

**Development and Characterisation of Novel Biocomposites
Fabricated Using Natural Fibres and Rapid Prototyping
Technology**

A Doctoral Thesis by

Lyes Azzouz

**Submitted in partial fulfilment of the requirements for the award of the
degree of**

Doctor of Philosophy

School of Physics, Engineering and Computer Science

University of Hertfordshire

May 2020

Abstract

This research project was motivated by the current development in the field of biocomposites and aims to explore various materials and techniques in the production of environmentally friendly composites. Initially, this study focused on establishing innovative methods of flax reinforcement with different polymeric compounds biodegradable and non-biodegradable based such as poly-lactic acid (PLA), polypropylene (PP), maleic anhydride polypropylene (MAPP) and put them under mechanical testing. One method which was employed here is comingling flax fibres with thermoplastic slivers forming continuous tapes and to be processed via thermal consolidation. Comparisons were made to their woven counterparts based off the tensile and flexural properties achieved by each category. The effects of fibre contents on the mechanical performance have also been evaluated. Similar approach was adopted for reinforcement with thermoset resins as both non-biodegradable unsaturated polyester (UPE) and biodegradable furan poly-furfural acid (PFA) resins were also considered for their development and characterisation. Effect of *in-situ* temperature on the tensile properties have also been studied for a selection of these biocomposites and their failure mechanisms discussed. A general trend of property decrease with temperature increase was observed as the combination of reinforcement architecture and thermal stability of the matrix control the tensile performance.

Another area of focus in this project is the Fused Deposition Modelling (FDM) of PLA parts using readily available 3D-printers. Tensile specimens were built and tested to correlate build parameters to internal configurations. Furthermore, the combined effects of *in -situ* temperature and filament build orientation have been investigated in terms of constitutive material parameters and final failure mechanism. The investigation involved the evaluation of properties deterioration including tensile strength, modulus, stress at failure, strain-to-failure and energy absorbed. They indicate that the internal structures coupled with *in-situ* temperature conditioning significantly affect the mechanical behavior of the specimens. The findings of this study are useful in defining the most appropriate raster orientation for FDM components on the basis of their expected in-service loading.

Lastly, three designs of lattice cores were proposed to assess the feasibility of using FDM process to produce lightweight polymer-based sandwich panels for structural applications. Effects of the shape topology on the compression in-plane and out of plane, shear and bending strength and stiffness have been experimentally investigated through a full mechanical characterisation. This category of core structures is well suited to compete with high performing honeycomb structures used for aerospace applications.

Keywords: Biocomposites; Flax; Mechanical properties; Additive Manufacturing; 3D-Printing; Lattice structures; *in-situ* temperature effects.

Acknowledgements

First of all, all thanks and gratitude go to my parents who supported me throughout my entire academic journey since the first day I stepped into the University of Hertfordshire to fulfil my academic aspirations from the undergraduate course to the doctoral programme. I would also like to dedicate a very special thanks to Rosemary Cargill for her support, encouragement and understanding for the entire duration of this programme.

I am also thankful to the University of Hertfordshire in general and doctoral college is particular for giving me the opportunity to pursue my research career by granting me a PhD position and allocating me with a supportive and experienced team of academics who have provided a great assistance in the conduct of my research.

I would like to sincerely acknowledge my principal supervisor Dr. Guogang Ren for his continuous support and valuable guidance during the entire period of this programme.

I am also thankful for the support of my second supervisor Dr. Leslie Mitchell with regard to sourcing the necessary resources to support the activities of this research.

I offer my thanks to all academics of the School of Physics, Engineering and Computer Science who offered any support or advice in the development of this project.

I am also grateful to the anonymous referees for their respective valuable comments on the manuscripts of journal articles.

Without a doubt the journey of a PhD candidate can be challenging but those difficult moments can be overcome with the support of fellow candidates who can be a source of refuelling to continue the journey. Therefore, I would like to thank all my research colleagues for their support and motivational discussions at times of difficulty.

Nomenclature

Acronyms

ABS	Acrylic Butadiene Styrene
AM	Additive Manufacturing
ASTM	American Society for Testing and Materials
CAD	Computer Aided Design
CM	Compression Moulding
DFM	Design for Manufacture
DMA	Dynamic Mechanical Analysis
DSC	Differential Scanning Calorimetry
FDM	Fused Deposition Modelling
FFF	Fused Filament Fabrication
FMF	Fibre Mass Fraction
FTIR	Fourier Transform Infrared Spectroscopy
GF	Glass fibre
GHG	Greenhouse Gases
ILSS	Interlaminar Shear Strength
IM	Injection Moulding
LCA	Life Cycle Assessment
LCL	Lower Control Limit
MAPP	Maleic Anhydride grafted Polypropylene
NF	Natural Fibre
NFC	Natural Fibre Composite
NMT	Natural fibre Mat Thermoplastic
ρ	Density in (g/cm ³) or (kg/m ³)
PC	Polycarbonate
PEEK	Polyetheretherkeytone
PEI	Polyetherimide
PFA	Polyfurfuryl Alcohol
PLA	Polylactic Acid
PP	Polypropylene
ROM	Rule of Mixtures
RP	Rapid Prototyping
RTM	Resin Transfer Molding
SD	Standard Deviation

SEM	Scanning Electron Microscope
SFTT	Single Fibre Tensile Test
SLS	Selective Laser Sintering
SMC	Sheet Moulding Compound
STL	Stereolithographic
TGA	Thermogravimetric Analysis
UCL	Upper Control Limit
UD	Unidirectional
UPE	Unsaturated Polyester
UTS	Ultimate Tensile Strength
V_f	Fibre Volume Fraction in %
VIP	Vacuum Infusion Process
2D	2Dimensional
3D	3Dimensional
3DP	3D Printing

Symbols

σ	Stress
τ	Shear Stress
E	Young's Modulus
E'	Storage Modulus
E''	Loss Modulus
ϵ	Strain
G	Shear Modulus
η	Efficiency Factor
Tan δ	Damping Factor
T_g	Glass Transition Temperature
T_m	Melting Temperature
U_t	Energy
wt%	Weight ratio percentage
X_c	Degree of Crystallinity

Units

cm^3	Cubic centimetre
GPa	Gigapascal

GSM	Grams per Square Meter
g	Gram
Hrs	Hours
J	Joule
kg	Kilogram
kN	Kilonewton
kPa	Kilopascal
N	Newtons
m ³	Cubic metre
mins	Minute
µm	Micrometre
mm	Millimetre
MPa	Megapascal
Pa	Pascal
°C	Degree Celsius
%	Percentage
±	Plus or Minus

Table of Contents

<i>Abstract</i>	i
<i>Acknowledgements</i>	ii
<i>Nomenclature</i>	iii
<i>Table of Contents</i>	vi
<i>List of Figures</i>	x
<i>List of Tables</i>	xvi
1. Introduction	1
1.1. Background	1
1.2. Research Aims and Objectives	5
1.3. Thesis Structure	6
1.4. Contributions and Achievements	7
2. Literature Review – Part I: Review of Biocomposites Based on Lignocellulosic fibres	9
2.1. Natural fibres overview	9
2.1.1. Chemical and morphological properties	11
2.1.2. Flax plant growth	15
2.1.3. Flax fibre isolation method	15
2.1.4. Single fibre mechanical tests	17
2.1.5. Production and utilisation of flax	18
2.2. Flax fibre architecture as a reinforcement	19
2.2.1. Continuous reinforcement	20
2.2.2. Discontinuous Reinforcement – Nonwoven mats	22
2.3. Selection of polymeric matrix and manufacturing technique	25
2.3.1. Polymer type	26
2.3.2. Biodegradable polymers	27
2.3.3. Composite manufacturing processes	37
2.3.4. Fibre and void contents	43
2.3.4.1. Fibre length and orientation factors	46
2.4. Mechanical properties	49
2.4.1. Tensile properties	49
2.4.2. Flexural Properties	52
2.4.3. Dynamic Mechanical Properties	56
3. Literature Review – Part II: A review of Additive Manufacturing Techniques	59
3.1. Additive Manufacturing: Types, Technology and Challenges	59
3.1.1. Additive Manufacturing Techniques	59
3.1.2. Additive Manufacturing Process and Technology	62
3.1.3. Materials Development for Additive Manufacturing	62

3.2.	Additive Manufacturing: Global Market Trend	63
3.2.1.	Market Value Growth	63
3.2.2.	Additive Manufacturing in Research	64
3.3.	Fused Deposition Modelling	65
3.3.1.	Process Parameters	66
3.3.2.	Effect of FDM Process Parameters: Process optimisation	67
3.3.3.	Material Selection and Compatibility for FDM	69
3.3.4.	Challenges and Limitations of FDM	70
4.	Materials and Methodology of Research	71
4.1.	Natural Fibre Composites: Materials, Manufacturing and Testing	71
4.1.1.	Selection and characterisation of materials and processes.....	71
4.1.1.1.	Differential Scanning Calorimetry	71
4.1.1.2.	Thermogravimetric Analysis	73
4.1.1.3.	Scanning Electron Microscopy	75
4.1.1.4.	Fourier Transform Infrared Spectroscopy.....	75
4.1.2.	Continuous - Unidirectional tape.....	78
4.1.2.1.	Thermoplastic based biocomposites	78
4.1.2.2.	Thermoset based biocomposite	84
4.1.3.	Discontinuous – Nonwoven mats	87
4.1.3.1.	Thermoplastic based biocomposite.....	87
4.1.3.2.	Thermoset based biocomposite	88
4.1.4.	Sample cutting and conditioning	89
4.1.5.	Characterisation and properties evaluation	90
4.1.5.1.	Tensile Properties.....	90
4.1.5.2.	Flexural Properties	91
4.1.5.3.	Thermo-mechanical Properties – DMA	92
4.1.6.	The effect of <i>In-Situ</i> Temperature on the Biocomposites	92
4.2.	3D Printed PLA Structures Specimen	93
4.2.1.	Materials and methods	94
4.2.1.1.	Geometry of tensile specimen.....	94
4.2.1.2.	Materials and equipment.....	95
4.2.1.3.	Specimen fabrication	97
4.2.2.	Experimental procedure.....	99
4.2.2.1.	Tensile testing	99
4.2.2.2.	The effect of temperature on extruded filament	100
4.2.3.	The effect of <i>in-situ</i> temperature on 3D printed Specimen	101
4.2.4.	Fractography analysis of 3D-printed and tested specimen	103

5. Results	104
5.1. Natural Fibre Composites	104
5.1.1. Continuous-Unidirectional	104
5.1.1.1. Thermoplastic based biocomposites	104
5.1.1.2. Thermoset based biocomposites	112
5.1.2. Discontinuous- Nonwoven	117
5.1.2.1. Thermoplastic based biocomposites	117
5.1.2.2. Thermoset based biocomposites	121
5.1.3. The effect of In-Situ Temperature on NFCs under Tension	123
5.1.3.1. Flax/Poly-lactic continuous reinforcement	124
5.1.3.2. Flax/Polypropylene nonwoven mats	125
5.1.3.3. Flax/Furan continuous reinforcement	127
5.2. 3D-Printed PLA Structures	128
5.2.1. Dimensional accuracy	128
5.2.2. Tensile testing	130
5.2.3. The effect of temperature on extruded filaments	133
5.2.4. The effect of In-Situ Temperature on Tensile Parameters	135
6. Discussions	141
6.1. Discussion of the biocomposites properties	141
6.1.1. Quasi-static Properties under Ambient Conditions	141
6.1.1.1. Continuous reinforcement	141
6.1.1.2. Discontinuous reinforcement	145
6.1.2. Tensile properties of conditioned specimen	152
6.1.3. Toughness and resilience of conditioned biocomposites	154
6.2. Discussion of 3D-Printed PLA properties	156
6.2.1. Effect of internal geometry	156
6.2.2. Extruded Filaments	159
6.2.3. Tensile Properties of 3D-printed Conditioned Specimen	159
6.2.4. Resilience and toughness of 3D-printed specimen	165
7. Case Study: Sandwich Panels of 3-D Printed Lattice Core and Biocomposite Skins	168
7.1. Introduction	168
7.2. Methodology	168
7.2.1. Lattice Structures	168
7.2.2. Manufacturing Procedures	169
7.2.2.1. Materials and equipment of the core	169
7.2.2.2. Printing problems resolution	170
7.2.2.3. Sandwich panels production	173

7.2.3.	Mechanical testing.....	173
7.2.3.1.	Tensile testing of NFC.....	174
7.2.3.2.	Compression testing of core lattice structures.....	174
7.2.3.3.	Shear testing of core lattice structures.....	175
7.2.3.4.	Flexural testing of sandwich panels.....	177
7.3.	Results and discussions.....	178
7.3.1.	Compression results of core lattice structures.....	178
7.3.2.	Shear results of core lattice structures.....	181
7.3.3.	Flexural results of sandwich panels.....	182
8.	Conclusions and Recommendations.....	187
8.1.	Conclusions.....	187
8.2.	Recommendations.....	190
	References.....	192

List of Figures

Figure 2-1 Components produced from natural fibres: a) spare wheel cover, b) car seatback, c) car door trim, d) car wheel arch, e) aircraft food galley. [Produced from source: (Ecotechnilin, 2017)].....	9
Figure 2-2 Classification of various reinforcement with natural fibres: cellulosic and non-cellulosic fibres.	10
Figure 2-3 Natural fibre market in the U.S by raw material- Projection 2013-2024 in USD Million (Grand.View.Research, 2018).....	11
Figure 2-4 Elementary fibre layer structure (Mohanty et al., 2005)	12
Figure 2-5 Flax secondary wall, S2 lamella contents with microfibril angle	14
Figure 2-6 Flax plant 12 growth stages.....	15
Figure 2-7 Cross section of the flax stem and elementary fibre production (Bos et al., 2002).....	16
Figure 2-8 Flax fibre world production 10 top countries in 2016.....	19
Figure 2-9 Production of unidirectional flax tape: a) alignment of flax yarns into uniform tapes, b) aligned flax tape along 0° direction, c) multi-layers laminated unidirectional flax to achieve the desired thickness.	21
Figure 2-10 Natural fibre nonwoven mats manufacturing stages.[Produced from source: (Ecotechnilin, 2017)]......	23
Figure 2-11 composite layer structure arrangement under flexural testing. LM: loading on mat; LUD: loading on UD (Habibi et al., 2017).....	25
Figure 2-12 Arrangement of molecules in a) Thermoplastic and b) Thermoset	26
Figure 2-13 The wide range of products and industries using bioplastics (European bioplastics, 2018).	27
Figure 2-14 Stages of PLA production using either condensation by direct polymerisation or catalyst ring opening polymerisation (Bajpai et al., 2014).....	28
Figure 2-15 Cradle to pellets Green House Gas emissions of a number of commonly used plastics (Vink et al., 2003)	29
Figure 2-16 Total energy from fossil resources required for plastics production (Vink et al., 2003)...	29
Figure 2-17 Proportions of various bioplastics contribution towards the global production capacity in 2018. Noticeably, PP and PEF are included in this chart inspite of their zero contribution, however, these are in developemnt to be available at commercial scale in 2023 (European bioplastics, 2018)..	30
Figure 2-18 Polypropylene structure.....	31
Figure 2-19 Representation of the cross linking mechanism of polyester resin (Mallick, 2007).	33
Figure 2-20 Chemical conversion of furfural through pre-condensation to produce furan pre-polymer	35
Figure 2-21 Variation of mechanical properties with respect to porosity variation levels- Comparison is based on reference $V_f=40\%$ for all processes (Hayward and Harris, 1990).....	45
Figure 2-22 Effect of autoclave pressure on the void content (%) (Phillips et al., 2013).....	45
Figure 2-23 Shear lag model predictions of the fibre length efficiency factor as a function of the fibre aspect ratio. Typical values for plant fibre composites are used in the calculations: $E_f= 50$ GPa, $G_m = 1$ GPa, $k = 0.785$, $V_f= 0.30$. (Madsen et al., 2009).....	47
Figure 2-24 Fibre orientation angle with respect to the loading axis for a 2-D reinforcement arrangement.....	49
Figure 2-25 a) Flexural strength, b) Flexural modulus of PLA reinforced with untreated hemp fibres and ALK (Alkali), SIL (Silane) and ALKSIL (Alkali and silane) treated fibres as a function of fibre contents (Sawpan et al., 2012)	53
Figure 2-26 a) Flexural strength, b) Flexural modulus of polyester reinforced with untreated hemp fibres and ALK (Alkali), SIL (Silane) and ALKSIL (Alkali and silane) treated fibres as a function of fibre contents (Sawpan et al., 2012).....	53
Figure 2-27 Failure mechanisms of tested specimen under SEM: dry flax (left) and wet flax (right) (Dhakal et al., 2014).....	54

Figure 2-28 Flexural modulus of glass, hemp and flax mat reinforced furan and polyester composites, average fibre contents $V_f=23\%$ (Arnold et al., 2009).	55
Figure 2-29 flexural modulus of furan/flax biocomposites (Arnold et al., 2009)	55
Figure 2-30 Loss factor at 1 Hz and 25 C for: a) UD composites and b) TW composites (Duc et al., 2014b).	56
Figure 3-1 the projected market value from 2015 to 2025 for individual industries	64
Figure 3-2 Quantification of the various AM techniques contribution in the global number of publications	65
Figure 3-3 Schematic diagram of the fused deposition modelling method with dual extruder providing build support (Mohamed et al., 2015)	65
Figure 3-4 Fishbone diagram of the causes and effects of DFM process parameters (Mohamed et al., 2015)	66
Figure 3-5 The FDM process variables: a) layer thickness, b) build orientation and c) nozzle path....	67
Figure 4-1 Schematic illustration of DSC working principle and mechanism	72
Figure 4-2 A sample signal of a DSC scan for PP fibres 30 -700 °C at heating rate of 10 °C/min covering melting and degradation phases	73
Figure 4-3 Mass loss % of flax fibres under isothermal exposure	74
Figure 4-4 Mass loss % of PP fibres under isothermal exposure	74
Figure 4-5 SEM images of flax fibre: a) outer surface of the fibre (elementary) with no visible micro-defects along its length, b) cross section of (technical) fibre showing a compacted number of microfibrils that provide tensile strength.	75
Figure 4-6 FTIR spectra of flax fibres	76
Figure 4-7 FTIR spectra of polypropylene	77
Figure 4-8 FTIR spectra of MAPP	77
Figure 4-9 a) Commingling process of flax staples and matrix staples, b) microscopic image of commingled slivers	78
Figure 4-10 The straightening stage of blended slivers: a) top and bottom fallers placed between roller, b) closer image of the bottom fallers, c) spread and aligned fibre web	79
Figure 4-11 A summary of the holistic process of individual slivers of flax and matrix into a comingled thin tape for biocomposite production	80
Figure 4-12 The process of thermal consolidation of aligned flax fibres and PLA to produce the Flax/PLA blended tape: a) Flax/PLA input blend, b) Flax and PLA being spread, c) the process of rolling the spread blend, d) a close image of pre-consolidated tape, e) thermal consolidation with the application of pressure between two heated rollers, and f) tape winding unit	80
Figure 4-13 Production of Flax/PLA panels out of comingled thin tapes: a) thermal press for thermal consolidation of panels, b) b) schematic representation of the heated consolidation zone, c) consolidated panels of three Flax/PLA ratios pressed at 170 °C and 20 bar for 20 minutes.	82
Figure 4-14 a) schematic diagram of the prepreg production, b) in-line impregnation of flax tape through a BioRez PFA bath, c) removal of resin excess by passing the prepreg through calander rollers, d) air oven drying of the prepreg, e) the final produced prepreg rolled ready for further consolidation	86
Figure 4-15 the manufacturing of polyester natural fibre mats: a) glass mat cleaned by acetone, b) resin mixture poured over the mats, c) resin wet mats arranged ready for consolidation, d) vacuum and absorption tissue inserted, e) vacuum applied to cure samples.	89
Figure 4-16 Electric guillotine used to cut the composite panels in dimensions corresponding to the specified standards	90
Figure 4-17 measurements taking of the various specimen types for the mechanical characterisation – this image is an example of geometry measurement of DMA samples.	90
Figure 4-18 a) Typical stress vs strain. Method of tensile modulus calculation using graphical method (BS EN ISO 527-5:2009); b) Specimen with aluminium end tabs; c) tensile test setup arrangement..	91

Figure 4-19 locations of stress concentration for the ASTM D638 dog-bone specimen with longitudinal extruded filaments (Ahn et al., 2002)	94
Figure 4-20 Modification of geometry including the contours (Ahn et al., 2002).....	94
Figure 4-21 Optimised geometry of standard based tensile specimen with nominal dimensions, improvement included the radius of curvature R=1000mm	95
Figure 4-22 Schematic arrangement of the specimen with different raster angle values 0°, 30° and 90° adopted to print the three infill orientations.....	98
Figure 4-23 schematic representation of internal arrangements of raster angles for the three orientations with respect to the loading line in tension mode.	100
Figure 4-24 In-situ temperature measurement using: a) thermocouples and b) Infrared camera	103
Figure 5-1 Biotex Twill 2x2 of flax fibres with different matrices PLA, PP and MAPP: comparison of tensile modulus and strength. Specimen consolidated with PLA showed the maximum modulus and strength, however the MAPP specimen exhibited improved strength as compared to the PP specimen.	104
Figure 5-2 Comparison of tensile performance of Flax/PLA in a 50:50 fibre to matrix ratio between two fabric architectures: 0°/90° tape and reference material Biotex Twill 2x2.....	107
Figure 5-3 optimisation of flax fibre to PLA matrix mix by weight ratio in terms of: a) tensile modulus and strength, b) flexural modulus and strength. It can be noted that the optimum results were reported for the 55:45 specimen.....	108
Figure 5-4 Comparison of: a) tensile performance of Flax/PP in a 50:50 fibre to matrix ratio amongst three fabric architectures: 0°/90°, UD tape and Biotex Twill 2x2. Reference specimen Twill 2x2 were only tested in tension mode, b) flexural performance between UD tapes and 0°/90°.....	110
Figure 5-5 Comparison of tensile performance of Flax/MAPP in a 50:50 fibre to matrix ratio between two fabric architectures: 0°/90° tape and Biotex Twill 2x2.....	111
Figure 5-6 Comparison of: a) tensile properties, b) flexural properties of Flax/MAPP in varying fibre to matrix ratio by weight of 0°/90° tape architectures: 40:60, 50:50 and 60:40	112
Figure 5-7 comparison of performance between three fabric reinforcements unidirectional (0°): Flax/glass veils ($V_f= 52\%$), Flax/PLA 90:10 ($V_f= 47\%$) and Flax Crystic laminate ($V_f= 33\%$). Fibre contents $V_f= 52\%$ for the hybrid mat due glass presence. This difference explains the superior tensile (chart a) and flexural (chart b) moduli and strengths.....	114
Figure 5-8 comparison of: a) tensile and b) flexural moduli and strengths of BioRez reinforced with two different fabric architectures in a mixture of 50:50, Tapes of Flax/PLA 90:10 and Non-Crimp Fabrics of Flax/PLA 90:10, both materials achieved similar fibre contents $V_f= 47\%$. While the Tapes were constructed in various orientations (UD 0°, 0°/90° and $\pm 45^\circ$), Non-Crimp Fabrics were limited to $\pm 45^\circ$ this is for process evaluation purpose. Twill 2x2 100% flax fabric were also used in the comparison.	116
Figure 5-9 comparison of: a) tensile and b) flexural moduli and strengths of Crystic polyester reinforced with Flax Laminates (Twill 2x2, UD 0° and 0°/90°) and BioRez reinforced with Twill Flax prepreg, both materials achieved similar fibre contents $V_f= 33\%$	117
Figure 5-10 Tensile test nominal stress vs strain curves of five Flax/PP specimen.....	118
Figure 5-11 Nonwoven Flax/PP panel cut direction for the purpose of testing in the longitudinal (along fibre direction) and transverse directions.....	120
Figure 5-12 tensile response comparison between nonwoven Flax/PP specimen tested in the longitudinal and transverse directions.....	120
Figure 5-13 Tensile nominal stress vs strain curves for three different nonwoven Flax/Polyester panels of varying fibre contents represented in their averaged values for: $V_f= 22\%$, $V_f= 18\%$, $V_f= 14\%$..	122
Figure 5-14 Flexural nominal stress vs strain curves for three different nonwoven Flax/Polyester panels of varying fibre contents represented in their averaged values for: $V_f= 22\%$, $V_f= 18\%$, $V_f= 14\%$	123
Figure 5-15 Tensile nominal stress vs strain averaged curves of five test repetitions of Flax/PLA panels tested under a range of temperatures 30°C- 70°C.....	125

Figure 5-16 Tensile nominal stress vs strain averaged curves of five test repetitions of nonwoven Flax/PP panels tested under a range of temperatures 30°C- 70°C	127
Figure 5-17 Tensile nominal stress vs strain averaged curves of five test repetitions of nonwoven Flax/Biorez panels tested under a range of temperature 30°C- 70°C.	128
Figure 5-18 Dimensions of all printed specimen compared to the UCL and LCL of the full population sample: a) width and b) thickness	129
Figure 5-19 Tensile curves of nominal stress vs strain for the three raster orientations each reported for five sample repetitions: a) 0°/90°, b) -30°/+60°, c) ±45°	132
Figure 5-20 Tensile stress vs strain of averaged samples of the three orientations overlapped, samples oriented in ±45° exhibit higher slope of elastic region indicating higher stiffness and higher peak corresponding to maximum UTS	133
Figure 5-21 Stress vs strain for printed PLA curve: tensile strength decreased while strain increased as temperature increases	134
Figure 5-22 Comparison of the Young's Modulus values of the three different orientations across temperatures (20-60 °C) – Standard deviations are included for all averages. For -30°/+60° and ±45° samples tested at 60°C low modulus values under 100 MPa and their respective standard deviations are presented but considerably low compared to the scale used.	136
Figure 5-23 Comparison of the tensile strength values of the three different orientations across temperatures (20-60 °C) – Standard deviations are included for all averages. For samples tested at 60°C low strength values under 1 MPa and their respective standard deviations are presented but considerably low compared to the scale used.	138
Figure 5-24 Comparison of the stress at failure values of the three different orientations across temperatures (20-60 °C) – Standard deviations are included for all averages. For samples tested at 60°C low values under 1 MPa and their respective standard deviations are presented but considerably low compared to the scale used.....	139
Figure 5-25 Comparison of the strain at failure values of the three different orientations across temperatures (20-60 °C) – Standard deviations are included for all averages. A very marginal influence of the temperature up to 40 °C after which total failure cannot be reached at 50 °C and 60 °C.	139
Figure 6-1 Tensile modulus and strength variations of flax/MAPP composites with respect to the increasing fibre wt%	143
Figure 6-2 Flexural modulus and strength variations of flax/MAPP composites with respect to the increasing fibre wt%	143
Figure 6-3 SEM images of internal geometry of flax/PP fractured samples: a) kink bands at the surface of the fibre; b) fibre internal pull-out of microfibrils; c) surface fracture of fibre under compressive load; d)a view of a dense zone of fibres damaged due to pull and twist loading.....	145
Figure 6-4 SEM image to show the variations of diameter and shape of fibres within the same sample.	146
Figure 6-5 The variation of tensile strength and modulus of flax/UPE composites with respect to fibre volume fraction increase	147
Figure 6-6 strain-to-failure linear reduction with increased fibre contents within the composites.....	147
Figure 6-7 SEM image of brittle fracture of flax fibres under the tensile load.....	148
Figure 6-8 The variation of flexural strength and modulus of flax/UPE composites with respect to fibre volume fraction increase.....	149
Figure 6-9 a) optical microscope image of bottom surface fracture with evident resin rich zones; b) microscopic image of through thickness view of the sandwich like arrangement of flax/UPE; c) mid-span damage initiation and propagation through the specimen thickness; d) failure of individual fibres due to stress concentration at the weak nodes due to bending	149
Figure 6-10 DMA results for the flax/UPE composites of three levels of fibre contents $V_f = 22\%$, $V_f = 18\%$, $V_f = 14\%$: a) storage modulus; b) loss modulus; c) $\tan\delta$	151

Figure 6-11 Effect of in-situ temperature increase on the tensile modulus and strength of Flax/PLA biocomposites, standard deviations values of the modulus are very small are difficult to see– a linear decrease with respect to temperature increase	153
Figure 6-12 Effect of in-situ temperature increase on the tensile modulus and strength of Flax/PP biocomposites – a linear decrease with respect to temperature increase	154
Figure 6-13 Effect of in-situ temperature increase on the tensile modulus and strength of Flax/PFA biocomposites – a linear decrease with respect to temperature increase	154
Figure 6-14 modulus of toughness and resilience of the biocomposites Flax/PLA, Flax/PP and Flax/PFA as temperature increases from 20-70°C.....	155
Figure 6-15 tensile strength and modulus variation of 3D-printed PLA with respect to the infill orientation of internal beads.....	156
Figure 6-16 cross section view of specimen of 0/90° orientation after the tensile test and full rupture of mid-section. Image portrays beads in criss-cross layering arrangement and bonding surfaces.....	157
Figure 6-17 Micrograph of tensile failure surface perpendicular along the slip plane	157
Figure 6-18 cross section view of specimen of -30°/+60° orientation after the tensile test and full rupture of mid-section. Image portrays beads in criss-cross layering arrangement and bonding surfaces	158
Figure 6-19 cross section view of specimen of ±45° orientation after the tensile test and full rupture of mid-section. Image portrays beads in criss-cross diamond arrangement and bonding surfaces.....	158
Figure 6-20 Micrograph of individual bead necking promoting local fracture and regions of air gaps between beads reducing the load bearing contribution of bonding surfaces.....	159
Figure 6-21 Contour plot of young’s modulus variation for 3D-printed PLA to illustrate the combined effects of temperature increase and infill orientation angle. Y-axis labels identification: 0= (0°/90°), 30= (-30°/+60°) and 45= (±45°)	160
Figure 6-22 Contour plot of strength variation for 3D-printed PLA to illustrate the combined effects of temperature increase and infill orientation angle. Y-axis labels identification: 0= (0°/90°), 30= (-30°/+60°) and 45= (±45°)	161
Figure 6-23 Optical images of fractured specimen ±45°: a) and b) for tests under 30°C, c) and d) for tests under 40°C	161
Figure 6-24 a) illustration of sliding movement of bonding surfaces under the induced shear due to tension acting on the adjacent beads; b) optical microscopic image close-up illustrated in a representative volume of shear failure within a cross section of fractured specimen.....	162
Figure 6-25 Microscopic images of specimen printed at: a) 0°/90°, b) -30°/+60° and c) ±45° after testing at 40°C.....	162
Figure 6-26 Contour plot of stress at failure variation for 3D-printed PLA to illustrate the combined effects of temperature increase and infill orientation angle. Y-axis labels identification: 0= (0°/90°), 30= (-30°/+60°) and 45= (±45°)	163
Figure 6-27 Contour plot of strain at failure variation for 3D-printed PLA to illustrate the combined effects of temperature increase and infill orientation angle. Y-axis labels identification: 0= (0°/90°), 30= (-30°/+60°) and 45= (±45°)	164
Figure 6-28 Fracture toughness and resilience of 3D-printed PLA of the three orientations and across a range of temperatures 20-60°C	165
Figure 6-29 Contour plot of resilience variation for 3D-printed PLA to illustrate the combined effects of temperature increase and infill orientation angle. Y-axis labels identification: 0= (0°/90°), 30= (-30°/+60°) and 45= (±45°)	166
Figure 6-30 Contour plot of modulus of toughness variation for 3D-printed PLA to illustrate the combined effects of temperature increase and infill orientation angle. Y-axis labels identification: 0= (0°/90°), 30= (-30°/+60°) and 45= (±45°)	167
Figure 7-1 (a) Lattice 1: BCC-Z structure, diamond design that has a vertical strut that runs through the middle of the unit cell (b) Lattice 2: cube-like format, circumferential rectangular pattern of 4 vertical struts on each corner, with 5 th vertical struts in the centre, and eight smaller struts that meet at	

the middle of the vertical strut in the centre of the cell, and (c) Lattice 3: diamond form BCC unit cell like that of unit lattice 1 without the vertical strut.	169
Figure 7-2 the effect of the reduced build pate adhesion and the plate levelling on the quality of the extruded filaments: a) the use of glue on surface build plate instead of raft; b) the plate/print-core nozzle spacing affects the quality of extrusion as shown is zones of poorly printed unit cells	171
Figure 7-3 Filament extrusion poor quality due to the inadequate printing temperature and the moisture content in the surrounding environment creates layers with multiple defects such as high porosity and geometrical faults.	172
Figure 7-4 Printing speed optimised to overcome the ghost layers of the complex parts: a) Lattice 2 printed at speed of 40 mm/s and missing layers are clearly noticed, b) Lattice 2 printed at speed of 15 mm/s which is defect-free	172
Figure 7-5 3D-printed PLA cellular lattice fabricated for compression test: (a) Lattice 1, (b) Lattice 2, (c) Lattice 3, (d) out-of-plane compression test set up.....	174
Figure 7-6 In-plane compression test set up: (a) inclined struts sanded down, (b) perfect alignment, (c) load line direction with specimen under testing, (d) illustration of manual sanding operation of a compression specimen.	175
Figure 7-7 (a) Dimensions of the tested core, (b) sample preparation, (c) test setup and loading direction.	176
Figure 7-8 (a) Specimen with lattice core bonded to the NFC skins, (b) sandwich panel flexural test set up.	177
Figure 7-9 Load vs displacement curves obtained from the out-of-plane compression test showing the three sample repetitions denoted as S1, S2 and S3: (a) Lattice 1, (b) Lattice 2, (c) Lattice 3 and (d) L2_S1 deformation mechanism with vertical struts fracture z	178
Figure 7-10 Load vs displacement curves from the in-plane compression test for the three repetitions with the observed in-situ deformation during and after testing: (a) Lattice 1, (b) Lattice 2 and (c) Lattice 3.	179
Figure 7-11 Deformation mechanisms of lattice structures under in-plane compression tests: (a) Lattice 1 shows layer by layer collapse through node rotation, (b) Lattice 2 shear band formation with stretch dominant deformation of bottom layer.....	180
Figure 7-12 Load vs displacement curves from the shear test of bonded core lattice: (a) Lattice 1, (b) Lattice 2, (c) Lattice 3 and (d) Comparison of the three structures	182
Figure 7-13 Failure mechanisms of the three core lattice structures under shear: (a) Lattice 1, (b) Lattice 2, (c) Lattice 3.....	182
Figure 7-14 Bending characteristics of sandwich panels shown on the load vs displacement. Three sample repetitions to show repeatability: (a) Lattice 1, (b) Lattice 2 and (c) Lattice 3.	183
Figure 7-15 Deflection and failure mechanisms under bending loading: (a) Lattice 1, (b) Lattice 2, (c) Lattice 3.	184

List of Tables

Table 1-1 Advantages and drawbacks of synthetic and natural fibres (Bensadoun, 2016).....	2
Table 2-1 Chemical composition (%) of natural plant fibres.....	13
Table 2-2 Natural fibres physical properties: Diameter, density and MFA with mechanical properties	14
Table 2-3 Comparison between thermoplastic and thermoset polymers	26
Table 2-4 Typical properties of cast thermoset polyester resin at 23 °C (Mallick, 2007).	34
Table 2-5 Performance requirements for automotive polyester and polyester composites.	34
Table 2-6 Manufacturing techniques used in the production of NFCs, process variables interrelated with composite parameters	43
Table 3-1 A summary of AM technologies and their corresponding materials	59
Table 3-2 Additive Manufacturing main process, materials, applications, benefits and drawbacks (Ngo et al., 2018)	61
Table 4-1 Draft ratio values for the 8 rollers in the slivers blend process	79
Table 4-2 Complete list of continuous thermoplastic based biocomposites considered in this research, materials types, processing parameters and reinforcement arrangements	83
Table 4-3 Typical physical and mechanical properties of Crystic 701PA tested in accordance with appropriate BS or BS EN ISO standards	84
Table 4-4 Complete list of continuous thermoset based biocomposites considered in this research, materials types, processing parameters and reinforcement arrangements	87
Table 4-5. Mechanical and physical properties of natural fibres and polyester 2-446PA	88
Table 4-6 Dimensions of tensile specimen	95
Table 4-7 PLA filament physical and mechanical properties	95
Table 4-8 Printing parameters used in the fabrication of 3-D tensile specimen on the MakerBot Replicator.....	96
Table 4-9 Samples considered for the testing plan	98
Table 4-10 DMA experimental plan on the PLA filaments.....	100
Table 4-11 Experimental Plan for the tensile testing	102
Table 5-1 Complete set of tensile and flexural tests results of flax reinforced biocomposites using different architecture of reinforcement and thermoplastics	106
Table 5-2 Complete set of tensile and flexural tests results of flax reinforced biocomposites using various reinforcement architectures and thermosets.....	113
Table 5-3 comparison of tensile properties between nonwoven Flax/PP specimen cut and tested in the longitudinal and transverse directions.....	119
Table 5-4 Tensile modulus and strength averaged values and their corresponding standard deviations (S.D.) of the five nonwoven Flax/Polyester specimen tested under tension for three levels of fibre volume contents.	121
Table 5-5 Flexural modulus and strength averaged values and their corresponding standard deviations (S.D.) of the five specimen tested under 3pt bending for three levels of fibre volume contents.	122
Table 5-6 Tensile modulus and strength averaged values of continuous aligned of Flax/PLA and their corresponding standard deviations (S.D.) of the five specimen tested under varying temperatures 30°C to 70°C.	124
Table 5-7 Averaged tensile modulus and strength values with calculated standard deviations of five test repetitions of Flax/PP panels tested under the effect of temperature 30°C- 70°C.....	126
Table 5-8 Averaged tensile modulus and strength values with calculated standard deviations of five test repetitions of thermoset based aligned continuous Flax/Biorez panels tested under the effect of temperature 30°C- 70°C.....	127
Table 5-9 Experimental values of tensile properties reported in terms of Young’s modulus, ultimate tensile strength, stress at failure and strain at failure	131
Table 5-10 Experimental result for neat and printed filaments from the tensile test	135

Table 7-1 Printing parameters used to manufacture all specimen considered for this study	173
Table 7-2 Maximum load values normalised with the nominal weight.....	185

1. Introduction

1.1. Background

Since the Paris Agreement 2015, a world-wide race to control the global warming which reached alarming levels in recent decades. One of the agreed NDCs – Nationally Determined Contributions– is limiting warming by 1.5-2°C above pre-industrial levels through the implementation of sustainable development and reducing Greenhouse Gases (GHGs) emissions. In consideration of this requirement, a pressing need for developing sustainable materials of which composites are not exempt due to their wide use in several industries. Natural fibres and flax in particular are cost-effective and offer specific mechanical properties comparable to those of glass fibres. Composites made of flax fibres with thermoplastic, thermoset, and biodegradable matrices have exhibited good mechanical properties.

Composite materials are formed from mixtures of two inherently dissimilar materials to create a new material emphasising the good properties while avoiding their drawbacks. Over recent years, the composites industry has increasingly shown an interest in reinforcement methods by natural fibres. Natural fibres such as flax, hemp and jute possess high reinforcing abilities in the presence of proper fusion with polymers. After decades of extensive development of synthetic fillers in the form of glass, carbon and aramid fibres, the focus has diverted to the bio-fibres, and resulted in the renewed interest in natural fibres on the basis of previous experiences during the last century such as the Henry Ford in 1941 where hemp and flax were used for the bodywork. The initiative was inspired by the increasing environmental consciousness and demands of legislative authorities related to the manufacture, use and removal of conventional composite structures (La Mantia and Morreale, 2011). However, the implementation of bio-fibres has to be integrated with the use of biopolymers to achieve the required biodegradability (Mohanty et al., 2000). As one of the current shortcomings of the existing composites, is the convenient removal and separation of fibres/matrix after the product end of life due to the firm interlinked components within the structure for stability purposes. The modern polymer technology dictates that all materials should be adjusted to the environment. Currently, the existing biopolymer systems do not possess the desired mechanical and thermal properties for load bearing applications. Therefore, the development of new high strength biodegradable polymers as a replacement for the synthetic counterparts is an ongoing research (Wool and Sun, 2011) (Faruk et al., 2014) (Pil et al., 2016).

The creation of bio-composites can be described as the insertion or reinforcing of natural fibres, e.g. flax, hemp or jute into bio-polymeric matrix in the form of cellulose, starch or lactic acid, etc. Currently, many researchers are working in the area of natural fibres and their composites for further development as a replacement candidate, to improve the necessary thermal and mechanical properties for engineering application and to endorse the biodegradability argument. Nevertheless the best performing plastics to be used as matrix are non-biodegradable synthetic based; as a result extensive studies achieved

remarkable performance when reinforcing bio-fibres into synthetic polymers. This has proposed a new category of composites even so not fully biodegradable (Zhu et al., 2013).

The benefits of bio-fibres over synthetic fibres, e.g. glass or carbon are low cost, low-density, high toughness, and renewability, satisfactory values of specific strength and specific modulus, good thermal and acoustic insulation due to their hollow and cellular nature (Bogoeva-Gaceva et al., 2007). A reduced tool wear and abrasion to machines, and reduced dermal and respiratory irritation, significant processing benefits as minor machinery adjustment are required. Moreover, additional advantages are the ease of separation and energy recovery when recycled. However, biodegradability, and the fact that these fibres compete with their synthetic counterparts in terms of specific strength and stiffness properties of natural fibres vary with location, origin and age of the plant (Pickering et al., 2016b). Despite the numerous advantages of bio-fibres, there are drawbacks associated with the fibres natural composition that have an effect during the composite manufacturing process. Due to their hydrophilic nature, the compatibility with the hydrophobic polymers is hugely reduced (Simão et al., 2016). Furthermore, Fibre degradation when exposed to high temperatures is critical; hence most bio-fibres are processed at maximum 200 °C (da Luz et al., 2018) (Chaishome et al., 2014).

Natural fibre composites are generally manufactured under different processing methods either with thermoplastics or thermosets (Maity et al., 2014) (Rana and Figueiro, 2016) (Mohanty et al., 2005). The chemistry of these two categories of polymer matrix is different which will consequently cause a variation in the composite properties. Firstly, thermoplastics are long linear chains very heat sensitive therefore this category is desired for low temperature applications such as automotive. Whereas thermosets are 3D crosslinked chains of monomers interlocked which cannot be molten or reshaped, this category is mostly used in high temperature applications such as aerospace. Table 1-1 summarises the commonly accepted advantages and drawbacks of using synthetic and natural fibre reinforcements.

Table 1-1 Advantages and drawbacks of synthetic and natural fibres (Bensadoun, 2016).

	<i>Synthetic fibres</i>	<i>Natural fibres</i>
<i>Advantages</i>	<ul style="list-style-type: none"> -Excellent mechanical properties/prices -Good adhesion with all resins -Temperature resistance -Incombustibility -Low thermal conductivity -Good dielectric properties -Good fire resistance 	<ul style="list-style-type: none"> -Very good mechanical properties -Biodegradable and renewable -Neutral CO₂ emissions -Good thermal and acoustic insulation -Non-toxic -Good resistance in aggressive environments -Low cost
<i>Drawbacks</i>	<ul style="list-style-type: none"> -Not environment-friendly -Premature aging in contact with water 	<ul style="list-style-type: none"> -Water sorption -Poor dimensional stability -Poor aging and thermal performance -Unknown long term properties: fatigue

Natural fibre-reinforced thermoset and thermoplastic composites have been widely utilised in different engineering applications especially in the automotive industry where they have successfully replaced non-structural components previously manufactured from glass fibre such as door panels, dashboards and trunk liners. Scientists and engineers motivation to employ advanced technology is driven by financial and environmental urges, to make a good use of natural resources in the production of competitive products. Sustainability is partly measured by the environmental burdens associated with the complete cycle of a material or product lifetime. However, “sustainable material “does not necessarily mean “environment friendly”. The fundamental loops during the holist processes contributing towards the creation of the material are included in the assessment, this is known for “Life Cycle Assessment” (LCA)(Association, 2011) (Dissanayake, 2011).

Freedom of design, mass customisation, waste minimisation and the ability to manufacture complex structures, as well as fast prototyping, are the main benefits of additive manufacturing (AM) or 3D printing (Ngo et al., 2018). The ASTM F42 Technical Committee defines additive manufacturing as “*Process of joining materials to make objects from three-dimensional (3D) model data, usually layer upon layer, as opposed to subtractive manufacturing technologies*”. The unique capabilities of AM technologies enable new opportunities for customization, very significant improvements in product performance, multi-functionality, and lower overall manufacturing costs. These unique capabilities include: **shape complexity**, in that it is possible to build virtually any shape fabricated from the microstructure through geometric mesostructure (sizes in the millimetre range) to the macrostructure part-scale; **material complexity**, in that material can be processed one point, or one layer, at a time; and **functional complexity**, in that fully functional assemblies and mechanisms can be fabricated directly using AM processes.

Design for manufacture and assembly (DFM) has typically meant that designers should tailor their designs to eliminate manufacturing difficulties and minimise manufacturing, assembly, and logistics costs (Gibson et al., 2010). Rapid prototyping (RP) is a freeform manufacturing process that allows users to fabricate a real physical part directly from a Computer-Aided Design (CAD) model. While prototypes enable the product development team to think, plan, experiment, and learn the processes while designing the product, AM technology supports low volume manufacturing in such manner that extra costs for the design and fabrication of moulds is eliminated. AM also enables easy integration of design changes and reductions of parts to greatly simplify product assembly.

In product development, time to market pressure is the main reason behind these technologies that evolved rapidly in the last few years. Therefore, the growing competition and the strive towards efficient production in many industries forced the transition of AM techniques focus from rapid prototyping fabrication to rapid tooling and rapid manufacturing (Liou, 2007). Through intensive research over the past two decades, significant progress has been made in the development and commercialization of new

and innovative AM processes, as well as numerous practical applications in aerospace, automotive, biomedical, energy and other fields (Nannan GUO, 2013). Furthermore, new applications are emerging as novel materials and AM methods are continuously being developed. One of the main drivers for this technology to become more accessible is attributed to the expiry of earlier patents, which has given manufacturers the ability to develop new 3D printing devices. Recent developments have reduced the cost of 3D printers, thereby expanding its applications.

Several industries consider AM technologies, for instance hearing aid manufacturers use Selective Laser Sintering (SLS) and Stereolithography machines to produce hearing aid shells. Furthermore, the production of clear dental braces at Align Technology employs Stereolithography to fabricate its moulds whereby tens to hundreds of thousands of uniquely customised based on person-specific geometric data can be achieved. SLS has been also used at Boeing and its suppliers in the production of ducts and similar parts for F-18 fighter jets (Gibson et al., 2010). The main drive of incorporating AM methods into any industry' operational strategies is to reduce the cycle time which has been reported to vary from 30 to 90%. For example, Pratt & Whitney in 1994 incorporated stereolithography into their investment casting process whereby 70 to 90% time and cost reduction were achieved. Molding operations are heavily affected by the long waiting time for parts to cool down between the material entering the mould and safe ejection, this is estimated to be as high as 75% of the total cycle time.

Sandwich structures are advantageous for structural applications exhibiting low-weight, high-stiffness and high energy absorption (Wadley et al., 2003) (Villanueva and Cantwell, 2003) (Nemat-Nasser et al., 2007). Depending on the industry standards and functional requirements, sandwich cores come in different forms and materials including honeycomb and metals for aerospace (Shafizadeh et al., 1999) (Herrmann et al., 2005) and marine applications (Mouritz et al., 2001), natural composites (Dweib et al., 2004) foam, balsa and wood for automotive and many other applications including construction (Davalos et al., 2001). Sandwich panels consist of two thin face sheet skins contributing to the flexural strength of the panel, whereas the core is responsible for the shear transfer between the skins. The core can also contribute to the overall flexural and compressive strength of the panel. Cellular core sandwich structures have been developed for various structural requirements in order to develop lightweight and adequately stiff and strong composites.

Advancement in additive manufacturing (AM) technology has led to the emergence of metallic core in the form of cellular honeycomb structures and truss-like structures specifically for high-performance mechanical properties typically used in lightweight energy absorbing products (Williams et al., 2011) (Brenne et al., 2013) (Meisel et al., 2012) (Yang, 2015). Much attention and development activities have been dedicated to produce optimised metallic structures through improved designs and build parameters (Rashed et al., 2016). There is a potential to use cellular honeycomb structures in polymer applications as well, but reinforced polymers and polymer composites would be preferred for improved mechanical

strength. A comprehensive study by Yazdani and co-authors. (Yazdani Sarvestani et al., 2018) covered the theoretical, numerical and experimental aspects of the geometry optimisation of 3D printed cellular cores for energy absorption applications.

Bio-composite materials offer the promise to improve sustainability and functionality compared to oil-derived polymer materials. 3D-printing (3DP) these materials for future applications because of geometric flexibility (e.g. honeycomb lightweight structures) is of particular interest (Compton and Lewis, 2014). Natural fibre (NF)-based composites have recently attracted interest due to the increased ecological concerns in global industry since issues of manufacturing-based energy burdens, recyclability and environmental safety become the centre of new materials and products developments (Saheb and Jog, 1999) (Pickering et al., 2016a). Among these natural fibres, lignocellulosic bast-fibres such as flax, hemp and jute are widely used for reinforcement of thermoplastic polymers. The reinforcement of renewable sourced polymers with flax fibres is encouraged due to their low density, good mechanical properties and low environmental impact.

Flax and polypropylene (PP) has been shown to be compatible for making high-quality composites (Van de Velde and Kiekens, 2003). Although PP can be printed, it is more challenging than the natural polymers polylactic acid (PLA), which is the most common fused filament fabrication (FFF)/fused deposition modelling (FDM) 3-D printed polymer, PLA is the primary printing material of choice. Due to its low melting temperature and ease of printing PLA can even be used by consumers to make finished products. The mechanical properties of FFF/FDM PLA are well established (Wittbrodt et al., 2013) (Tymrak et al., 2014), their chemical resistance is also known (Wittbrodt and Pearce, 2015) as well as their thermal behaviour (Grasso et al., 2018). PLA has also been successfully used in a number of polymer matrix composites for 3D-printing (Wang et al., 2017), such as PLA wood fibre biocomposites (Le Duigou et al., 2016) (Tao et al., 2017), and synthetic fibres such as short carbon fibres (Ferreira et al., 2017).

1.2. Research Aims and Objectives

The aim of the research presented herein is to:

- ❖ Develop flax based biocomposite materials with various matrix systems, bio and non-bio based polymers, and characterise them for their quasi-static mechanical properties.
- ❖ Implement Fused Deposition Modelling (FDM) in the development of composite-like structures to be incorporated in the design of novel biocomposite materials.

Another aim of this research is to combine both field's advancements i.e. natural fibre composites and additive manufacturing technology to propose a novel bio-inspired structure for use in sandwich material applications. In order to fulfil these proposed aims, the following activities and objectives were planned:

- Conduct a critical review of the existing literature covering the progression of biocomposites and establish the current state of the art
- Conduct a critical review of the current additive manufacturing techniques and establish the most suitable method for use with respect to materials availability and sustainability as well as process parameters implications and challenges.
- Manufacture of a number of flax reinforced polymers using selections of architectures (comingled tapes, nonwoven mats and woven) with bio-based and non-based thermoplastics or thermosets in suitable blend ratios before consolidation into flat biocomposite panels.
- Evaluate the quasi-static properties, primarily tensile and flexural, of all biocomposites to weigh the benefit of enhanced performance against the associated fabrication implications such as cost, processing steps, energy intensity and materials availability.
- Investigate the combined effects of *in-situ* temperature conditioning and tensile loading on selected flax biocomposites to assess the extent of tensile properties deterioration
- Employ FDM technique to fabricate composite-like parts in various raster orientations and investigate the combined effects of *in-situ* temperature conditioning, raster orientation and tensile loading on 3D-printed parts to assess the extent of tensile properties deterioration.
- Implement FDM in the design of bio-inspired sandwich panels through fabrication of novel truss-like structures to be used as core for flax based biocomposites face sheets and conduct a full mechanical characterisation of individual constituents as well as combined.

1.3. Thesis Structure

Chapter 1 provides a general introduction on the various elements of this research including an overview of biocomposites, advancement of rapid prototyping techniques and the applications of both fields. The project aims and objectives are also defined herein.

Chapter 2 covers Part I of the literature review focusing on natural fibre composites including their processing and manufacturing methods, physical and thermal characterisation, mechanical characterisation and biocompatibility.

Chapter 3 is the continuation of literature review Part II, this reviews the main 3D printing methods, materials and their development in trending applications. Furthermore, this chapter will particularly focus on the use of Fused Deposition Modelling (FDM) in the fabrication of structural components and evaluate the feasibility and effect of process parameters on scaling-up this technology.

Chapter 4 covers all the materials considered for this research as well as their manufacturing techniques. This includes all biocomposites i.e. lignocellulosic based fibres combinations, including the continuous unidirectional and discontinuous nonwoven natural fibres, reinforced with various types of matrices (PLA, PP, PFA and UPE). The corresponding manufacturing techniques and procedures are also included. In addition, the 3-D printing procedures, materials and equipment are covered within this

chapter. Moreover, the experimental methods defined in established international standards that were adopted in this research are detailed in this chapter.

Chapter 5 details the results of the experimental activities conducted which covered the characterisation of the mechanical and thermo-mechanical properties of the different combinations of biocomposites as well as the 3D-printed parts produced via FDM.

Chapter 6 provides a thorough discussion of results presented in Chapter 5 through extrapolation of results generated in the respective sections of Chapter 5 and provide further analysis of key experimental outputs.

Chapter 7 draws from the aspects and outputs of biocomposites and additive manufacturing parts of this thesis to design and develop a thorough characterisation of sandwich structures using bio-inspired truss-like lattice internal structures and biocomposites face sheets. This chapter is a direct extract of the published work developed as part of this project (Azzouz et al., 2019)

Chapter 8 presents the main conclusions from all aspects of this research project and highlights points of recommendations for future work.

1.4. Contributions and Achievements

The dissemination of the work presented here has included in the form of peer-reviewed journal articles, participating posters and presentations in various local and international events. Furthermore, the academic training obtained in this process has helped the author to be invited independent reviewer and undertake review of journal papers to be published in *Rapid Prototyping Journal* (Emerlad) and *Composites Part B* (Elsevier).

Peer-Reviewed Journal papers

Two original research peer-reviewed publications have emerged from the work described in this thesis.

1. Azzouz, L., Chen, Y., Zarrelli, M., Pearce, J. M., Mitchell, L., Ren, G. & Grasso, M. 2019. Mechanical properties of 3-D printed truss-like lattice biopolymer non-stochastic structures for sandwich panels with natural fibre composite skins. *Composite Structures*, 213, 220-230.
2. Grasso, M., Azzouz, L., Ruiz-Hincapie, P., Zarrelli, M. & Ren, G. 2018. Effect of temperature on the mechanical properties of 3D-printed PLA tensile specimens. *Rapid Prototyping Journal*, 24, 1337-1346.

Conferences, Posters and Attendance

1. Materials Research Exchange, UK Advanced Materials Research, Coventry UK, 25 February 2014

2. A multidisciplinary Conference on the Use of Thermal Analysis and Calorimetry to Support Product Development, GSK R&D Ware, Hertfordshire UK, 1-2 April 2014
3. Digimat Users' Meeting, Barcelona , Spain 29 September- 1 October 2015
4. Materials and Renewable Energy, University of Hertfordshire, 26-28 July 2017
5. Materials Research Exchange, UK Advanced Materials & Investor Showcase, London UK, 12-13 March 2018

2. Literature Review – Part I: Review of Biocomposites Based on Lignocellulosic fibres

2.1. Natural fibres overview

Generally, natural fibres can be classified according to origin, which part of the plant they are extracted from and whether animal or mineral. Plant based fibres also known as cellulose based fibres can be bast, leaf and other fibres or seeds. The common feature within these different categories is the internal micro-design represented by individual cells and group of cells which promote the strength and stiffness of the plant fibre reinforced plastic. Ongoing research and modification of these resources have resulted in the optimisation of the cell functions. The dominant constituent of plant fibres is found to be cellulose which is a natural polymer known for its high strength and stiffness to weight ratio. Cellulose is the base unit cell which makes up the building material of long fibrous cells. The whole plant can be fiberised and used for different structural and non-structural applications maximising its exploitation and minimising waste. The fibres obtained from the stem are called bast and few of these such as flax, hemp, jute or kenaf are used in automotive applications when reinforced with thermoplastics and thermoset matrix due to their low density and low cost compared to glass fibre. For instance, Mercedes-Benz used 46 kg of renewable materials including natural fibres in the production of 87 various components of the S-class cars (John and Thomas, 2008). Furthermore, natural fibres can be adequate for use in aircrafts and railway carriages interiors' cladding. Figure 2.1 illustrates the various applications of natural fibres.



Figure 2-1 Components produced from natural fibres: a) spare wheel cover, b) car seatback, c) car door trim, d) car wheel arch, e) aircraft food galley. [Produced from source: (Ecotechnilin, 2017)]

Natural fibres are grouped into two categories, cellulosic and non-cellulosic, Figure 2-2 illustrates the classification of reinforcing fibres. Bast fibres are subset of the plant fibres of which flax, jute, hemp and kenaf are the most commonly used due to their remarkable tensile strength and stiffness.

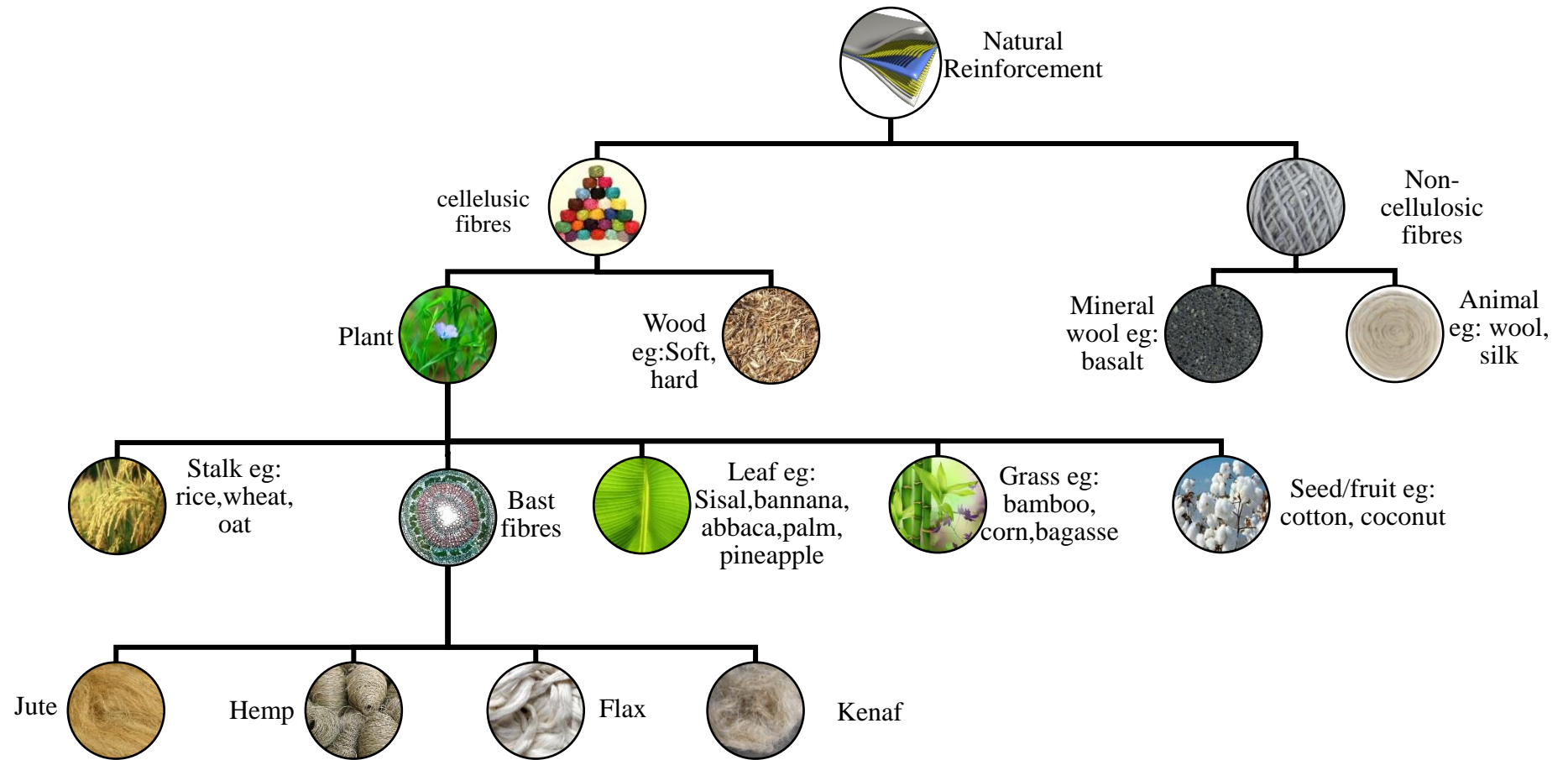


Figure 2-2 Classification of various reinforcement with natural fibres: cellulose and non-cellulosic fibres.

The estimated market size of natural fibre revenues by 2024 will be approximately USD 11 billion according to the published report of U.S natural fibre composites market size 2013-2024 with a 245% increase in market growth from the USD 4.46 billion in 2016, Figure 2-3. In terms of European production, natural fibre and wood-based composites accounted for 10 - 15% of the total composites production in 2012 which was equivalent of 350,000 tons of biocomposites. The spiralling demand for lightweight products from the automotive and construction sectors due to their thermal insulation, also the growing awareness regarding green products fuelled the increased interest in these natural resources. However, the moisture sensitivity of natural fibres composites and other structural scarcities are still hindering the further market growth.

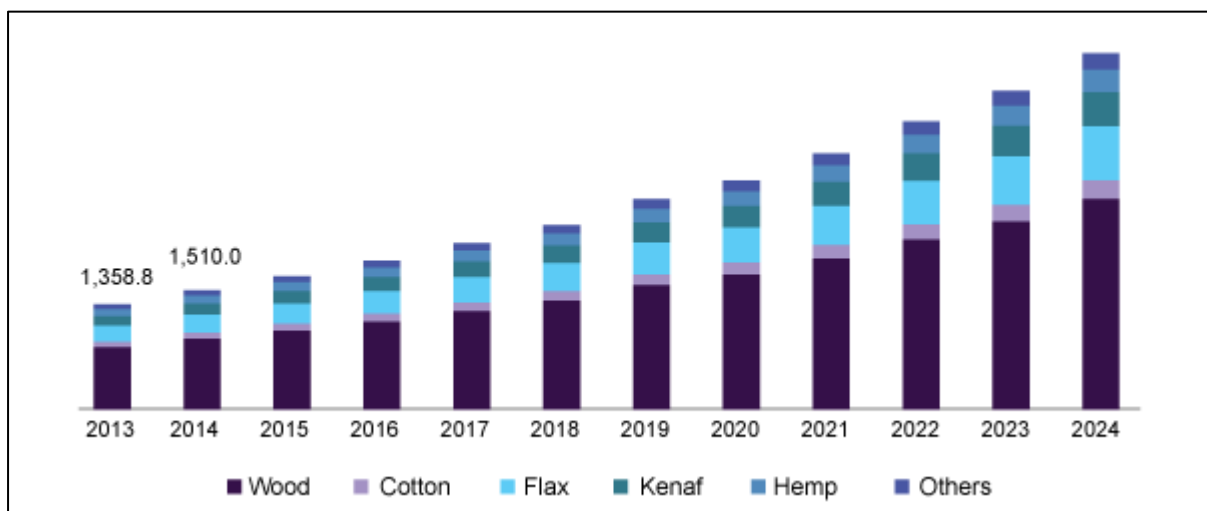


Figure 2-3 Natural fibre market in the U.S by raw material- Projection 2013-2024 in USD Million (Grand.View.Research, 2018)

2.1.1. Chemical and morphological properties

Bledzki and Gassan have expansively contributed to the knowledge of natural fibres composition analysis via various publications and books (Bledzki and Gassan, 1999, Bledzki et al., 2002, Gassan and Bledzki, 2001). Since natural fibres are extracted from different types and parts of plants, individual chemical compositions in terms of their amounts of cellulose, hemicellulose, lignin and other compounds vary slightly. The common feature of all these natural fibres is the dominant cellulose contents as represented by the high weight presence; Table 2-1. The basic unit of cellulose macromolecule consist of linear chain of bonded anhydro-glucose units, which contains three alcoholic hydroxyl groups (—OH) (Bledzki et al., 1996). Hydrogen bonds are created within the cellulose itself at intramolecular level as well as with other macromolecules in the intermolecular bonding form, whereas the third hydroxyl group is bonded with air. As a result, all natural fibres are hydrophilic in nature, as the moisture content ranges from 8% to 22%. There are other natural substances that

constitute the natural fibres beside cellulose, as Table 2-1 shows the second significant content is lignin and then several waxes. Lignin is a phenolic compound acting as cementing material that bonds the individual cells of hard NF, and whereby fibre structure, properties and morphology are influenced (Reimschuessel, 1985). Lignin is a biochemical polymer, which functions as a structural support material in plants. Lignin is also resistant to biological degradation, but the fibre pre-treatment with the organic solvent to extract waxy substances to enhance the adhesion render it vulnerable to the cellulose enzyme (David and Fornasier, 1986). Lignin keeps water within the fibre and acts as a hardener to promote its resistance to gravity forces and wind (Kalia et al., 2009). During synthesis of plant cell walls, polysaccharides such as cellulose and hemicellulose are laid down first, and lignin fills the spaces between the polysaccharide fibres, cementing them together. This lignification process causes a stiffening of cell walls, and the carbohydrate is protected from chemical and physical damage (Mohanty et al., 2000).

Although the exact mode of linkages in bio-fibre is not well known, lignin is believed to be linked with the carbohydrate moiety through two types of linkages, one alkali sensitive and the other alkali resistant. The alkali sensitive linkage forms an ester-type combination between lignin hydroxyls and carboxyl of hemicellulose uronic acid as shown in Figure 2-4.

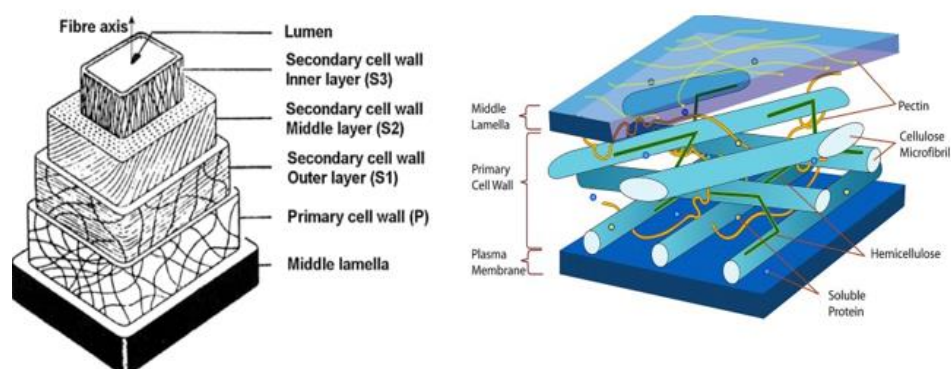


Figure 2-4 Elementary fibre layer structure (Mohanty et al., 2005)

The ether-type linkage occurs through the lignin hydroxyls combining with the hydroxyls of cellulose. The lignin, being polyfunctional, exists in combination with more than one neighbouring chain molecule of cellulose and/or hemicellulose, making a cross-linked structure. The lignocellulosic material possesses many active functional groups like primary and secondary hydroxyls, carbonyls, carboxyl (esters), carbon-carbon, ether and acetal linkages.

Table 2-1 Chemical composition (%) of natural plant fibres

Fibre	Cellulose	Hemi-cellulose	Pectin	Lignin	Fat and waxes	Moisture
Flax	71-78	18.6-20.6	2.3	2.2	1.7	8-12
Hemp	70-74	17.9-22.4	0.9	3.7-5.7	0.8	6.2-12
Jute	61-71.5	13.6-20.4	0.2	12-13	0.5	12.5-13.7
Kenaf	45-57	21.5	3-5	8-13		
Ramie	68-76	1.31-16.7	1.9	0.6-0.7	0.3	7.5-17
Sisal	66-78	10-14	10	10-14	2	10-22
Abaca	56-63	17.5-21	1	12-13.1	3	5-10
Cotton	85-90	5.7	0-1	0.5-1	0.6	7.85-8.5
Wood	40-45	20-30		26-34		

Sources: (Franck, 2005), (Akil et al., 2011), (Bledzki et al., 2015), (Bogoeva-Gaceva et al., 2007)

Inconsistencies within the reported values of natural fibres chemical constituents, therefore ranges provided in this table should be considered with caution. Furthermore, the physical properties of these natural fibres such as diameter, density and most importantly the microfibril angle MFA have direct effects on the tensile strength, Young's modulus and elongation at break, Table 2-2. Bast fibres are extracted from the inner bark of phloem dicotyledonous plants that provide strength and rigidity to the plant stem. A layer of thin bark underneath which bundles of fibres run parallel down along the stem length for approximately 100 cm and a 1 mm width, some of these bast fibres possess an aspect ratio of 1000.

Natural fibres are composed of a number of elementary fibres bonded together by the middle lamella resulting in the so-called a technical fibre. In order to achieve the highest potential of each natural fibre, the stiffness and strength needs to be measured and which are dependent on crucial physical characteristics such as the fibre dimensions, defects, and structure. These characteristics are irregular from fibre to another and also can vary within a single fibre design along its length in terms of cellulose content and spiral angle, which results in varying performance (Faruk et al., 2012). A recent study proposed the impregnated fibre bundle test method (IFBT) implemented by carbon and glass fibre manufacturers to measure the stiffness of flax and hemp fibres (Bensadoun et al., 2017). It was observed that the stiffness has a very low scatter compared to other results obtained at different laboratories which

confirm the certainty. Whereas strength is highly sensitive and demonstrated a wide-ranging variation mainly due to imperfections and flaws (Pil et al., 2016).

Table 2-2 Natural fibres physical properties: Diameter, density and MFA with mechanical properties

Fibre	Diameter (μm)	Density (g/cm^3)	MFA ($^\circ$)	Modulus (GPa)	Strength (MPa)	Elongation (%)
Flax	40-600	1.5	5-10	27.6	350-1500	2.7-3.2
Hemp	25-500	1.47	2-6.2	70	690	1.6
Jute	25-200	1.3-1.49	8	13-26.5	393-800	1.16-1.5
Kenaf	180-240	1.19-1.45	–	53	930	1.6
Ramie	–	1.55	7.5	61.4-128	400-938	1.2-3.8
Sisal	50-200	1.45	10-22	9.4-22	468-700	3-7
Abaca		1.5	–	9.8-35.1	430-760	3.4-11.1
Cotton	12-38	1.5-1.6	–	5.5-12.6	287-800	7-8
Wood (soft)	–	1.5	–	8.9-12.3	70-92	1.5

Source: (Mohanty et al., 2005), (Bledzki et al., 2015), (Bogoeva-Gaceva et al., 2007)

Fibres cellulose content, microfibril angle orientation and the diameter of single fibre determine the mechanical properties of each fibre type in terms of their tensile strength and elongations at failure (Bledzki et al., 2015). Gassan and co-workers (Gassan et al., 2001) calculated elastic modulus of single fibre and found that it decreases with increasing spiral angle as well as the degree anisotropy whereas maximum shear modulus was recorded for spiral angle of 45° . Fibre modulus also decreases with diameter increase. Figure 2-5 illustrates the microfibril orientation within the internal structure of flax fibres.

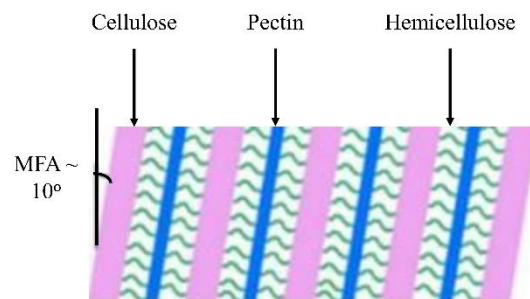


Figure 2-5 Flax secondary wall, S2 lamella contents with microfibril angle

2.1.2. Flax plant growth

Flax (*Linum usitatissimum* L.) is a plant first growth and cultivation dates back to the ancient Egyptian civilisation and later brought to Europe 2000 years ago by export traders. Flax plant growth requires a specific climate and typically sown in the period March- May during which temperature remains below 30° C. According to the Flax Council of Canada, the life cycle of flax plant observes 12 distinct stages from vegetative to flowering then maturation period. The first 30 days after planting, fibre cells develops and roots develop through seed germination and initial signs of growth where the first true leaves emerge out of raising stem. Afterwards, flowering period, a daily growth of 1-3 cm producing 2.4 leaves out of the progressive stem extension between 50- 60 days, during which the number of fibre cells can be determined as no further cells are produced. Finally, once flowering period is over, maturation period initiates lasting between 30-40 days and during which concentric layers of cellulose are deposited within the hollow fibre cells rendering them heavier. Figure 2-6 represents the 12 stages aforementioned.

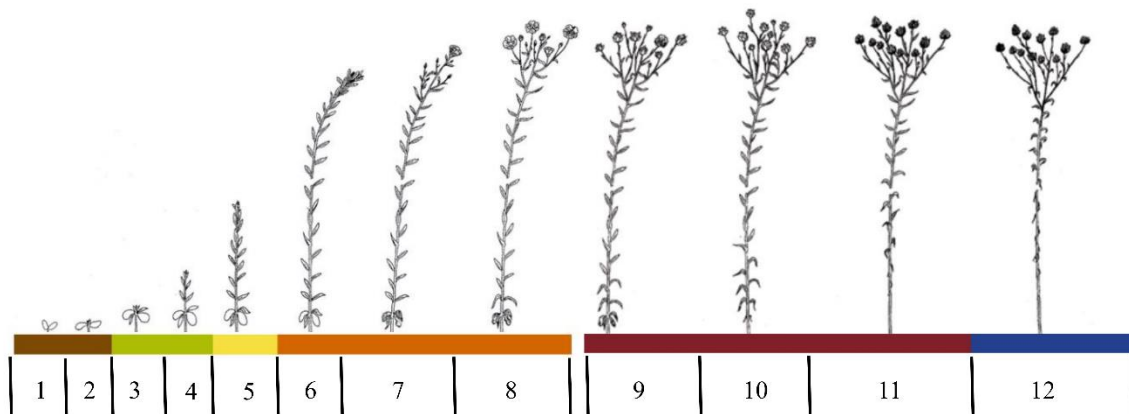


Figure 2-6 Flax plant 12 growth stages

Once maturity is reached, fibre flax stems varieties; estimated to near 20 categories however only major four represent 90% of areas sown in western Europe; can reach 80 – 120 cm height with a diameter of about 3 mm. Primary fibres cemented by pectin amalgamates rapidly developing into bundles inwards through the stem diameter with outermost bundles first. These bundles simultaneously elongate until the end of flowering stage by then representing 25 % of the dry weight of the stalk. The flax stalk can contain 20 – 40 fibre bundles of which each bundle contains 20 – 40 primary fibre.

2.1.3. Flax fibre isolation method

Flax plant undergoes various isolation process to yield the fibres directed to various end products (flaxseed, linen, flax oil...etc.) and by products including reinforcement for composites production. These processes affect the mechanical properties therefore this performance dependence requires a careful process selection. The stem being the main source of both long and short flax fibres in the form

of technical fibres located in a layer below the outer waxy skin as illustrated in Figure 2-7. Retting is the process of subjection of the crop or deseeded straw to biological or chemical treatment to easily separate the fibre bundles from the woody core. Flax can be dew retted, water retted or chemically retted. Water retting the most preferred and oldest method first used in Europe yields the best fibre quality, however it gradually vanished due to the associated intensive labour and water shortages. This process involves stem immersion in cold or warm water between 4 days and several weeks depending on the temperature and minerals in water.

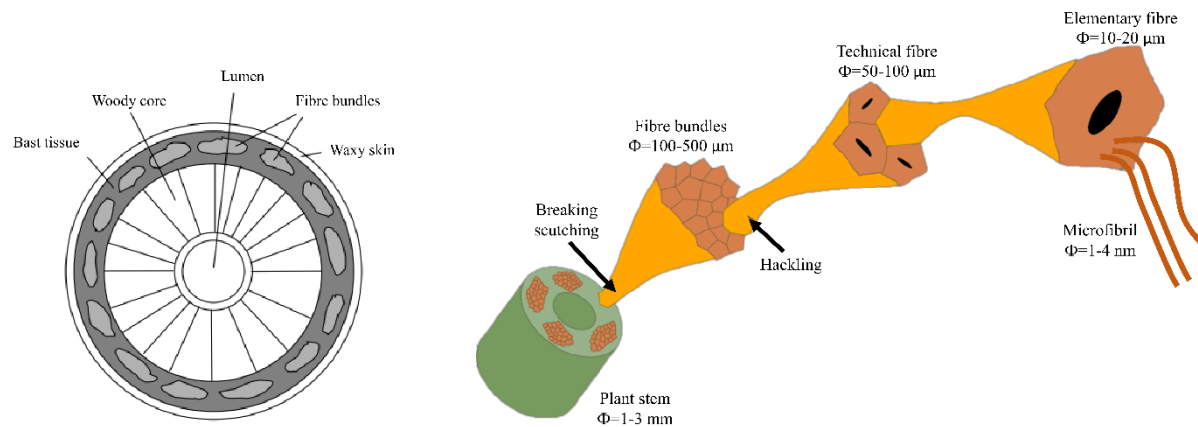


Figure 2-7 Cross section of the flax stem and elementary fibre production (Bos et al., 2002)

The flax plant growth as described before lasts for approximately 100 days, after maturation, the plant stem is pulled out and left on the field grounds for 6 weeks to promote the degradation of pectin that surrounds the fibre bundles which loosen the flax fibres, this process is called dew-retting. This process of degradation relies on microorganisms and needs continuous rotation of the stem to alternate exposure to the sun and soil contact. Furthermore, retting process if done on good knowledge, it yields optimum mechanical properties due to the fibre dependence on weathering. Chemical retting also referred to as bio-retting utilise enzymes e.g. pectinase to digest the binding pectin, however failure to terminate this process on time can damage the actual fibres and consequently reduce their mechanical properties.

Next step is the scutching process, this entails breaking the woody core to produce shives and the loosened fibres are removed from the cortical skin. Scutching of flax plant is a sequence of operations to isolate the fibres from the plant stem to produce long fibres also known as line and also by-products such as short fibres or also known as tow, seeds and woody plant matter known as shiv or shives. The separated fibres both long and short are rough and thick which require refining through hackling process producing fine technical fibres and by-products i.e. shives and tows. The short fibres can be later carded into slivers and low cost compounds or transformed into mats for injection molding. A scutching line consists of several progressive operations rippling; drafting the straw layer; breaking the stems; grading and baling the line fibres produced. The quality of scutched fibres is dependent on effective retting process, since in the case of poor retting the presence of pectin holding the fibres firmly together can

prevent the easy separation process resulting in undue damage to fibres. For structural applications requiring unidirectional long fibres, fibres can be spun into yarns and roving. Biagotti and co-workers (Biagotti et al., 2004a) in their published work emphasised on the importance of the steps of refining process in achieving the best fibre quality and a selection of which to be retted industrially. The monitoring of fibre quality at the beginning of the raw material production is essential, this is achieved using microbiological and microscopic (light and electron microscopy) testing. The aim of good retting process is to effectively separate from the retted straw the maximum ratio of long fibres to the short fibres. The latter is considered less profitable as it can be sold, ten times or more, cheaper than long fibres. However, it is important to mention that excessive retting can also cause enzymatic attack and consequently weakens the fibres which then leads to fibre breakage during the scutching process.

2.1.4. Single fibre mechanical tests

This method is widely used to determine the single fibre tensile and elastic modulus. Single Fibre Tensile Test (SFTT) is the most common method to determine fibre properties and have been widely adopted and reported in literature (Joffe et al., 2003, Baley, 2002). The procedure involves gluing individual fibres on a paper frame with an epoxy adhesive, cutting the edges of the paper is necessary to eliminate the frame loading. Unlike synthetic fibres natural fibres have irregular cross section and being not uniform along the fibre length affects the accuracy of tests results. Tensile test of fibres is the typical approach to calculate the modulus and ultimate strength using the conventional method to determine the fibre diameter on an optical microscope. Therefore, due to the diameter variation natural fibres including flax, testing will result in inaccurate properties with large standard deviation.

Hu (Hu et al., 2010) proposed an improved test method based on ASTM D 3822 to minimise the inherent flax property variation by implementing modification to the sample selection for testing and accuracy of cross section determination at the failure location. Tensile strength tests of three types of extracted flax fibres Canadian grown including water retted and enzyme retted achieved low standard deviation of 11% measuring 354.4 (± 25.4) MPa and 465.5 (± 33.9) MPa respectively. Reports on effects of clamping gauge distance showed variation of fibre strength due to the kink bands and defects in the composite like technical fibres. To ascertain the importance of the number of defects and diameter variation on the tensile strength of elementary flax fibres, Baley performed tensile testing of 10 mm and 1 mm long fibres (Baley, 2004). Results indicated an average modulus of 54080 ± 15128 MPa and a tensile strength of 1339 ± 486 MPa for the 10 mm long fibres. For the 1 mm long fibres, results were limited to tensile strength due to the low length which was found to be 1030 ± 383 MPa. A pretesting fibre observation with an optical and polarised light microscopy assisted Baley in determining the fibres diameter in the range 14 – 40 μm and an average defect spacing along the 10 mm fibre of 101 ± 39 μm . The highly oriented crystalline cellulose within the elementary flax fibre makes the fibres stiff and strong and found significantly higher than the technical fibre at the same clamping length due to the

bundle effect (Bos et al., 2002). Furthermore, hand decorticated elementary fibres were found free of kink bands along the fibre length as compared to the standard decorticated fibres hence tensile strength of 1834 ± 900 MPa and 1522 ± 400 MPa respectively. During the elementary fibre separation from the technical fibre i.e. bundle cell, damage of the fibre may occur which consequently lead to tensile strength decrease. Fibre handling during its processing strongly affects its dimensional stability especially the cross section.

In another study on the effects of environmental conditioning of flax fibres on the mechanical properties (Stamboulis et al., 2001), green and Duralin treated hand decorticated flax have been tested with two gauge lengths 3.5 mm and 8 mm. Duralin treated flax displays surface morphology modification and render it hydrophobic. Based on moisture absorption tests and single fibre tests under varying humidity, all strengths confirmed the inversely proportionality with gauge length as higher strengths were recorded for both fibres green and Duralin at 3.5 mm gauge. Test results also showed that 66% relative humidity yielded optimum tensile strength as compared to 30 and 90 %, however time of exposure to certain humidity conditions typically after 3 days affects the mechanical properties due to the fungus development on the fibre surface causing degradation. Temperature effects on property degradation have been reported in a study (Hornsby et al., 1997) on flax and wheat straw fibres, both elastic modulus and strength decreased with temperature increase, micromechanical tests also confirmed the strength dependency on gauge length.

Enzyme treatments have been widely studied at the USDA group of D.E Akin (Adamsen et al., 2002, Akin et al., 2004, Akin et al., 2001) in which retting process takes place through chemical fibre pre-treatments using different enzyme mixtures have been developed and applied under well controlled conditions concluding that enzyme retting although it improves fibre fineness but decreases fibre strength. Early attempts in the Netherlands and other European countries to establish a large scale production of enzyme retting never materialised despite being well optimised as this process can yield a fibre strength of 800 to 1000 MPa. In another method of fibre separation, the steam explosion process has been described in (Kessler et al., 1998) in terms of associated effects on fibre structure and properties, a significant decrease of strength in steam exploded fibre is commonly observed as opposed to standard scutched fibres. This process was also found to be easily controllable to produce high quality fibre with minimum loss in fibre yield.

2.1.5. Production and utilisation of flax

Throughout the world, flax is mainly grown for its seeds used in many food products to produce flax oil or as a food additive (e.g. bread), and is known as “seed flax”. In Europe, the cultivated flax types called “fibre flax” is mainly destined to the production of flax yarns for linen fabric production. The flax fibre is extracted from the bast of the stem and has a soft, lustrous and flexible feel. The best quality fibres are used for the weaving of linen fabrics destined to the fashion industry, lace and sheeting and

coarser grades are used for twine and rope. Flax can also be used for the manufacturing of high-quality paper or for printed banknotes (Bensadoun, 2016).

According to the Barometer of European Flax 2015, every year flax growth in Europe captures 250,000 tons of CO₂ yielding saving equivalent to driving a Renaults Clio around the earth 62,000 times. Natural fibre world production is in constant increase to serve the various industries and applications. Among these applications we can find the automotive industry making the most of this category of natural resource growth. A market analysis report indicates the top 10 flax fibre producers in the world with Europe representing over 80% of the world production mainly located in France and Belgium, Figure 2-8. A notable end of flax production growth in Belgium of 26% per year in the period 2007-2015.

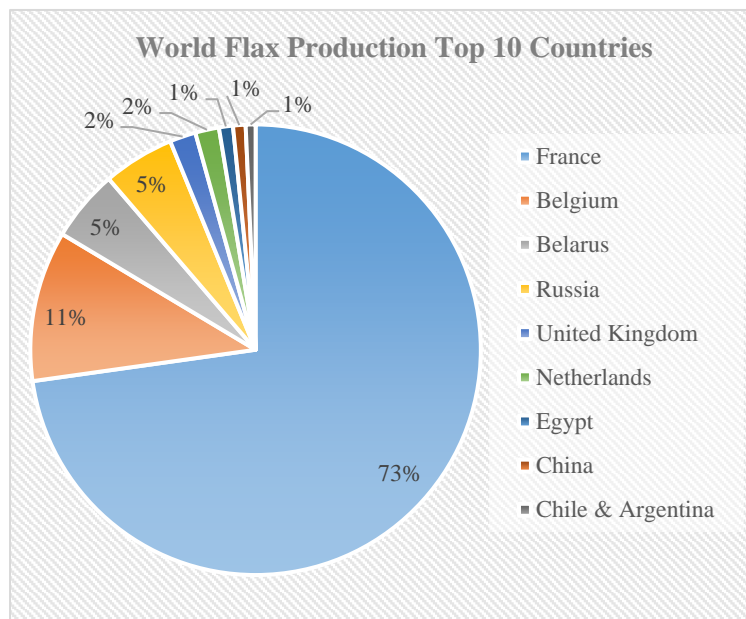


Figure 2-8 Flax fibre world production 10 top countries in 2016

2.2. Flax fibre architecture as a reinforcement

Flax plants are cultivated for their fibres production onto line flax (long fibre), flax tow (short fibre), flax spinning and flax yarns, and also other types of fabrics. These various forms serve specific industrial applications depending on the final product design and performance requirements. Flax plants yield various types of fibres used in the manufacturing of composites. For example yarn preparation and spinning has been inspired by the cotton spinning method. Spinning can be achieved by two methods dry and wet. Continuous fibres are spun into yarns to produce the unidirectional long fibres which are used in the manufacture of unidirectional composites layers whereas the short fibres can be oriented or randomly dispersed within a matrix to form mats and fabrics. As described in (Habibi et al., 2017) yarn production yields tailored textiles which allow a higher fibre volume fraction composites due to better fibre packing, however this technique is associated with high energy consumption. Furthermore, in order to achieve strong yarns enough to survive the textile machines processing, off axis orientation of twisted yarns fibres should be reduced to prevent the deterioration of mechanical

properties. Otherwise, discontinuous flax and its by-products such as shives can be filtered and manipulated into nonwoven mats. However, in order to obtain high performance composites in terms of strength and stiffness, it is desirable to utilise long continuous fibre or woven non crimp fabrics.

Fibre architecture is defined as the fibre arrangement within the composite which affects both the properties and necessary processing. Fibre continuity, orientation, yarn twist, crimping and interlocking mechanisms are characteristics that heavily influence the mechanical properties. Furthermore, composites consolidation using fibre reinforcement and the matrix flow through the fibres determines the void content, fibre wetting, fibre distribution i.e. fibre rich zone (dry).

2.2.1. Continuous reinforcement

If continuous fibres are used, the fibre architecture can be one-dimensional, two-dimensional or three-dimensional. Typical production techniques of one-dimensional architecture can be pultrusion.

i. One-dimensional - Unidirectional prepreg and tape

In this method fibre strands or known as yarns are aligned in one direction to produce textile preforms to be further processed into prepregs or dry fabrics. Unidirectional orientation of natural fibres in a polymer composite ensures the highest efficiency of reinforcement. Furthermore, better alignment of the reinforcing fibres clearly improves stiffness and strength of the composite in the axial direction (Andersons and Joffe, 2011). However, in order to hold the primary fibres in position a small amount of binding fibres can be employed. Though, it is argued that the use of 0/90° term by weavers is only acceptable to be unidirectional if 75 % by weight or over of primary fibres are oriented in one direction while others claim at least 90%. Common unidirectional usually possess primary fibres in the 0° i.e. along the roll called a **warp UD** but can also be oriented at 90° to the roll called a **weft UD** (Rana and Fanguero, 2016).

There are various methods of maintaining the primary fibres in position in a unidirectional including weaving, stitching, and bonding (Figure 2-9). As with other fabrics, the surface quality of a unidirectional fabric is determined by two main factors: the combination of tex and thread count of the primary fibre and the amount and type of the secondary fibre. The drape, surface smoothness and stability of a fabric are controlled primarily by the construction style, while the area weight, porosity and (to a lesser degree) wet out are determined by selecting the appropriate combination of fibre tex and numbers of fibres per cm.

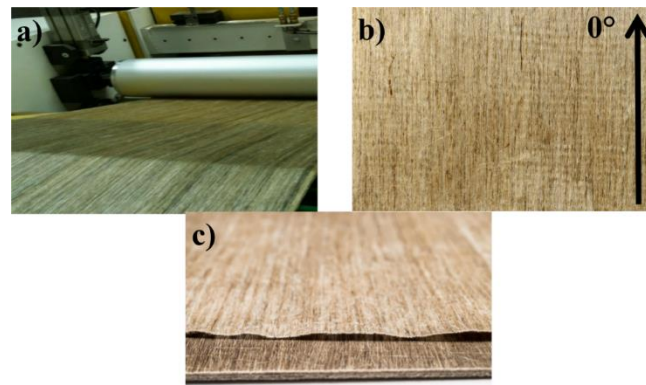


Figure 2-9 Production of unidirectional flax tape: a) alignment of flax yarns into uniform tapes, b) aligned flax tape along 0° direction, c) multi-layers laminated unidirectional flax to achieve the desired thickness.

Warp or weft unidirectionals can be made by the stitching process. However, in order to gain adequate stability, it is usually necessary to add a mat or tissue to the face of the fabric. Therefore, together with the stitching thread required to assemble the fibres, there is a relatively large amount of secondary, parasitic material in this type of UD fabric, which tends to reduce the laminate properties. Furthermore the high cost of set up of the 0° layer of a stitching line and the relatively slow speed of production means that these fabrics can be relatively expensive.

An example of thermoset matrix application as unidirectional Cordenka CR fibres were incorporated within Furan resin to produce a bio-composite through laminates hot pressing (Malaba and Wang, 2015). This process achieved high fibre/matrix ratios with fibre mass fractions FMF as high as 51 - 64 % which enhanced the tensile properties to an optimum before composite deterioration as FMF reached 75 %.

ii. Two-dimensional - Woven Fabrics

The two-dimensional architecture with continuous fibres which can be either bidirectional or multiaxial. These provide an opportunity to tailor the structural performance of the composite as it compensates the lower strength and modulus in the transverse to the fibre direction. To reduce the variation of strength and modulus of the final composite architecture with respect to fibre angle of orientation, multi-layered laminates can be achieved through stacking several unidirectional architectures. However, the interlaminar properties of multi-layered can be affected due to the early failure by delamination as shear stresses inherently cause layers separation.

The bidirectional structure is achieved through weaving or interlacing fibre yarns together in two mutually perpendicular directions usually referred to as warp and fill representing 0° and 90° respectively. Crimping the fibre yarns as they move up and down to form the interlaced architecture can be varied accordingly to obtain optimised properties in certain directions by changing the number of fibre yarns per unit width in the warp and fill directions. For example, a balanced fabric can be tailored by combining the same number of fibres in both warp and fill direction which maximise

properties in the 0° and 90° direction but maintained low in other directions. Otherwise, in order to improve these properties in other directions, the flax yarn can be interlaced to produce the multidirectional fabrics such as $0^\circ/\pm\theta^\circ$ or $0/90/\pm\theta$. The $\pm\theta$ orientation represents the direction at which the yarns are laid down i.e. $+\theta$ or $-\theta$ relative the warp direction (0° direction).

Other methods to produce 2-D architecture include knitting and biaxial braiding as a process of fibre yarns interlooped instead of interlaced and intertwining two continuous yarns respectively. Knitted fabrics provide more flexibility than woven fabrics and are more suitable in making shapes with tight corners.

iii. Three-dimensional

Due to the inherent weakness within the one-dimensional and two-dimensional architecture along the z-direction composites fail in delamination mode through thickness. To overcome this weakness fibres are integrated in the thickness direction producing the three-dimensional architecture. A process of 3-D fabric fabrication by stitching woven fabrics through the z-direction using a stitching thread, otherwise weaving or braiding can be employed.

2.2.2. Discontinuous Reinforcement – Nonwoven mats

Nonwoven mats or fabrics are defined as web structures bonded through interlocking fibres or filaments using mechanical, thermal or chemical methods. Discontinuous fibre nonwoven mats are produced by Vacuum Assisted Resin Transfer Molding (VARTM) for thermosets use and compression moulding using the film stacking method for thermoplastics. These fibres are generally oriented in various directions following a random or statistical distributions. The mechanical properties of nonwoven fabrics depend on raw materials i.e. fibre quality due to its growth and isolation process, fibre aspect ratio and fibre arrangement. Typical failure modes of the nonwoven include fibre rupture, de-bonding and fibre slippage as a result of high volume voids.

The most common method to achieve these mats is air-laying as separated short discontinuous fibres are suspended in air and dropped by gravity on a moving conveyor whereby a web-like structure of fibres is formed. The constant fibres feeding mechanism requires binding through reciprocating needle-punch process using barbed needles moving perpendicular to the fibre web. The punching process parameters include the areal density, needle-punch density and the needle-punch depth. The density of the nonwoven mats is affected by the process of compounding method of the fibres as such in the case of needle punching mechanisms parameters of fibres as illustrated in Figure 2-10. The in-plane alignment of fibres within the web structure is achieved through the carding machine followed by the cross lapping process of veils to attain the desired areal density of the mat. This step is then followed by needles penetration that engage some fibres already oriented along the in-plane direction to reorient along the thickness i.e. out of plane direction. Control of amount of fibres deposited over unit area

which is measured in grams per square meter (GSM) allow yield various areal densities. Similarly, mat thickness is controlled by the needle punch density (P) which is the number of punches per square centimetre of the mat. Therefore, the thickness of mats is dictated by the areal density (GSM) and the needle punch density (P). Natural fibre composites strengths as replacement to synthetic composites rely on their functional properties i.e. the improved specific properties as mechanical properties to weight ratio increases for a constant thickness.

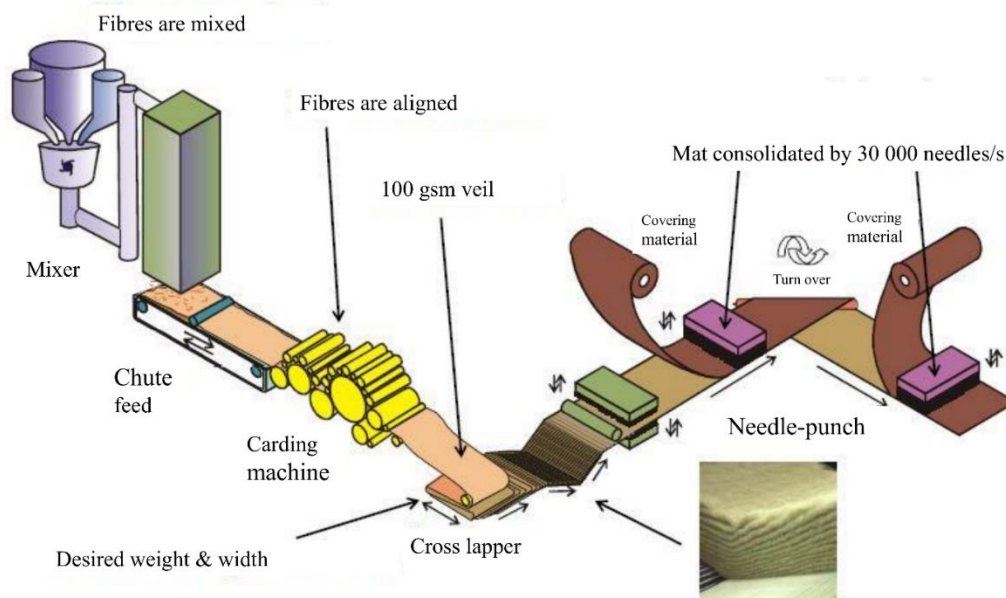


Figure 2-10 Natural fibre nonwoven mats manufacturing stages.[Produced from source: (Ecotechnilin, 2017)].

In contrast to glass nonwoven mats which have been extensively researched and are commercially available with well-defined properties, studies reporting on natural fibre mats are limited. In spite of the under-development of natural fibres mats composites, this review of literature encompasses the critical studies published up to date.

The density of these composites fabricated through the use of nonwoven mats is heavily controlled by the areal weight and void contents of the 3D web structures. The individual fibre density and resin density with their weight fractions are considered when calculating the fibre contents fraction which is heavily process dependant as mats pass through various stages illustrated in Figure 2-10. Fibre volume fraction V_f of a mat is inversely proportional to its thickness. To calculate the fibre volume fraction V_f of the needle punched multiplayer prior to consolidation into panels, Eq. (2-1) can be used:

$$V_f = \frac{n \cdot \beta}{\rho \cdot t} \quad \text{Eq. (2-1)}$$

Where n , β , ρ and t are the number of layers, areal weight (g/cm^2), density of fibre (g/cm^3) and thickness in cm respectively. Alternatively the most commonly used equation to calculate fibre volume fractions and the composite density, Eq. (2-2) and Eq. (2-3) can be used:

$$V_f = \frac{\frac{W_f}{\rho_f}}{\frac{W_f}{\rho_f} + \frac{W_m}{\rho_m}} \quad \text{Eq. (2-2)}$$

$$\rho_c = \frac{1}{\frac{W_f}{\rho_f} + \frac{W_m}{\rho_m}} \quad \text{Eq. (2-3)}$$

W_f , W_m , ρ_f , ρ_m and ρ_c are fibres weight fraction, matrix weight fraction, fibre density, matrix density and composite density respectively.

Yu and co-authors (Yu et al., 2009) successfully developed non-woven bio-fibre mats using Canadian grown and cultivated flax and hemp via consolidation by needle-punching and thermal bonding and using three matting methods: scan-feed, wet-lay and air-lay. Bio-composites panels were manufactured using the bio-fibre mats and a vinyl ester resin through a vacuum assisted RTM maintaining a 20 % fibre volume fraction. The authors then conducted tests in tension, flexure and short beam shear modes and discussed their potential use in the manufacturing of bus components. Comparatively, air-lay mats were more uniform than other mats. The mats were soft and easy to conform to tooling surface offering a good balance of efficiency, quality and productivity; however, the pressure needed to achieve compaction was greater with the air-lay than the wet-lay mats. They reported that hemp composites outperformed the other flax and flax/hemp blends bio-composites which may be attributed primarily to the irregularity of the flax mats and the noticeable fibre agglomeration.

A potential approach to precisely control the reinforcement architecture by combining continuous yarns of twisted fibres and textile techniques proved by a group of researchers to improve NFC properties (Habibi et al., 2017). They examined the effects of two assembly stacking sequences using two reinforcement types, short flax fibre mats and unidirectional (UD) layers of flax yarns, within epoxy matrix. The samples were produced via RTM process with various number of layers depending in order to achieve the minimum plate thickness imposed by the ASTM standards. Experimental activities included the tensile and flexural testing in both longitudinal and transverse directions. Acoustic emission (AE) data was collected with the use of multivariable analysis to monitor damage evolution. Different damage behaviours have been identified through a clear description of different damage modes, their evolution and their contribution to the overall composite failure. Figure 2-11 illustrates the layers arrangements of the UD and mat with respect to the loading applied under flexural testing. A significant improvement to the reinforcement stability of flax yarns during manipulation, cutting and impregnation when using short fibres as a binder. This proposed technique saves energy, cost and maintain the fibre integrity with less twisted yarns.

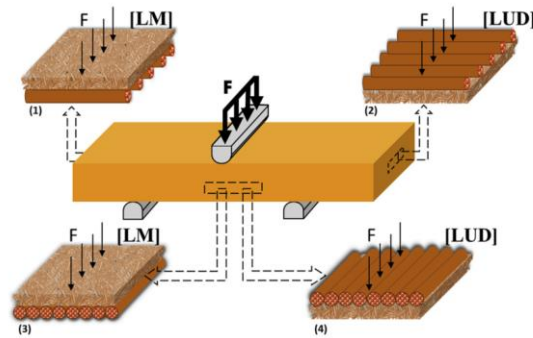


Figure 2-11 composite layer structure arrangement under flexural testing. LM: loading on mat; LUD: loading on UD (Habibi et al., 2017)

2.3. Selection of polymeric matrix and manufacturing technique

The roles of a matrix within a fibre reinforced composites are to keep the fibres in place, to transfer stresses between fibres and protect fibres against environmental i.e. chemical and mechanical i.e. surface abrasion degradation. Although the matrix has a minor role in tensile load carrying capacity of a composite structure, the matrix serves a major role in the compressive, interlaminar shear and in-plane shear properties of the composite. In particular, fibre buckling can be overcome by the matrix lateral support under compressive loading thus improving the compressive strength of the composite. Under bending loads, the interlaminar shear strength is crucial whereas in-plane shear strength is important under torsional loads and therefore the interaction between the fibres and matrix is key in the design process of damage tolerant structures.

Matrix selection is primarily dependent on the desired mechanical properties of the final composite. Therefore, the end application as well as the desired mechanical performance dictate the polymer type. For high performance composites the matrix properties need to be:

- High tensile modulus which affects the compressive strength of the composite,
- High tensile strength which controls the intraply cracking in laminated composites,
- High fracture toughness which controls the ply delamination and crack growth.

In-service environmental impact on the mechanical properties while using a polymeric matrix should be also considered such as the elevated temperature on the dimensional stability and resistance to moisture and solvents. The former usually means that the polymer must have a high glass transition temperature T_g . In practice, the glass transition temperature should be higher than the maximum use temperature. Resistance to moisture and solvent means that the polymer should not dissolve, swell, crack (craze), or otherwise degrade in hot-wet environments or when exposed to solvents. Some common solvents in aircraft applications are jet fuels, de-icing fluids, and paint strippers. Similarly, gasoline, motor oil, and antifreeze are common solvents in the automotive environment.

2.3.1. Polymer type

Polymers are divided into two broad categories: thermoplastics and thermosets. In a thermoplastic polymer, individual molecules are not chemically joined together. They are held in place by weak secondary bonds or intermolecular forces, such as van der Waals bonds and hydrogen bonds.

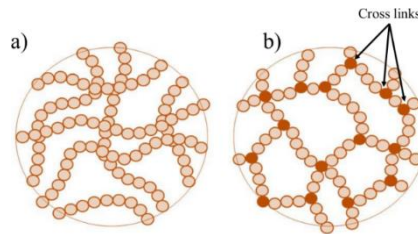


Figure 2-12 Arrangement of molecules in a) Thermoplastic and b) Thermoset

With the application of heat, these secondary bonds in a solid thermoplastic polymer can be temporarily broken and the molecules can now be moved relative to each other or flow to a new configuration if pressure is applied on them. Upon cooling, the molecules can be frozen in their new configuration and the secondary bonds are restored, resulting in a new solid shape. Thus, a thermoplastic can be heat-softened, melted, and reshaped as many times as desired. On the other hand, in a thermoset polymer, the molecules are chemically joined together by cross-links during polymerisation forming a rigid three-dimensional network structure, Figure 2-12. Thermosets however cannot be melted and reshaped with the application of heat but if the cross-links count is low these thermosets can soften at elevated temperatures. Therefore, polymer selection is typically based on the end- use application requirement as depicted in Table 2-3

Table 2-3 Comparison between thermoplastic and thermoset polymers

	Thermoplastic	Thermoset
Molecular Structure	Linear	3-D cross-links
State	Solid	Liquid
Impact Strength	High	Low
Viscosity	High	Low
Processing Pressure	High	Low
Processing Temperature	High	Low
Processing Time	Short	Long
Chemical reaction	No	Yes
Consolidation	By cooling	By chemical reaction
Reversibility	Can be reshaped	Cannot be reshaped
Recyclable	Yes	No
Reinforcements	Optional	Necessary
Fibre contents	Low	High
Manufacturing	Injection, extrusion	Hand lay-up, Vacuum bagging, Compression moulding

2.3.2. Biodegradable polymers

Polymers can be categorised as synthetic or bio-derived i.e. natural. Growing concerns over the current situation of manufacturing, use and disposal of traditional composites made of non-degradable polymers required more effort in the research and design of biodegradable polymers. Generally biopolymers originate from renewable sources or can be synthesised microbially such as Polyhydroxylalkanoates PHAs (Moralejo-Gárate et al., 2011, Osman et al., 2016) or from petroleum based compound such as Polypropylene and Polyethylene (Harding et al., 2007). Replacing the conventional polymers with biopolymers in various applications proved of environment benefits however at the cost of economic loss. Bioplastics have attracted a number of markets, from packaging, catering products, consumer electronics, automotive and transport, textiles and other consumer goods, Figure 2-13.

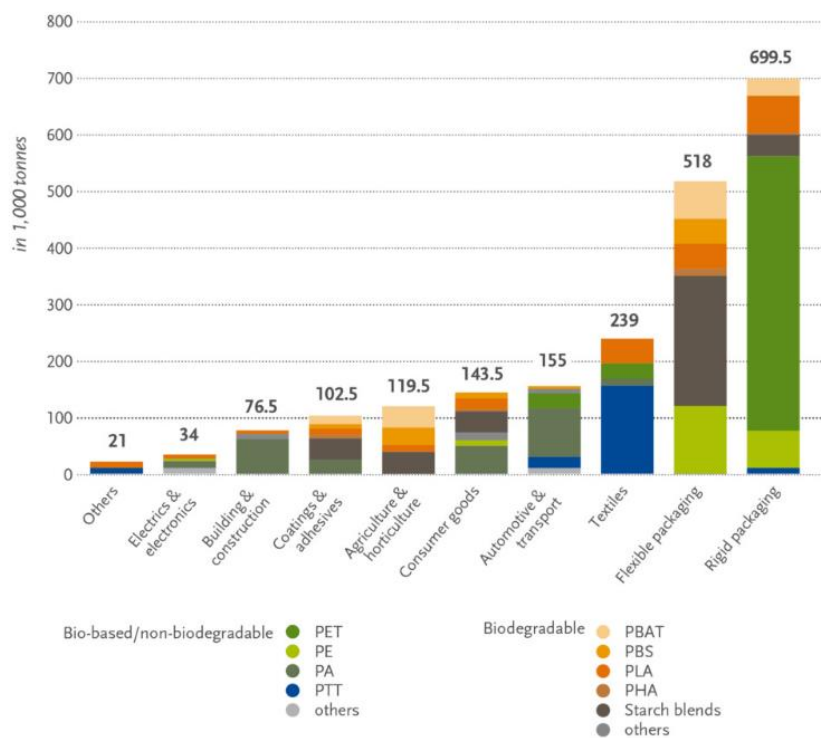


Figure 2-13 The wide range of products and industries using bioplastics (European bioplastics, 2018).

In the early days of polymer sciences and engineering, the development of biopolymers was based exclusively on chemical modification. The term bio-derived or bio-based represents the primary monomers which are sourced from nature and man-made into organic polymers, there are three principal ways to produce bio-based plastics (Nassiopoulos, 2015):

- Make use of natural polymers which may be modified but remain intact to a large extent (e.g. starch and cellulose based plastics);

- To produce bio-based monomers by fermentation or conventional chemistry and polymerize these monomers in a second step (e.g. poly-lactic acid);
- Produce bio-based polymers directly in microorganisms or in genetically modified crops.

Although plastics are temporary products due to their low durability but also suffers from serious drawbacks such as resistance to degradation resulting in its accumulation in the environment at a high rate of 25 million tons per year. The plastic abundance is increasing at an alarming rate affecting life on our planet and more specifically in the marine environment, therefore an emphasis on monitoring and mitigation of plastic debris (Ryan et al., 2009, Cózar et al., 2014). Therefore design of biodegradable polymers should consider the end of life phase of a product in such a way that a biocomposite made of biofibre and biopolymer should display stability during storage and usage but also degrade once disposed-off (Foruzanmehr et al., 2016). European bioplastics estimates the current annual global plastic production about 335 million tonnes of which bioplastics represent 1 %. According to the latest market data compiled by the later (European bioplastics, 2018). Bioplastic production is set to increase from around 2.11 million tonnes in 2018 to approximately 2.62 million tonnes in 2023 with an average compound annual growth rate CAGR of 4.4%. Furthermore, in 2018, the proportions of bioplastics that are bio-based / non-biodegradable and biodegradable represented 56.8 % and 43.2 % respectively.

i. Poly-lactic acid - PLA

PLA is a thermoplastic biopolymer which can be semicrystalline or totally amorphous in nature. The fermentation of agricultural products produces lactic acid which can be further polymerised through direct condensation and ring-opening polymerisation of the cyclic lactide. During PLA synthesis, agricultural products such as corn, rice, potatoes, sugar beets or other agricultural wastes are converted into dextrose. Dextrose is then converted into lactide by fermentation in the presence of catalyst, Figure 2-14 illustrates this process. Afterwards, vacuum distillation purifies the lactide compound and then polymerised to obtain the PLA polymer which is considered a sustainable and biodegradable material. It is derived from annually renewable resources and composted through conversion into water and carbon dioxide used for growing more agricultural products and then again consumed in PLA production in a closed cycle (Bajpai et al., 2014).

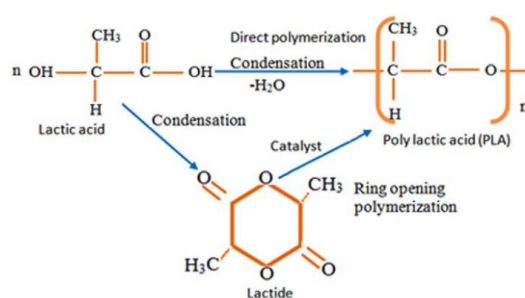


Figure 2-14 Stages of PLA production using either condensation by direct polymerisation or catalyst ring opening polymerisation (Bajpai et al., 2014)

Figure 2-15 presents the net Green House Gas emissions considering cradle to pellets for a number of materials, PLA not only produce the least CO₂ per tonne produced but over long term i.e. PLA Year 5+ can absorb a substantial amount equivalent to that released by other plastics production cycles. Life Cycle Assessment LCA studies on environmental sustainability reports the energy consumption during production taking into account the feedstock generation phase as well as the process energies. In contrast to traditional petroleum based polymers rely on limited oil reserves and also fossil resources take millions of years to regenerate, PLA monomers are generated from annual renewable resources which takes about 100 days but inevitably a certain amount of fossil fuels is required to produce the raw materials. This is an important factor to determine and maximise production efficiencies, Figure 2-16 compares the total energies (feedstock and process) of pellet production for conventional plastics to the projected production of PLA in 5 years and longer term.

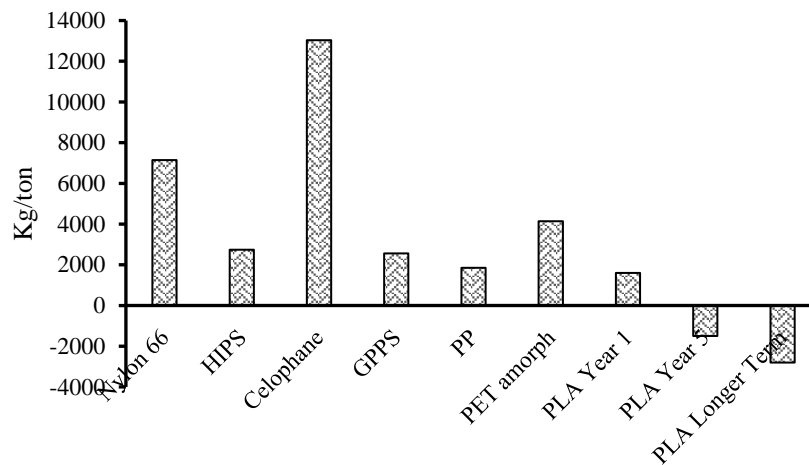


Figure 2-15 Cradle to pellets Green House Gas emissions of a number of commonly used plastics (Vink et al., 2003)

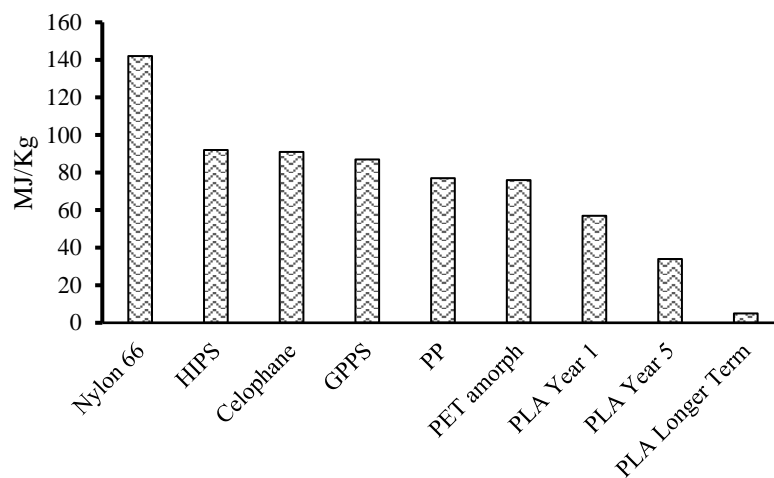


Figure 2-16 Total energy from fossil resources required for plastics production (Vink et al., 2003)

PLA possess comparable mechanical properties to the widely used non-biopolymers such as polyethylene terephthalate and polypropylene which are petroleum based. It is also a hydrophobic polymer because of the incorporation of the CH₃ side chain, however PLA is still very compatible matrix for natural fibre reinforcement due to its considerably high but safe processing temperature window of about 185– 190 °C because of the high melting point (175 °C) which is below the first stage degradation of natural fibres. PLA is brittle and have a relative narrow glass transition temperature about 50 to 60 °C making it undesired for upper service temperature. This processability drawback can be overcome with the addition of small amounts of D (-) lactide to L (+) lactide producing a PDLA which can decrease the melting temperature. However, PDLA suffers low impact resistance due to high stiffness and brittleness which can be moderated by blending low molecular weight plasticizers. In the same way, PLAs are often blended with other resins for various reasons e.g. to lower the cost or increase biodegradability and more commonly to enhance its performance. High performance PLA grades exhibit versatile properties promoting its candidacy as an excellent replacement for Polystyrene (PS), Polypropylene (PP) and Acrylic Butadiene Styrene (ABS) in more demanding applications. Most commercial high-purity grades PLA are semicrystalline having high yield and tensile strength equivalent to twice that of HDPE. PLA is produced into its primary form of pellets which can then be converted into various forms such as films and sheets via standard forming methods or can be directed for thermoforming, extrusion or injection molding (Auras et al., 2006).

PLA production which represents 10.3 % of the global bioplastic production capacity has been dominated by the joint venture of Cargill Corporation and Dow Chemical (NatureWorks) with estimated manufacturing of 95 % of the global production. Main PLA grades commercialised by NatureWorks LLC under the trademark Ingeo are directed for multiple further processing options (Murariu and Dubois, 2016). Production capacities of PLA are expected to grow by 60 % in the period 2018 to 2023. Figure 2-17 displays the different types of bioplastics in varying proportions contributing to the global production.

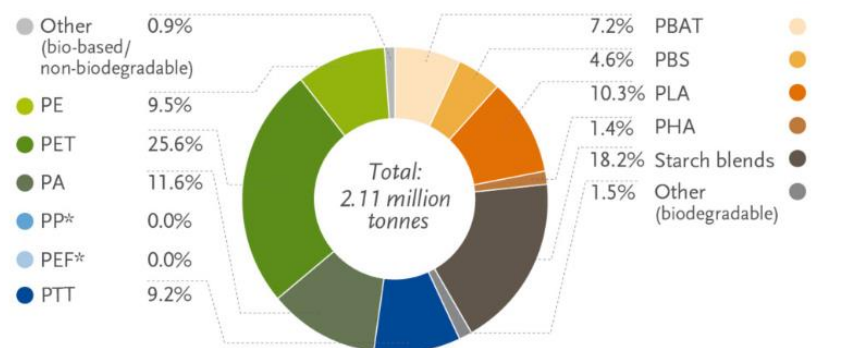


Figure 2-17 Proportions of various bioplastics contribution towards the global production capacity in 2018. Noticeably, PP and PEF are included in this chart inspite of their zero contribution, however, these are in developemnt to be available at commercial scale in 2023 (European bioplastics, 2018)

Typical applications of PLA are disposable tableware articles like drinking cups, cutlery, trays, food plates and food containers. Some other potential applications include soil retention sheathing and other agriculture films, waste and shopping bags, and the use as packaging material in general. PLA can also be spun into fibres which could be used for the manufacture of woven and non-woven biodegradable one-use fabric articles such as disposable garments, feminine hygiene products, and diapers. 3-D printing filaments represents a new market for PLA production, as pellets are transformed into continuous spools through extrusion process.

ii. Polypropylene - PP

Polypropylene (PP) is a petroleum based thermoplastic made from the combination of propylene monomers. Initial work by Ziegler in Germany in producing stereoregular polymers was later perfected by Professor Giulio Natta in Italy. Natta further developed the concept into the production of the first polypropylene resin in Spain in 1954. However, commercial production began later in 1957. Propylene molecules are derived from three major sources, most commonly from the steam-cracking process of naphtha which is a fraction of crude oil. Typically, this process is targeted to produce ethylene monomer whereas propylene is a by-product produced at various ratios depending on the crude oil feedstock. Gasoline refining process and, most recently, a new process by which propane is dehydrogenated to capture propylene monomer. Afterwards the polymer is produced through the process of addition polymerisation in which high energy radiation and an initiator or a catalyst are added to combine monomers together. PP is a versatile material i.e. diversity in structural designs and a range of mechanical properties are achievable. The grades of polypropylene can be derived with the addition of filler or reinforcing agents and blending PP with copolymer components which change the molecular weight distribution along with the process conditions result in variation of the final properties. These conditions are the four different routes of polymerisation: solution, suspension, bulk and gas-phase polymerisation. Polypropylene is a linear hydrocarbon polymer expressed as C_nH_{2n} , PP is also considered a vinyl polymer represented in Figure 2-18 in which every carbon atom is attached to a methyl group. The presence of methyl group attached to alternate backbone chain carbon atom can alter the properties. A possible stiffening effect of the chain resulting in increased melting point of the crystalline chain, or interfere with the chain symmetry hence decreasing crystallinity and melting point.

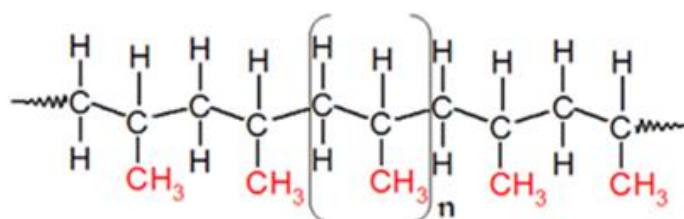


Figure 2-18 Polypropylene structure

PP is typically in a semicrystalline state with 40– 60 % crystallinity (Arroyo et al., 2000), lightweight with a density of 0.9 g/cm³, semi rigid, offers good chemical and electrical resistance at higher temperatures, tough, good fatigue and heat resistance, high softening point as PP melting point at ca. 160 °C. PP can be utilised in two forms: homopolymer and copolymer and selection is generally based on non-technical criteria.

When the PP matrix is reinforced, typically using natural fibres which are polar due to the hydroxyl groups, acetal and ether linkages. PP on the other hand is nonpolar, and fibre-matrix adhesion is to a large extent affected. Therefore, to overcome the interface properties, extensive research suggests modification to the chemistry of PP by attaching polar groups onto the molecular backbone e.g. acrylic acid, MA (Kim et al., 2007) (Mohanty et al., 2004, Han et al., 1981) and many other coupling agents (Gonzalez et al., 2002). In particular, significant improvement to the interface properties and consequently the composite strength when maleated PP (MAPP) is used (Shubhra et al., 2013). The tensile and impact strengths have been evaluated and results suggested that MAPP improved the stress transfer from the matrix to the fibre (Ashori and Nourbakhsh, 2009). The mechanism which improves the interface properties is obtained through hydrogen bonding between hydroxyl groups of natural fibres and carbonyl groups of the MA segment of the MAPP. The Hydrogen bonding reduces the rate of moisture absorption thus strength of the composite increases.

Polypropylene production takes various forms depending on the end use and intended performance. PP is suitable in packaging applications due to its good barrier properties, high strength, good surface finish and low cost. PP in packaging can be in both flexible form, PP films are suitable for food use due to its excellent optical and low moisture-vapour transmission (Ramos et al., 2012), and rigid form such as blow molding for bottles, cups and pots production (Raheem, 2013). PP films come in two important forms depending on the end user requirements: 1) cast PP film known as CPP; 2) Biaxially Oriented Polypropylene (BOPP). The consumer goods market has also benefited from the invention and development of PP in various uses such as housewares, appliances, luggage, toys etc. The automotive sector uses PP for its low linear thermal expansion, good processability and balanced impact /stiffness (Lummerstorfer et al., 2019) in parts such as trays, bumpers, fender liners, interior trim, instrumental panels and door trims (Moritomi et al., 2010). Furthermore, fibres and fabrics market segment benefits from PP in the form of tape, strapping, bulk continuous filament, staple fibre, spun bound and monofilament extrusion (Maddah, 2016). PP sheets/thermoforming (Macauley et al., 1998) and injection moulding are also considered key processes of PP global production (Kalay and Bevis, 1997).

iii. Unsaturated Polyester – UPE

The unsaturated polyester resin is a thermoset (*UPE*), capable of being cured from the liquid or solid state when subjected to the right conditions. Saturated polyester, on the other hand, cannot be cured this way. It is common to refer to unsaturated polyester resins as “polyester resins” or simply “polyesters”.

The base material for the polyester thermoset matrix is an unsaturated polyester resin formed of a chain containing a number of double carbon bonds C=C. This compound is achieved by the reaction of maleic anhydride and ethylene glycol or propylene glycol (Dholakiya, 2012). Saturated acids, such as isophthalic acid or orthophthalic acid, are also added to modify the chemical structure between the cross-linking sites; however, these acids do not contain any C=C. According to US Patent (Hatton, 1974), depending on the desired properties of the produced article such surface and strength, the resin formulation should be prepared by condensing maleic anhydride and propylene glycol or by condensing the later with addition to dipropylene glycol and isophthalic acid. Polyesters also have a limited storage life as gelling initiates uncontrollably over a long period of time, though, often small quantities of inhibitor are added during the resin manufacture to slow this gelling action. To improve handling of the polymeric liquid, viscosity of the compound is reduced through dissolving using a reactive polymerisable diluent e.g. styrene. The diluent acts as a cross linking agent through its double bonds C=C by bridging the adjacent polyester molecules at their unsaturation points to cure from a liquid to a solid state (Sanchez et al., 2000). Figure 2-19 illustrates the cross linking of polyester resin.

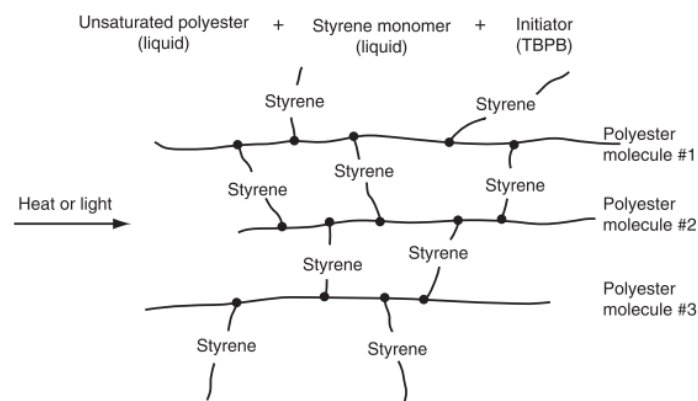


Figure 2-19 Representation of the cross linking mechanism of polyester resin (Mallick, 2007).

To prevent premature polymerisation of the polyester during storage, small amounts of inhibitors are mixed with the liquid resin. However, specific ratios of catalyst to polyester resin are normally prescribed by manufacturers to initiate the curing cycle. Furthermore, with the application of heat curing is accelerated through the rapid decomposition of the catalyst into free radicals which then react with the styrene molecules and break their C=C bonds (Hsu and Lee, 1991). Styrene radicals, in turn, join with the polyester molecules at their unsaturation points and eventually form cross-links between them resulting in solid polyester resin (Suh et al., 2000). (Cao and Lee, 2003) investigated the combination of low temperature and curing agents based on the reaction kinetics and conversion profiles. Curing reactions can be hindered due to the restrained chain mobility, therefore research suggests an increased temperature, heating rate or further heat exposure post-cure to overcome such a network interlock effect and achieve maximum conversion (Lin et al., 1999) (Yang and Lee, 1988). The curing time for polyester resins depends on the decomposition rate of the catalyst, which can be increased by increasing the

curing temperature (Parker and Moffett, 1954). Unlike other thermosetting resins, polyester curing reactions does not produce any by-product enabling it to be moulded, cast and laminated at low pressures and temperatures. For use in moulding, a polyester resin requires the addition of several secondary products such as: 1) catalyst, 2) accelerator and, 3) additives (Thixotropic, pigment, filler...etc.).

Polyester resins have gained a lot of interests in various applications such as aerospace, automotive, marine and load bearing infrastructure due to their excellent ease of processability, high flexural modulus, outstanding chemical resistance and low cost (Mallick, 2007). Polyester resins are similar to epoxies when it comes to properties as they are heavily affected by the cross-link density. The modulus, glass transition temperature, and thermal stability of cured polyester resins are improved by increasing the cross-link density, but the strain-to-failure and impact energy are reduced. The major factor influencing the cross-link density is the number of unsaturation points in an uncured polyester molecule. Polyester resins can be formulated in a variety of properties ranging from hard and brittle to soft and flexible. Its advantages are low viscosity, fast cure time, and low cost, however, high volumetric shrinkage of polyesters presents a major drawback when compared to using epoxies.

Table 2-4 Typical properties of cast thermoset polyester resin at 23 °C (Mallick, 2007).

Density (g/cm³)	1.1 – 1.43
Tensile strength (MPa)	34.5 – 103.5
Tensile modulus (GPa)	2.1 – 3.45
Elongation (%)	1 – 5
Cure shrinkage (%)	5 – 12

Typical end use of polyesters as matrix systems in the production of composites, represent about 75 % of total resin used, particularly for the maritime (due to flame retardancy, water and fire resistance properties) (Tran et al., 2018) and automotive (Table 2-5) industries.

Table 2-5 Performance requirements for automotive polyester and polyester composites.

Automotive parts	Requirement	Material / Reinforcement
Seat covers	Abrasion and UV resistance, aesthetic	Polyester / wool
Carpets	Light fastness, moldability	Polyester
Seat belts	Tensile strength, abrasion and UV resistance	Polyester
Hoses, belts	Heat resistance, tensile strength, dimensional stability, adhesion and chemical resistance	Polyester / aramid
Headliners, boot-liner	Stiffness, strength, light weight, energy dissipation/absorbing and thermal stability	Polyester / Glass, carbon, aramid

There are two types of polyester as standard laminating systems in the composite industry: orthophthalic (ortho) and Isophthalic (iso). The former is essentially composed of orthophthalic acid

contains 35 – 45 % of styrene ideal for applications that do not require high temperature, high corrosion resistance or high mechanical properties. The latter contains 42 – 50 % of styrene and better suited for high demanding applications such as severe environments and greater mechanical properties. Although UPE resins are commonly used as the matrix in synthetic glass fibre composites, it has been modified to make it more compatible with cellulosic natural fibres. (Aziz et al., 2005) investigated the compatibility of four chemically modified polyester through determining their effect on the flexural, impact fracture and dynamic mechanical properties. Haghdan and Smith reviewed the available literature on the effects of chemical treatments on fibre-matrix interfacial adhesion and the wettability of many natural fibres by polyester (Haghdan and Smith, 2015). Other researchers also examined various fibre surface treatments such as alkali (Aziz and Ansell, 2004), γ -MPS, acrylonitrile and UPE-MEKP (Mehta et al., 2006). Mehta et.al confirmed the improved adhesion which resulted in the increase of tensile (strength and modulus), flexural (bending strength and modulus of elasticity), impact strength, dynamic storage and loss moduli compared to the control polyester untreated fibres, however, less damping was observed in the chemically treated fibres.

iv. Poly-furfuryl alcohol - PFA

Polyfurfuryl alcohol (PFA) represents a promising, highly ecological, carbon neutral and fully non-toxic resin. PFA is a thermally cross-linked polymer that is synthesized from the precursor furfuryl alcohol (FA). Furfural is an aldehyde derived from the hydrolysis of renewable saccharidic biomass such as agricultural residues of corn, sugarcane, wheat, oat, cottonseed hulls, rice hulls, birch wood and hazelnut shells (Deka et al., 2013) . The monomer FA is liquid at room temperature and has high solubility in water and many organic solvents, and its polymerization can be carried out under flexible conditions (Wang and Yao, 2006). Polyfurfuryl alcohol (PFA) is a common thermosetting resin that is usually synthesized by the cationic condensation of its monomer furfuryl alcohol (FA). Many studies have been devoted to the understanding of FA polymerization mechanism and the characterization of PFA (Choura et al., 1996, González et al., 2002). Importantly, PFA is compatible with many organic polymers and inorganic materials, and it gives high carbon yield when undergoing pyrolysis (Nanni et al., 2019).

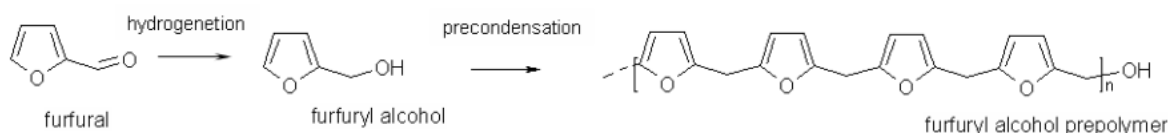


Figure 2-20 Chemical conversion of furfural through pre-condensation to produce furan pre-polymer

The conversion of furfural into furfuryl alcohol (FA) by the process of derivatisation. The controlled polymerization of FA results in polyfurfuryl alcohol (PFA) of the black colour, chemical conversion shown in Figure 2-20. To enhance processability of PFA, the viscosity needs to be reduced with a solvent

which can be simply water, however, the solvent amount and poly-condensation reaction require a distinct process and curing control in order to avoid foaming, other formation defect or incomplete PFA cure thus adverse effects on its overall performance properties. However the condensation reactions are hardly controlled and that is what limited its use as a resin in the past 50 years. When PFA polymerisation is conducted for academic research, the cross-linking activation process is carried out either slowly by gradually increasing the temperature from 20 °C to 80 °C or by isothermal stepwise temperature increase between 90 °C and 160 °C. Both methods span over a period 2 – 8 hours and are considered time consuming and unfeasible for industrial scale production, therefore short cycles times are required.

A US patent (Nordlander, 1946) clearly mentioned that it is impossible to cure PFA at low temperature, also at high temperature the risk of explosion is difficult to control as reactions go out of control. Above 80° C, exothermic reaction occurs due the condensation polymerization of FA according to the patent report; also cooling it does not allow controlling the reaction kinetics neither. As soon as the exothermic reaction starts, a significant increase in the polymer viscosity causing a non-workable state for the resins. At some cases, despite the elimination of the explosion effect, the objects will blister or cracks develop once the exothermic reaction initiates. A Belgian leading manufacturer of PFA TransFurans Chemicals (TFC bvba, Belgium) specialises in the conversion of hemicellulose into furfural which is then polymerised to produce the thermoset resins systems Furolite and BioRez. Furolite unique and excellent resistance to high temperatures make it hard to ignite providing an inherent fire resistance for fibre reinforced composite production for aerospace, rail, public transport and offshore. For the composite production, Furolite is available in various formulation for different processing techniques: snap cure compression moulding, prepreg technology, resin transfer molding. BioRez PFA typical application in the automotive and furniture for the biocomposite with lignocellulosic natural fibres and green technology production due the excellent adhesion properties.

In the European collaborative project BIOCOMP (2005- 2008) aimed at developing new classes of biocomposite materials from renewable resources, a study investigated the suitability of furan thermosetting bio-resins as a matrix for flax fibres (Arnold et al., 2009). The incorporation of flax into biorez (TFC, Belgium) required modifications to the two-part resin by mixing with a catalyst (up to 6% by weight). The curing cycle was a stepwise isothermal in the sequence of 150 minutes at 20 °C, 45 minutes at 50 °C and 45 minutes at 80 °C with constant vacuum being applied throughout the cycle to restrict the amount of laminates shrunk and evacuate any additional water produced. Control samples of glass/polyester and glass/furan have been prepared for comparison. Findings revealed stiffness of flax/furan similar to the reference synthetic samples, the process development produced better surface finishes. Furan composites also maintained its mechanical performance at high temperatures.

Previous results have been achieved on the flax reinforced thermoset PFA composites by (Kumar and

Anandjiwala, 2013). Rakesh and Rajesh have initially investigated the thermal stability of the matrix PFA, which was found to be very high with T_{\max} of 482 °C and 60 % of char yield at 700 °C compared to that of the PA possessing two lower T_{\max} (195 and 443 °C). In order to determine the performance of the resultant biocomposite and to estimate the effects of the matrix addition, the ratio of PFA/fabric in the biocomposite was 60:40 prepared in two conditions dry and wet. In another study samples, compression moulded of flax/PFA and cellulose acetate butyrate (CAB) were investigated for rheological, mechanical and dynamic properties. Results showed that reinforcement with flax fibres increased the storage modulus (Toriz et al., 2003).

2.3.3. Composite manufacturing processes

Traditional manufacturing techniques, which have been designed and developed for the conventional fibre reinforced polymer composites and thermoplastics, are also adopted in the natural fibre polymer composites fabrication. These techniques include hand lay-up; spray lay-up; filament winding; pultrusion; extrusion and injection moulding; carding and hot pressing; film-stacking and hot pressing; compression moulding; resin transfer moulding (RTM) or resin infusion; sheet moulding compounding (SMC) and hot pressing. Selection of the appropriate method of consolidation is dependent on many factors, fibre type and orientation, fibre content, moisture content of fibre, matrix i.e. polymer type and rheology, thermal stability, the overall properties of the final composite...etc. Furthermore, processing temperature limitations of the natural fibres need to be considered, as they cannot be processed at over 180 – 200 °C or over 175 °C for prolonged periods without a significant decrease in mechanical properties (Gassan and Bledzki, 2001) (Wielage et al., 1999). Due to this restriction, suitable matrix systems need to be chosen with care. As discussed in the previous section (2.3.2) most biopolymers also have low processing temperatures; for example PLA has a glass transition and melting point of 58 °C and 130- 230 °C respectively, therefore, compatibility with natural fibres (Henton et al., 2005). An extensive literature on the processing techniques of NFCs is available and categorise them based on the matrix system used i.e. thermoplastic and thermoset based (Faruk et al., 2012). ***Natural fibre reinforced thermoplastic*** include compression moulding, extrusion, injection moulding, hot pressing and long fibre thermoplastic- direct (LFT-D). ***Natural fibre reinforced thermoset*** include resin transfer moulding (RTM), filament winding, sheet moulding compound (SMC) or known as thermoset compression moulding, hand lay-up and spray lay-up, vacuum resin infusion and pultrusion (Faruk et al., 2014).

i. Compression Moulding

Compression Moulding (CM) is generally used for thermoplastic matrices with loose chopped fibre or mats of short or long fibre either randomly oriented or aligned, however this technique can be also with thermoset matrices. The fibres are stacked alternately with thermoplastic matrix sheets before pressure and heat are applied (Pickering et al., 2016b). Compression moulding is a forming process in which a plastic material is placed directly into an open, heated metal mould cavity, then is softened by the heat,

and forced to conform to the shape of the mould as the mould closes. The mould temperature is maintained using electric heaters, and the mould is held shut with a hydraulic cylinder, or toggle clamp. Material is placed in the mould, and it is closed under high pressure and high temperature. Contact with the heated mould surface softens the material, allowing it to fill in the entire cavity and initiating a chemical reaction, which cures the part. Cure time is determined by the thickest cross section, mould temperature, material type and grade. After curing, the mould opens and the part is ejected. Hydraulic press is the common type of compression moulding machine. Unlike some of the other processes, the fact that materials are usually measured before moulding prevents the excess flash.

There are various types of reinforcements which can be used in advanced composite thermoplastics. These reinforcements can be unidirectional tapes, woven fabrics, randomly oriented fibre mat, or chopped strands. Thermoplastic resins may be loaded into the mould either in the form of pellets, film, sheet, solution, fibre, or the mould may be loaded from a plasticising extruder. Thermoplastic materials are heated above their melting points, formed and cooled. For both thermosets and thermoplastics, adequate distribution of material over the mould surface during the compression step is ensured through a good material feed (Alimuzzaman, 2014). The incorporation of fibres into thermoplastic resins used to suffer low fibre wet-out due to high viscosity thermoplastics compared to low-viscosity thermoset resins, however new techniques have been developed to commercially produce thermoplastic prepregs. These will have long storage life and can be consolidated into a laminated composite by applying heat and pressure (Mallick, 2007). **Thermoset compression moulding** process entails spraying rather than immersing the natural fibres mats with resin then compress into the final part in a hot tool. Typical applications of this process in the automotive industry include interior parts such as door trims, seatbacks, vehicle under-trays.

ii. Sheet moulding compounding (SMC)

Sheet moulding compound (SMC) is a thermoset based compression moulded composite which is mainly used for producing thin, strong, stiff and light weight structural parts. Common thermoset resins for SMC sheets are polyester and vinyl esters, whereas epoxies longer cure time has limited their use in SMC. SMC composites are manufactured in a two-step production process, first step is the preparation of the so-called prepreg and compression moulding being the second step (Sawallisch, 1984). Prepregs of fibres, in the form of continuous roving or nonwoven mat or woven fabrics, impregnated with predetermined amounts of uniformly distributed resin. Prepregging process uses a bath containing a resin liquid of a controlled viscosity by applying appropriate solvent to the catalysed resin. Unlike other processes which can sometimes damage fibres due to the rotating screw for example in the extrusion or injection moulding, CM eliminates such damage as the fibres can be gently placed inside the mould without shear stress or vigorous motion, thus preserving the isotropic properties of the composite. Chopped glass fibre in thermosetting resins used to be the conventional SMC process output, however

nowadays, the process has been developed for natural fibres such as flax (van Voorn et al., 2001), hemp (Ren et al., 2009) and jute (Lautenschläger et al., 2017). Furthermore, the moulding temperature and pressure affect the mechanical properties of natural fibre composites. On one hand higher temperature reduces the thermoplastic viscosity hence better fibres wetting but on the other hand there is a risk of fibre degradation (Summerscales and Grove, 2014). Simultaneously, sufficient moulding pressure is important to remove air trapped inside the mould and reduce void contents (Khondker et al., 2006).

iii. Hand lay-up

Hand lay-up, the simplest method of composite manufacturing, suitable for natural fibre composites although it does not necessarily involve the application of heat but labour intensive process and is widely used for prototype part manufacturing and in the marine industry. This process yield low fibre fraction contents compared to hot pressing and compression moulding and consequently produces only moderate mechanical properties. The process entails fibre wet-out with the application of resin on the reinforcement layers continuously until the required thickness is achieved, then allowed to cure. In a study on the impact and fatigue behaviour of non-woven hemp polyester composites, hand lay-up process using dead weight (~ 40 kPa) during curing produced a low fibre weight fraction of 16 % fibre. However, to provide a significant reinforcing effect it was necessary to apply higher pressure using moulder (~2 MPa) which resulted in much higher fibre fraction of 44 % (Yuanjian and Isaac, 2007). Similar results reported in a study by (Cicala et al., 2009), the measurements of fibre volume fractions were found as low as 8 -11% due to the low compaction pressure of such process and porous structure of natural fibres that increase the amount of resin absorbed when lamina are impregnated. Alternatively, a higher volume fraction of 30 % could be achieved if liquid molding techniques RTM were employed.

iv. Resin Transfer Moulding

Liquid composite moulding processes encompass Resin Transfer Moulding (RTM) which its basic approach is to separately inject the liquid resin into the bed of stationary preforms. In the RTM technique, firstly the two-part mould needs to be cleaned and coated with a release agent. Once these coats are cured, dry fibre preform or porous preform having the mould size is placed into the cavity. Then, the two matching mould halves are clamped tightly to avoid leakage of resin during injection process. A pressurised molten resin is then injected into the heated mould through single or multiple ports depending on the final part complexity. Once the mould is filled with resin and after cooling cycle has been completed, the part can be removed. Post-cure is often required to allow the chemical reaction between the resin and its catalyst. This technique is capable of serving industries with high volume production demands at effective costs, as it bridges the gap between labour intensive hand lay-up and capital intensive compression moulding. The main variables of RTM process are mould temperature, injection pressure, resin viscosity, preform architecture and permeability, preform placement, gate location and configuration and vent control (Ho et al., 2012). Generally, low viscosity resin is achieved

at higher temperature allowing fast resin flow at higher injection pressure, as a result shorten the manufacturing cycle time. However, an excessive injection pressure may cause deformation of the mould and wash-out of the fibre preform. An excessively high mould temperature may induce premature resin gelation and cause short shot (Ho et al., 2012). Lower temperature requirements of natural fibre to avoid thermomechanical degradation making RTM the preferred process over other processes (Francucci et al., 2012). In a comparative study between RTM and CM Sisal reinforced polyester composites elucidated the benefits of the former process in reducing the void contents and water absorption. Tensile and flexural properties of the RTM composites were higher than the CM fabricated composites due to the good fibre/matrix interaction (Sreekumar et al., 2007).

Other advantages associated with the RTM process are: lower investment and operating cost, dimensional accuracy, manufacturing of complex parts, good surface finish, low volatile emission due to closed moulding process. Specifically, the incorporation of natural fibres in RTM process reduce the risk of abrasiveness for the tooling unlike glass fibres. In the same context, absence of airborne particles reduces respiratory problems for workers. However, the limitations are complex tooling design and also substantial trial-and-error experimentation or flow simulation modelling is required for manufacturing the complex parts. Compaction in this process is also affected by the structure of natural fibres including the effect of lumen closing and due to lower degrees of fibre alignment, natural fibre composites are less compactable than glass fibre composites.

v. *Resin infusion- Vacuum Infusion Process*

Resin infusion also known as vacuum infusion process (VIP) or vacuum bagging is also considered one of the liquid composite moulding whereby only vacuum is used to drive the resin flow and the laminates are enclosed in a one sided mould covered with a bag (Summerscales and Grove, 2014). This technique is basically an extension of the hand lay-up process, it is referred to as open mould process. Vacuum bagging involves layering the preform with peel ply, resin infusion film and resin infusion mesh then sealing the wet laid-up laminate with a sealing plastic film to form a vacuum bag. Air under the bag is then extracted by a vacuum pump thus the laminate is consolidated through pressure effect of one atmosphere. The pipe work consists of two parts, on one side of the preform applying vacuum so that extra air is removed. On the other side, resin is infused through a tube from a container (cup or glass) into the sealed bag. Vacuum causes the resin to flow through the preform and proper wetting of the fibres is achieved. Unlike hand lay-up, vacuum bagging achieves higher fibre contents and lower void contents and better fibre wet-out resulting in: i) stronger interface strength thus increased strengths and moduli, ii) minimise fibres abrasion thus eliminate damage and fracture, iii) avoid crack initiation and growth due to void (Boey and Lye, 1992). Although the process reduces volatiles emission during cure, it is costly for consumables and labour intense which require specialist skills to carry out the steps of mixing and controlling the resin flow and content (Williams et al., 1998). Biocomposite panels, for

large structures like trucks and automotive parts, of soybean oil resin reinforced with various natural fibres mats were prepared using vacuum-assisted resin transfer moulding (VARTM) and cured at room temperature due to the associated cost inefficiency with post-cure at elevated temperature (O'donnell et al., 2004). The static and dynamic test results of these panels proved that VARTM is suitable for the manufacture of large-scale components without the need to generate a large mechanical force via a press for molding.

vi. Film stacking and hot pressing

This technique employs alternate layers of dry fibres and polymer, most commonly thermoplastic, films followed by heating and compressing the stack using hot press to force the thermoplastic into the reinforcement layers and thus form prepregged sheet. Initially, this technique involves converting the polymer resin into a film form by heating and compressing the polymer pellets. The reinforcement fibre can take many forms such as nonwovens or continuous comingled, wrapped and coveaved fibre arrangement. The reinforcing fibres are then cut to the desired dimensions and shape then placed between the heating plates equipped with a hydraulic press. The stack of the layered polymer films and fibres achieving the desired thickness is then placed for processing. The assembly is heated and pressed and once the polymer has melted the composite is cooled to room temperature under constant pressure. Process parameters, time and temperature as well as pressure, are dependent on the nature of composite constituents i.e. polymer and fibres and are controlled as these parameters have an effect on the melting temperature and viscosity but also on the degradation of the reinforcing fibres. Jute fibres have been consolidated with polypropylene films using a combination of film stacking and compression moulding to produce samples for mechanical and optical characterisation. A pressure of 2 MPa, holding time of 15 minutes and cooling at ambient temperature were used for three moulding temperatures 140, 150 and 160 °C produced samples of fibre volume fraction 49.2 %. Optical micrographs revealed visible voids caused due to the incomplete fusion of polypropylene films and partly melted matrix of samples pressed at 140 and 150 °C hindered the adequate impregnation of the reinforcing jute yarns. In contrast, composites moulded at 160 °C PP films were adequately fused and its complete melt penetrated the fibre bundles (Khondker et al., 2005). In another study, biocomposite samples were manufactured by stacking alternate layers of treated kenaf fibres and PLA films. The whole assembly was then placed between heated platens with controlled temperature of 190 °C and two-stage pressure process of 700 psi for 12 minutes and 1700 psi for 5 minutes followed by cooling under pressure. At 90 °C, the mould platens were opened and composite of various fibre volume fractions namely 27, 37, 47 % were removed for conditioning then testing (Huda et al., 2008).

vii. Injection moulding

Injection moulding (IM) of composites is a process that forces a measured amount of mixture which contains molten polymer and fibre into mould cavities. This process can be employed in the production

of NFCs. This technique is capable of producing in great numbers parts of complex geometries with accurate dimensions while the process being fully automated (Faruk et al., 2012). Other advantages include economics of scale, minimum warping and shrinkage high function integration and possibility of using recycled materials. Difficulties associated with achieving high fibre fraction and longer fibre limit the use of injection moulding in the production of natural fibre biocomposites. Although this process was originally designed for plastic pellets to produce thermoplastic components however this process was later adopted for fibre reinforced composites. In such process, the pellets with chopped fibres are fed individually through a funnel-shaped feed hopper into a heated compression barrel with a rotating screw. The solid pellets are transformed into a viscous liquid, the mixture is then channeled through the sprue nozzle effect and finally forced into the tightly clamped mould cavities against the injection pressure. The closed mould is then cooled allowing the polymer to solidify and locking the fibres in place. Finally, once the assembly is sufficiently cooled, the composite is ejected from the closed mould to form the desired part.

Fibres used in the injection moulding are usually chopped first into short fibre according to the critical fibre length criterion to ensure efficient load transfer assuming a good fibre/matrix interfacial bonding is resulted. However, the fibre length in practice is normally shorter than the predicted fibre length due to the high shear rate in the barrel. In extreme cases where the fibre length is less than the critical fibre length, therefore inability to carry load effectively or even worse by acting as a defect in the material. A possible solution is to increase the fibre content which would theoretically improve the strength and stiffness, but a risk of fibre cluttering in the narrow gate and sprue would limit the amount of fibres to be injected. Many studies have been conducted to assess the potential of using IM in the natural fibre composite production.

Extrusion is an essential pre-IM step and often considered for producing pre-cursor for IM process. This is because injection moulding machines and screws are much shorter than extruders and therefore, the ratio of length to diameter for injection moulding screws is lower than for extruders. The lower length to diameter ratio of the screw in injection machine makes it less efficient in mixing and non-homogenous melt comparison with extruders. For this reason, if the composite is processed by injection moulding, prior extrusion compounding is necessary for the materials.

viii. Other composite processes

Pultrusion process is a less commonly used method in the production of NFCs. In this process, fibres are pulled from creel through a resin bath and then on through a heated die to form composite shapes with constant cross section. Typical components produced via pultrusion are rods, beams, channels, tubes, walkways and bridges, handrails, light poles, etc. However, a variant known as pulforming allows for some variation in the parts cross section. This process is continuous, low cost and high volume manufacturing.

Filament winding is primarily used for making tubular parts, generally circular or oval sectioned, for application-specific structures like pressure vessels, pipes and tanks. The process involves passing fibre tows through a resin bath before the impregnated fibres are wound in a variety of orientations angle over a rotating mandrel. The fibres moving through the resin bath and after impregnation they move back and forth by means of the guide while the mandrel rotates at a specified speed. The desired angle is achieved by controlling the motion of the guide and the mandrel.

In summary, NFCs are manufactured through various processes depending on the application specifications, geometry, final product performance and most importantly costs at high volume production. Careful consideration to a number of factors such as the properties degradation during processing, fibre loading and porosity i.e. void contents when choosing a manufacturing technique for NFCs. Table 2-6 provides a summary of NFCs manufacturing techniques in relation with composite parameters.

Table 2-6 Manufacturing techniques used in the production of NFCs, process variables interrelated with composite parameters

Manufacturing technique	Consolidation pressure (bar)	Fibre volume fraction (%)	Porosity volume fraction (%)	Matrix used
Injection moulding	>1000	Up to 45% (Typically 15-30%)	None	Thermoplastic
Compression moulding	Up to 40 (typically 20-30)	Up to 85% (Typically 25-50%)	Up to 25% (Typically 2-8%)	Thermoplastic or Thermoset
Prepregging (with autoclave)	0-10 (typically 4-6)	Up to 60% (Typically 35-50%)	Up to 10% (Typically 0-4%)	Thermoset
VIP/(RTM)	0-4 (typically 0-2)	Up to 60% (Typically 25-50%)	Up to 10% (Typically 1-4%)	Thermoset

2.3.4. Fibre and void contents

The mechanical properties of a composite are dependent not only on the properties of the constituents, but more so on the individual volumetric composition of the composite. In fact, the fibre volume fraction V_f is the single-most important factor in the rule of mixtures model. Increasing the fibre volume fraction improves many mechanical properties including stiffness and strength (tensile, flexural, compressive, shear) and impact energy absorption. Other factors such as the fibre-matrix interface and fibre architecture including fibre geometry (i.e. length, diameter and aspect ratio), fibre orientation (Miao and Shan, 2011) and packing arrangement which extend the scope of the basic rule of mixtures for strength and stiffness presented in Eq. (2-4) and Eq. (2-5) respectively:

$$\sigma_c = V_f \cdot \sigma_f + (1 - V_f) \cdot \sigma_m \quad \text{Eq. (2-4)}$$

$$E_c = V_f \cdot E_f + (1 - V_f) \cdot E_m \quad \text{Eq. (2-5)}$$

Where E_c , σ_c , E_f , σ_f , E_m , σ_m and V_f are the composite modulus, composite strength, fibre modulus, fibre strength, matrix modulus, matrix strength and fibre volume fraction respectively.

A comprehensive study on the mechanical properties of polypropylene reinforced with short flax fibre bundle samples processed using injection moulding and fibre contents varied from 0 to 60% weight fractions (Arbelaiz et al., 2005). Shah and co-workers investigated the effect of fibre volume fraction on the physical and tensile properties of aligned flax fibre reinforced in polyester matrix. Samples of five different volume fractions were fabricated using vacuum infusion technique, while in order to achieve varied V_f the number of unidirectional mat layers of flax yarns (low twist 50 tpm and high twist 190 tpm) was increased. As previously mentioned, although compression moulding is preferred to produce much higher V_f , vacuum infusion is suitable for large components manufacturing (Shah et al., 2012). They concluded that no clear correlation between fibre volume fraction and porosity, however, low V_f NFCs are susceptible to intra-yarn voids whereas high V_f NFCs are prone to inter-yarn voids. Peijs and co-authors reported in a number of publications on the effect of fibre volume fraction on the mechanical performance of all cellulose composites (Qin et al., 2008) and flax mat reinforced polypropylene fabricated by means of film stacking method (Peijs et al., 1998). Experimental results suggested a correlation with the Cox-Krenchel prediction model (Cox, 1952) (Krenchel, 1964) as the increase of flax fibre contents yielded an increase in tensile strength and modulus. Peijs's study concluded that while the flax/PP mat (NMT) tensile modulus is equivalent to the glass/PP (GMT) model-predicted modulus, the tensile strength of NMT require further optimisation to enable its use for strength critical applications.

Porosity an almost inevitable phase in composite fabrication, has a significant detrimental effects on the final composite performance. In particular, plant based composites suffer low compactibility therefore these need to be further compressed to achieve high fibre V_f and reduce void contents. The variability of composite properties produced by hand lay-up process is more manifested compared to other available mechanised processes (Harris, 1999). According to literature, as illustrated in Figure 2-21, the void presence in various composite manufacturing methods is classified in the following order: hand lay-up, compression moulding, RTM, vacuum assisted resin infusion and with the minimum porosity values, (as low as 0%) as shown in Table 2-6, prepregging with autoclave although porosity can be as high as 10% if low autoclave pressures (<3 bar) are used, Figure 2-22 illustrates the decrease in porosity with the increase of applied pressure. It is acceptable that thermoset based composites yield significantly lower void contents compared to their counterpart based on thermoplastic matrices due to the low viscosity of several magnitude.

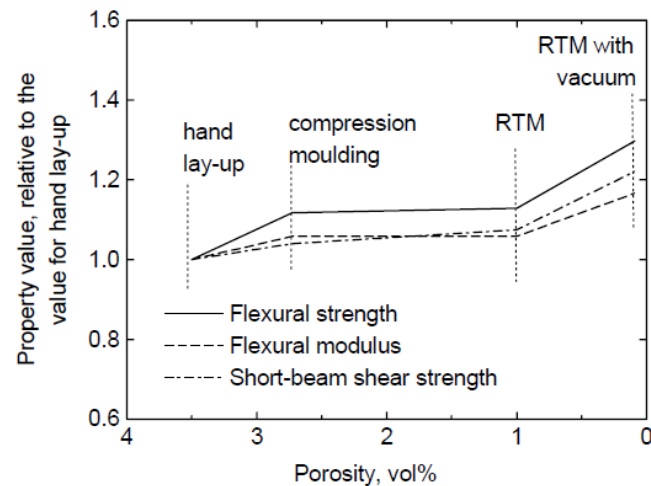


Figure 2-21 Variation of mechanical properties with respect to porosity variation levels- Comparison is based on reference $V_f = 40\%$ for all processes (Hayward and Harris, 1990).

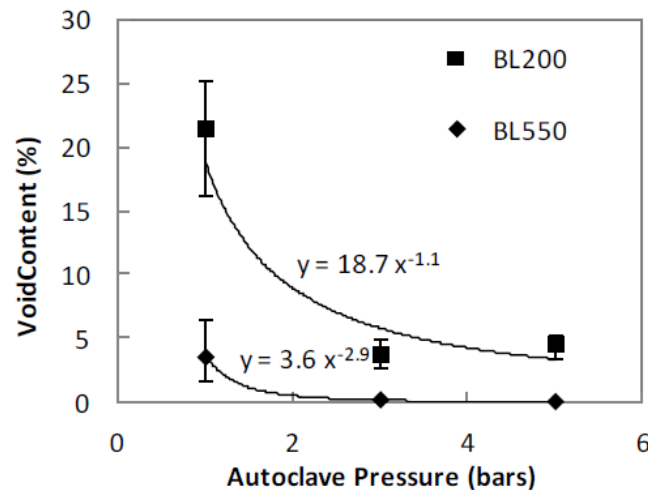


Figure 2-22 Effect of autoclave pressure on the void content (%) (Phillips et al., 2013)

Madsen et al, developed a theoretical model based on data best fitting in order to describe the composite volumetric interaction between contents of fibre, matrix and porosity (Madsen and Lilholt, 2003) (Madsen et al., 2007). The composites used for this study have been manufactured from filament wound flax yarns and polypropylene foils through film stacking then vacuum heating (190 °C for 15 minutes) and press consolidation (2.2 MPa for 1 minute). The eight laminates manufactured samples had fibre weight fractions in the range 50 -75% equivalent to fibre volume fraction of 41 - 55% and porosity in the range of 4 -8%. Some interesting assumptions were made, instead of assuming the porosity is constant, the porosity is assumed to be a variable function of the fibre weight fraction. It was concluded that for high fibre volume fractions and high porosity content, the proposed corrected model improved the accuracy of axial properties prediction but failed to fully predict the transverse properties (Madsen and Lilholt, 2003).

2.3.4.1. Fibre length and orientation factors

The effects of fibre length on the elastic properties of short fibre reinforced polymer composites have been analysed mathematically in the early 1950s (Cox, 1952). The stiffness and strength of FRPs have been shown to critically depend on the fibre length and fibre orientation distributions FLD and FOD respectively, particularly, for the injection moulded FRP composites (Hine et al., 1995). To attain the full reinforcement potential of natural fibres, it is crucial that the highest reinforcement efficiency is utilised. The reinforcement geometry i.e. fibre length and aspect ratio affect the length factor efficiencies for the stiffness η_{IE} and strength η_{IS} . High aspect ratios and reinforcement fibres longer than the critical fibres maximise these factors η_{IE} and η_{IS} . A comprehensive study addressed the theoretical modelling of the optimum V_f of short discontinuous short fibre composites and their potential to attain the highest strength using the well-known shear lag theory. It also covered the determination of the fibre length efficiency factor η_l (Pan, 1993). According to the shear lag (the elastic stress transfer) theory originally developed by Cox (Cox, 1952) which introduced the expression of η_l in Eq. (2-6) and Eq. (2-7):

$$\eta_l = 1 - \frac{\tanh \frac{\beta L}{2}}{\frac{\beta L}{2}} \quad \text{Eq. (2-6)}$$

Where β is shear-lag parameter and is given by:

$$\frac{\beta L}{2} = 2 \frac{L}{D} \sqrt{\frac{G_m}{E_f \ln \left(\frac{k}{V_f} \right)}} \quad \text{Eq. (2-7)}$$

Where L is the fibre length, D is the fibre diameter, G_m is the matrix shear stiffness, E_f is the fibre tensile modulus and k is a constant controlled by the geometrical packing pattern of the fibres e.g. for continuous parallel hexagonally packed ($k=0.907$) and for squared packed ($k=0.785$). The fibre length efficiency (η_l) can be calculated as a function of the fibre aspect ratio (L/D) which the model in Figure 2-23 illustrates. The model shows that η_l is rapidly increasing towards about 0.8 when L/D is increased towards about 20, and thereafter η_l is asymptotically approaching 1.0 when L/D is increased towards infinity. At L/D equal to 50, η_l is equal to 0.93. It was also proved that if $L/D > 50$, the influence of η_l variations in the calculations of composite stiffness is minor (Madsen et al., 2009).

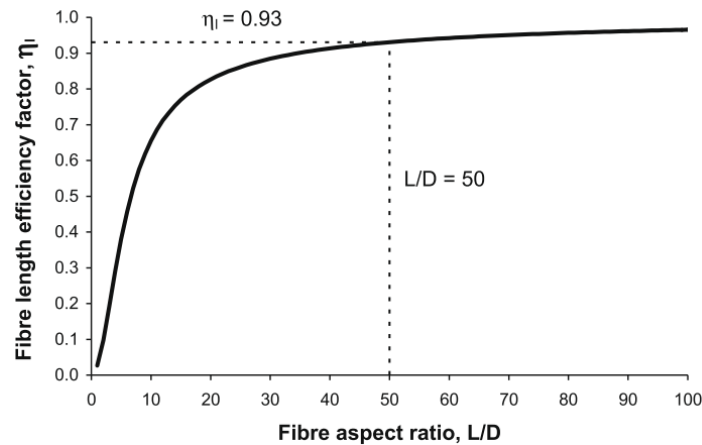


Figure 2-23 Shear lag model predictions of the fibre length efficiency factor as a function of the fibre aspect ratio. Typical values for plant fibre composites are used in the calculations: $E_f = 50$ GPa, $G_m = 1$ GPa, $k = 0.785$, $V_f = 0.30$. (Madsen et al., 2009)

Several factors and parameters including fibre fracture, interfacial bond strength, interfacial debonding, interface and matrix plastic deformation control the fibre critical length l_c . The variation of these factors makes determining the exact value of l_c difficult. Many studies employed this Single fibre fragmentation test (SFFT) technique with the Kelly-Tyson theory as micromechanics modelling approach to evaluate the critical fibre length and interfacial shear strength (IFSS) for elementary and technical flax fibres (Van den Oever and Bos, 1998) and also predicting strength of hemp PP composite (Beckermann and Pickering, 2009). Critical fibre lengths for bast fibre reinforced PFRPs have been measured to be in the range of 0.2- 3 mm. While a majority of bast fibres are typically >30 mm in length and have high aspect ratios typically between 100-2000. The composite manufacturing route dictates the appropriate fibre length and aspect ratio which can be much lower. Furthermore, the fibre critical length is a valuable parameter in the optimisation of composites mechanical properties versus processability. For instance, injection moulding employs fibres with lengths of 1-3 mm and aspect ratios <20; the resulting length efficiency factors are thus <0.30. In another study (Ausias et al., 2013) short flax fibre averaged lengths measured at 1.98 ± 0.18 mm, 1.07 ± 0.14 mm, and 0.42 ± 0.07 mm were cut and used for multiple extrusion cycles (once and twice) after being blended with PP. Injection moulded flax-PP composites were then used to assess the effect of processing on the initial fibre length and number of extrusion or injection cycles on average fibre length and aspect ratio. Both fibre length and aspect ratio decreased with further extrusions but unexpectedly longer fibres (2 mm) i.e. original without extrusion yielded lower tensile strength and modulus which can be explained by higher shear rate experienced compared to shorter fibres.

Fibre orientation of the discontinuous fibre composites is an important factor when considering enhancing strength and stiffness properties, therefore, it is desirable to orient the fibres in the loading direction. However, achieving perfect alignment or complete random distribution has been proven to be very difficult, if not impossible particularly for natural fibres as they exhibit a complicated

anisotropic structure (Cichocki Jr and Thomason, 2002). Fibre orientation efficiency factor η_o is dependent on the form of reinforcement and processing conditions. For continuous fibre composite where all fibres are aligned in the loading direction $\eta_o=1$ and $\eta_l=1$. Several studies used micromechanical models to determine this parameter and variations were reported based on statistical methods, whereby an established function form to describe the fibre orientation probability density as detailed in Pan's study (Pan, 1993). For instance, injection moulded NFCs fibres exhibit 3D-random orientation therefore an estimated orientation factor η_o in the range of 0.2- 0.28 has been reported (Bos et al., 2006) and (Garkhail et al., 2000) whereas other studies (Vallejos et al., 2012) (Serrano et al., 2013) reported higher orientation factors 0.27- 0.37 based on composites with same fibre loadings of 20, 30, 40 and 50 %. In contrast to the case of injection moulded parts whereby fibre orientation distribution is independent of the base angle orientation if the direction of flow is along the composite principal axis, for sheet moulding compounds fibres are assumed planar reducing the problem to two-dimensional. For a 2-D random fibre orientation it has been shown that $\eta_o=3/8$, which was also found to be valid for the natural fibre nonwoven mats. Furthermore, following the method of Bowyer and Bader (Bowyer and Bader, 1972), Bos and co-authors back-calculated the virtual orientation factor η_{ov} for Random flax/PP composites 20% and 40% V_f fabricated via a wet laid process then hot pressed, found η_o to be 0.411 and 0.396 respectively (Bos et al., 2006).

Composites reinforced with multiaxial textile fabrics may have a range of orientation distribution factors, depending on the ply orientation. For composites with balanced biaxial reinforcements in a [0,90] and [± 45] stacking sequence, it can be shown that $\eta_o = 0.5$ and $\eta_o = 0.25$, respectively. Finally, unidirectional fibres ensure the orientation distribution factor η_o to be close to unity.

The Cox-Krenchel model describes the contribution of both orientation and length factors to the overall composite strength and stiffness and is derived from both models of Cox's shear lag theory (Cox, 1952) and Krenchel orientation factors (Krenchel, 1964). Eq. (2-8) and Eq. (2-9) have been widely used in the prediction of composite properties:

$$\sigma_c = \eta_l \cdot \eta_o V_f \cdot \sigma_f + (1 - V_f) \cdot \sigma_m \quad \text{Eq. (2-8)}$$

$$E_c = \eta_l \cdot \eta_o V_f \cdot E_f + (1 - V_f) \cdot E_m \quad \text{Eq. (2-9)}$$

Where E_c , σ_c , E_f , σ_f , E_m , σ_m , V_f , η_o and η_l are the composite modulus, composite strength, fibre modulus, fibre strength, matrix modulus, matrix strength, fibre volume fraction, fibre orientation factor and fibre length factor respectively. The Krenchel orientation factor allows for the possibility of a distribution of fibres having different orientations with respect to a reference axis as illustrated in Figure 2-24, and is given by:

$$\eta_o = \sum_n a_n \cos^4 \Phi_n \quad \text{Eq. (2-10)}$$

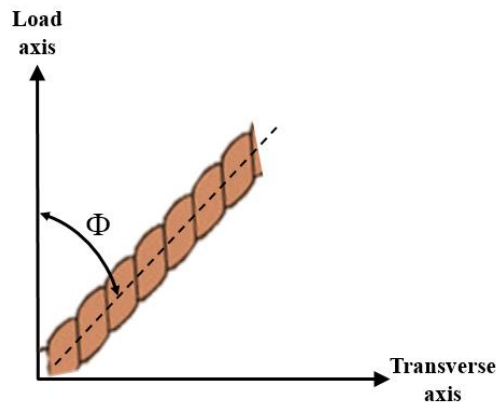


Figure 2-24 Fibre orientation angle with respect to the loading axis for a 2-D reinforcement arrangement

2.4. Mechanical properties

The following section reviews the current literature of mechanical properties of bio-composites primarily made of natural fibres as reinforcement in its various architecture (discussed in section 2.2.2). In mechanical characterisation studies, composite materials testing is considered in two scenarios namely quasi-static and dynamic. The difference between these two being the load rate i.e. the progressive time step in applying load or strain. The quasi-static approach covers a range of testing modes such as tensile, compressive, flexural (3Pt and 4Pt bending) and shear (interlaminar shear) tests. Dynamic testing mode is typically conducted under impact mode using various methods e.g. the falling weight impact test (or drop test), hammer impact, induced vibration ...etc. While considering shock, vibration or impact analysis, it is important to understand the changes in mechanical properties in either the time or frequency domain in order to have a reliable prediction.

2.4.1. Tensile properties

Tensile properties are the most widely reported properties for NFCs and various studies investigated the effects of the intrinsic properties of the individual constituents i.e. fibre and matrix and also the interaction between them. Theoretically, since the fibres high tensile strength and stiffness contribute the most towards increasing the composite strength and modulus, many studies proved that increasing the fibre volume fraction V_f increase the overall strength however this can be at the expense of reduced strain at failure. Singleton and co-workers tested biocomposites made of flax mats and recycled HDPE through film stacking and compression, this process produced varying compositions with samples of 10, 18, 20 and 30% V_f (Singleton et al., 2003). Authors reported an increase of flax/HDPE strength and modulus with fibre loading, whilst a moderate increase in yield stress and strength (as much as 25%) a significant increase in modulus from 1.2 GPa that of the HDPE to 8 GPa. However, a 5% strain failure for the biocomposite which was lower compared to the 20% for recycled HDPE as ductility falls with increasing fibre reinforcement. A large scatter of data for specimen of 30% V_f was also reported. Upon

comparison with theoretical predictions based on a simple ROM and a random fibre orientation factor of 3/8, it was found that experimental results agree well with the theoretical ROM behaviour.

Oksman and his colleagues manufactured two categories of biocomposites from hand-made roving flax with PLA and PP through twin screw extruder then compression moulded, test samples of 30 and 40 wt% were compared for their tensile properties (Oksman et al., 2003). Results revealed no significant improvement to the tensile strength to be gained from flax reinforcement for both used matrices PP (28 MPa) and PLA (50 MPa). This was attributed to poor fibre/matrix as load cannot be transferred from the matrix to the strong fibres. In contrast, an observed increase in modulus to 8.3 and 5 GPa from 1.6 and 3.4 GPa of virgin PLA and PP respectively concerning the 30 wt% specimen. Further increase of 7.6 GPa was recorded for the flax/PP, whereas the flax/PLA 40 wt% experienced reduced modulus to 7.3 GPa which can be explained by the fibres orientation difference during the composite compression moulding (Oksman et al., 2003).

In an attempt to assess the applicability of the rule of mixtures and orientation averaging based models, flax fibre composites with thermoset and thermoplastic polymer matrices have been manufactured and tested for stiffness and strength under uniaxial tension. Coextruded polypropylene and MAPP with flax were compounded then hot pressed, while flax mats with vinyl ester (VE) and acrylic resin (AR) were manufactured through RTM process (Andersons and Joffe, 2011). All tested composites showed an increase in modulus for both thermoset (VE and AR) based specimen in the range of 8- 10 GPa and thermoplastic modulus fell in the range of 3- 5 GPa with a clear advantage of MAPP over pure PP across three levels of V_f 13, 20 and 29%. Similar trend was observed for the tensile strength as values ranged between 70- 90 MPa for thermoset based whereas thermoplastic based specimen ranged between 25- 40 MPa. The rule of mixtures proved effective in the stiffness prediction for thermoplastic/ flax extruded based and thermoset/ flax mat based specimens, however for strength, it proved sensitive to the matrix and adhesion properties depending on the fibre ineffective length.

Similarly, the orientation averaging approach was applied towards the prediction of stress–strain diagrams in tension of flax/polypropylene composites with different fibre volume fractions. This FEM model used the deformation of misaligned short fibre composite to analyse and describe the behaviour of the unit cell response under selected loading modes (Modniks and Andersons, 2013). The prediction model was in agreement with experimental results obtained elsewhere in literature (Andersons and Joffe, 2011) for flax/PP and flax/MAPP samples of 13, 20 and 29% V_f up to strain limit of 1.5% in the linear region of the stress-strain curve. However beyond this strain, in the non-linear deformation range, the stress at given strain was markedly overestimated. The non-linear deformation was predominately attributed to the imperfect mechanical interlocking-dominated adhesion of flax fibres to the polymeric matrix as the both fibre debonding and matrix yielding contribute to the non-linearity.

A study into the effect of fibre volume fraction on the tensile strength, modulus and strain at failure of UD Hermès flax epoxy composites proved similar behaviour whereby strength and modulus increase quasi-linearly with increased fibre contents whereas strain at failure decreased significantly up to 15% V_f beyond which strain remains constant (Yan et al., 2014). The same study reported that tensile characteristics of these composites are heavily dependent on fibres location on the stem. Fibres size variation along its longitudinal axis and chemical composition of their cell walls explain the higher values of tensile strength of 1795 MPa and modulus of 76.7 GPa for the fibres extracted from the middle of the stem (Charlet et al., 2007).

Kumar and Anandjiwala manufactured and characterised 100% biocomposite made of woven flax fabric (FF) 180 gsm reinforced into bio-based PFA resin. 10 layers of flax fabrics were dipped into the PFA resin producing prepregs prior to consolidation through stacking and compression moulding into panels of 4 mm thickness and composition of 60:40 fibre to resin ratio (Kumar and Anandjiwala, 2013). Comparison of tensile strength among the virgin PFA (15.65 MPa), FF/PFA-D (dry) (15.53 MPa) and FF/PFA-W (wet) (10.07 MPa) showed that PFA reinforcement with dry FF did not offer any significant improvement, while a decrease of approximately 36% in strength for reinforcement with wet FF when compared to both virgin PFA and FF/PFA-D. On the other hand elongation at break increased with reinforcement for dry and wet.

A separate study compares the mechanical properties of two types of unidirectional flax composites using PLA as the matrix, one made with layers of aligned flax roving alone (187.5 gsm) and the other containing an additional paper layer (226.2 gsm) fabricated using paper making techniques. The process and machinery employed in this work has been detailed in (Couture et al., 2016). 4mm plaques were achieved through stacking 7 layers of prepregs (4.2 mm thickness) with all fibres aligned in the same direction within the 4 mm thick steel frame, the excess 0.2mm compresses the stack during PLA melting, thus allowing the trapped air between the prepreg layers to escape along with the excess PLA. At the end of this process, the fibre volume fractions V_f for the UD Flax/PLA and UD Flax-paper/PLA were 44.3 and 56.1%. The presence of fibres leads to significantly higher tensile strengths than that of virgin PLA, by a factor of 5.5 ($339 \pm 23/62 \pm 1.4$ MPa) for the flax/PLA and 5.1 ($316 \pm 14/62 \pm 1.4$ MPa) for the flax-paper/PLA composites. Furthermore, the increase factors in tensile modulus are 5.9 ($19.6 \pm 1.3/3.4 \pm 0.1$ GPa) and 6.1 ($20.8 \pm 0.9/3.4 \pm 0.1$ GPa) for the flax/PLA and flax-paper/PLA composites, respectively (Couture et al., 2016).

A film stacking method and compression moulding process for the fabrication of biocomposite made of different weaves. Flax (basket and plain weaves), jute (plain weave) and cotton (basket weave) with no chemical treatments added into two grades of PLA matrix, 3260HP and 10361D commonly used as binder for natural fibres, transformed from pellets into film sheets of 0.5mm thickness (Rubio-López et al., 2015). The compression moulding process parameter were varied to determine their effects on the

tensile strength of the final biocomposite, temperature ranged between 175 °C and 200 °C, pressure from 0.8 MPa to 40 MPa and number of plies from 2 to 4. Reinforcement proportion in terms of weight fraction was evaluated at 65%. Tensile test results revealed that basket weave flax- 3260HP PLA processed at a temperature of 185 °C and pressure of 32 MPa exceeded the other combinations of materials and processing parameters with strength of 116.33 MPa. Notably, both flax weaves performed better than jute and cotton fabrics due to the high inherent tensile strengths of basket flax 271.62 MPa and plain flax 225.39 MPa compared to that of jute 136.18 MPa and 116.5 of cotton. Furthermore, bilayer biocomposites (2 layers) exhibited marginally higher strengths compared to 4 layers counterpart, however these differences were smaller than the standard deviation thus deemed insignificant. Considering the full data set, it was also concluded that processing temperature of 180 °C produced better tensile strengths averaged at 110 MPa. Whereas the pressure effect was found to have a better and constant effect on strength averaged at 112 MPa over the range 8 – 32 MPa (Rubio-López et al., 2015).

2.4.2. Flexural Properties

Flexural strength and modulus of chemically modified hemp fibres, short (averaged 4.9 mm) random and long (65 mm) aligned, reinforced in two matrices polylactide (PLA) and unsaturated polyester (UPE) were investigated over a range of fibre content (0–50 wt%) (Sawpan et al., 2012). Composites form short fibre and PLA pellets were compounded (10, 20 and 30 wt% fibre), twin screw extruded then injected moulded. Whereas the polyester based composites were fabricated by compression moulding of poured polyester resin over weighed hemp fibres at 30, 40 and 50 wt%. Fibres were randomly oriented when hand-laid in the mould cavity then left to cure for 5 hours under ambient temperature and 5 MPa pressure, post-cure at 80 °C for 3 hours. For long reinforcement, PLA based samples were manufactured by compression moulding using film-stacking at three different fibre contents (30, 35 and 40 wt%). Finally, the manufacturing technique employed for the UPE/short random fibre was also followed to fabricate polyester long hemp aligned fibres. All composite plaques described were cut to desired shapes using a computer numerical controlled (CNC) mill (Sawpan et al., 2012). Five specimen of each category with geometry with length (span) to depth ratio $L/D = 16$ were tested in flexure.

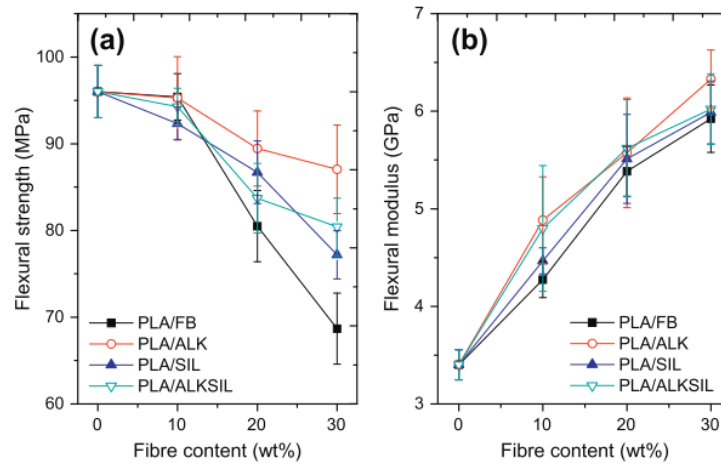


Figure 2-25 a) Flexural strength, b) Flexural modulus of PLA reinforced with untreated hemp fibres and ALK (Alkali), SIL (Silane) and ALKSIL (Alkali and silane) treated fibres as a function of fibre contents (Sawpan et al., 2012)

A general trend was observed for all PLA composite combinations, while flexural modulus increased with increased fibre contents, flexural strength decreased with increased fibre contents, as can be seen in Figure 2-25. Similar trend was observed for the polyester hemp composites as shown in Figure 2-26.

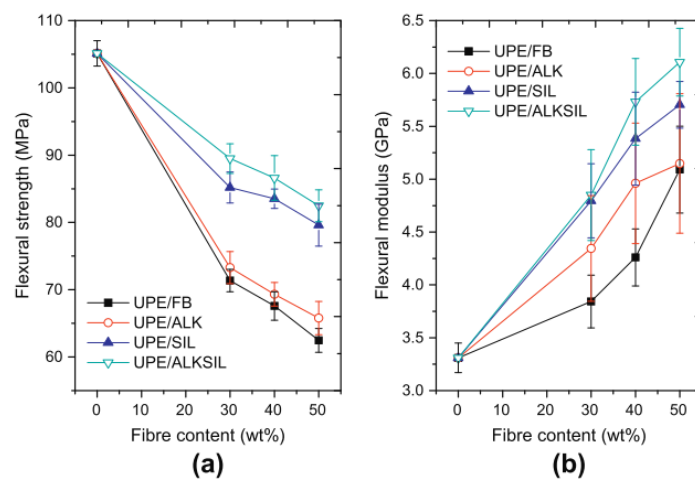


Figure 2-26 a) Flexural strength, b) Flexural modulus of polyester reinforced with untreated hemp fibres and ALK (Alkali), SIL (Silane) and ALKSIL (Alkali and silane) treated fibres as a function of fibre contents (Sawpan et al., 2012).

The behaviour of these composites under flexure can be explained by the mixed mode of loading of tension and compression. Microscopic analysis supported this suggestion as signs of compressive fracture characterised by stress whitening whereas at the tension site smooth brittle-like fracture is evident (Sawpan et al., 2012). The compression of fibres within the matrix can be subjected to kinking instead of compression wave form presenting weak spot i.e. defects in the fibres. In turn, the kinks will induce stress concentration points in the matrix which could act as sites of potential crack initiation, fibre/matrix debonding and the overall source of failure. Therefore increasing the fibre contents increase the number of stress concentration points, consequently flexural strength decreases. In contrast, flexural modulus increases as fibre contents increase due to the contribution of stiff fibres.

Dhakal and co-authors investigated the effects of water immersion by flexural characterisation of biocomposites made of flax and jute fabrics with bio-sourced epoxy resin (Dhakal et al., 2014). Specimen manufactured through hand lay-up technique of balanced 0/90 plain weave fabrics of flax 200 gsm and jute 305 gsm whereby eight and five laminates for flax and jute samples respectively and epoxy resin poured over then processed through vacuum bagging. This process produces 3 mm thickness plates of total fibre weight fraction was 41% and void content was 4.6% for both reinforcement types to allow valid like-for-like comparison. Flexural tests under three point bending of specimen with span to depth ratio 20:1. Results reported as averaged values with flexural strengths of 102.48 and 111.84 MPa and modulus of 3.57 and 4.98 GPa for flax and jute respectively. However these were reduced after immersion in water as strength reductions as much as 40.4 and 60.4% while modulus dropped by 69.2 and 80.0% compared to dry samples (Dhakal et al., 2014). Upon microscopic examination of tested samples, the failure of a dry flax specimen exhibiting a definitive fracture line due to the tension created under the three-point bending test is shown in Figure 2-27. While the dry specimen exhibited a clean brittle fracture, the wet specimen showed a ductile fracture with the main fracture line as well as the formation of secondary cracks. De-bonding along with delamination between the fibre reinforcement and the matrix initiate these smaller secondary cracks as a result of the water absorption. This would explain the lower mechanical performance of the wet samples compared with the dry ones (Dhakal et al., 2014).

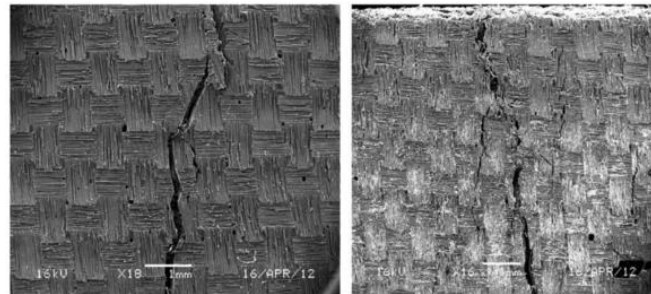


Figure 2-27 Failure mechanisms of tested specimen under SEM: dry flax (left) and wet flax (right) (Dhakal et al., 2014)

Various laminates have been produced by vacuum infusion using two-part furan resin Biorez with glass (450 gsm) mats and non-woven natural fibres mats, flax (570 gsm) and hemp (740 gsm), furthermore, similar reinforcement was used with Crystic polyester for reference (Arnold et al., 2009). Laminates were all vacuum infused with fibre volume fractions in the region of 23%. Results elucidated the poor performance of furan based composites as seen in Figure 2-28, explained by the action of acids can cause hydrolysis in cellulose chains and other binding materials, thereby degrading the fibre bundle mechanical properties. It was therefore evident that the two- part furan resin was unsuitable for use with hemp and flax fibre due to the acidic catalyst used to cure it.

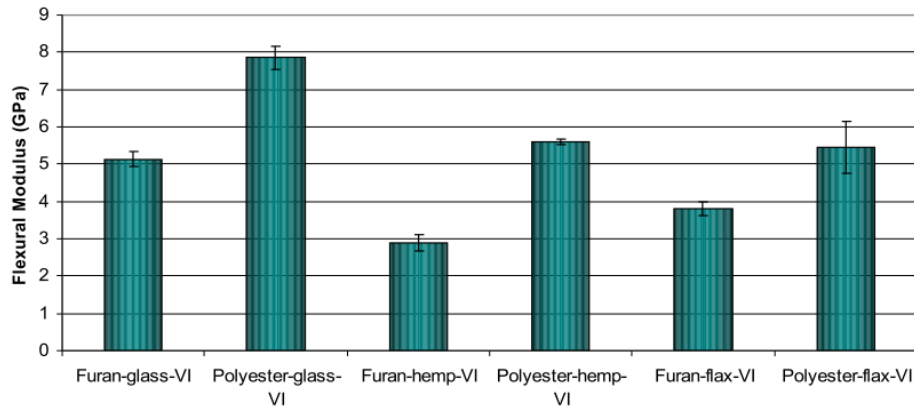


Figure 2-28 Flexural modulus of glass, hemp and flax mat reinforced furan and polyester composites, average fibre contents $V_f=23\%$ (Arnold et al., 2009).

Arnold and co-authors extended the scope of the study to eliminate the fibre degradation with significant alteration to the two-part furan resin, a specifically developed pH neutral (4-5) Furo-lite. A further modification to the process of manufacturing as resin was diluted in solvent (water) to reduce its viscosity and improve fibre wet out. Fabrics employed were: 1) loosely woven plain weave flax fabric with highly twisted yarn (170gsm), 2) tightly woven plain weave flax fabric with highly twisted yarn (106gsm) and 3) unidirectional stitched flax fabric with loosely twisted yarn (230gsm). The latter reinforcement was laid-up as a biaxial laminate to ensure comparability. This procedure yielded flax fabrics prepregs impregnated with up to 60% by weight of furan resin. Laminates using natural fibre prepreg were made by vacuum consolidating the materials at 150°C for 15 minutes. Laminates were approximately 40% fibre by volume. Positive effects were reported as a result of the modifications in comparison with previously tested biocomposites as crimp and twist clearly affects their flexural modulus, as illustrated in Figure 2-29. In particular, the unidirectional stitched flax fabric/furan exhibited flexural modulus of 9.6 GPa and strength of 99.4 MPa.

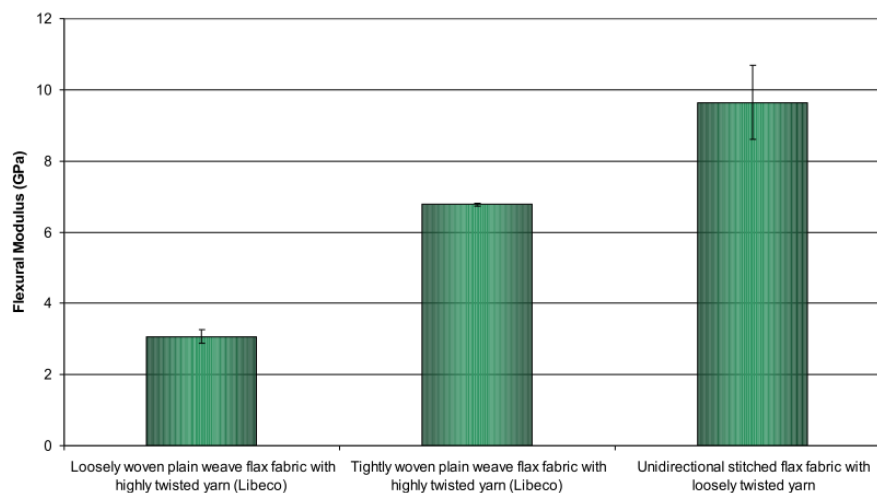


Figure 2-29 flexural modulus of furan/flax biocomposites (Arnold et al., 2009)

2.4.3. Dynamic Mechanical Properties

Dynamic mechanical analysis (DMA) is a versatile technique that complements the information provided by the more traditional thermal analysis techniques such as differential scanning calorimetry (DSC), thermogravimetric analysis (TGA), and thermal mechanical analysis (TMA). The dynamic parameters such as storage modulus (E'), loss modulus (E''), and damping factor ($\tan \delta$) are temperature dependent and provide information about interfacial bonding between the reinforced fibre and polymer matrix of a composite material.

Saba and co-authors reviewed an extensive pool of research articles on the dynamic mechanical properties of natural fibres reinforced thermoset, thermoplastic and bio-polymers composites (Saba et al., 2016). Damping properties of unidirectional (UD) flax and twill 2/2 (TW) flax reinforced in epoxy, polypropylene and polylactide and results were compared to those of carbon and glass (UD and TW) but only reinforced in epoxy resin. The processing techniques employed in this study were RTM for epoxy based composites and compression moulding with 1 mm thickness films PP and PLA obtained from Twin Screw Prism extruder biocomposites. All samples produced for characterisation under static tensile loading and dynamic loading consistently contained $V_f=40\%$ (Duc et al., 2014b).

Tensile properties of the composites considered in Duc's study which expectedly revealed that UD carbon and glass epoxy samples outperformed the flax reinforced composites, however, among the flax samples UD flax/epoxy increased strength and modulus to 258.2 MPa and 20.2 GPa respectively. Regarding the dynamic properties, specimen cut to 35 x 10 x 2.5 mm were tested in the single cantilever mode to characterise the damping behavior of the composites under flexural conditions. At each frequency (0.1 Hz, 1 Hz and 100 Hz), the composites were heated from $-40\text{ }^\circ\text{C}$ to $120\text{ }^\circ\text{C}$ at $2\text{ }^\circ\text{C}/\text{min}$ at a constant deformation of 0.01% and the preload force was set to 0.0001 N. Figure 2-30 reports the optimum damping ratio of flax, UD and TW, reinforced with PP composites. It was observed that PLA based UD flax and TW flax loss factors were competitive to those of carbon and glass epoxy composites. In this case researchers find the best compromise between stiffness and damping with flax fibre reinforced in semi-crystalline renewable and biodegradable PLA (Duc et al., 2014b).

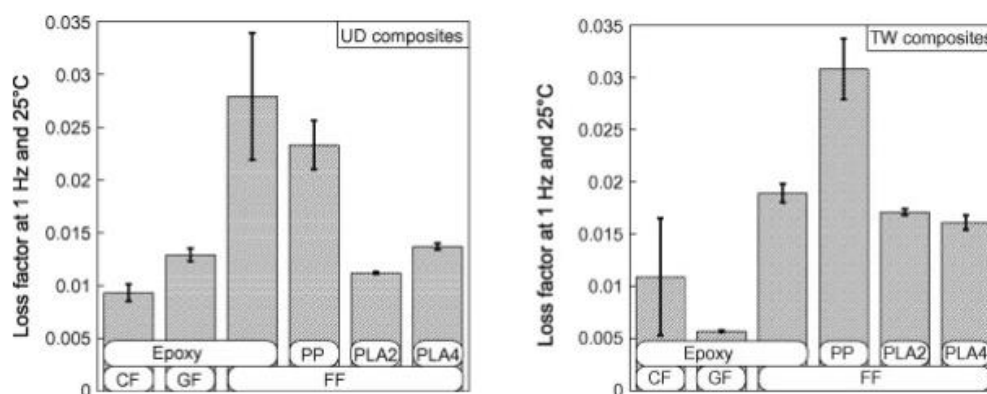


Figure 2-30 Loss factor at 1 Hz and 25 C for: a) UD composites and b) TW composites (Duc et al., 2014b).

Pothan and co-authors studied the dynamic characteristics of polyester reinforced with banana fibres. They reported maximum storage modulus for the neat polyester at lower temperatures i.e. in the glassy region, whereas at temperatures above T_g , the E' values are found to be maximum for composites with 40% fibre loading. This indicates that the incorporation of banana fibres in polyester matrix substantially induces reinforcing effects at higher temperatures. The incorporation of fibres lowers the loss modulus and damping peaks whereby the height of the damping peaks depended on the fibre content. An additional peak in the $\tan \delta$ curve at higher fibre content, suggesting micro-mechanical transitions due to the immobilized polymer layer was evident. These results were in agreement with a study on the dynamic and thermal analysis of vinyl ester matrix with alkali treated and untreated jute fibres (Ray et al., 2002). Increase of the jute fibre contents in the composite from 23%, 30 % to 35 % increases the E' values as a result of more interfacial stress transfer, on the other hand $\tan \delta$ values are observed to decrease after jute incorporation. Jute fibres restricted resin molecules mobility shifting T_g by 28 °C compared to that of vinyl ester. Alkali treatment of fibres for 4 h and 8h degraded the fibres as corresponding loss modulus value was highest in the 4 h treated composites with minimum defect concentration and decreased again in the 8 h treated composites, this could be due to the increased crystallinity index of the 8 h treated fibres, having higher defect concentration.

Other researchers studied the effects of fibre reinforcement with thermoplastic matrices and found similar trends, as stiffness increases with fibre contents increase due to its increased crystallinity but damping ratio decreases. Furthermore, fibre modification by chemical treatment improves fibre/matrix interlocking consequently good stress transfer at the interface level. DMA results of wood flour polypropylene (PP) composites, shows that the storage modulus improved and loss factor decreased in the presence of maleic anhydride grafted polypropylene (MA-PP) (Guo et al., 2006). Etaati et al., reported the same findings as the study focused on vibration damping characteristics of short hemp fibre reinforced with polypropylene composites with varying fibre contents (0- 60wt%) and compatibilizers (maleic anhydride-grafted polypropylene and maleic anhydride-grafted polyethylene octane) under applied frequencies of 1 to 200 Hz (Etaati et al., 2014). Dry and moisture-saturated samples of injection moulded jute reinforced with two kinds of PP homopolymer and maleic anhydride grafted PP (MAHgPP) were investigated for their thermal, dynamic mechanical and aging behaviour (Doan et al., 2007). The storage modulus of matrix modified composites showed an improved value compared with non-modified polypropylene at the same fibre content, for as prepared and for aged samples. (Rana et al., 1999) reported the same behaviour of short jute fibre reinforced polypropylene, as the storage modulus increases with increase in fibre content. Moreover, addition of compatibilizer improves molecular interaction between jute and MAPP further increase in values is also observed. Similarly, the transition, that is $\tan \delta$ peak, is shifted to higher temperature with fibre loading increase.

Viscoelastic properties of needle-punched (400 gsm) nonwoven surface modified (alkali treated) jute fibre with polypropylene composites and prepared through compression moulding having 23- 33 wt%

jute content were investigated (Karaduman et al., 2014). Both effects of the fibre loading and stacking sequence of nonwoven layers enhanced the storage and loss moduli due to the reinforcement. The interface adhesion characteristics between fiber and matrix were quantitatively analyzed using adhesion efficiency factor (A) and reinforcement effectiveness coefficient (C) (Karaduman et al., 2014).

Flax fibres received in tow form transformed into nonwoven by dry laying and mechanical entanglement (untreated or previously helium plasma treated) and unsaturated polyester (UPE) poured over then compressed under ambient temperature and 15 MPa pressure. DMA measurements were carried out in the single cantilever bending mode over a range of frequencies 1, 2, 5, 10 and 20 Hz (Gouanve et al., 2006). This study discussed the effects of plasma treatment and styrene content within the polyester resin on the dynamic parameters and relaxation in such a manner that the maximum rate of styrene used to build the UPE network is equal to 95% which was reduced to 88% with the presence of flax fibres. Furthermore, for a given temperature, the value of the relaxation time constant increases as the content of styrene decreases. However, the quantity of styrene which participated in the relaxation decreased in the presence of flax fibres.

Hodzic and co-authors reported storage moduli of untreated and silane treated flax reinforced with hydrophobic and hydrophilic PP of around 10- 12 GPa at 10 Hz frequency which was four times higher than that of the pure commercial PP. These values were far superior compared to those of flax reinforced PLA 1- 2 GPa. The hydrophilic PP – (hydrophobic) flax fibre system showed the best mechanical properties due to a polar bond contribution. The hydrophobic PP – (hydrophobic) flax system showed slightly inferior performance (Hodzic et al., 2002).

3. Literature Review – Part II: A review of Additive Manufacturing Techniques

3.1. Additive Manufacturing: Types, Technology and Challenges

3.1.1. Additive Manufacturing Techniques

The American Society for Testing and Materials (ASTM) classifies the AM techniques into seven main process categories of which some are currently commercially available and some in research and development stage whereas others are not currently developed. Table 3- summarises the AM technologies and their corresponding materials where it is clear that polymers are the most developed due to the ease of manufacturing.

Table 3-1 A summary of AM technologies and their corresponding materials

AM Technologies							
Materials	Powder Bed Fusion	Direct Energy Deposition	Material Jetting	Binder Jetting	Material Extrusion	Vat Photo-Polymerisation	Sheet Lamination
Polymers	Green	Red	Green	Green	Green	Green	Red
Metals	Green	Green	Yellow	Green	Yellow	Red	Yellow
Ceramics	Red	Red	Yellow	Green	Green	Yellow	Red
Composites	Red	Red	Red	Red	Green	Red	Green
Biological	Red	Red	Red	Red	Yellow	Red	Red

Commercially developed	Green	In R&D stage	Yellow	Not developed yet	Red
------------------------	-------	--------------	--------	-------------------	-----

Powder Bed Fusion (PBF): This process uses thermal energy from a laser or electron beam to selectively fuse powder in a powder bed; **Directed Energy Deposition (DED):** Utilizes thermal energy, typically from a laser, to fuse materials by melting them as they are deposited; **Material Jetting (MJ):** This process, typically, utilizes a moving inkjet-print head to deposit material across a build area; **Binder Jetting (BJ):** This process uses liquid bonding agent deposited using an inkjet-print head to join powder materials in a powder bed; **Material Extrusion (ME):** Push material, typically a thermoplastic filament, through a nozzle onto a platform that moves in the x, y, z plane, also known as the Fused Deposition Modelling (FDM); **Vat Photo-polymerization (Vat-P):** These machines selectively cure a liquid photopolymer resin in a vat using light, this process is also known as Stereolithography (SLA); **Sheet Lamination (SL):** This process uses sheets of material bonded to form a three-dimensional object (Li et al., 2016).

Methods of additive manufacturing (AM) have been developed to meet the demand of printing complex structures at fine resolutions. Rapid prototyping, the ability to print large structures, reducing printing defects and enhancing mechanical properties are some of the key factors that have driven the development of AM technologies. The most common method of 3D printing that mainly uses polymer filaments is known as fused deposition modelling (FDM). In addition, additive manufacturing of powders by selective laser sintering (SLS), selective laser melting (SLM) or liquid binding in three-dimensional printing (3DP), as well as inkjet printing, contour crafting, stereolithography (SLA), direct energy deposition (DED) and laminated object manufacturing (LOM) are the main methods of AM, full details are included in Table 3-2. The processes of additive manufacturing consist of various and complex physical phenomena including melting/solidification and vaporization, heat and mass transfer etc.

Table 3-2 Additive Manufacturing main process, materials, applications, benefits and drawbacks (Ngo et al., 2018)

AM Process	Materials	Applications	Benefits	Drawbacks	Resolution
Fused deposition modelling	Continues filaments of thermoplastic polymers Continuous fibre-reinforced polymers	Rapid prototyping Toys advanced composite parts	Low cost High speed Simplicity	Weak mechanical properties Limited materials (only thermoplastics) Layer-by-layer finish	50-200 μm
Powder bed fusion (SLS, SLM, 3DP)	Compacted fine powders Metals, alloys and limited polymers (SLS or SLM) ceramic and polymers (3DP)	Biomedical Electronics Aerospace Lightweight structures (lattices) Heat exchangers	Fine resolution High quality	Slow printing Expensive High porosity in the binder method (3DP)	80-250 μm
Inkjet printing and contour crafting	A concentrated dispersion of particles in a liquid (ink or paste) Ceramic, concrete and soil	Biomedical Large structures Buildings	Ability to print large structures Quick printing	Maintaining workability Coarse resolution Lack of adhesion between layers Layer-by-layer finish	Inkjet: 5–200 μm Contour crafting: 25–40mm
Stereolithography	A resin with photo-active monomers Hybrid polymer-ceramics	Biomedical Prototyping	Fine resolution High quality	Very limited materials Slow printing Expensive	10 μm
Direct energy deposition	Metals and alloys in the form of powder or wire Ceramics and polymers	Aerospace Retrofitting Repair Cladding Biomedical	Reduced manufacturing time and cost Excellent mechanical properties Controlled microstructure Accurate composition control Excellent for repair and retrofitting	Low accuracy Low surface quality Need for a dense support structure Limitation in printing complex shapes with fine details	250 μm
Laminated object manufacturing	Polymer composites Ceramics Paper Metal-filled tapes Metal rolls	Paper manufacturing Foundry industries Electronics Smart structures	Reduced tooling and manufacturing time A vast range of materials, Low cost, Excellent for manufacturing of larger structures	Inferior surface quality and dimensional accuracy Limitation in manufacturing of complex shapes	Depends on the thickness of the laminates

3.1.2. Additive Manufacturing Process and Technology

There are many different RP processes, but the basic operating principles are very similar. First, construct the CAD model to specify the physical object with 3D data as electronic information input. Typically a computer model achieved through a CAD package but can be also obtained from a physical model though digitising or scanning. Once the 3D data is available, the CAD model is then converted into STL file format, a file extension from STereoLithography. In STL format, the file consists of the X, Y, and Z coordinates of the three vertices of each surface triangle, with an index to describe the orientation of the surface normal. The capability to export CAD files into STL format is supported by most current CAD packages. The key advantage of using STL format is making the AM process more robust and reliable allowing the user to transfer the slicing operation into a routine of finding the interactions between lines and triangles. The File is then transferred to a software whereby the model can be sliced to form layers and generate support structures if needed as part of the print parameters specifications. Finally, the 3D physical model is produced then removed and post-processed where applicable.

3.1.3. Materials Development for Additive Manufacturing

In its early development, AM technology was applied to produce plastic prototypes, and many AM processes (i.e., SLA, SLS, FDM, 3DP) have been developed to produce parts with various plastics. After intense development and exploration, AM technology has become more and more capable of producing complex net-shaped or nearly net shaped parts in materials that can be directly used as functional parts including metals, ceramics and composites (Nannan GUO, 2013). To be successful, materials must be formed into proper feedstock, have appropriate characteristics for processing in the specific AM fabricator, and must have acceptable service properties. Enhancing materials performance and suitability for AM processes will remain a key ongoing research area. Reliability, traceability and the specific development of materials which have comparable properties to ‘bulk’ equivalents but are optimized to AM processes have formed the basis of significant levels of research. Research attention is currently focused on understanding the origin of defects in AM parts and eliminating them. These include porosity, binding defects (Utela et al., 2008), interfaces and microstructural effects (Singh et al., 2017). Bourell and co-authors detailed the process of appropriate materials selection as per individual AM process identified in the ASTM and based on extensive materials databases such that of Ashby. The review suggested adopting the manufacturability index as a measure of overall success of a particular material processability (Bourell et al., 2017). The index, whether qualitative or semi quantitative, would essentially be process specific and would therefore provide designers and developers with useful data for selecting materials for specific applications.

3.2. Additive Manufacturing: Global Market Trend

3.2.1. Market Value Growth

A substantial growth of the global AM market since 2010 as this industry' products and services expanded over the first decade of this millennium however it still only represents 0.02% of the global manufacturing activities estimated at \$25 trillion in 2014. Moreover, the use of 3D printers is expected to grow by a further 40% in the period 2010-2020 as more manufacturers embrace the AM processes for their numerous benefits, thus price per printer is forecasted to drop significantly. According the Wohler's report 2014, the global market value is expected to rise to \$21 billion in 2020 with average CAGR up to 30% ranging from 18% (Academics & Education) to 36% (Medical prosthetic device) for different market segments. This growth will contribute positively in overcoming the AM technical and commercial challenges. The AM market can be divided into two subcategories the industrial market and the DIY consumer market. The former includes users from commercial enterprises, ranging from larger scale (e.g. Airbus for components in their plane) to smaller scale (e.g. Beltone for its high valued hearing aids). These users will typically buy more advanced industrial AM systems that sell for \$5,000 or more. The latter includes users of small residential consumption or hobbyists who will normally buy home desktop systems under \$5,000. The academic researchers utilise both industrial and desktop AM machines to conduct AM research.

The global AM market in 2015 was dominated by the top five industries represented in Figure 3-1, with automotive sitting at the top of the list. Consumer products, business and industrial equipment, aerospace and prototyping captured majority of the market. In the scope of market projection up to 2025, the primary segments will maintain their strength with automotive holding a lead position and aerospace moving up to third place. A noticeable fast growth is forecasted for the medical sector including dental diagnostic and prosthetic devices.

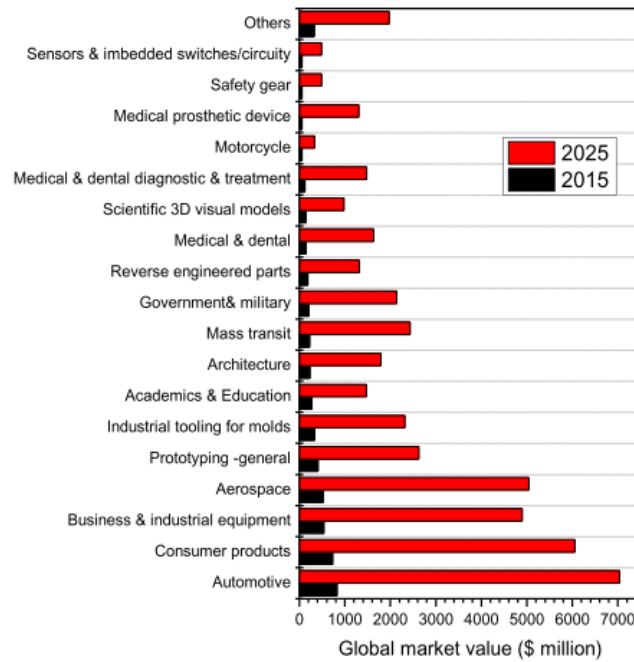


Figure 3-1 the projected market value from 2015 to 2025 for individual industries

The UK will follow the overall rising global trend in applications such as satellite parts production and aircraft components for the aerospace, also for the healthcare and medical sector e.g. orthopaedic implants, dental crowns. Other applications in creative industries e.g. tailored jewellery, furniture and motorsport sectors as most active in using AM technology with niche products being developed and sold on small scale. Energy generation and the remainder of the automotive sector are less proactive, for example in power generation, gas turbine manufacturers are happy to follow the lead of aerospace gas turbine technology research in the field of AM.

3.2.2. Additive Manufacturing in Research

Similarly, since the early 1980s, global research has seen a significant increase in the funding allocated for AM academic activities and subsequently the number of publications. With the EU allocating more than €160 million to fund research in the period of 2007-2013, this is mainly under the EU FP7 program up until 2013, after which it was replaced by the Horizon 2020 program. These funding schemes were fruitful as a total of publications per year in excess of 3000 globally with the USA, China, Germany and the UK being the four leading contributors with the highest amount of publications between 2014 and 2016. The UK is represented by the University of Sheffield, University of Nottingham and Loughborough University as they are identified as key players in AM research globally. The mostly widely studied AM technologies are identified as: SLM, FDM, SLA, SLS, and EBM, with the number of publications shown in Figure 3-2. It can be clearly noticed that SLM and FDM attracts the most interest being widely reported in literature.

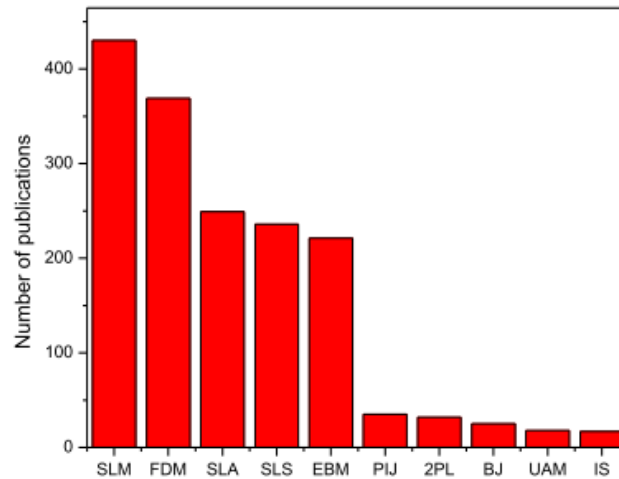


Figure 3-2 Quantification of the various AM techniques contribution in the global number of publications

3.3. Fused Deposition Modelling

The demand of printing complex structures at fine resolutions required the development of additive manufacturing (AM) methods in order to optimise some key factors such as the ability to print large structures while reducing printing defects and enhancing mechanical properties. The most common method of 3D printing is a type of extrusion-based AM as defined by ISO/ASTM 52900:2015, this process mainly uses polymer filaments which is known as fused deposition modelling (FDM). In 1992, Startasys Ltd (formerly Startasys Inc), pioneered this technology while Adrian Bowyer started the RepRap project with first online appearance in 2004, providing open source designs for FDM machines. Fused Deposition Modelling is a term trademarked by Stratasys, this process is synonymous to as Fused Filament Fabrication (FFF). In this method, a continuous filament of a thermoplastic polymer is used to 3D print layers of materials, see Figure 3-3 .

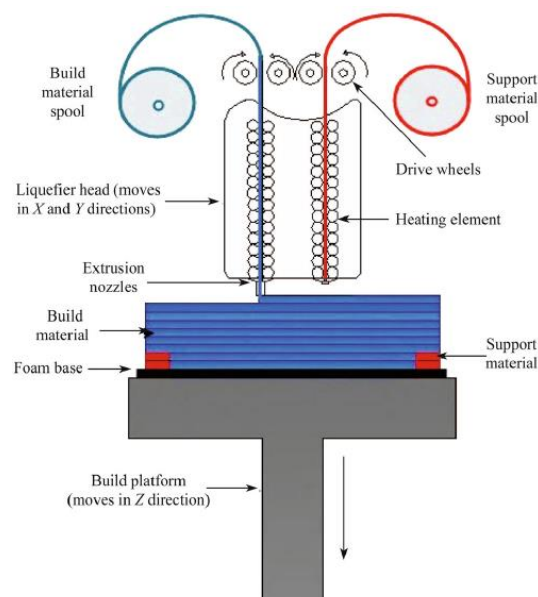


Figure 3-3 Schematic diagram of the fused deposition modelling method with dual extruder providing build support (Mohamed et al., 2015)

The nozzles are continuously fed with solid filaments through rotating gears which then deposit a thread of molten thermoplastic in orthogonal planar directions X and Y on a movable platform along the Z direction. The filament is heated at the nozzle to reach a semi-liquid state and then extruded on the platform or on top of previously printed layers. The thermo-plasticity of the polymer filament is an essential property for this method, which allows the filaments to fuse together during printing and then to solidify at room temperature after printing. The material is heated up to 1 °C above its melting point, so that it solidifies right after extrusion and subsequently welds to the previous layers (Bikas et al., 2016). As illustrated in Figure 3-3, the complexity of the desired geometry dictates whether a support structure is required whereby a second nozzle is employed.

3.3.1. Process Parameters

The quality of FDM processed parts mainly depends on careful selection of process variables, thus, it is imperative to identify the process parameters that significantly affect it. The layer thickness, width and orientation of filaments and air gap both in the same layer and between layers are the main, but not limited to, processing parameters that affect the mechanical properties of printed parts, Figure 3-4 shows all the process variables that need to be studied and optimized in FDM process. Low cost, high speed and simplicity of the process are the main benefits of FDM. On the other hand, weak mechanical properties, layer-by-layer appearance, poor surface quality, inter-layer distortion were found to be the main causes of this process limitations.

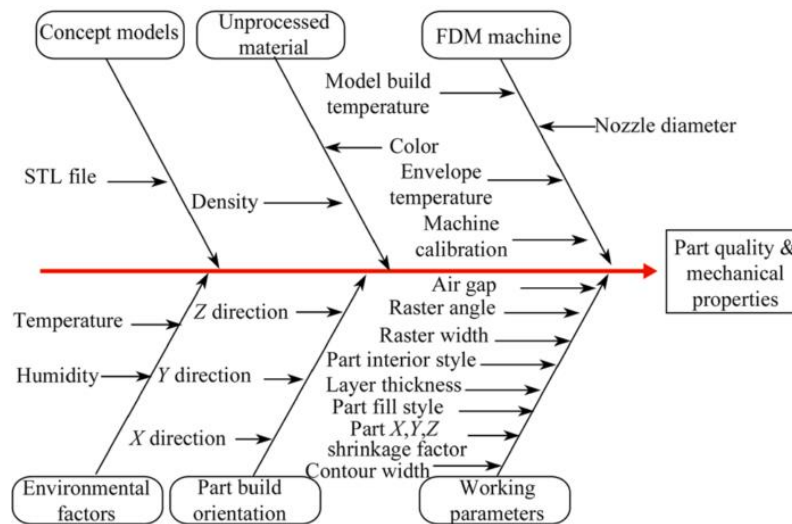


Figure 3-4 Fishbone diagram of the causes and effects of FDM process parameters (Mohamed et al., 2015)

(i) **Build orientation** refers to the way in which the part is oriented inside the build platform with respect to X, Y, Z axes as shown in Figure 3-5 b). (ii) **Layer thickness** is the thickness of layer deposited by nozzle tip, as shown in Figure 3-5 a). The value of layer thickness depends on the material and tip size. (iii) **Air gap** refers to the gap between adjacent raster tool paths on the same layer, as shown in Figure 3-5 c). (iv) **Raster angle** refers to the angle of the raster pattern with respect to the X axis on the bottom

part layer. Specifying the raster angle is very important in parts that have small curves. The typical allowed raster angles are from 0° to 90° . (v) **Raster width** is the width of the material bead used for raster. Larger values of raster width produce parts with stronger interior while using smaller raster width values reduce production time and material. The value of raster width varies based on nozzle tip size. (vi) **Contour width** refers to the width of the contour tool path that surrounds the part curves. (vii) **The number of contours** to build around all outer and inner part curves is shown in Figure 3-5 c). Additional contours may improve perimeter part walls. (viii) **Contour to contour air gap** refers to the gap between contours when the part fill style is set to multiple contours. (ix) **Perimeter to raster air gap** refers to gap between the inner most contour and the edge of the raster fill inside of the contour.

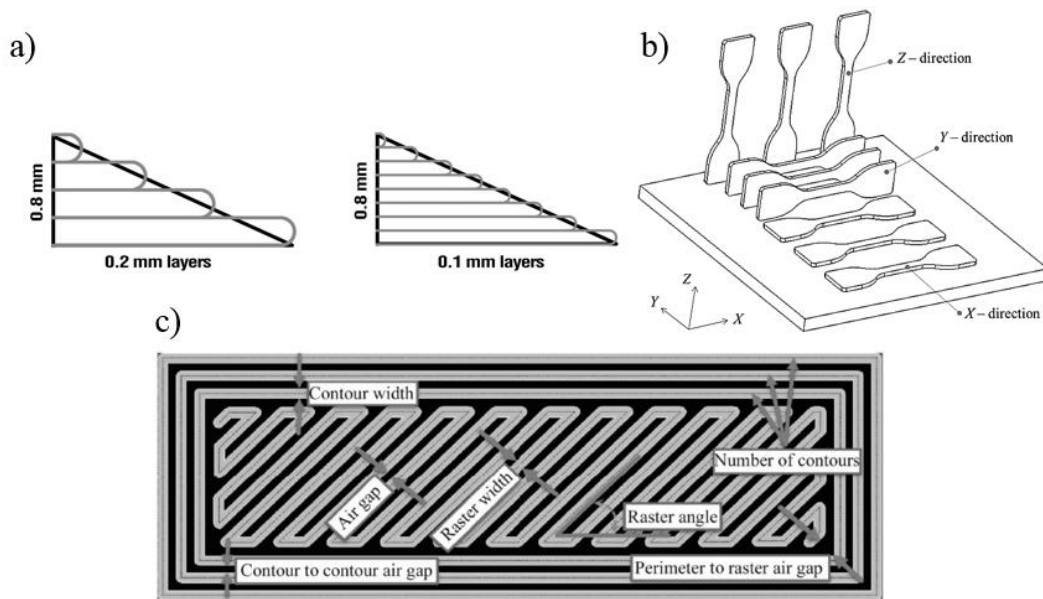


Figure 3-5 The FDM process variables: a) layer thickness, b) build orientation and c) nozzle path

Further parameters that can affect the quality and functionality of the printed parts are nozzle/printing temperature, deposition speed, build plate temperature, infill pattern, infill density and most importantly the material type (Ćwikła et al., 2017).

3.3.2. Effect of FDM Process Parameters: Process optimisation

FDM is a complex process that exhibits a large number of conflicting parameters that will influence the part quality and its mechanical properties. Therefore, the determination of the optimum process variables in the correct combination have been the focus of many researchers in recent years as it not only maximise the mechanical properties but also improve dimensional precision, avoid unacceptable wastes and large amount of scraps, enhance productivity rates and reduce production time and cost. Several studies optimised the FDM process parameters using statistical modelling methods and experimental data. Design of Experiment (DOE) is viable technique to reduce experimental sampling size for multiple levels of variables using the Taguchi method. The main objective of employing Taguchi method is to identify the general influence of each factor, then establishing whether higher or

lower values produce the preferred result and finally analysis of variance (ANOVA) to determine the relative percent of influence and significance of each factor. Notably, most reported investigations on process optimisation focused on acrylonitrile butadiene styrene (ABS P400).

Sood and co-authors studied the functional relationship between FDM process parameters (layer thickness, orientation, raster angle, raster width and air gap) and ABS P400 specimen. Strengths including tensile, flexural and impact from reduced experimental runs based on central composite design (CCD) and results displayed using response surface plots (Sood et al., 2010). While they reported less significant influence of layer thickness, build orientation and raster width on the considered mechanical properties (Sood et al., 2012), other parameters such as raster angle and air gap between two successive beads were proven to affect mechanical properties. It was found that increasing raster angle enhances tensile strength as confirmed by Vega and co-workers study which reported the highest tensile, flexural and impact strengths for samples with 90° raster angle, however, this orientation is referred to as 0° or arborator in Vega's paper (Vega et al., 2011). In another study (Dawoud et al., 2016) a raster angle layup of $\pm 45^\circ$ proved to offer maximum tensile and impact strength, whereas highest flexural strength was recorded for a 0°/90°. The dependence of FDM fabricated parts strength on the raster build orientation was explained by the anisotropic behaviour of these parts as reported in Ahn co-authors' study which also revealed that optimum tensile strength with 90° raster orientation and zero air gap (Ahn et al., 2002). A comprehensive parametric investigation on the effects of FDM process variables on 3D-printed tensile PLA samples (Lanzotti et al., 2015), confirmed the superior tensile properties (strength and modulus) of 90° specimen. Other variables influence were also investigated using an empirical model for tensile strength, a sequential approach to experimentation, based on central composite design (CCD) (Lanzotti et al., 2015). Raster build orientation is the direction of beads relative to the loading direction of the part. Therefore, it is important to take into account the variation of reference axis when reviewing discussions from literature on the raster orientation or angle effects. For example, if the beads are oriented along the tensile loading direction this raster angle is commonly referred to as 0°, however, others may report this orientation as 90°.

Air gap is the space between the beads, this parameter is typically set to zero by default meaning adjacent beads just touch. However it can be set at a positive value resulting in beads not touching which offers a rapid build process but produces loosely packed structure. On the other hand, a negative air gap produces partially overlapping beads resulting in a dense structure. There are different views regarding the impact of raster air gap on the FDM fabricated parts. A group suggests that a positive air gap was proposed to allow material flow towards adjacent layers thus contributing to the enhancement of mechanical properties (Sood et al., 2010). Whereas others claim the opposite stating a negative air gap between rasters, no less than -0.03mm to avoid excess material build up (Ahn et al., 2002), enhance the tensile properties. This phenomena was also reported and explained by the density increase of -0.05mm air gap FDM parts (Dawoud et al., 2016). From a cost perspective, the main reason to print

less than 100% infill parts is to reduce costs as printing time, energy and material consumption can be reduced to the extent without deteriorating drastically the strength of the partial-infill sample relative to the solid ones (Ćwikła et al., 2017). However, implementing high negative air gap increases raster overlap and consequently induces dimensional inaccuracy.

Correspondingly, increased number of contours effects on the tensile strength and stiffness was investigated from both the experimental and the numerical points of view, results from both methods revealed increase in properties with as little errors as 4% (Croccolo et al., 2013). A lack of literature regarding the effects of contouring on the fabricated parts strength, however it was emphasized that offset contours that followed the perimeter of the sample were used to relieve the stress concentrations (Ahn et al., 2002). Another study reported an increase in tensile strength with increased number of contours (perimeter shells) from 2 to 6 due to the increase in number of filaments aligned along the loading direction as the number of perimeters increase (Lanzotti et al., 2015).

3.3.3. Material Selection and Compatibility for FDM

Specific in-service properties, functional requirements and physical specifications of FDM fabricated parts for a given application necessitate the use of materials exhibiting acceptable microstructure and geometric tolerances, minimum porosity, reduced roughness and improved finish surfaces. Therefore, input material feedstock must be formed into a state compatible with FDM process nature. Categorically plastics are listed as amorphous and semicrystalline thermoplastics or thermosets. FDM being a material extrusion process, it is mainly used for amorphous polymers as it involves thermal layer adhesion, its large viscous softening temperature range makes it most suitable for successfully depositing the bead of plastic. These amorphous thermoplastic polymers, including ABS, Polycarbonate (PC) and their blends PC/ABS as well as PLA, Polyamide (polymer bound) and Polyetherimide (PEI) soften over a wide range of temperature up to the so called glazing temperature, forming a high viscosity material ideal for material extrusion through a narrow range of nozzle diameter (0.2–0.5 mm).

In contrast, the semicrystalline state is less desired for the FDM process due its narrow softening temperature range and uncontrollable flow characteristics during the extrusion process due to the abrupt change of the polymer's viscosity. Nevertheless, this class of materials can be still employed including, thermoplastic Polyurethane (elastomer for flexible parts), Polyetheretherkeytone (PEEK) and Polypropylene (PP). While PEEK is quite expensive and the need for a well-performing high temperature 3D printer (nozzle temperature 370- 410 °C) to achieve good quality parts, PP is considered challenging to 3D-print due to its high warpage.

Material extrusion processes (i.e. FDM) often require support structures to overcome the overhangs. This can be achieved through lattice scaffolding designs either using the same material with low strength connections to the actual part (single nozzle) or using dual nozzle head with the support made of wax-

based material or Poly-vinyl alcohol (PVA). The support structure is then removed by melting or dissolving as part of 3D-printing post-processing, a common combination is PLA with PVA water soluble supports.

3.3.4. Challenges and Limitations of FDM

Among the many possible challenges associated with FDM, one can find material related the most influential of all. As an example, since FDM relies on liquid fusion binding which is a rapid mass transport mechanism, low viscosity flow is a commonplace for plastics whereby a heated plastic is fused to the previous layer upon deposition. This phenomena makes the 3D-printed part prone to defects such as porosity which can be detrimental to the functionality of component. Void formation between subsequent printed layers can reduce interfacial bonding and thereby causing inferior and anisotropic mechanical properties. Moreover, since the FDM binding mechanism is driven by the temperature change, gravity and only capillary forces pores can be formed due to shrinkage, lack of fusion/melting/binding or material feed shortage. Distortion and delamination induced by warpage and deflection originating from stresses caused by the change in material volume. In FDM the large thermal gradient of the extruded filament causes contraction of some deposited layers and subsequently delamination and splitting of the part.

Poor surface finish as a consequence of various factors such as the staircase effect induced by the layer thickness and build orientation, coarse bead (raster) width as well as the filament spool aging if not appropriately stored in between operation. Atmospheric conditions including humidity and oxygen contents if not controlled can induce depolymerisation by oxidation and cause undesirable degradation of filament.

4. Materials and Methodology of Research

4.1. Natural Fibre Composites: Materials, Manufacturing and Testing

4.1.1. Selection and characterisation of materials and processes

The creation of biocomposites can be described as the insertion or reinforcing of natural bast fibres (NF), e.g. flax, hemp, kenaf or jute into bio-polymeric matrix in the form of cellulose, starch, lactic acid, furfural alcohol etc. In this research, one of the objectives is to produce a biocomposite system with different flax reinforcement textile styles, including unidirectional aligned, twill 2x2 (7ends/cm, 7picks/cm) and nonwoven mats. Different forms of matrix were used for the reinforcement namely PP (also compared to MAPP) films/slivers and PLA slivers for thermoplastics otherwise PFA and UPE represented the thermoset resins. Reinforcement was mainly developed and fabricated at Tilsatec (Wakefield, UK) while consolidation and various biocomposites manufacturing was performed at Netcomposites (Chesterfield, UK)

Thermal analysis may be regarded as the experimental procedures and examinations used to evaluate chemical, physical and structural changes a material experiences when exposed to a heat source. In principle, temperature is a fundamental state variable that affects most chemical reactions, physical properties and structural transformations. Thus, as a general concept, any scientific or technological characterization of a material, in which temperature is varied as an experimental parameter, could be considered as thermal analysis. However, this term has long been limited to specific techniques related to thermogravimetric and calorimetric effects also known as TGA and DSC respectively.

4.1.1.1. Differential Scanning Calorimetry

Differential scanning calorimetry (DSC) is a technique widely used in the study of thermal characteristics such as mass state transitions and reactions that a substance experiences when exposed to heat. Identifying these characteristics is very important in order to put the materials into production and achieve the performance required, such as glass transitions, melting points, crystallisation point and other physical and chemical reactions. The mechanism of DSC as illustrated in Figure 4-1, the working principle is measuring the heat flow difference between a sample and a reference. The DSC is equipped with two crucibles in one of which a specific amount of material is required to yield acceptable results. There are two types of crucibles that can be used in thermal analysis DSC, open pan and closed pan. Typically crucible are made of alumina or aluminium, for which calibration is required to obtain the thermal correction constants.

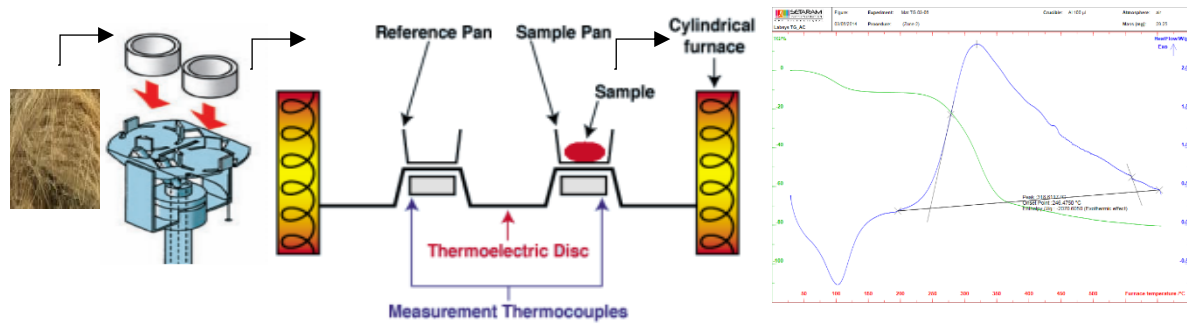


Figure 4-1 Schematic illustration of DSC working principle and mechanism

As part of the biocomposite production process such that of compression moulding, the thermoplastic based mainly, polymeric fibres are heated to their melting temperature to bond the loose fibres and crystallise by cooling to form a rigid panel. Therefore, by performing DSC tests on polymeric fibres that involves heating the samples gradually to a certain temperature (this is decided according to the polymer nature), then cooling it down at different rate to investigate the different transitions associated with this cycle.

Thermoplastic fibres were filled in alumina Al₂O₃ crucible of 100 µl capacity then placed on a gravitational scale within a combined capability TGA/DSC SETARAM Labsys 1600 (Caluire, France). The experiment involved heating a mass of 25 (±5mg) from ambient temperature to high temperatures to capture all thermal transitions and their corresponding enthalpies as shown in Figure 4-2. The aim to carry out these scans is to identify the melting temperature to design the appropriate composite manufacturing process ensuring using appropriate parameters. Furthermore the degree of crystallinity is another vital property to affect the composite manufacturing, the crystallinity can be calculated using the following relationship in Eq. (4-1):

$$X_c (\%Crystallinity) = \frac{\Delta H_m}{\Delta H_{m100\%}} \times 100 \quad \text{Eq. (4-1)}$$

where ΔH_m is the enthalpy of fusion under melting and is obtained via integration of the corresponding endothermic peak of the melting, and $\Delta H_{m100\%}$ is the melting enthalpy of a totally crystallized thermoplastic sample.

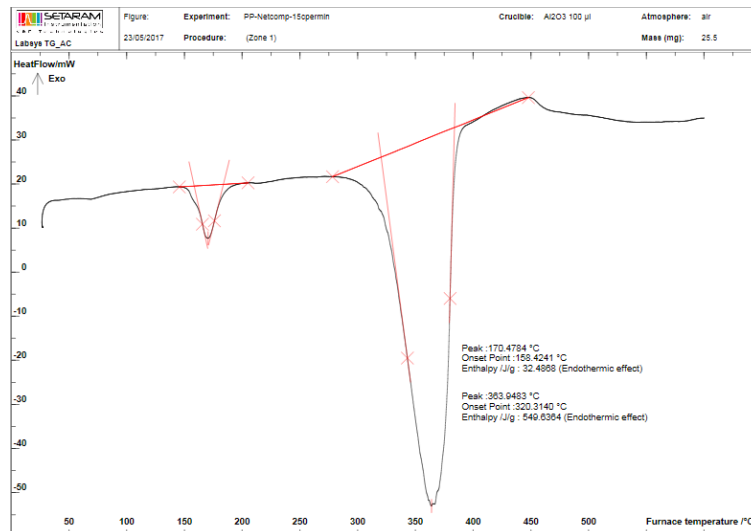


Figure 4-2 A sample signal of a DSC scan for PP fibres 30 -700 °C at heating rate of 10 °C/min covering melting and degradation phases

A typical DSC thermogram of a thermoplastic such as PP and PLA manifests distinctive heat flow deviations (endothermic and exothermic) from a baseline indicating specific events such as glass transition, melting, crystallisation and pyrolysis. It is worth noting that some transitions do not appear explicitly and it may be difficult to identify them due to the heating rate i.e. for fast heating scans. For the case of PP as shown in Figure 4-2, two distinct endotherms that indicates melting at temperature peak of 170 °C and degradation at temperature peak of 383 °C. Although, polymer reference materials with 100 % crystallinity are rarely available for comparison purposes. However, the heats of fusion values for 100 % crystalline polymers may be determined by indirect methods such as extrapolation using the Flory equation. The melting enthalpy of 100% crystalline PP as published by TA Instruments Technical Note is $H_m = 207 \text{ J/g}$ (Blaine, 2002) while a 100% crystalline PLA has $H_m = 93 \text{ J/g}$. Therefore, for instance by taking the experimentally measured melting enthalpy as 32.4J/g and then applying Eq. (4-1) the degree of crystallinity of PP fibres ($X_c\%$) = 15%. Likewise, PLA crystallinity is found to be 33% as the melting enthalpy was experimentally evaluated at 31.1J/g.

These results demonstrate that both polymers have amorphous characteristics, but as these undergo heating cycling during processing or annealing a more crystalline structure can be achieved. Previous studies have shown that incorporating natural fibres with such thermoplastics of semicrystalline nature promotes the crystallisation process as their surface roughness and topography act as nucleating agents.

4.1.1.2. Thermogravimetric Analysis

Fibres and polymers, mainly thermoplastic category, are processed into a biocomposite through heating to a certain temperature high enough to initiate melting. It has been established in literature that natural fibres in general and flax in particular is susceptible to thermal degradation as temperature reaches 200 °C (Baley et al., 2016). Isothermal exposure of flax fibres and PP slivers using the same equipment and method described in the previous section 4.1.1.1 was conducted. A range of temperatures from 160°C

which the lowest limit for melting to initiate up to 240°C which is considered above the first degradation stage of flax fibres, time of exposure can also be a factor causing detrimental degradation.

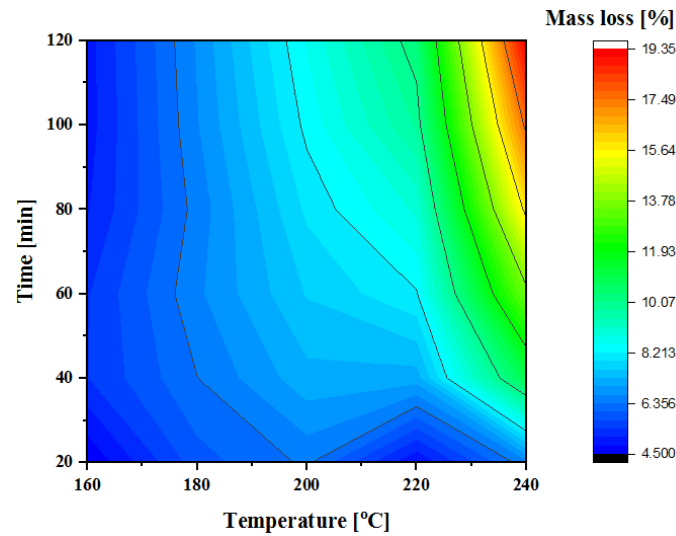


Figure 4-3 Mass loss % of flax fibres under isothermal exposure

Figure 4-3 and Figure 4-4 represent the mass losses of flax and PP fibres respectively. For the polymer, above the melting temperature 160-180°C it starts to endure thermal degradation that is dependent on the temperature as well as the exposure duration. As the temperature approaches 240°C, degradation becomes more pertinent >5% for periods as short as 40mins while the highest mass loss >20% at this temperature when exposure reaches 2 hours. In parallel, flax fibres exhibit less thermal stability with magnified effect of temperature and exposure time as the highest mass degradation recorded for maximum temperature 240°C and 2 hours exposure is found to be almost doubled of that of PP. Therefore, during thermal consolidation of these materials together to produce the natural fibre composite, it is permissible to use a temperature in the range of 160-190°C for a cycle of no more than 40 minutes before degradation of flax fibres initiates.

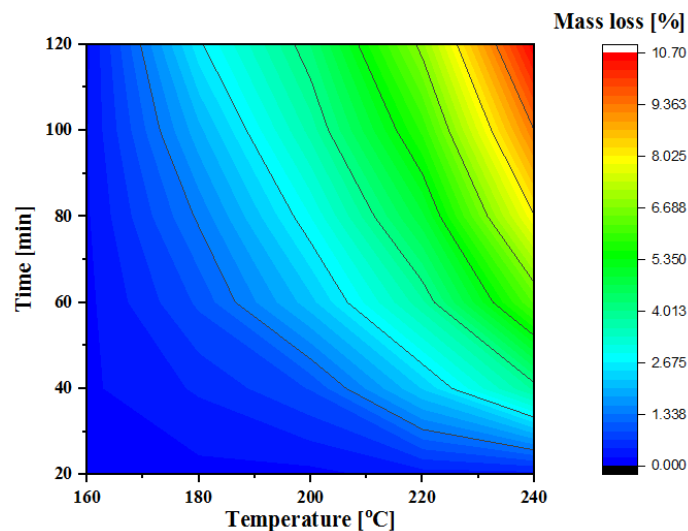


Figure 4-4 Mass loss % of PP fibres under isothermal exposure

4.1.1.3. Scanning Electron Microscopy

A scanning electron microscope (SEM), JEOL JCM-5700 CarryScope operated at an accelerating voltage of 20kV. The samples were sputter-coated with a gold, gold-palladium layer before taking the images to prevent charging, this was achieved using Sputter Coater EMITECH (Quorum Technologies, East Sussex, UK). The thickness of the sputter-coated layer had a thickness about 10–15 nm. These images were used to examine the microdefects and general microstructure of individual flax fibres, as illustrated in micrographs presented in Figure 4-5. As discussed in the literature chapter, kink bands or fractured fibres will inherently affect the biocomposite when subsequently reinforced with polymers.

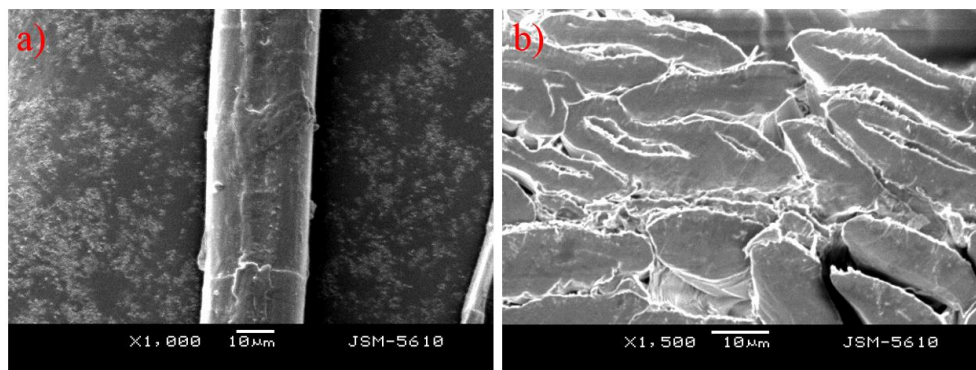


Figure 4-5 SEM images of flax fibre: a) outer surface of the fibre (elementary) with no visible micro-defects along its length, b) cross section of (technical) fibre showing a compacted number of microfibrils that provide tensile strength.

4.1.1.4. Fourier Transform Infrared Spectroscopy

Fourier Transform Infrared Spectrum is a technique widely used in the materials science including solids, liquids and gases whereby different engineering materials such as polymers and fibres whether natural or petrochemical based. There are three types of FTIR spectrometers depending on the required range of Infrared region; near-infrared region ($12800 - 4000 \text{ cm}^{-1}$), mid-range region which is the most commonly used region ($4000 - 400 \text{ cm}^{-1}$) and far-infrared region ($30 - 400 \text{ cm}^{-1}$). In the current study, a PerkinElmer® spectrum 100 mid-range region with spectral resolution of $0.4 - 64 \text{ cm}^{-1}$ and wavelength accuracy of $\pm 0.1 \text{ cm}^{-1}$ ($\pm 0.02 \text{ cm}^{-1}$ achievable) was used for the structural characterisation. Samples of bast flax fibres and polypropylene (MAPP as well) slivers were scanned in transmittance mode from $4000 - 500 \text{ cm}^{-1}$ to determine the composition and evaluate the potential chemical bonding mechanisms when these are consolidated into composites. Figure 4-6 depicts the main peaks indicating various chemical bonds of the flax fibre constituents.

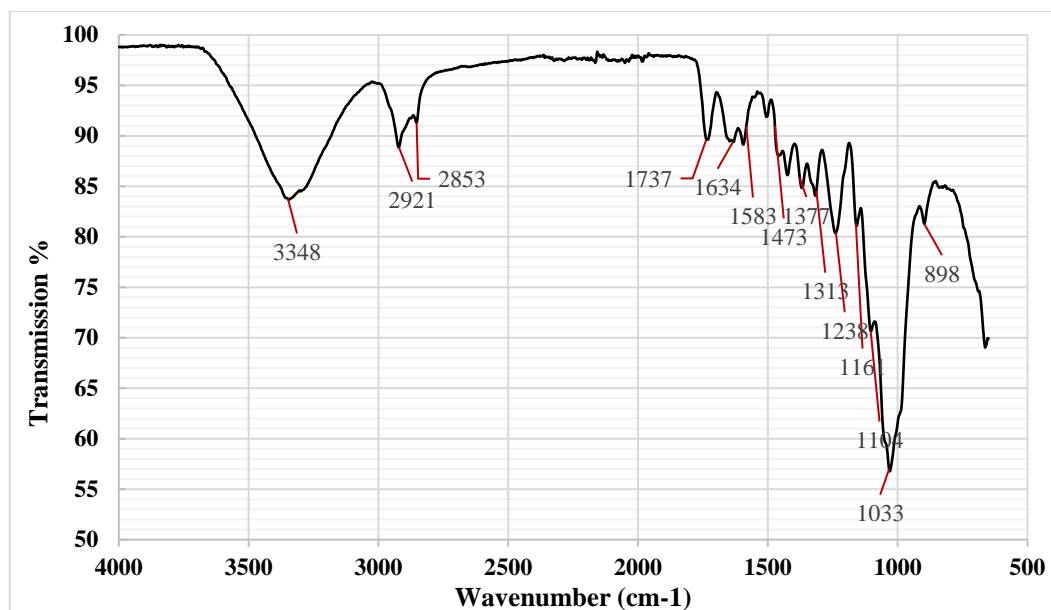


Figure 4-6 FTIR spectra of flax fibres

Infrared spectra of flax are displayed, a broadband spectra observed in the range $3350-3300\text{ cm}^{-1}$ which is associated with the presence of the polysaccharides hydroxyl as a result of the O–H linked shearing (Zaini et al., 2013). Also the double peaks at 2921 and 2853 cm^{-1} due to the C–H symmetrical stretching which indicates the presence of polysaccharide and the CH_2 symmetrical stretching indicating the existence of wax (Le Troedec et al., 2008). Several peaks have been recorded below 2000 cm^{-1} and are linked to various compounds vibrations. The peak recorded at 1737 cm^{-1} is related to the unconjugated stretching of carboxylic acid or ester (Hemicellulose) C=O (Biagiotti et al., 2004b). Water (OH) is detected at a waveband 1634 cm^{-1} , as commonly reported in several studies (Nacos et al., 2006) (Biagiotti et al., 2004b) (Le Troedec et al., 2008). The symmetrical stretching of the aromatic compound C=C is observed in the vibration peaks at 1591 and 1634 cm^{-1} referring to lignin contents. The presence of pectin, lignin, hemicelluloses and calcium pectates is noticed within the significant peak at 1425 cm^{-1} due to the CH_2 symmetric bending and C=C stretching in aromatic groups. Similar response in a study carried out by Sun and co-authors (Sun et al., 2005), as the vibration peak logged at 1473 and 1377 cm^{-1} due to the in-the-plane C–H symmetric and asymmetric bending of polysaccharides respectively.

Figure 4-7 represents the wideband spectra of polypropylene fibres, the bands at 1456 cm^{-1} and 1376 cm^{-1} are the characteristic of polypropylene as these respectively refer to deformation vibration asymmetrical and deformation vibration symmetrical of the CH_3 . The bands at 2950 cm^{-1} , 2917 cm^{-1} , 2868 cm^{-1} and 2838 cm^{-1} are respectively associated with CH_2 asymmetrical stretching vibration, CH_3 asymmetrical stretching vibration, CH_3 symmetrical stretching vibration and symmetrical stretching

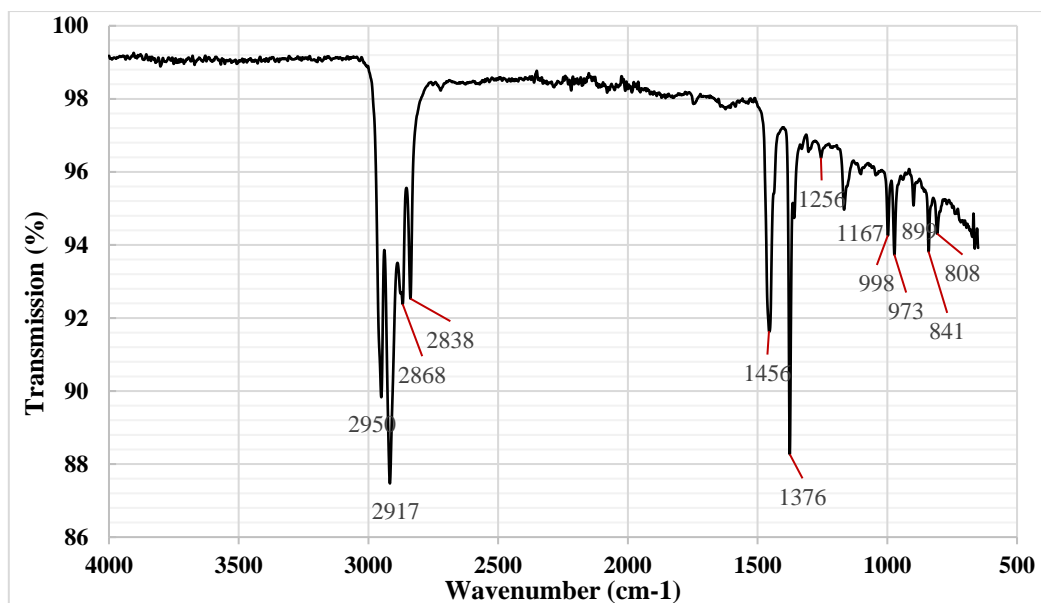


Figure 4-7 FTIR spectra of polypropylene

vibration of CH_2 . With multiple peaks in the range $1400\text{--}750\text{ cm}^{-1}$ of which bands between $1300\text{--}865\text{ cm}^{-1}$ refer to carbon lattice pulsation. Bands 1359 cm^{-1} and 1305 cm^{-1} indicate wagging vibration of $\text{CH}_2\text{-CH}$ and CH_3 whereas 1167 cm^{-1} is for deformation vibration of CH_2 . In the case of MAPP as seen in Figure 4-8, all peaks detected for the PP are also detected for MAPP in addition to absorption band observed at 1750 cm^{-1} which is assigned to the absorption of carbonyl groups (C=O) of MA.

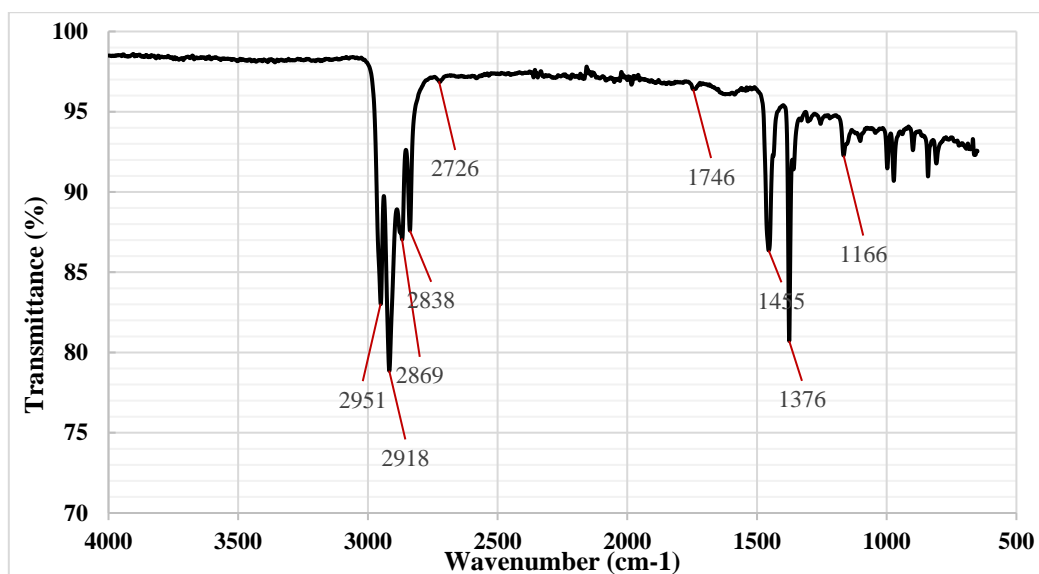


Figure 4-8 FTIR spectra of MAPP

4.1.2. Continuous - Unidirectional tape

4.1.2.1. Thermoplastic based biocomposites

i. Tape Production

Development of natural fibre-based tapes with thermoplastics also known as Natural fibre Mat Thermoplastics (NMT) for the biocomposite production have been carried out at Tilasatec whereby commingled blends were trialled. The combination consisted of a number of reinforcements using primarily flax fibres with various matrix types. Trials were aimed at developing fibre spreading and aligning specifically identifying the machine speed, temperature for thermal consolidation and air pressure requirements; hence optimising the process and quality of the final product. The process of fibre commingling consists of firstly the fibre staples (natural fibre i.e. flax and matrix i.e. PP, MAPP and PLA) conversion into continuous slivers, followed by comingling of the slivers as shown in Figure 4-9a). In the diagram, eight slivers are assembled in a creel then fed into two sets of rollers, back and front spaced 230 mm apart as the gear assembly was modified to adjust the tension between the creel and back rollers. The comingled slivers will form a blend as seen under the microscope and illustrated in Figure 4-9b) to be then passed into the straightening stage in the machine to be spread and aligned, this takes place between the back and front rollers, as shown in Figure 4-10.

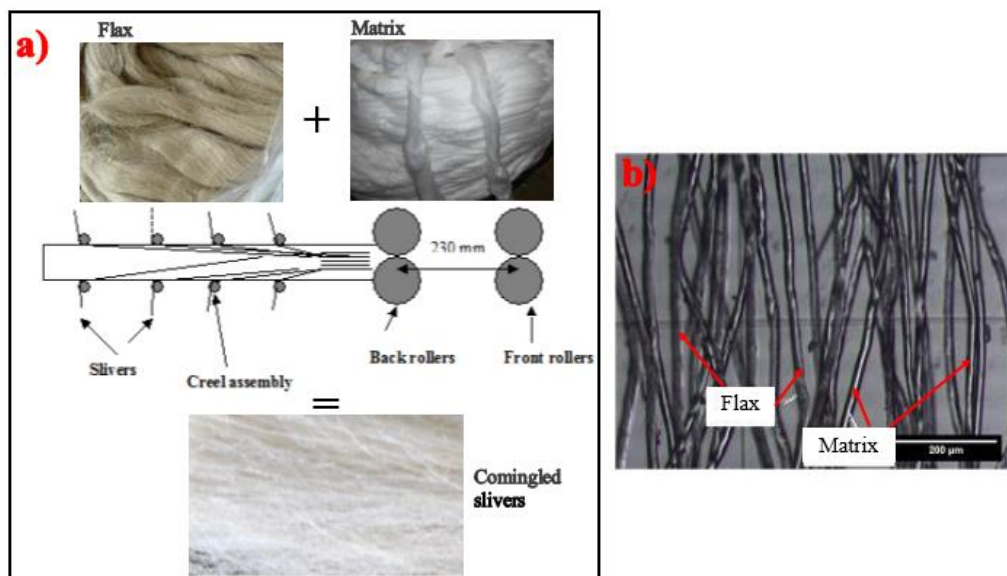


Figure 4-9 a) Commingling process of flax staples and matrix staples, b) microscopic image of comingled slivers

Straightening the sliver assembly is important via spreading and alignment process whereby for good results correct amount of draft is required. Drafting, also called drawing, in yarn manufacture, process of attenuating the loose assemblage of fibres called sliver by passing it through a series of rollers, thus straightening the individual fibres and making them more parallel. Each pair of rollers spins faster than the previous one. Optimum draft values vary for different types of fibres and slivers weight. In this study, several attempts have been carried out to understand the effect of draft on the blend composition,

values of draft ratios and designations are presented in Table 4-1. Higher draft ratio values break the slivers whereas lower values yield poor spreading and alignment. Images from the process in operation are shown in Figure 4-10.

Table 4-1 Draft ratio values for the 8 rollers in the slivers blend process

		Rollers draft ratios							
Roller		1	2	3	4	5	6	7	8
1 st		2.10	2.07	2.03	1.98	1.94	1.90	1.86	1.82
2 nd		1.83	1.80	1.76	1.72	1.68	1.64	1.62	1.58
3 rd		1.59	1.56	1.53	1.50	1.47	1.45	1.44	1.39
4 th		1.38	1.36	1.33	1.30	1.28	1.26	1.23	1.21



Figure 4-10 The straightening stage of blended slivers: a) top and bottom fallers placed between roller, b) closer image of the bottom fallers, c) spread and aligned fibre web

The final stage of the tape production is thermal consolidation process of the commingled slivers already blended during the drafting phase whereby appropriate parameters were optimised were identified. These parameters were: *i*) machine speed i.e. feed speed at 3-4 m/min, *ii*) maximum temperature of 220 °C to avoid fibre degradation, *iii*) air pressure of 7 mbar (700 Pa), *iv*) calendar pressure of 2 bar, *v*) contact dwell time (CDT) 0.7-0.9 seconds as feed speed decreases from 4 to 3 m/min calculated from Eq. (4-2), similarly, *vi*) heat dwell time (HDT) 0.91-1.2 seconds calculated from Eq. (4-3). The complete process produces a thin tape ready for composite panel fabrication as summarised in Figure 4-11. The need to produce flexible tapes requires the addition of veils which can be either random glass fibres (17gsm) producing hybrid tapes, or PP fibres (12gsm) also PE/PP bi-component can be used. Initial trials to use flax/glass veils produced tapes of 450gsm with 80% fibre wt%, this was primarily directed to the production of thermoset panels as described in the next section.

$$\text{Contact Dwell Time (CDT)} = \frac{\text{Contact Area}}{\text{Delivery/feed speed}} \quad \text{Eq. (4-2)}$$

$$\text{Heat Dwell Time (HDT)} = \frac{\text{Heating Length}}{\text{Feed Speed}} \quad \text{Eq. (4-3)}$$

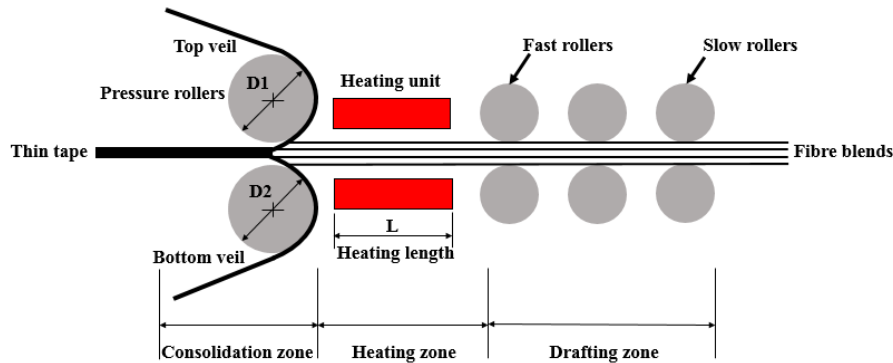


Figure 4-11 A summary of the holistic process of individual slivers of flax and matrix into a comingled thin tape for biocomposite production

An example of these trials is comingled pre-impregnated blends of flax/PLA developed at Tilasatec using a Poly (L -lactide) acid (PLA) based on lactides attained from corn starch fermentation. Aligned flax fibres and PLA fibres were spread with few blend fibre to matrix weight ratios (40/60, 50/50 and 60/40). Preliminary mechanical results suggested further investigation of the 55/45. The continuous reinforcement used was the combination of flax sliver of 1.45 g/cm^3 fibre density and PLA sliver with 1.25 g/cm^3 blended into tape making unit. Once the fibres are aligned and the required blend weight fraction is on target, the tape was produced by thermal consolidation with a machine speed 3 m/min and operating temperature of $165 \text{ }^\circ\text{C}$ resulting in the consolidated part of average tape areal weight 176 gsm and reduced thickness of approximately 0.3 mm from 0.8 mm due the pressure exerted on the blend within the rollers. This process is illustrated in Figure 4-12.

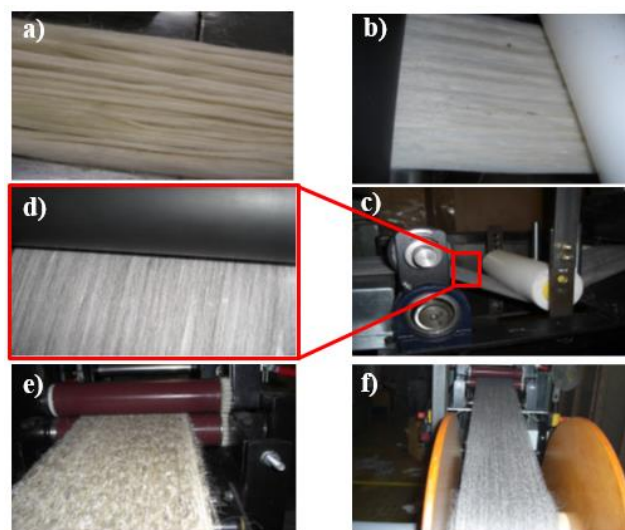


Figure 4-12 The process of thermal consolidation of aligned flax fibres and PLA to produce the Flax/PLA blended tape: a) Flax/PLA input blend, b) Flax and PLA being spread, c) the process of rolling the spread blend, d) a close image of pre-consolidated tape, e) thermal consolidation with the application of pressure between two heated rollers, and f) tape winding unit.

ii. Flat panels production

Initial stage of this research was dedicated to experimenting a variety of materials combinations as well as their processing parameters in order to optimise the final chosen panel for the subsequent holistic testing for full characterisation. The details of these materials and corresponding process parameters are included in Table 4-2, the only process adopted in panels production is the compression moulding using the thermal press shown in Figure 4-13a). A compression moulding machine consists of the main frame unit, pump unit, heating and cooling unit. This technique enables obtaining composites with higher amounts of fibre reinforcement (Fages et al., 2012).

The aforementioned Flax/PLA tape is considered as a reference to describe the compression moulding process. The next stage of the process is the composite thermal consolidation whereby samples of rectangular geometry were prepared at NetComposites using a hot press moulding process with 16 layers with 0°/90° balanced and mirrored for the 3 mm final thickness plaque as shown in Figure 4-13c). The panels were moulded at 175 °C and held at maximum temperature for 20 mins under a pressure of 20 bar before cooling the samples to room temperature. The composite density was calculated using Eq. (2-2) at 1.3-1.35 g/cm³. The fibre volume fractions were also calculated using Eq. (2-3). The process of compression moulding for all was as follows:

- PET sheets were used as non-stick material to avoid sample sticking to the mould after cure. The required number of layers (this depends on the desired thickness) were wrapped within PET sheets.
- The stacked layers with the PET easy release sheets were then sandwiched between the two mould unit metal platens and the hot press was switched on with the target temperature set.
- The pressure control valve of the hydraulic pump unit was opened to release the pressure when the temperature was raised to 100 °C, and then moving the bottom platen down creates an open space between platens for the sample. The contact between platens and sample happens at this temperature to avoid the instantaneous melting effect of the thermoplastic matrix during the process temperature which ranges between 165–180 °C considering all types included in Table 4-2
- Once the melting temperature of the matrix was achieved, the pressure was increased to reach the pre-set moulding value and maintained throughout the length of sample consolidation under the effect of temperature as well.
- After the completion of the moulding cycle as shown in Figure 4-13 b), the heat is removed and cold water is pumped around the mould cavities to cool down the sample to room temperature under maintained pressure effects.
- Once stabilised at room temperature, by releasing the hydraulic pressure, the mould platens are moved apart to allow the removal of the consolidated panel.

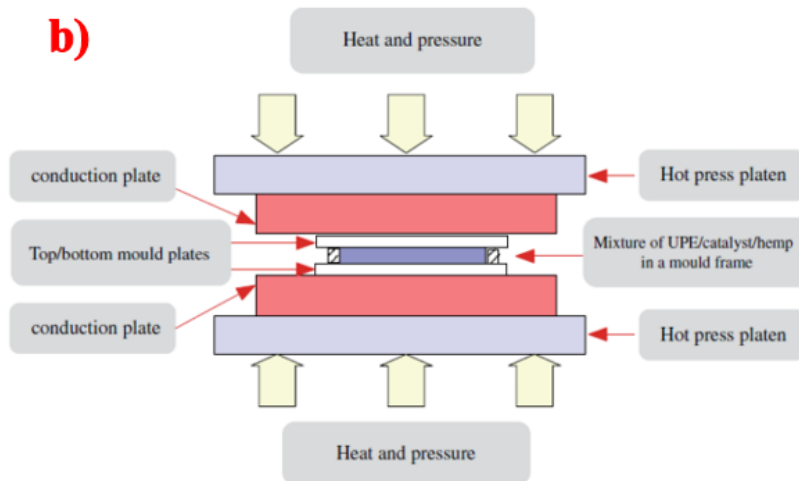
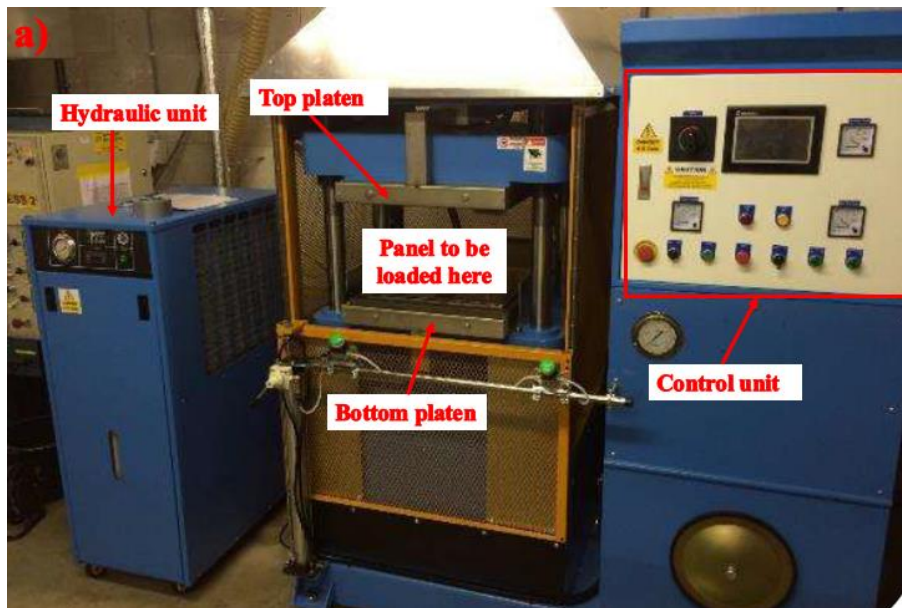


Figure 4-13 Production of Flax/PLA panels out of comingled thin tapes: a) thermal press for thermal consolidation of panels, b) schematic representation of the heated consolidation zone, c) consolidated panels of three Flax/PLA ratios pressed at 170 °C and 20 bar for 20 minutes.

Table 4-2 Complete list of continuous thermoplastic based biocomposites considered in this research, materials types, processing parameters and reinforcement arrangements

Reinforcement Type	Matrix	Fibre/Matrix wt%/wt%	Tape areal weight (gsm)	Consolidation arrangement	Press Pressure (Bar)	Press Temperature (°C)	Press Time (mins)	Fibre Volume Fraction ^c V_f (%)	Density ^c (g/cm ³)
Flax 2x2 twill	PP	50:50	400	12 layers of 0.3mm ply thickness	20	180-200	20	37.5	1.12
(For reference only ^a)	MAPP	50:50	400	12 layers of 0.3mm ply thickness	20	180-200	20	37.5	1.12
	PLA	50:50	400	12 layers of 0.3mm ply thickness	20	180-200	20	40	1.34
		40:60	170	12 layers, 0°/90° balanced, mirrored	20	175-180	20	29.3	1.06
	MAPP	50:50	170	12 layers, 0°/90° balanced, mirrored	20	175-180	20	38.3	1.11
		60:40	170	12 layers, 0°/90° balanced, mirrored	20	175-180	20	48.2	1.16
	Flax UD tape ^b	PLA	40:60	176	16 layers, 0°/90° balanced, mirrored	20	165-170	20	36.5
50:50			176	16 layers, 0°/90° balanced, mirrored	20	165-170	20	46.3	1.34
60:40			176	16 layers, 0°/90° balanced, mirrored	20	165-170	20	56.4	1.36
PP		55:45	175	16 layers, 0°/90° balanced, mirrored	15	175	20	51.3	1.35
		50:50	150	16 layers, 0°/90° balanced, mirrored	15	180	20	38.3	1.11
		50:50	150	16 layers, UD	15	180	20	38.3	1.11

^a For comparison, Biotex 400gsm 2x2 Twill Flax Fibre were used, fibre density of 1.5 g/cm³. These reference samples were only tested for their tensile properties, strength and stiffness.

^b the UD tapes were processed through slivers commingling of flax fibre (density 1.45 g/cm³) and either PP (density 0.9 g/cm³), MAPP (density 0.9 g/cm³) or PLA (density 1.25 g/cm³)

^c The densities and V_f of all panels produced are theoretically calculated from Eq. (2-2) and Eq. (2-3)

4.1.2.2. Thermoset based biocomposite

The fabrication of thermoset based biocomposites focused on two types mainly for comparison purposes namely unsaturated polyester resin (UPE) and polyfurfuryl alcohol (PFA) sourced from East Coast Fibreglass Supplies (Newcastle, UK) and TansFurans (TFC) Chemicals bvba (Geel, Belgium) respectively. While the former is partially bio-based the latter is 100% bio-based typically from agricultural wastes e.g. sugarcane.

Unsaturated Polyester: Among the desired properties when handling and using thermoset resins is the pot life and gel times, UPE Crystic 701PA a pre-accelerated isophthalic polyester resin was selected due to its low viscosity and controllable exothermic characteristics. Furthermore, these characteristics make it particularly suitable for the manufacture of large structures by vacuum injection methods. Additionally, Crystic 701PA have excellent strength retention in wet environments and very compatible for use with various reinforcement types including natural fibres. The manufacturer's recommendations indicate the best methods and conditions when handling Crystic 701P, the user is to allow the resin to attain the workshop temperature which should be stabilized at 18- 20 °C. For optimum results in no circumstances the resin, the mold or the workshop temperature is below 15 °C before curing is carried out. To initiate the curing, catalyst M (Butanox M50) is recommended to be added in small amounts of 1-2 % depending on the required crosslinking speed. For effective use the catalyst should be thoroughly mixed with the resin to be fully incorporated either manually or using a low shear mechanical stirrer where possible. It is widely accepted that in order to accelerate the cure cycle of polyester resin, a maximum possible amount of catalyst needs to be added up to a limit at which handling time is significantly reduced hence low processability. For instance, for Crystic 701PA, if cure is carried out at the lowest temperature (15 °C) a minimum of 2% of M catalyst is required to initiate the crosslinking process which lasts for 149 minutes as specified in the datasheet. This is considered the worst case scenario and processing times are reduced as temperature increases. The full list of this Crystic 701PA resin properties and curing formulations are summarised in Table 4-3.

Table 4-3 Typical physical and mechanical properties of Crystic 701PA tested in accordance with appropriate BS or BS EN ISO standards

Property	Crystic 701PA ¹
Appearance (Liquid resin)	Mauvish
Viscosity at 25 °C [poise]	1.6
Specific gravity at 25 °C	1.11
Gel time at 25 °C with 1% catalyst [minutes]	85
Deflection temperature under load² (1.80 Mpa) [°C]	75
Water absorption [mg]	10
Tensile strength² [MPa]	66
Tensile modulus² [MPa]	3580
Elongation at break [%]	2.5
Barcol Hardness	35

¹ Unfilled casted resin was fully cured in the following schedule: 24 hrs @ 20 °C, 3 hrs @ 80 °C

² Specimen tested in tensile mode were cured as follows: 24 hrs @20 °C, 5 hrs @ 80 °C, 3 hrs @ 120 °C

Polyfurfuryl Alcohol: Continuous effort has been dedicated towards the development of high performance thermosets based on renewable resources, PFA in particular attracts much attention due to its highly ecological properties being carbon neutral and fully non-toxic. BioRez 080101 supplied by TFC bvba is a self-crosslinking resin with high compatibility to natural fibres containing 78- 80 wt% of furfuryl alcohol prepolymer and diluted in 20-22 wt% water with very small amount of free furfuryl content (<0.5 wt%). This BioRez has a density of 1.33 g/cm³, a shelf life of 3 months at room temperature but storage stability is extendable if the resin is refrigerated. The dilution in water is required to reduce the viscosity to facilitate its use and handling in composite production processes. Typical viscosity values measured at 20- 25 °C range between 100- 200 cP (1- 2 Poise), these values increase during storage at room temperature from initial value of 147 cP to 179 cP after two weeks then 186 cP and 208 cP after three and four weeks respectively. However, a process limitation associated with the high water contents in particular during the processing of fibre reinforced polymer as PFA generates water which slows down the process speed and may adversely affect the overall material properties. This shortcoming limits its application in many sectors of industry that require fast and efficient mass production through short cycle ideally several minutes maximum. Reinforcement PFA with hydrophilic natural fibres enhances quality of composites while reducing cycle times due to its ability to absorb the excess water. Existing academic research on processing PFA based biocomposites suggest the crosslinking to be done either by gradually and slowly increase the temperature from 20 to 80°C or isothermal stepwise at temperatures between 90 and 160 °C. In both cases the processing times range between 2 and 8 hours hindering its market share.

The working procedure of BioRez 080101 as prescribed by the manufacturer, recommends to dry the impregnated fibres in air oven to a moisture content less than 5%. This resin was delivered as ready mix with acid hardener already formulated into the binder however additional acid can be added to speed up the curing process. For curing with contact heat press at 140 °C, 1.5 minutes/mm material thickness is required but for shorter cycle times higher temperature up to 160 °C can be used.

i. Prepreg production

Three types of reinforcement were employed in this category of biocomposites fabrication through impregnating with BioRez PFA, this included unidirectional carded flax with top and bottom glass veils tapes produced at Tilsatec using the tape production technique described herein in Section 4.1.2. The latter is a hybrid reinforcement and considered for toughening option. The second type being Flax/PLA comingled tape in a mix ratio of 90:10 also produced at Tilsatec facilities using the same tape production technology. The presence of PLA within the 90:10 tape holds the aligned flax fibres in place. Additionally, the third type is a non-crimp fabric produced with multiaxial technology available at Formax Ltd. (Leicester, UK) whereby Flax/PLA 90:10 ratio stitched using PLA thread in the ±45°. For comparison purpose, flax Twill 2x2 fabrics sourced from Composites Evolution Ltd. (Chesterfield, UK) were also impregnated with BioRez PFA. The impregnation process consisted of continuously feeding

the flax tapes/fabrics through a bath of resin whereby a full immersion takes place, then the impregnated tapes are passed through calendar rollers to remove the excess resin. The prepreg is then moved into drying stage as it travels through a forced air oven. The prepreg production is illustrated in Figure 4-14.

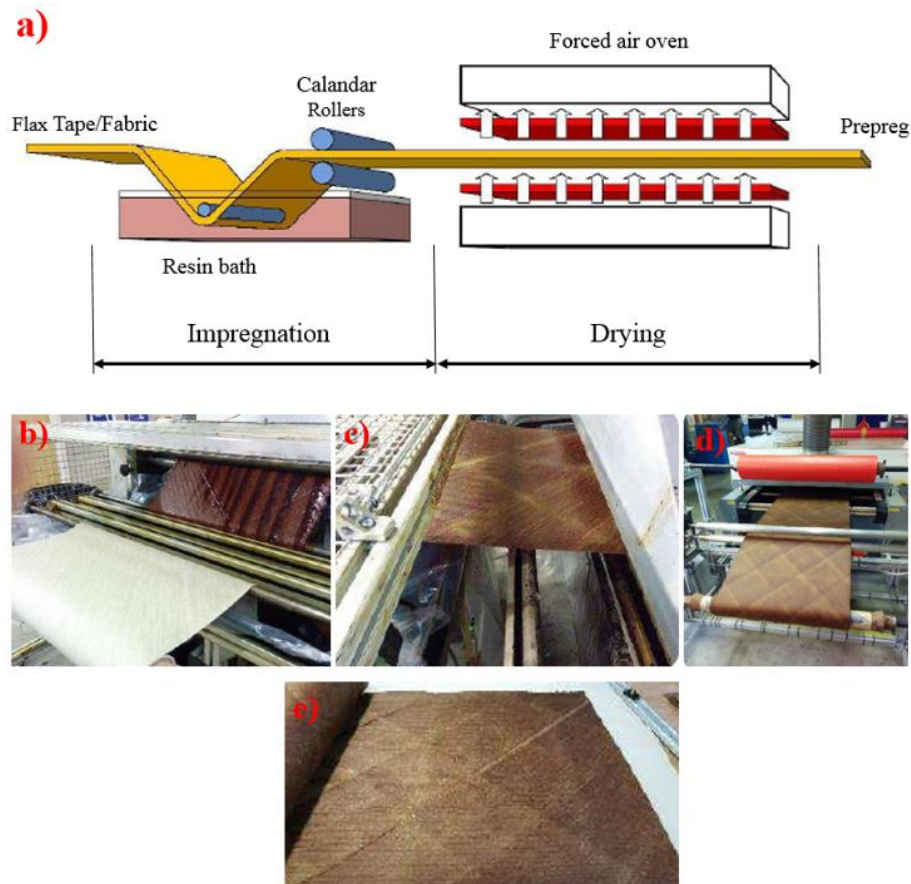


Figure 4-14 a) schematic diagram of the prepreg production, b) in-line impregnation of flax tape through a BioRez PFA bath, c) removal of resin excess by passing the prepreg through calender rollers, d) air oven drying of the prepreg, e) the final produced prepreg rolled ready for further consolidation

ii. Flat panels' production

The biocomposite panel production depends on the resin used i.e. the use of PFA based prepreps entailed consolidation through compression moulding process whereas for the UPE vacuum infusion process was employed. The compression moulding procedure for the thermoset is identical to that of the thermoplastic samples described in the previous section, the full details are included therein. The vacuum assisted resin infusion process has been discussed in Section 2.3.3. Similarly to the thermoplastic based panels, experimentation on various combinations of reinforcements and thermoset resins were carried out and the details of the considered specimen and their processing parameters are included in Table 4-4.

Table 4-4 Complete list of continuous thermoset based biocomposites considered in this research, materials types, processing parameters and reinforcement arrangements

Reinforcement Type (gsm)	Matrix	Fibre:Resin (wt%:wt%)	Orientation	Consolidation parameters	V _f ^a (%)	Density ^a (g/cm ³)
Flax/Glass veil 80/20 (450)		55:45	UD (0°)	4 layers pressed hot @ 120 °C, 12 bar for 20 minutes – loaded hot removed cold	52.8	1.4
Flax Prepreg (400)		50:50	Twill 2x2	4 layers pressed hot @ 120 °C, 12 bar for 20 minutes – loaded hot removed cold	48	1.4
Flax/PLA 90/10 (170)	PFA BioRez	50:50	UD (0°) 0°/90° ±45°	Compression moulding of 16 layers @ 140°C and 12 bar for 20 minutes – cooled under pressure	47	1.4
NCF-Non-crimp Fabric Flax/PLA 90/10 (363)		52:48	±45°	Compression moulding of 4 layers @ 140°C and 12 bar for 20 minutes – cooled under pressure	46	1.4
Flax Laminate (400)	Crstyic 701PA UPE	41:59	Twill 2x2 UD (0°) 0°/90°	Vacuum resin infusion, 24 h @ ambient, post-cure 3 h @ 80 °C	35 33 33	1.23 1.3 1.3

^aThe densities and V_f of all panels produced are theoretically calculated from Eq. (2-2) and Eq. (2-3) respectively.

4.1.3. Discontinuous – Nonwoven mats

This category of reinforcement i.e. discontinuous or nonwoven mats was used with both thermoplastic and thermoset matrices, therefore the production methods of these mats are identical. However, the conversion of these mats into flat composite panels vary depending on the matrix used. The production of the flax nonwoven mats considered in our research are primarily needle-punched based, nevertheless according to literature, thermal consolidation of mats reduces the risk of mechanical damage to fibres in comparison to needle-punched based mats . The full description of these methods is included in Section 2.2.2.

4.1.3.1. Thermoplastic based biocomposite

The selected matrix to be used with discontinuous flax fibres for the nonwoven mat thermoplastic (NMT) was Polypropylene (PP). The preforms made of Flax/PP with a mix ratio of 52:48 were interlocked via needle-punch process at Echotechnilin, Ltd (Cambridgeshire, UK), these are marketed under the commercial name fibriplast sheets. The technology used at their premises is illustrated in Figure 2-10 equipped with penetrating 30,000 needles/s capable of producing mats of various thicknesses and areal weights in the range of 300- 2400 gsm. In this research, a single mat of 1200 gsm, with fibres laid down along the machine direction also referred to herein as longitudinal, was used to

produce the flat composite panels through compression moulding i.e. thermal press. The procedure of this operation is similar to that described in the previous Section 4.1.2, whereby consolidation with applied pressure of 20 bar and temperature of 120 °C for 5 minutes yielding a reduced thickness of 2 mm.

4.1.3.2. Thermoset based biocomposite

The polyester resin used as the matrix for the composite panels manufacturing was purchased from East Coast Fiberglass Supplies Ltd (Tyne and Wear, UK). The resin is Crystic 2-446PA which is an orthophthalic pre-accelerated and low styrene emission and thixotropic unsaturated polyester resin. This grade of polyester is a versatile use resin for general purpose moulding including hand lay-up mouldings of composites. Catalyst/ hardener M which is a medium grade Methyl Ethyl Ketone Peroxide was also purchased from East Coast Supplies Ltd to accelerate cure cycle and reduce gel time. A manufacturer recommendation to mix 70:30 resin to hardener ratio for cold curing formulation, manual stirring of the mixture for 2 minutes to achieve a homogenous compound. A minimum requirement of 15 °C room temperature for the curing to take place. The reinforcement employed in this study, needle punched nonwoven mats 100% Flax, fabric areal weight of 600 gsm were obtained from Ecotechnilin (Cambridgeshire, UK). Table 4-5 summarises the mechanical and physical properties of the polyester and Flax fibre used for the fabrics used in this study.

Table 4-5. Mechanical and physical properties of natural fibres and polyester 2-446PA

Material	Density (g/cm ³)	Tensile strength (MPa)	Young's Modulus (GPa)	Elongation (%)
Flax	1.4	400 – 1500	40 – 80	2.7 – 3.2
Polyester*	1.2	50	3.8	1.5

* The values considered with the cure time, temperature and post cure procedure as described by manufacturer.

Hand lay-up with vacuum bagging method was adopted in the preparation of the composite samples. A glass bed was cleaned with acetone to remove any contamination and dirt then double tapped around the edges. Polyester resin/formulated catalyst mixture in the ratio of 70:30 was poured on square shaped fabrics which were cut from the flax roll and pre-weighed then placed on the glass. To achieve certain sample thicknesses multiple layers were arranged on the glass which was firstly coated with release agent and the Mylar sheet placed on the surface to maintain the vacuum. Trapped air was continuously removed by vacuum and air bubbles gently squeezed out using a roller. A range of densities have been achieved through hand wetting with controlled amounts of polyester as one layer fabric for specimens used in the tensile, flexural, impact hammer, Dynamic Mechanical Analysis and two layers of fabrics for specimens used in short beam test. Fibre volume contents and densities for the manufactured specimen have been calculated using Eq. (2-2) and Eq. (2-3).

The procedure followed in the hand lay-up of the samples was as follows:

- Firstly, the glass mat was cleaned by acetone in order to remove any contaminants and dirt and double tape was attached to the edges of the glass mat to create a boundary.
- The required resin was mixed with the catalyst in the ratio of 70:30 parts; followed by 2 min of manual stirring for homogenization.
- All samples with required layers of nonwoven mats were arranged on the glass mats.
- The mixture was applied to each sample, using a brush and roller.
- A flat weight was placed on top of each sample, a vacuum valve and absorption tissues was placed on each glass mat.
- To create the required vacuum condition, on top of each glass mat, a Mylar sheet was attached to the double tape of glass mat.
- Vacuum was applied continuously in order to get rid of air trapped and hence cure the samples, then the samples were left to cure for 24 hours under room temperature ($\sim 20^{\circ}\text{C}$).

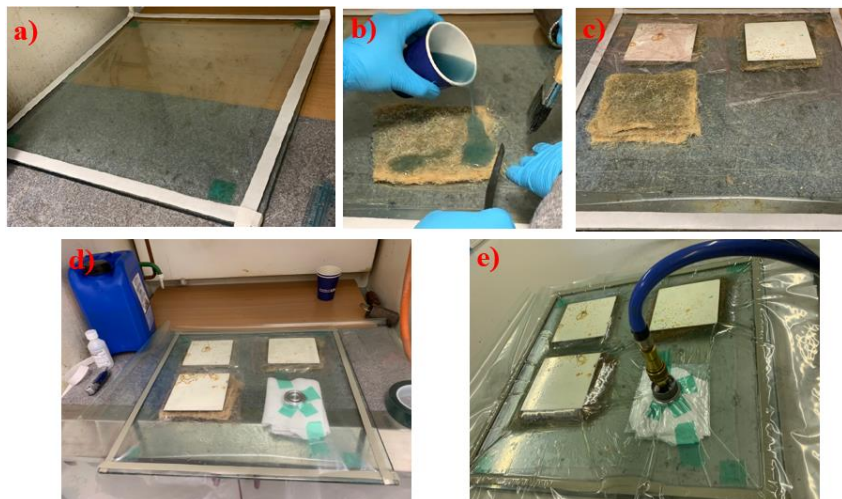


Figure 4-15 the manufacturing of polyester natural fibre mats: a) glass mat cleaned by acetone, b) resin mixture poured over the mats, c) resin wet mats arranged ready for consolidation, d) vacuum and absorption tissue inserted, e) vacuum applied to cure samples.

This fabrication process and the inherent properties of fibres in terms of the low packing ability of flax fibres limit the maximum obtainable fibre volume fraction, low fibre contents have been achieved namely 14%, 18% and 22%.

4.1.4. Sample cutting and conditioning

The samples considered for mechanical testing were cut from rectangular panels using two main machines, the electric guillotine (Figure 4-16) and laser cutter.



Figure 4-16 Electric guillotine used to cut the composite panels in dimensions corresponding to the specified standards

The geometry measurement after cutting were obtained using a caliper whereby lengths, widths and thicknesses were measured and three readings taken from different locations then averaged.



Figure 4-17 measurements taking of the various specimen types for the mechanical characterisation – this image is an example of geometry measurement of DMA samples.

4.1.5. Characterisation and properties evaluation

4.1.5.1. Tensile Properties

For the tensile characterisation of the composites at least five specimens cut from the panels produced and listed in the previous sections 4.1.2 and 4.1.3 in the dimensions 250 x 25 mm have been tested according to BS EN ISO 527-4:1997. Samples have been subjected to tensile load with a testing speed of 2 mm/min using an electromechanical UTM Tinius Olsen (Surrey, UK) model 50 ST equipped with a 50 kN load cell. The testing machine was controlled with a hand held interface and a virtual machine interface running on a Tinius Olsen Horizon software connected to a PC. The specimen were clamped within the jaws of the machine with care to avoid any prestressing effects as such stress can be generated from centring the sample or can be caused by gripping pressure. However, to some extent, this can be beneficial to avoid a toe region on the stress vs strain curve which is the initial non-linear portion of the curve. For materials for which the initial portion of the curve is linear, the strain zero may be corrected for preload by extending the initial straight portion of the stress-strain curve to zero load and measuring strain from that point. The strain value at the zero-load intercept is commonly called the “foot correction” and is subtracted from readings taken from strain scale (Davis, 2004). The wedge grip inserts should be contained within the grip body or crosshead, and the specimen tabs should be fully engaged by the grips. Acquired data including the force, the distance travelled by the grips and time are

collected and exported as an excel file for the derivation of the tensile parameters as per standards procedures and recommendations. British Standard BS EN 527-1:2012 (E) describes the alternative method to record strain from a tensile test in the case of absence of extensometer. The nominal strain is based on the increase of distance between the grips relative to the initial gripping distance. It is also acceptable to record the crosshead displacement instead of measuring the distance between the grips. The nominal stress and strain are calculated from Eq. (4-4) and Eq. (4-5):

$$\sigma = \frac{F}{A} \quad \text{Eq. (4-4)}$$

$$\varepsilon = \frac{L_t}{L} \quad \text{Eq. (4-5)}$$

Where σ is the stress in MPa, F is the measured force in Newtons (N) and A is the initial cross area measured in mm^2 . Similarly, ε is the nominal strain expressed as a dimensionless ratio or percentage (%), L_t is the increase of gripping distance occurring from the beginning of the test expressed in mm and L is the initial gripping distance. In order to obtain the tensile modulus E_t , the initial slope from the stress vs strain in the strain interval $\varepsilon_1 = 0.05\%$ and $\varepsilon_2 = 0.25\%$ as shown in Figure 4-18a).

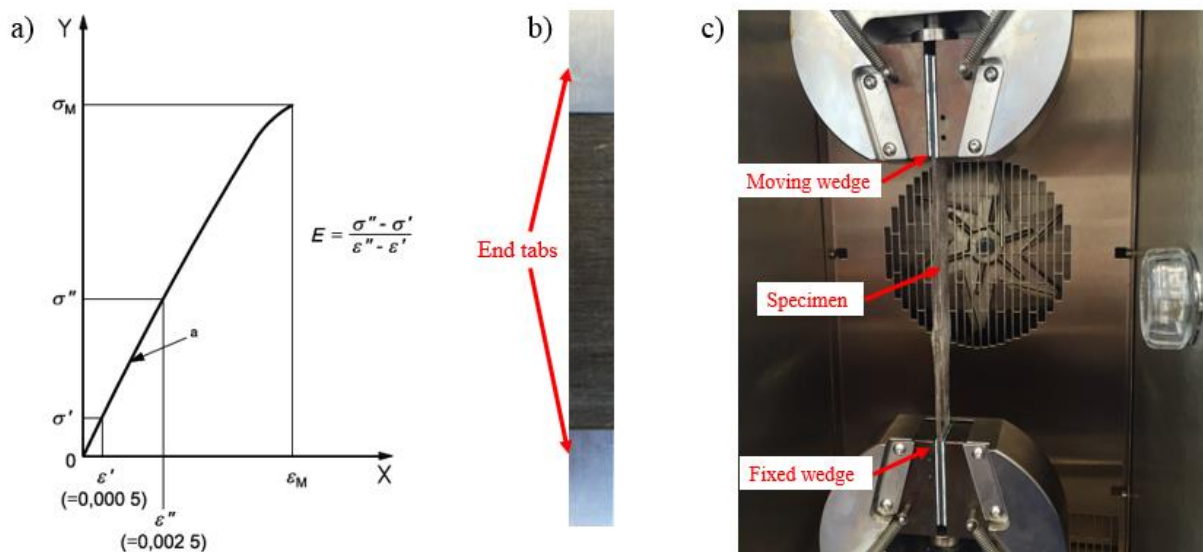


Figure 4-18 a) Typical stress vs strain. Method of tensile modulus calculation using graphical method (BS EN ISO 527-5:2009); b) Specimen with aluminium end tabs; c) tensile test setup arrangement

4.1.5.2. Flexural Properties

Three-point bending tests were performed according to BS EN ISO 14125:1998 to determine the flexural parameters. Five specimens of each sample with dimensions of Class II obeying to the requirement of length to thickness ration 20:1 and width of 15 mm were cut from the panels. These specimens were tested on the same UTM equipment Tinius Olsen (Surrey, UK) model 25 ST equipped

with 25 kN load cell. The tests were conducted at a cross-head speed 2 mm/min. The flexural stress σ_f , strain ϵ_f and modulus E_f were calculated using equations Eq. (4-6), Eq. (4-7) and Eq. (4-8) respectively:

$$\sigma_f = \frac{3FL}{2bh^2} \quad \text{Eq. (4-6)}$$

$$\epsilon_f = \frac{6sh}{L^2} \quad \text{Eq. (4-7)}$$

$$E_f = \frac{L^3}{4bh^3} \left(\frac{\Delta F}{\Delta s} \right) \quad \text{Eq. (4-8)}$$

Where σ_f is the flexural stress expressed in MPa, F is the load in Newtons, L is the span of the specimen in mm, h is the thickness of the specimen in mm and b is the width of the specimen in mm. S is the midpoint deflection in mm, ΔF is the difference in load between F'' and F' at deflections S'' and S' respectively.

4.1.5.3. Thermo-mechanical Properties – DMA

To determine the effects of the type and amount of reinforcement on the damping properties, DMA tests on small coupons off-cuts from the flexural panels to measure storage modulus (E'), loss modulus (E'') and damping ratio ($\tan \delta$). The choice of the fixture depends on the material used and the desired results. While thin films are often measured in tension because of the low stiffness of the material and lack of bending rigidity, a three-point bending configuration is widely employed for composites, because it eliminates the combined loading induced by a single or double cantilever mode and it produces measurable strains in relatively stiff materials (Goertzen and Kessler, 2007). A DMA 8000 manufactured by Perkin Elmer Ltd. (Buckinghamshire, UK) was used to record the dynamic parameters of samples of the dimensions 50 x 10 x 2mm were loaded in the three-point bending configuration at a displacement of 0.025mm and 1 Hz frequency. Samples were heated from 25 °C to 180 °C at a heating rate of 5 °C/min.

4.1.6. The effect of *In-Situ* Temperature on the Biocomposites

In light of what has been historically reported for NFCs, a gap in the current literature on the mechanical performance under thermal effects creates a need to explore the topic and establish new knowledge. Thermal degradation of natural fibres under elevated temperatures poses a limitation on its use within certain environments. This restriction also varies depending on the matrix used, thermoplastics in particular are prone to softening as temperature approaches the glass transition which is typical in the range of 50- 70 °C. This phase change of the matrix weakens the overall mechanical performance as it represents the medium which transfers load to the fibres. On the other hand, thermosets are considered

of high thermal resistance due to the high cross-linking which inherently promotes its mechanical performance. Specimen of flax fibres, continuous and discontinuous mats based, reinforced with thermoplastic and thermoset matrices have been investigated for their tensile properties degradation with increasing temperatures. The characterisation involved testing standard specimen under the combination of static loading mode and *in-situ* environmental conditioning, to support the dynamic mechanical study using DMA in understanding this phenomena. The static testing provides indications of property deterioration (Young's modulus, UTS and strain at failure) under isothermal condition. Whereas DMA provides dynamic quantities such as storage modulus, loss modulus and damping ratio over a ramping temperature to capture the phase change i.e. glass transition of the composite.

The test method and equipment utilised for the *in-situ* characterisation of the biocomposites is identical to that employed for the 3D-printed parts included in section 4.2.3.

4.2. 3D Printed PLA Structures Specimen

3-D printing (3-DP), Rapid Prototyping (RP) or Additive Manufacturing (AM) are three synonyms used to describe a range of processes which makes it possible to fabricate parts, by various materials, through an additive process, layer upon layer, starting directly from a computer-aided design (CAD) model. One of these processes is the Fused Deposition Modeling (FDM) which is considered low cost 3-D printing method due to its availability as open source since the expiration of the FDM patent in 2009. Nowadays, there are many low-cost 3D printers available on the market (< £500). They fall into three categories: not-assembled "DIY" (Do It Yourself) open-source, fully assembled open-source and commercial systems with proprietary software (Lanzotti et al., 2015). One of the best-known open-source 3D printer project was developed in 2005 by Dr Adrian Bowyer, from the University of Bath (UK) and is known as the Replicating Rapid prototyper (Rep-Rap) Project. This started off as a self-replicating equipment using the fused filament fabrication (FFF) technique commonly using materials such as polylactic acid PLA and acrylonitrile butadiene styrene (ABS) to fabricate about 50 % of its own parts (Pearce, 2012). This then extended to other materials as this technology evolved to include composites such as carbon and natural fibre reinforced polymers (Young et al., 2016). Different official 3D printing machines have been released in the course of Rep-Rap Project and currently there are hundreds of variations.

Initial use of 3D printers was limited to applications for conventional prototyping and engineering tooling, customizing scientific equipment or in research activities whereby tools can be designed and printed to cut cost and time. However, progress made and easy access to low-cost 3D printers triggered several researchers to investigate the mechanical properties of 3-D printed parts. Numerous studies aimed at process optimisation investigated the effects of printing parameters on the mechanical properties through applying statistical methods to experimental data. This study aims to firstly evaluate the effects of printing orientation on the tensile properties of PLA specimen under static loading within this chapter, then extend the investigation with varying *in-situ* temperatures.

4.2.1. Materials and methods

4.2.1.1. Geometry of tensile specimen

The geometry used for this study was based of the optimised version from ASTM 638-14 Type I as proposed by Ahn and his colleagues (Ahn et al., 2002). The basis of this modification is the problems associated with the shape as added complications to the loading of the 3D printed parts that caused them to fail prematurely. These complications included large stress concentrations caused by the termination of the longitudinal roads used to approximate the large radii of the dog-bone shape specimen as shown in Figure 4-19.

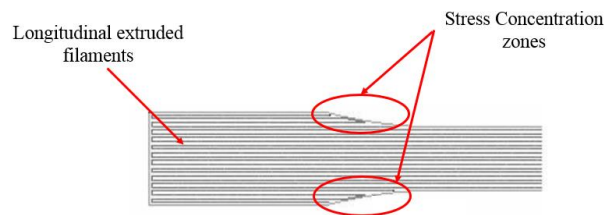


Figure 4-19 locations of stress concentration for the ASTM D638 dog-bone specimen with longitudinal extruded filaments (Ahn et al., 2002)

Introducing offset contours around the perimeter as corrective measures to eliminate this effect as shown in Figure 4-20, this modification was expected to relieve the stress concentrations. However, this approach maintained high stress near the curvature zone with partial stress shifted towards the center of the specimen due to gaps causing complex modes of loading as opposed to pure tension as desired in the ASTM standards.

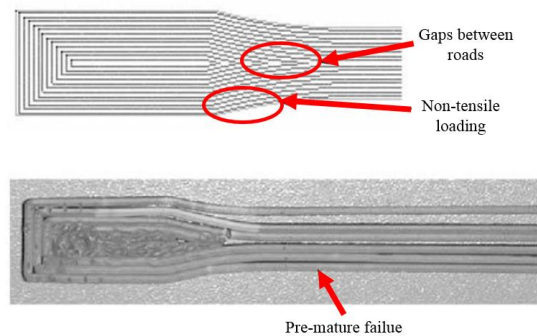


Figure 4-20 Modification of geometry including the contours (Ahn et al., 2002)

As a result, a further modification to the geometry was needed to ensure that the dominating mode is tension and the failure occurs within the gauge length of the specimen as proposed and implemented by Lanzotti co-authors (Lanzotti et al., 2015). A parabolic profile has been modified. For such a purpose, a parabolic profile for the fillet was used in combination with a curvature radius equal to 1,000 mm for the opposite faces of the central portion. This modification allows the reduction of the stress concentration due to the curvature variation and ensures the failure of the specimen at the minimum

cross section. Therefore, the geometry adopted in this research is shown in Figure 4-21, and full dimensions are included in Table 4-6.

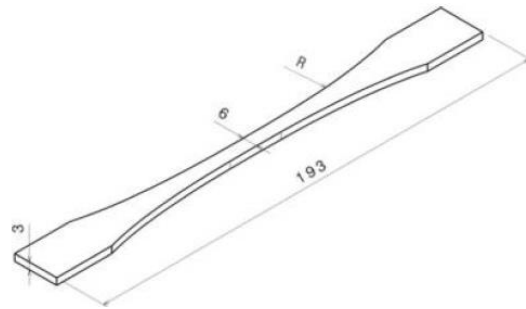


Figure 4-21 Optimised geometry of standard based tensile specimen with nominal dimensions, improvement included the radius of curvature $R=1000\text{mm}$

Table 4-6 Dimensions of tensile specimen

Geometry	Dimensions (mm)
Total length	193
Width of narrow section	6
Width of ends	20
Length of wide ends	25
Radius of fillet	1000
Distance between grips	150
Thickness	3

4.2.1.2. Materials and equipment

A MakerBot Replicaor Desktop 3D printer (MakerBot Industries, Brooklyn, USA), which is available at the materials laboratory of University of Hertfordshire, was used to produce the tensile specimen. The printer uses the FDM technology to extrude filaments through a nozzle diameter of 0.4 mm over a build plate, the printer has a build volume of $252 \times 199 \times 150$ mm limited to printing only polylactic acid (PLA). PLA is widely used in emerging technologies such as 3D printing as is characterised by low operating temperatures, specifically the glass transition temperature T_g and the melting temperature T_m which are preferable characteristic for both the softening during the deposition stage (T_g) and avoiding localised degradation process because of hot spot in complex geometry (T_m). The extruder head is capable of printing filaments of 1.75 mm diameter, the filament feed made of PLA was delivered from MakerBot distributor as a continuous spool wound around a plastic holder, essential properties provided in Table 4-7 as reported from manufacturer in its accompanying data sheet.

Table 4-7 PLA filament physical and mechanical properties

Property	Test Method	Typical values
Density	ASTM 1505	1.24 g/cm ³
Tensile strength	ASTM D638 (50mm/min)	62 MPa
Tensile Modulus	ASTM D638 (50mm/min)	3600 MPa
Strain at yield	ASTM D638 (50mm/min)	>4.4 %
Flexural Modulus	ASTM D790 (15mm/min)	2600 MPa
Heat Deflection	ASTM 648	52- 49 °C
Melt Flow Index	ASTM D1238	6g/ 10min

The selected printing parameters have been continuously tuned to achieve the optimum print quality, this included the most critical ones namely layer thickness, number of shells and overlapping which directly affect the infill density. Furthermore, this tuning was primarily based on the quality of the print out specimens in terms of dimensions, smoothness of the outer surfaces however the volume of material needed to print the samples and the speed in which the required number of samples is produced are important too. The full list of parameters considered for tensile specimen printing is included in Table 4-8.

Table 4-8 Printing parameters used in the fabrication of 3-D tensile specimen on the MakerBot Replicator

Parameters	Value	Unit
Layer height	0.18	mm
Infill layer height	0.18	mm
Number of shells	2	–
Feed rate	1	mm/s
Travel feed rate	10	mm/s
Print temperature	215	°C
Filament diameter	1.75	mm
Nozzle diameter	0.4	mm
Infill density	40%	–
Floor thickness	1.5	mm
Support angle	68	degrees
Support density	20%	–
Cooling fan speed	50%	–
Infill pattern	Linear	–

In our study, the selected infill density is 40% having a zero air gap whereby the density of the final part, amount of material and time are reduced as compared to using a 100 % infill density and a negative air gap. Using negative air gaps between individual rasters is able to reach 98% of the maximum possible density equivalent to parts fabricated via injection moulding (Dawoud et al., 2016). In contrast, FDM parts produced at a positive air gap are much lower in density. It was estimated that a reduction of 9% in finished part density when using +0.05 mm air gap compared to -0.05 mm. This can be related to the fact that a positive air gap causes adjacent rasters to barely touch along a line resulting from the cylindrical raster shape, whereas a negative raster gap, designed for overlapping rasters causes adjacent filaments to partially squeeze and fill in the air gap in between. However, negative air gap any lower than -0.08 as discussed by Ahn (Ahn et al., 2002) cannot build well due to excess material build up on the nozzle and the part itself besides degrading surface quality and dimensional tolerances. In light of current literature, our focus was to solely investigate the effects of raster orientation on the tensile properties as opposed to using a negative air gap whereby this effect is diminished. The implications of this is that the 3D printed part can no longer be considered as a composite structure.

4.2.1.3. Specimen fabrication

The fundamental issue in designing 3D-printed components is the identification of strength and stiffness (Qin et al., 2015) as several authors have carried out experimental tests to investigate the mechanical behavior. For instance, de Obaldia and co-authors (de Obaldia et al., 2015) suggested that 3D-printed materials exhibit highly anisotropic behavior in both their stiffness and strength properties in a similar manner to a reinforced composite. This anisotropy is due to the internal arrangement of filaments known as infill orientation. These orientation arrangements include unidirectional bead lay-up and criss-cross bead lay-up in which the beads of adjacent layers are separated by 90° (Thomas and Renaud, 2003). In both of these cases, the effect of the infill orientation on the stiffness and strength of the component have been found similar to that of composite materials (Rodríguez et al., 2001). Nevertheless, the main difference between 3D-printed parts in the proposed orientations (i.e. $0/90^\circ$, $-30^\circ/+60^\circ$ and $\pm 45^\circ$) and composite materials is the shear stress transfer mechanism among adjacent layers. In the case of 3D-printed components, adjacent beads, from a layer-upon-layer configuration viewpoint, are blended rather than attached via a substrate material as typically encountered in fibre-reinforced polymers. Therefore, the overlapping surface in 3D-printed components could be varied by modifying the parameters related to the deposition phase such as temperature, deposition rate or contact pressure. The extension of bonding surfaces plays an essential role for the 3D-printed parts, by withstanding the tangential load acting on the element while in long fibre-reinforced polymer composite, the shear performance is related to the strength of the matrix mainly.

The geometry adopted for this study to produce the 3-D samples was generated with CAD software CATIA V5 (Dassault Systemes, Velizy-Villacoublay, France). The stereolithographic files (STL) were then generated in order to be transferred into the printer as it is the only file format readable by the operating system of such 3-D printers. These files are script of coding text that embeds the specified parameters for the slicing process, this is achieved using MakerWare 2.2.0 control software as a free download from manufacturer website. Since this study focuses on the effect of infill (also known as beads or roads) orientation on the tensile properties, three different orientations ($0/90^\circ$, $-30^\circ/+60^\circ$ and $\pm 45^\circ$) have been selected based off previous findings reported in literature and three separate STL files have been generated. As illustrated in Figure 4-22, the specimen were printed in the x - y plane and rotated around the z -axis with a raster angle of 0° , 30° and 90° to generate the infill orientation $0/90^\circ$, $-30^\circ/+60^\circ$ and $\pm 45^\circ$ respectively. The horizontal build direction of the test specimen as reported in literature produces the maximum tensile strength, minimum production time and acceptable support material consumption (Durgun and Ertan, 2014). Three specimen of the same orientation were printed at a time due the limited surface area as well as the potentially decreased quality of the printed parts as it was noticed that the thermal bonding to the build plate decreases when moving away from the centre of the build plate.

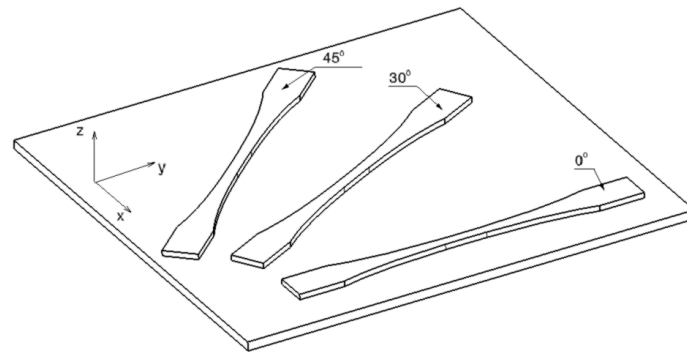


Figure 4-22 Schematic arrangement of the specimen with different raster angle values 0° , 30° and 90° adopted to print the three infill orientations

The total number of 3-D printed specimen to be considered for tensile testing is 15 as five repetitions were necessary as required per ASTM standards, also to ensure statistical significance, for each of the three of orientations. The specimen were coded using orientation O1 ($0/90^\circ$), O2 ($-30^\circ/+60^\circ$) and O3 ($\pm 45^\circ$) followed by the number of sample being tested as presented in the testing plan in Table 4-9 and to be also used in subsequent graphs in the analysis of tensile properties of the samples. For example, sample No.1 for the $0/90^\circ$ orientation is denoted as O1_1. After the completion of printing process and prior to testing, dimensions of all samples including overall length, thickness and width of the central part (narrow area) were measured with a Bathy digital caliper (Bowers Group, Camberley, UK) with a precision of $\pm 10 \mu\text{m}$ and an average of three measurements is reported in Table 4-9.

Table 4-9 Samples considered for the testing plan

Test Model	Layer Thickness [mm]	Infill Orientation [°]	Number of shells	Length [mm]	Width [mm]	Thickness [mm]	Area [mm ²]
O1_1	0.18	0	2	192.00	6.48	3.53	22.87
O1_2	0.18	0	2	191.00	6.43	3.45	22.18
O1_3	0.18	0	2	192.00	6.44	3.47	22.35
O1_4	0.18	0	2	192.00	6.43	3.43	22.05
O1_5	0.18	0	2	191.00	6.44	3.48	22.41
O2_1	0.18	30	2	192.00	6.57	3.36	22.08
O2_2	0.18	30	2	193.00	6.50	3.40	22.10
O2_3	0.18	30	2	192.00	6.59	3.37	22.21
O2_4	0.18	30	2	192.00	6.58	3.37	22.17
O2_5	0.18	30	2	192.00	6.58	3.38	22.24
O3_1	0.18	45	2	192.00	6.47	3.30	21.35
O3_2	0.18	45	2	193.00	6.48	3.37	21.84
O3_3	0.18	45	2	193.00	6.43	3.35	21.54
O3_4	0.18	45	2	193.00	6.46	3.37	21.77
O3_5	0.18	45	2	192.00	6.48	3.36	21.77

All samples are expected to have dimensions similar to the nominal solid model dimensions from the CAD file. The part quality including surface finish and dimensional accuracy is largely influenced by printing parameters such as thermal factor which affects the quality of bonding besides deposition speed. Process capability study is the ability of the process to meet the design specifications for a service or product. Therefore, a statistical analysis was conducted to assess the geometrical deviations of printed specimen with respect to the nominal CAD geometry. The considered tolerances for this analysis were based on ASTM: D638-14 standards.

From comparison of the measured dimensions as reported in Table 4-9 with nominal dimensions it can be clearly noticed that both width and thickness are consistently higher than that of the nominal geometry. Therefore, the nominal values were instead chosen to be the historical average population of all samples and from which the individual deviations of the measured dimensions were reported. The acceptance test was based on the population ± 3 standard deviations (σ_p) with boundaries represented by the upper control limit (UCL) and lower control limit (LCL) through calculations using Eq. (4-9), Eq. (4-10) and Eq. (4-11) respectively:

$$\sigma_p = \sqrt{\frac{\sum_{i=1}^n (X_i - \bar{X})^2}{n}} \quad \text{Eq. (4-9)}$$

$$UCL = \bar{X} + 3 \sigma_p \quad \text{Eq. (4-10)}$$

$$LCL = \bar{X} - 3 \sigma_p \quad \text{Eq. (4-11)}$$

where X_i , \bar{X} and n are the individual values from the population, the population mean and the size of the population respectively.

4.2.2. Experimental procedure

4.2.2.1. Tensile testing

Tensile mechanical tests were carried out on the standard PLA 3-D printed samples of the three orientations $0/90^\circ$, $-30^\circ/+60^\circ$ and $\pm 45^\circ$ using an INSTRON electromechanical testing machine D3367 Dual Column System (INSTRON, UK). The load was measured with a 30 kN load cell having an accuracy of ± 0.5 per cent. Each specimen was clamped to the flat specimen grips at a specified grip separation of 150 mm and loaded along the longitudinal axis with a crosshead speed of 2mm/min, displacement was set to automatically stop once specimen reaches failure. Acquired data including the force, the distance travelled by the grips and time are collected and exported as an excel file for the derivation of the tensile parameters. The tensile test procedure for data analysis in terms of stress and strain is identical to that used in the biocomposite characterisation in section 4.1.5.1, nominal stress and

nominal strain are also calculated using Eq. (4-4) and Eq. (4-5) included therein. The load was applied along the specimen length which induced different load scenarios within the composite-like structure as raster orientation varies among the three beads arrangements as shown in Figure 4-23.

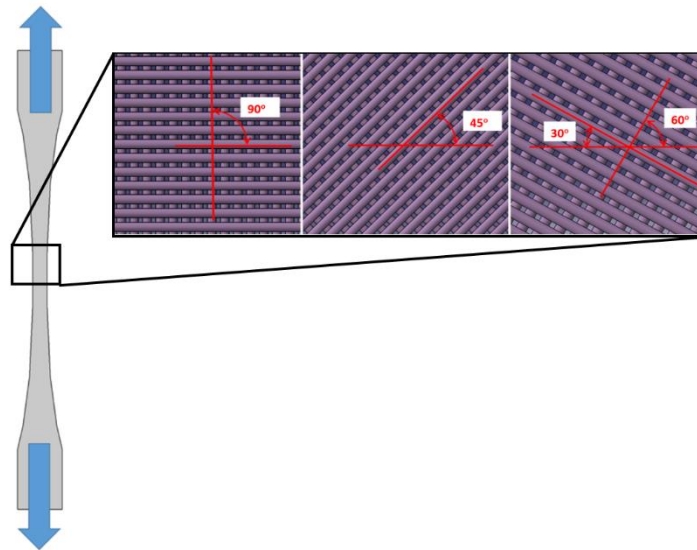


Figure 4-23 schematic representation of internal arrangements of raster angles for the three orientations with respect to the loading line in tension mode.

4.2.2.2. The effect of temperature on extruded filament

To assess the potential physical change in the feeding material because of the time-temperature profile undergone by the system during the deposition stage, preliminary mechanical tests were carried out on plain and on freely extruded PLA filament samples, that is those that are left to run for a few seconds as part of the filament loading process and cleared from the build plate before printing takes place. Each test was repeated five times for statistical significance. In Table 4-10, the plain and freely extruded wire-like samples are reported along with the considered temperatures and the number of performed test repetitions.

PLA filaments, both plain and extruded, were tested by using a Dynamic Mechanical Analyser, model Q800 DMA (TA Instruments Italy), equipped with a fibre tension clamp. The tension tests were force controlled up to the maximum 18N by using a force ramp of 1 N/min. Nominal dimensions of the cylindrical wire-like filament were 15 mm in length and 1.75 mm and 0.60mm in diameter for plain and extruded filaments respectively.

Table 4-10 DMA experimental plan on the PLA filaments

Filament	T (°C)	Repetitions
Plain PLA filament	20-30-40-50-60	5
Extruded PLA filament	20-30-40-50-60	5

4.2.3. The effect of *in-situ* temperature on 3D printed Specimen

Despite the rapid growth in the number of AM-related publications over the past five years, approximately 3,500 per year, there is still a gap in the open literature regarding the effect of temperature on the mechanical properties of 3D-printed components. Furthermore, *in situ* mechanical testing over a range of in-service temperatures is a significant factor in identifying failure modes, that is, whether the fracture is brittle or ductile. Considering the viscoelastic nature of polymeric materials, the elastic proportion of stress-strain curve followed by a sudden drop in stress with no further extension is said to be a brittle fracture failure. However, in ductile dominant failure, the elastic and plastic proportions are merged with a decreased value of maximum stress and a prolonged extension which is sometimes infinite. These effects are controlled by the addition of plasticizers or temperature variation (Kendall and Siviour, 2014).

The scarce knowledge on the impact of temperature on the strength and stiffness of the 3D-printed materials justifies the need of their investigation; ultimately benefiting the selection of 3D printing processing parameters or conditions, rather than just being a geometric specification, according to the required applications. Therefore, in this chapter, the thermal, mechanical properties of 3D-printed PLA specimens have been investigated by considering different raster angles and environmental temperatures, 20°C-60°C. The heat-induced variations of the feeding material have also been studied by performing mechanical tests on the plain filaments, referring to the filaments before the extrusion process takes place, and the extruded filaments in tensile mode configuration. This was done with the aim of assessing potential property changes related to the physical variation of the polymeric material. Thus, the UTS, Young's modulus, strain at failure and stress at failure of these 3D-printed samples were determined at different temperatures to evaluate final material performance along three bead orientations, namely, 0°/90°, -30/+60° and ± 45°, while the temperature was kept constant over several values ranging between 20°C and 60°C.

A total of 75 standard tensile specimens were produced and tested, within which, each of the three different infill orientations was tested at five different temperatures from 20 to 60°C. The tensile tests were repeated five times to ensure statistical significance. Table 4-1 reports the experimental plan for all PLA samples manufactured at different infill orientations and temperatures. The ID indicated in Table 4-11 is composed of two parts; the first signifies the temperature value (T1, T2 and T3) and the second signifies the considered orientation (O1, O2 and O3).

Table 4-11 Experimental Plan for the tensile testing

Sample ID	Infill orientation	T (°C)	Repetitions
T101	0°/90°	20	5*
T201	0°/90°	30	5
T301	0°/90°	40	5
T401	0°/90°	50	5
T501	0°/90°	60	5
T102	-30°/60°	20	5*
T202	-30°/60°	30	5
T302	-30°/60°	40	5
T402	-30°/60°	50	5
T502	-30°/60°	60	5
T103	±45°	20	5*
T203	±45°	30	5
T303	±45°	40	5
T403	±45°	50	5
T503	±45°	60	5

*These specimen have been already tested and results reported within Section 5.2.2.

The quasi-static tensile tests of 3D-printed samples were performed using an Instron electromechanical testing machine D3367 Dual Column System (Instron, UK) equipped with Bluehill software also equipped with an environmental chamber 3119-610.

To ensure that temperature testing of these specimen achieve stabilisation state within the specified temperatures within Table 4-11, a preconditioning procedure to record the time needed to reach a specified temperature was carried out. Samples were heated from room temperature to the desired temperature value and the time for each temperature increment was recorded. Initially, temperature readings were taken by means of thermocouples, KM07-C K Type (TME Technology in Temperature, West Sussex, UK) attached to the wide end surface of the specimen using a sticky 13×18 mm thermopads as shown in Figure 4-24a). The temperature of the chamber was set on a digital control located on the side of the chamber while temperature of the specimen was monitored on a TES-1319 K Type Thermocouple Thermometer (TES Electrical Electronic Corp., Taiwan) with a resolution of 0.1 °C and a range of -50 to 1300 °C. Once the temperature of the chamber stabilizes, the time needed for the specimen to reach the set temperature was recorded. However, this method lacked accuracy as the thermocouples failed to adequately record the actual temperature of the specimen, instead, the readings

represented the surrounding temperature. Therefore, to obtain more representative readings, an infrared (IR) camera FLIR TG165 (FLIR Systems, USA) with measurement resolution of 0.1 °C, range of -25 to 380 °C and 9 Hz frame rate and image resolution of 4,800 pixels, was employed to identify the temperature distribution in the gage length of each tested specimen. A uniform temperature distribution over the central part of the specimen and a temperature within an acceptable deviation from the nominal value of ± 1 °C is captured. This can be seen in Figure 4-24b) for the gage length of one of the samples tested at 60°C. The times required for the 3D-printed samples to stabilize at the given temperatures of 30°C, 40°C, 50°C and 60°C were found to be 3, 7, 10 and 15 min, from the time chamber stabilises respectively.

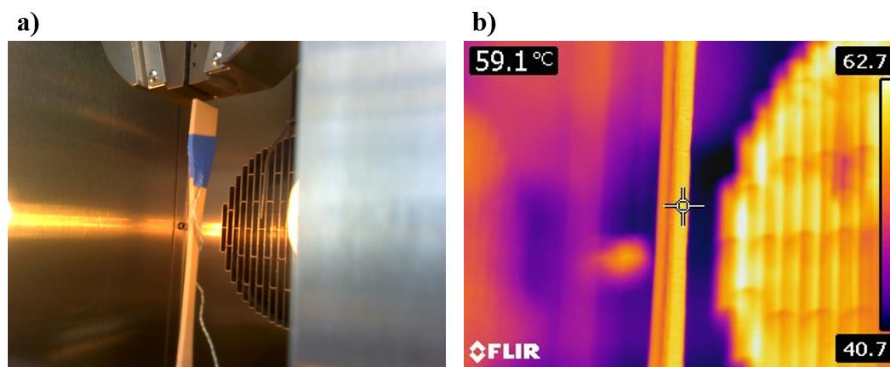


Figure 4-24 In-situ temperature measurement using: a) thermocouples and b) Infrared camera

4.2.4. Fractography analysis of 3D-printed and tested specimen

Fracture surfaces of the tensile test specimens were examined using a LEICA DFC295 digital microscope colour camera (Leica Microsystems, UK) with a resolution of $2,048 \times 1,536$ pixels (3 megapixels). The fracture surfaces contain necking as well as voids because of the printing imperfection and the fracture process itself. The fracture surfaces were scanned for these features and as a way of confirming the nature of the failure mechanism. The microscopic observations of the samples tested at different temperature values highlighted porosity because of the printing process. The specimens examined at 50 °C and 60 °C did not reach complete separation and were therefore not analysed.

5. Results

5.1. Natural Fibre Composites

The preliminary work on the potential of using flax fibres in different architectures and forms consolidated with various thermoplastics and thermosets have been conducted as described in chapter 4 and reported herein. The experimental procedures involved the use of adequate number of specimen to ensure representative results are obtained, therefore in this study, a minimum of five specimen was maintained for both tensile and flexural tests. In this section of chapter 5, results of tensile and flexural tests in terms of strength and modulus are split into two subsections continuous and discontinuous reinforcements which are further divided into thermoplastic based and thermoset based materials.

5.1.1. Continuous-Unidirectional

The tensile and flexural properties of both thermoplastic and thermosets reinforced with continuous flax fibres are reported in section 5.1.1.1 and 5.1.1.2 respectively, with values of all experimental tensile and flexural tests conducted in Table 5-1 and Table 5-2 respectively.

5.1.1.1. Thermoplastic based biocomposites

With the aim to evaluate the impact of matrix type on the mechanical performance of the biocomposites, a number of panels have been produced from twill 2x2 flax fabrics and one of the polymers PLA, PP or MAPP. All considered specimen consisted of equivalent 50:50 fibre to matrix ratio by weight, resulting in V_f of 40%, although final panels densities varied from PLA which is higher than that of PP and MAPP due to inherent higher density of PLA. Figure 5-1 presents the tensile modulus and strength of these biocomposites.

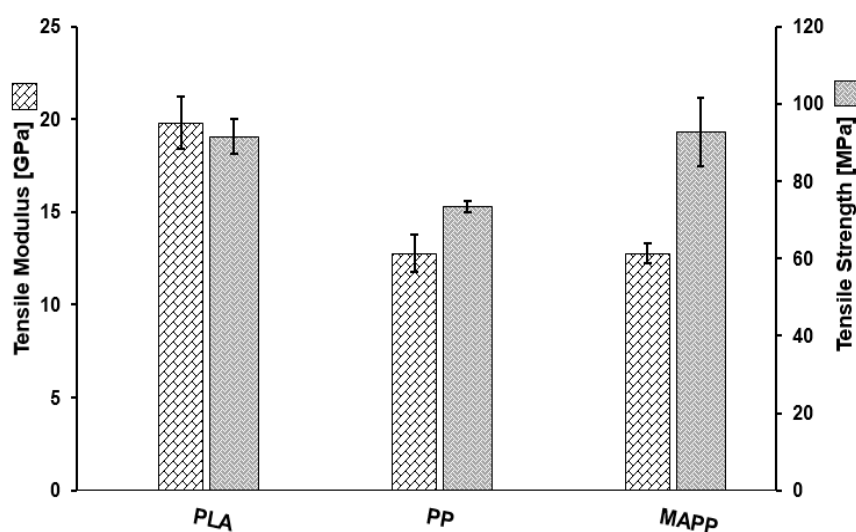


Figure 5-1 Biotex Twill 2x2 of flax fibres with different matrices PLA, PP and MAPP: comparison of tensile modulus and strength. Specimen consolidated with PLA showed the maximum modulus and strength, however the MAPP specimen exhibited improved strength as compared to the PP specimen.

Regarding tensile modulus, PLA based samples exhibited superior stiffness (19.8 GPa) compared to PP and MAPP, which showed similar values (12.7 GPa), with a calculated variation of 55% compared to that of PLA. Similarly, a strength increase of 24% when PLA is used instead of PP, this variation in strength and modulus is anticipated due to the fact that PLA properties are higher than PP. The pure PLA has a tensile strength of 50 MPa and a modulus of 3.4 GPa compared to 28MPa and 1.3 GPa of pure PP. It was however found that the incorporation of maleated PP (MAPP) results in an increased strength equivalent to that reported for the PLA based biocomposite. This clearly suggests a better fibre matrix interaction enabling the mechanism of load transfer to the stiff fibres. Previous work on the effect of reinforcing flax with PLA and PP revealed similar trends i.e. PLA superiority to PP based biocomposites (Oksman et al., 2003). It also proved that increasing flax content within the PP based is less significant compared to PLA based biocomposite. Interestingly, the tensile strength of 50:50 glass/PP conveyed in a review article (~80 MPa) is comparable to the 74 MPa we report here for the 50:50 flax/PP. Meanwhile our reported modulus (12.77 GPa) is considerably higher than the glass/PP (~7 GPa) (Shubhra et al., 2013). Although the review does not specify the form of reinforcement, but the results presented here validates the possibility of replacing GF with NF.

Table 5-1 Complete set of tensile and flexural tests results of flax reinforced biocomposites using different architecture of reinforcement and thermoplastics

Material		Tensile Modulus [GPa]		Tensile strength [MPa]		Flexural Modulus [GPa]		Flexural strength [MPa]	
		Average	S.D.	Average	S.D.	Average	S.D.	Average	S.D.
Flax/PLA Tape	40:60	15.06	0.81	58.13	16.67	4.88	1.68	65.72	24.44
	50:50	14.79	2.28	57.37	16.30	10.13	1.35	143.11	14.07
	55:45	13.98	0.65	87.35	7.04	13.22	1.03	148.28	11.48
	60:40	18.09	2.65	88.82	21.11	8.72	0.76	108.63	15.93
Flax/PP Tape 50:50	UD (0°)	14.57	0.75	154.33	7.47	16.23	0.70	161.37	5.72
	0°/90°	9.05	1.46	53.64	8.35	10.20	1.11	81.34	5.28
Flax/MAPP Tape	50:50	14.62	1.07	104.87	11.09	6.18	1.01	92.77	16.89
	60:40	12.92	1.10	105.38	5.55	9.67	0.66	112.94	5.04
	40:60	11.28	0.66	88.99	6.55	7.37	0.95	80.67	7.31
BIOTEX 50:50 Twill 2x2*	PLA	19.81	1.39	91.48	4.44	N/A	N/A	N/A	N/A
	PP	12.77	1.01	73.33	1.48	N/A	N/A	N/A	N/A
	MAPP	12.77	0.54	92.59	8.89	N/A	N/A	N/A	N/A

*The BIOTEX samples were tested for their tensile moduli and strengths only, therefore, N/A represents not assessed.

In order to further determine the implication of reinforcement architecture on the mechanical properties of Flax/PLA in a 50:50 ratio, $0^\circ/90^\circ$ stacked tapes and twill fabrics (also bi-directional) were compared for their tensile performance. In spite of difference in final panel's densities, a comparison can still be made. Figure 5-2 highlights the lower strength 37% and stiffness 25% of $0^\circ/90^\circ$ samples as compared to the twill weave. A possible explanation is that woven fabrics have reduced crimp which promotes its wettability and enhance the fibre/matrix interaction which is most desired in tension mode. The cross-over effect may have contributed to this response as twill woven fabrics are soft and pliable due to less interlacing which can positively affect the stiffness of the composite. This is because Young's modulus is less sensitive to the state of adhesion between the reinforcing fibres and matrix than the tensile strength.

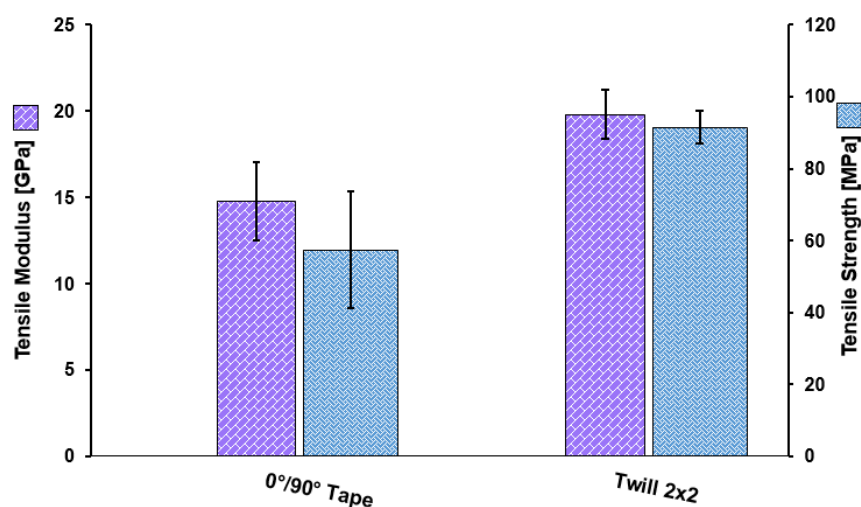


Figure 5-2 Comparison of tensile performance of Flax/PLA in a 50:50 fibre to matrix ratio between two fabric architectures: $0^\circ/90^\circ$ tape and reference material Biotex Twill 2x2

The above comparison can be extended to consider the effect of fibre contents on the tensile and the flexural properties. For this reason, $0^\circ/90^\circ$ Flax/PLA tapes of different weight ratios were produced and tested, namely 40:60, 50:50, 55:45 and 60:40 as provided in Figure 5-3. It can be observed that for 55:45, tensile modulus is unaffected but a significant increase of 52% in strength in comparison to the 50:50 samples. For 60:40 samples, modulus is found to increase by 22% while strength increase of 54% from those recorded for 50:50. The improved strength and stiffness with increasing the fibre content are equivalent to the flax twill fabric. Therefore it can be claimed that while an increase of fibre content results in a gradual increase in strength, the stiffness is constant at low contents before it surges for 60:40 samples. The current tendency agree with published research, an example is Bodros and co-workers study in which they reported a modulus as 2.5 times high as the pure PLA when reinforced with $V_f = 30\%$ (Bodros et al., 2007).

In light of the tensile results, flexural properties show a different sensitivity to fibre contents as the maximum flexural strength and stiffness corresponds to the 55:45 samples. From Figure 5-3b), a decrease in flexural strength and modulus as fibre content increased to 60 wt% to even a lower level

than those samples of fibre content of 50 wt%. This suggests that flexural behaviour is highly dependent on fibre/matrix interaction which is affected by the level of fibre wetting. Visual examination of the 60 wt% fibre contents specimens showed insufficient fibre wetting on top and bottom surfaces which hinders the load transfer. Furthermore, the inherent defects (kinks) of individual fibres induce stress concentration points causing reduction of flexural strength could be due to fibre defects (kinks). As a result crack initiation, fibre/matrix debonding and early failure before the load is fully transferred from matrix to fibre contribute towards this performance deficiency. Overall, when considering the combined performance in terms of tensile and flexural, samples produced with 55:45 weight ratio outperformed all others. This is taking into account the significant variation in the tensile strength recorded for the 60 wt% fibre content (88.8 ± 21 MPa) compared to the 55 wt% specimens (87.3 ± 7 MPa) which is thought to be caused by limitations of the manufacturing process at high fibre contents.

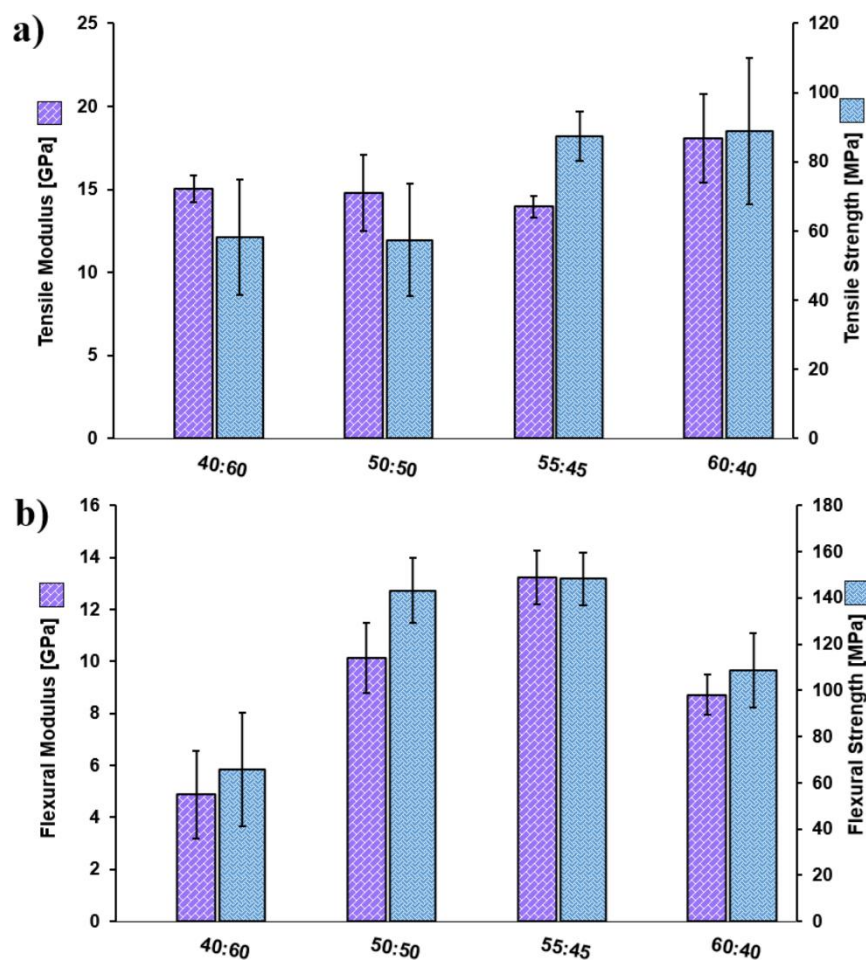


Figure 5-3 optimisation of flax fibre to PLA matrix mix by weight ratio in terms of: a) tensile modulus and strength, b) flexural modulus and strength. It can be noted that the optimum results were reported for the 55:45 specimen.

Similarly, three biocomposites Flax/PP in 50:50 ratio have been produced, of which two unidirectional tapes layered in UD (0°) and cross ply $0^\circ/90^\circ$ then thermally pressed to produce thick panel. A third panel made of twill fabric to be used as a reference sample. Fibre contents by volume of these panels was consistent in the range 37.5-38.5%, this made the comparison valid. As expected, the panels having

unidirectional layers of fibres aligned along the load direction possessed the highest tensile properties, see Figure 5-4. The UD samples modulus was only 14% superior to the twill counterparts while being 38% higher than the $0^\circ/90^\circ$ modulus. The tensile strength recorded for the UD samples was significantly higher than the twill and the $0^\circ/90^\circ$ samples with a factor of 2.1 and 2.9 respectively. These results can be classified according to their tensile performance in an ascending order as follows: $0^\circ/90^\circ$, twill, UD. Samples of $0^\circ/90^\circ$ arrangement exhibited the lowest performance due to the balanced amount of fibres oriented in the orthogonal directions i.e. only half of the fibres contribute in the load bearing. On the other hand, twill samples although are considered a bidirectional 2D fabrics, fibres can be arranged in a bias orientation which in this case is clearly the loading direction. Existing literature, (Romhányi et al., 2003), reported similar findings with flax reinforced starch biocomposites produced via film stacking technology. Furthermore, Kannan and co-authors reported similar observation for Flax/PP with 40% V_f as comparisons were made among different stacking arrangements of 6-ply panels: $(0^\circ)_6$, $(45^\circ)_6$, $(60^\circ)_6$, $(90^\circ)_6$ and cross laminated $(0^\circ/90^\circ)_6$ s with 3-ply with 0° and 3-ply with 90° . The tensile strength ratio of the $(0^\circ)_6 : (0^\circ/90^\circ)_6$ s samples was as high as 2.7 (Kannan et al., 2013). In such scenario, the failure of the UD (0°) samples can be attributed to the fibre rupture along their axial directional arrangement, fibre/matrix interfacial failure, matrix shear failure or matrix tensile failure. While the cross laminated ($0^\circ/90^\circ$) samples failure is dominated by local failures at fibre/matrix interface of half of the layers orthogonal to load direction as the remaining layers only exhibit half of the properties utmost.

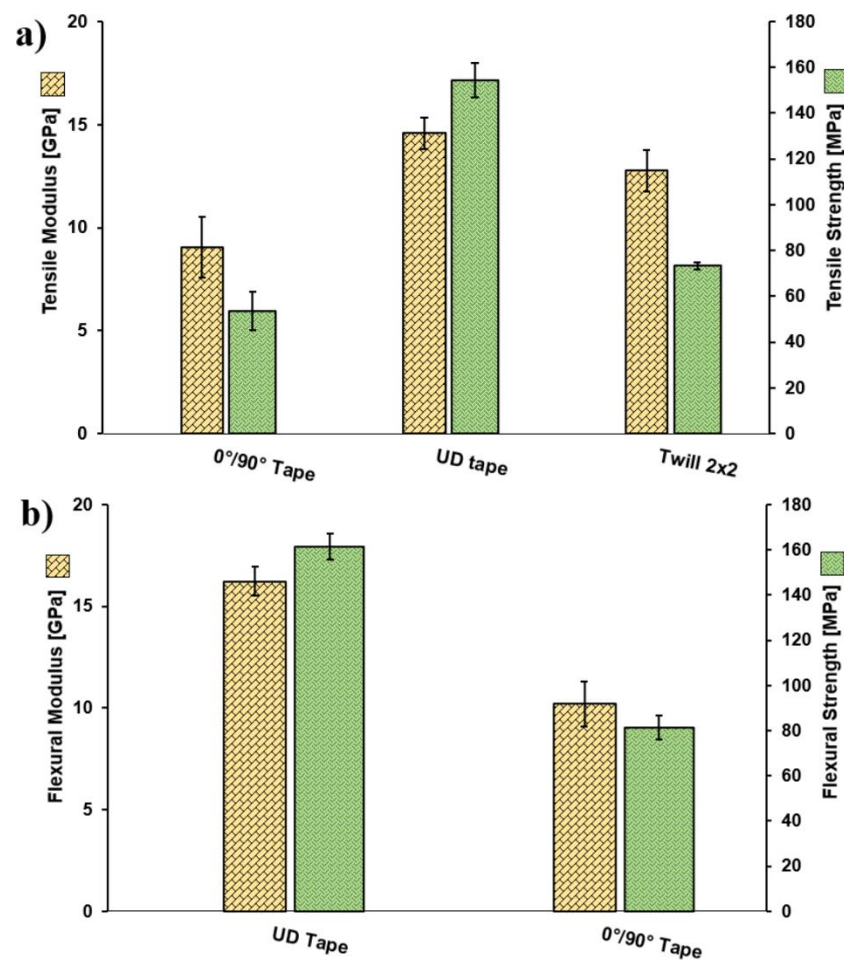


Figure 5-4 Comparison of: a) tensile performance of Flax/PP in a 50:50 fibre to matrix ratio amongst three fabric architectures: 0°/90°, UD tape and Biotex Twill 2x2. Reference specimen Twill 2x2 were only tested in tension mode, b) flexural performance between UD tapes and 0°/90°

Flexural performance of the Flax/PP panels was limited to only UD 0° and 0°/90° orientations, it can be seen from Figure 5-4 b) that the former displayed optimum flexural strength and modulus in values as twice and 1.5 times respectively compared to the latter. These results can also be explained by the directional arrangement of reinforcement in a manner that for UD 0° samples under flexure, the fibres were aligned along the longest side of specimen. Knowing the combined mode of flexure test, the bottom layer experiencing tension was supported by the longitudinal fibres, while the twill specimen bidirectional arrangement increased its flexibility.

With regard to the effect of a modified matrix, maleated PP (MAPP), the 0°/90° and twill fabric based specimen showed apparent similarity in terms of tensile strength and modulus, see Figure 5-5. A slight advantage of 13% in both stiffness and strength when comparing the 0°/90° to twill fabrics. The tape production technology proved adequate to achieve inter-layer and intra-layer efficacy to distribute the load over the specimen and eliminate zones of stress concentration that can be detrimental to a composite. Furthermore, the addition of coupling agent to the PP matrix improved strength substantially by 96% while stiffness recorded a 38% increase in comparison to the unmodified PP.

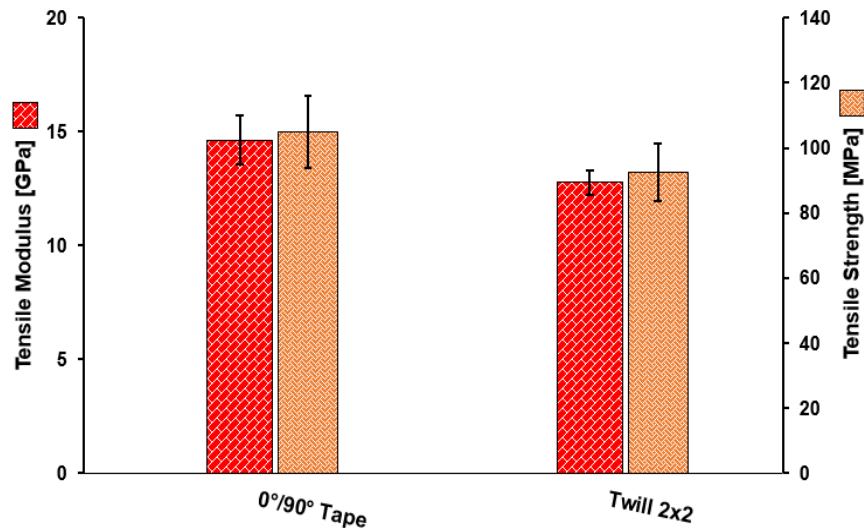


Figure 5-5 Comparison of tensile performance of Flax/MAPP in a 50:50 fibre to matrix ratio between two fabric architectures: 0°/90° tape and Biotex Twill 2x2

To further examine the combined effect of this type of coupling agent and fibre contents, tensile and flexural tests have been conducted on 40, 50 and 60 flax wt% and results are presented in Figure 5-6. It was difficult to distinguish a clear relationship between the fibre contents and tensile performance since although samples of 50 wt% displayed slightly better stiffness and strength. Noting that the tensile modulus peaked for this level of reinforcement before reducing again for 60 wt%, the maximum increase was calculated for a fibre content increase from 40 to 50 wt% to be 22%. Maximum tensile strength was found at fibre loading of 50 wt% and 60 wt% reaching a high value of 105 MPa which is equivalent to 15% increase from the 40% samples. In contrast, flexural strength increased linearly as fibre contents increased from 40 to 60 wt%, flexural modulus however was found to only increase once fibre content reached 60 wt% by 32% as compared to an average value of 6.8 GPa obtained for both 40 and 50 wt%.

In summary, for valid comparison, the 50:50 wt% of 0°/90° tapes across the three matrices have been considered, a noticeable impact of PP modification (MAPP) in improving the tensile modulus to a level comparable to the PLA based biocomposites (>14 GPa). In addition, there was a remarkable doubling of tensile strength for MAPP based specimen compared to those of PP and PLA based. In terms of flexural performance, this was not quite the case as PLA based biocomposites surpassed both PP and MAPP.

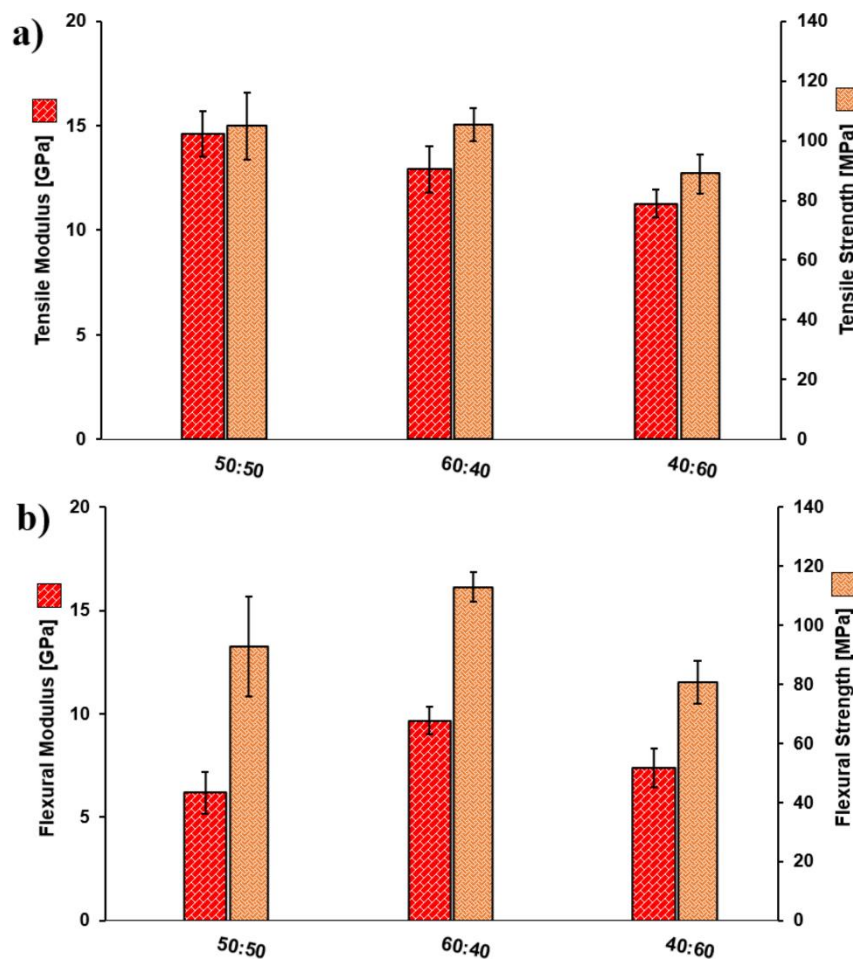


Figure 5-6 Comparison of: a) tensile properties, b) flexural properties of Flax/MAPP in varying fibre to matrix ratio by weight of 0°/90° tape architectures: 40:60, 50:50 and 60:40

5.1.1.2. Thermoset based biocomposites

Similar approach of mechanical characterisation and comparison adopted in the previous section 5.1.1.1 will be followed here, although this entails thermoset polymers and their associated fabrication processes. A trial of flax hybridisation using 100% flax tapes and glass veils layered in the UD (0°) as a reference material is also included. This technique has been considered by many researchers, a review states (Jawaid and Khalil, 2011) to provide an insight on how lower density of materials can be achieved. Hybridisation can yield relatively light weight composites with acceptable specific properties, low cost and ease of separation with enhanced energy recovery (Jusoh et al., 2016). Table 5-2 summarises all the tensile and flexural results obtained for various reinforcement architecture with either Biorez PFA or Crsytic UPE, the achieved fibre contents by volume and densities have also been included. Further to the tabulated results, charts have been also produced to capture comparisons of selected specimen either on the orientation basis, reinforcement type or any combination of the three.

Table 5-2 Complete set of tensile and flexural tests results of flax reinforced biocomposites using various reinforcement architectures and thermosets

Reinforcement	Matrix	Fibre:Resin	Orientation	V _f ^a (%)	Density (g/cm ³)	Tensile Modulus [GPa]		Tensile Strength [MPa]		Flexural Modulus [GPa]		Flexural Strength [MPa]	
						Average	S.D.	Average	S.D.	Average	S.D.	Average	S.D.
Flax/Glass veil 80/20 UD (0°)		55:45 (450gsm)	UD (0°)	52.8		24.3	1.77	240	10.3	19.4	1.3	252.00	9.4
Flax Prepreg Twill 2x2		50:50 (400gsm)	Twill 2x2	48		10.5	0.97	69	7.9	9.6	0.89	100.00	6.3
Flax/PLA 90/10	BIOREZ	50:50 (170gsm)	UD (0°)	47	1.4	16.90	0.85	144.60	14.30	13.90	0.49	166.60	7.7
			0°/90°			8.80	0.34	81.60	3.85	8.50	1.73	125.20	13.3
			±45°			13.40	1.64	87.90	18.00	11.06	1.88	155.00	11
Non-crimp Fabric Flax/PLA 90/10		52:48 (363gsm)	NCF ±45°	46		14.27	2.66	103.00	9.30	9.52	2.25	158.20	14.9
Flax Laminate	CRYSTIC	41:59 (400gsm)	Twill 2x2	35	1.23	7.20	0.79	68.30	6.70	4.00	0.83	97.40	7.70
			UD (0°)	33	1.3	17.20	1.24	165.50	40.80	13.70	1.50	188.90	13.9
			0°/90°	33	1.3	11.00	1.45	107.40	8.40	9.50	1.19	140.40	8.9

Firstly, a performance comparison among panels of Biorez PFA reinforced with aligned flax tapes as UD (0°), either hybrid i.e. combined with glass veil 80:20 (wt%) or commingled with PLA 90:10 (wt%). Another panel fabricated from Crystic polyester and 100% flax laminates were also part of the comparison. Figure 5-7a) indicates that the maximum properties for tensile modulus and strength among these biocomposites is associated with the hybrid (glass veil) specimen. The other two appear to bear similar tensile properties. Tensile modulus is found to be 44% greater than that of the comingled flax/PLA tapes and flax/Crystic laminate, the latter two exhibit similar stiffness of ~ 17 GPa. Tensile strength is also 66% greater for the hybrid than the comingled fabric and 45% greater than of the flax only laminate.

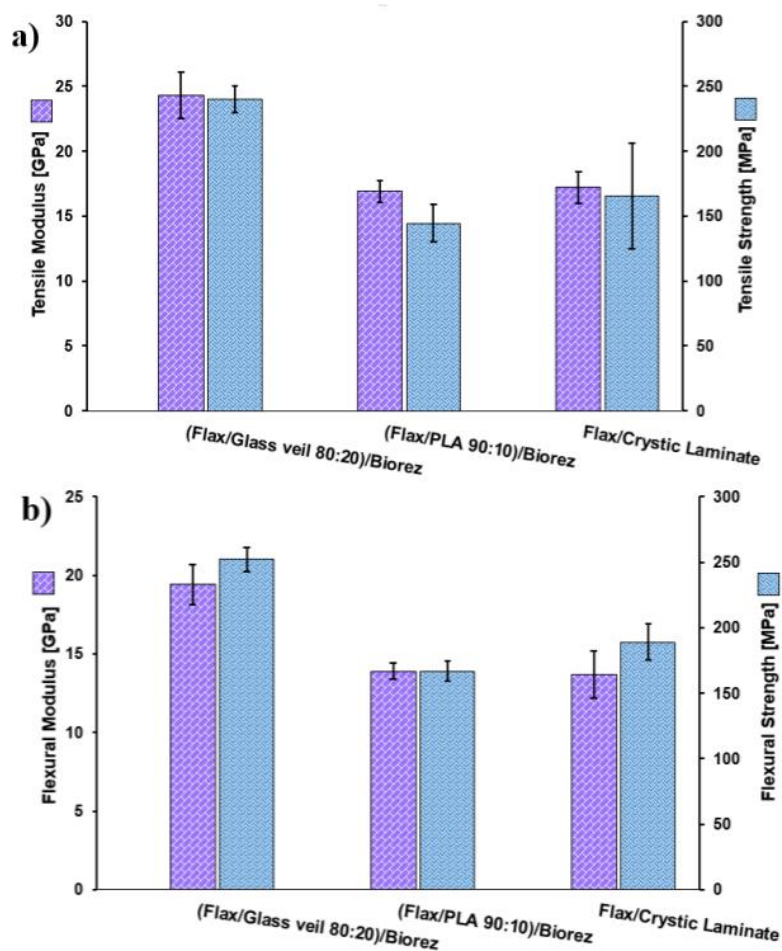


Figure 5-7 comparison of performance between three fabric reinforcements unidirectional (0°): Flax/glass veils ($V_f=52\%$), Flax/PLA 90:10 ($V_f=47\%$) and Flax Crystic laminate ($V_f=33\%$). Fibre contents $V_f=52\%$ for the hybrid mat due glass presence. This difference explains the superior tensile (chart a) and flexural (chart b) moduli and strengths.

Likewise, the flexural properties revealed the same trend as the hybrid specimen outperformed the comingled flax/PLA and flax only laminate. Flexural modulus of hybrid samples was found to be 40% greater than those of the comingled flax/PLA and flax only laminate, the latter two exhibited similar flexural stiffness of ~ 13.8 GPa. The highest attained flexural strength corresponded to the hybrid specimen at 252 MPa, which is 51% and 33% greater than those of comingled flax/PLA and only flax

laminate respectively. The results reported herein are in agreement with other work, as incorporation of GF plies to sandwich NF tapes for improved mechanical properties have been extensively explored (Ahmed and Vijayarangan, 2008). The superior properties of the hybrid specimen are attributed to the stiffer glass fibres laid along the flax fibres.

Further investigation into the tensile and flexural performance of flax reinforced Biorez PFA with respect to methods of plies stacking, direction and sequence have been conducted as depicted in Figure 5-8. Among these considered specimen, the highest tensile modulus and strength related to the flax/PLA tapes UD (0°) specimen, values of 16.9 GPa and 144.6 MPa respectively as fibres are aligned along the load direction. The second highest values, 14.3 GPa and 103 MPa, correspond to the non-crimp specimen aligned along the $\pm 45^\circ$ direction. Similar results of the multi-layered $\pm 45^\circ$, but slightly lower, stiffness 6% and strength 14.6% as compared to the NCF $\pm 45^\circ$. This small variation is expected as it can be attributed to the extra stitching in the z-direction which improved the inter-laminar strength. A further decrease of tensile properties for the bidirectional specimen, $0^\circ/90^\circ$ having 8.8 GPa modulus and 81 MPa strength, while twill fabrics showed a higher modulus 10.5 GPa but a lower strength of 69 MPa.

With regard to the flexural properties, the UD (0°) specimen maintained their dominance over the other biocomposites although this was marginal compared to the observed trend for tensile behaviour. In terms of flexural modulus, again the UD (0°) claimed the highest value of 13.9 GPa which was 20% and 31% higher than those of the multi-layered $\pm 45^\circ$ and NCF $\pm 45^\circ$ respectively. Interestingly, the twill specimen exhibited equivalent average modulus values to the NCF $\pm 45^\circ$ specimen. Although this statement does not hold when standard deviations are considered, the NCF $\pm 45^\circ$ generally are comparable to the multi-layered $\pm 45^\circ$. Meanwhile, the lowest flexural modulus was found for specimen oriented in the $0^\circ/90^\circ$ with an average value of 8.5 (± 1.73 GPa) which, again based on S.D. implications, is comparable to the twill specimen. Similar observation was found for the flexural strength, the highest recorded 166 MPa while a marginal decrease for both the multi-layered $\pm 45^\circ$ and NCF $\pm 45^\circ$ at 155 MPa and 158 MPa respectively. A further decrease of strength for the $0^\circ/90^\circ$ to 125 MPa which continues to drop to a lowest level 100 MPa for the twill specimen.

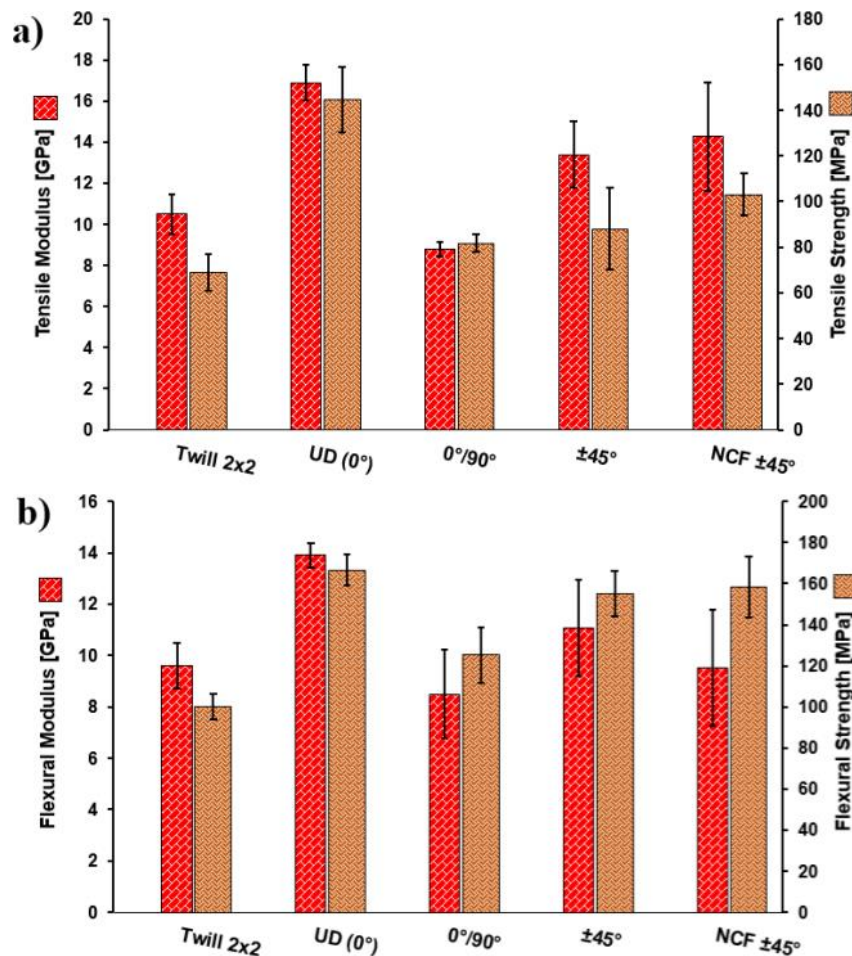


Figure 5-8 comparison of: a) tensile and b) flexural moduli and strengths of BioRez reinforced with two different fabric architectures in a mixture of 50:50, Tapes of Flax/PLA 90:10 and Non-Crimp Fabrics of Flax/PLA 90:10, both materials achieved similar fibre contents $V_f = 47\%$. While the Tapes were constructed in various orientations (UD 0°, 0°/90° and ±45°), Non-Crimp Fabrics were limited to ±45° this is for process evaluation purpose. Twill 2x2 100% flax fabric were also used in the comparison.

Polyester based specimen with reinforcement architectures similar to those considered for the bio-based resin (PFA), with the exception of the ±45° orientation, have also been investigated, tensile and flexural results are presented in Figure 5-9. With no major deviations from what have been previously reported here with regard to the effect of architecture on the performance. The highest tensile modulus and strength tallied 17.2 GPa and 165.5 MPa respectively was associated with the unidirectional orientation (UD 0°). The second best performer was the 0°/90° as 11 GPa modulus and 107.4 MPa strength have been obtained, 36% and 35% respective reduction with reference to the 0° orientation. The lowest performance for Crystic based specimen was linked to specimen fabricated from twill fabrics as a further reduction of 35% modulus and 36% strength as compared to the 0°/90° specimen. A possible explanation of the unexpectedly lower performance of the twill arrangement compared to 0°/90°, is the in plane waviness of fibres which can be associated with the vacuum infusion process. Further, this waviness induces complex loading on the structure resulting in highly non-linear response followed by multiple stages failure with matrix cracking and fibre breaking and a result affecting the global strength and stiffness. The direction of applied load whether in the warp or weft orientation, crimp and fibre

twist values and general quality of fibres can also affect the tensile response. For like-to-like architecture comparison using bio-based PFA and UPE, the former exhibited higher modulus while tensile strength was identical.

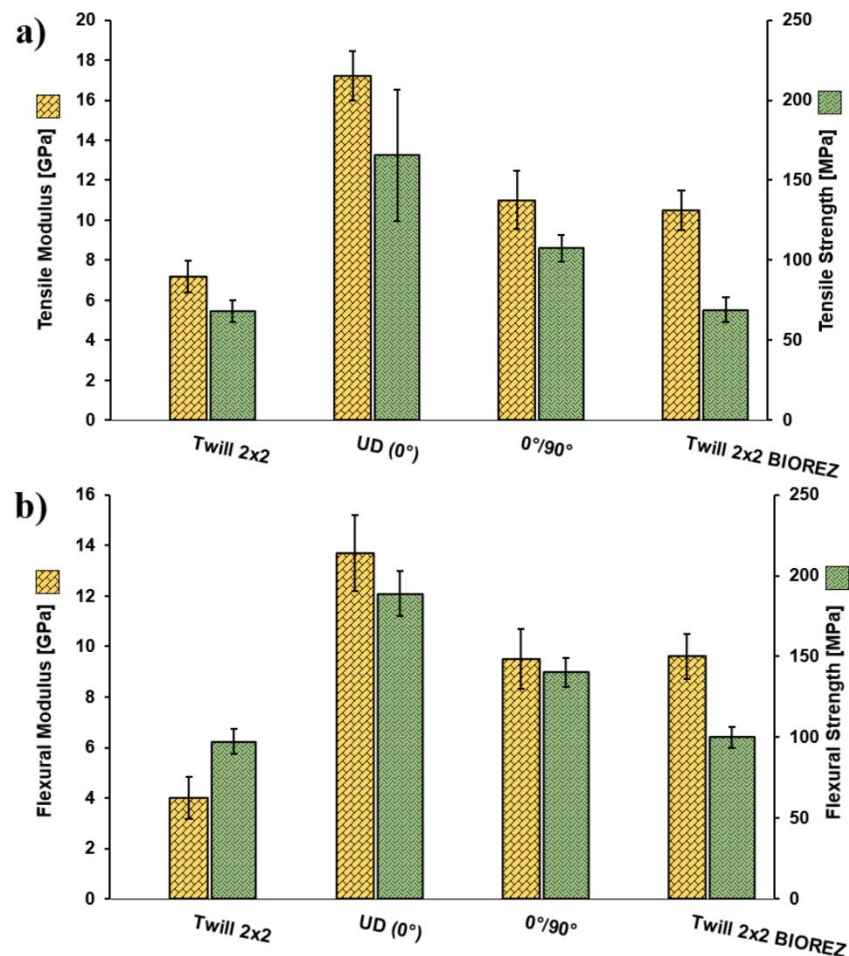


Figure 5-9 comparison of: a) tensile and b) flexural moduli and strengths of Crystic polyester reinforced with Flax Laminates (Twill 2x2, UD 0° and 0°/90°) and BioRez reinforced with Twill Flax prepreg, both materials achieved similar fibre contents $V_f = 33\%$.

The flexural properties were found in agreement with the reported trend of tensile properties. The highest flexural modulus of 13.7 GPa and flexural strength 189 MPa were obtained for the UD (0°) as these decreased limit by 71% and 48% respectively for the twill/polyester representing the lowest limit. On the other hand, the bidirectional 0°/90° specimen fell somewhat in the middle as they displayed a modulus of 9.5 GPa and strength of 140.4 MPa. Note that although the direct comparison of twill reinforcement with Biorez (PFA) and Crystic (UPE) revealed a superior performance (both modulus and strength) of the former specimen, a similar modulus (1% variation) with the 0°/90° was reported.

5.1.2. Discontinuous- Nonwoven

5.1.2.1. Thermoplastic based biocomposites

The thermoplastic specimen considered for characterisation, nonwoven Flax/PP, covered only the tensile test whereby the stiffness and strength have been evaluated. Figure 5-10 represents the tensile

nominal stress plotted against the nominal strain for all specimen put under test. Three zones can be distinguished. The behaviour is linear at the beginning of the loading, and a change occurs in the slope indicating the first damage as this nonlinearity increases with the load. Finally, the stress decreases with a slight plastic strain followed by failure of the tensile specimen. The initial part of the curves suggest consistent stiffness with an average of 1785 (± 102 MPa). The linear trend observed for all specimen extends up to a strain of 0.5%. The non-linear response thereafter can be explained by the three-phase mechanism as described in the literature: a) microcracks initiation at fibre end matrix interphase that propagates along the fibre lengths, b) plastic deformation of the matrix, and c) microcrack opening in the matrix and the slow crack propagation through the deformed matrix (Panthapulakkal and Sain, 2007). The fibre pull-out from the matrix initiates catastrophic crack propagation through the matrix. Stiffness in composites is generally attributed to the fibres, though to bring out the best stiffness from fibres, adequate fibre/matrix interface for efficient load transfer is essential. The tensile strength however, taken as the highest point on the curve, indicates variations among the tested specimen with an average of 15.3 (± 0.7 MPa). Since the fibre matrix interface is responsible for the strength of composites, this variation is likely to be caused by the inherent voids present within the samples which vary due to processing. Furthermore, the adhesion of the flax fibre and PP matrix is apparently insufficient to provide enhancement of the NFC strength above that of the polymer matrix.

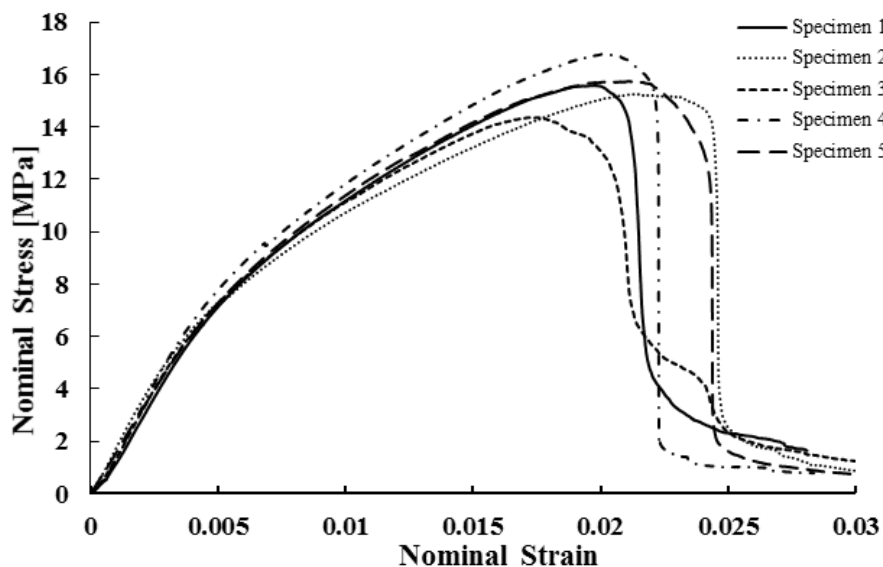


Figure 5-10 Tensile test nominal stress vs strain curves of five Flax/PP specimen

The strain at failure as can be seen from the curves of Figure 5-10 was found to be in the range 2 – 2.5% which signifies the presence of fibres. The composite exhibits a brittle-like failure as denoted by the sudden drop of load at a certain displacement. Notably, the strain at failure of pure PP, although not evaluated in this study, a similar grade of PP has been tested in several studies and elongation values were in excess of 10% (Martin et al., 2016) (Vas and Bakonyi, 2012).

Tensile properties of composites are dependent on the stress direction as found and reported in Table 5-3. Both modulus and strength values decreased when the tensile load was aligned perpendicular to the fibre arrangement, as the former decreases from an average value of 1785 MPa for longitudinal direction to 1204 MPa for the transverse direction. Similarly, tensile strength decreases from an average value of 15.3 MPa for longitudinal to 10.4 MPa for transverse direction. This is attributed to the inherent anisotropic property of nonwoven fabrics. The mechanical interlocking of fibres to produce needle-punch fabrics may cause some distortion in fibre alignment at the micro-level which results in variations of the composite macro-level behaviour. This observation is in agreement with literature as the tensile strength of the parallel web or random web was found to decrease with increasing angle of cut of the specimen for strength measurement (Maity and Singha, 2012). Another study (Miao and Shan, 2011) employed a modified process which is simpler and cheaper method of converting fibres directly into a mat without involving the spinning and weaving operations. This involved an additional drawing operation into the parallel-laying nonwoven process. The drawing operation considerably improves the fibre alignment in the final mat, leading to a significant increase in mechanical performance of the final composite. Although, the tensile properties reported in Miao and co-authors study are considerably higher than the values reported herein as their panels consisted of stacking 6 layered mats instead of only one layer used in our study.

Table 5-3 comparison of tensile properties between nonwoven Flax/PP specimen cut and tested in the longitudinal and transverse directions

Test Direction	Tensile Modulus [MPa]		Tensile Strength [MPa]	
	Average	S.D.	Average	S.D.
Longitudinal	1785	±102	15.3	±0.77
Transverse	1204	±108	10.74	±0.74

Figure 5-12 presents the directional tensile response of specimen cut from the same panel in two directions (Figure 5-11), longitudinal and transverse. The specimen cut along the fibre alignment i.e. longitudinal exhibited higher strength and modulus but also higher strain to failure of ~2.5% compared to that recorded (>2%) for the specimen tested along the cross direction i.e. transverse. This can be explained by the combination of potential voids and fibre rich zones aligned perpendicular to the load direction.

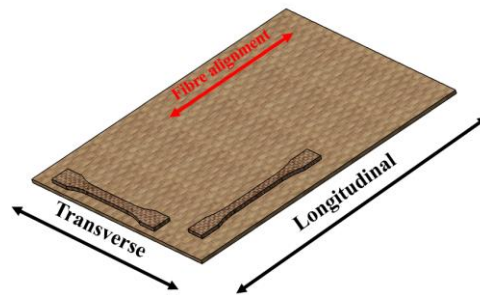


Figure 5-11 Nonwoven Flax/PP panel cut direction for the purpose of testing in the longitudinal (along fibre direction) and transverse directions

The given results confirm that a degree of fibre alignment has been achieved through the parallel-laying method, a less commonly adopted nonwoven process. This method preserves the partial fibre alignment in the carded web as opposed to cross-laying the carded web, used to form most carded nonwoven mats, resulting in a reduction of fibre alignment in the final mat. As reported in literature (Anandjiwala and Boguslavsky, 2008), the practice of producing nonwoven mats by web formation and cross-laying results in different strengths in the machine direction and cross direction. The tensile properties of nonwoven fabrics change in the different directions of the fabric due to structural anisotropy resulting from the process of fabric formation.

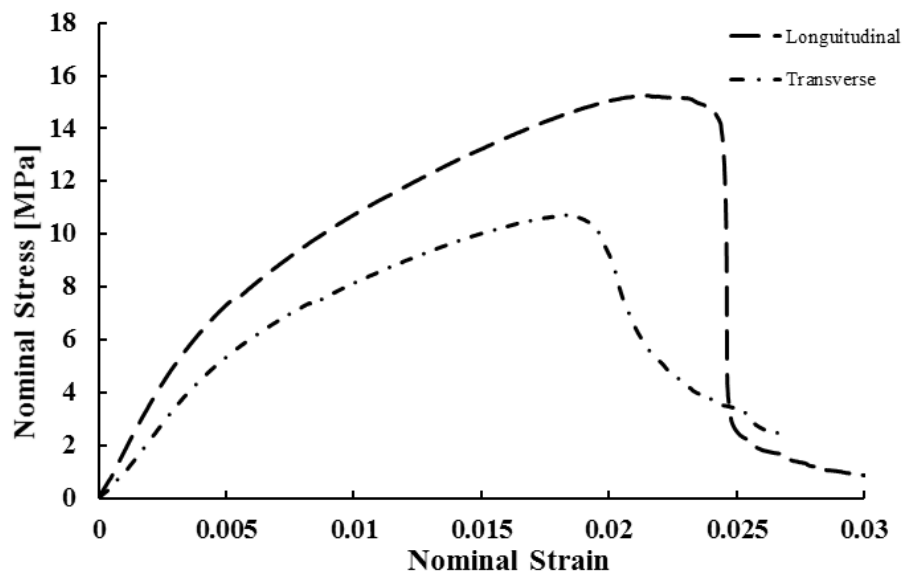


Figure 5-12 tensile response comparison between nonwoven Flax/PP specimen tested in the longitudinal and transverse directions

Thermo-bonding process used in the fabrication of nonwoven mats is responsible for the formation of interlock points between different flax fibres to allow their easy handling. In the case of high fibre contents, the matrix is unable to form aggregates of melted PP/flax which in turn results in lack of adhesion.

5.1.2.2. Thermoset based biocomposites

The effect of fibre volume fraction on the physical and tensile properties of discontinuous aligned natural fibre composites Flax/UPE produced via vacuum infusion has been investigated. There is no clear correlation between fibre volume fraction and tensile strength due to uncertainty on the void contents associated with this method of composite type production. However, according to Shah and co-authors low fibre content NFCs are prone to intra-yarn voids, while high fibre content NFCs are prone to inter-yarn voids. This is due to changing resin flow dynamics with increasing fibre content (Shah et al., 2012). In our study, tensile modulus and strength of a single layer of nonwoven flax mat impregnated with polyester resin have been evaluated, results are presented in Table 5-4.

Table 5-4 Tensile modulus and strength averaged values and their corresponding standard deviations (S.D.) of the five nonwoven Flax/Polyester specimen tested under tension for three levels of fibre volume contents.

Fibre volume content ($V_f\%$)	Tensile Modulus [MPa]		Tensile Strength [MPa]	
	Average	S.D.	Average	S.D.
14	1936	± 155	34.1	± 1.76
18	2385	± 280	28.6	± 2.75
22	3115	± 93	31.2	± 1.92

The tensile behaviour of Flax/UPE as depicted in Figure 5-13, highlights the effects of flax fibres when reinforced with a resin matrix as the non-linear stress-strain response of natural fibres has been transferred to the biocomposite. This can be clearly observed from the linear part of the curves attributed to the stiffness which appears to be extended as fibre contents decrease indicating the elastic behaviour of the matrix to be dominant. Yet this linear elastic response shrinks with increasing fibre contents but with increased slope, this correlates with the tensile modulus values recorded in Table 5-4 as they increase from 1936 (± 155 MPa) for $V_f=14\%$ to 3115 (± 93 MPa) for $V_f=22\%$. On the other hand, strength of these samples taken as the highest point on the curves appeared to reveal a different behaviour as the highest strength value of 34.1 (± 1.76 MPa) was associated with the minimum fibre contents at $V_f=14\%$. Meanwhile the lowest strength of 28.6 (± 2.75 MPa) corresponded to fibre contents $V_f=18\%$ and a median strength of 31.2 (± 1.92 MPa) for specimen of $V_f=22\%$. However, considering their standard deviations, these variations are insignificant and therefore they are considered to have equivalent strengths.

The effect of fibre contents on the strain at failure is demonstrated through the observed decrease in extension of the curves of Figure 5-13 with increased fibre contents to 2.3%, 2% then 1.7% as fibre contents increase from 14% to 18% then 22% respectively. While a strain at failure of virgin polyester is around 1.5%, this value suggests that flax reinforcement introduces an increase in strain at failure.

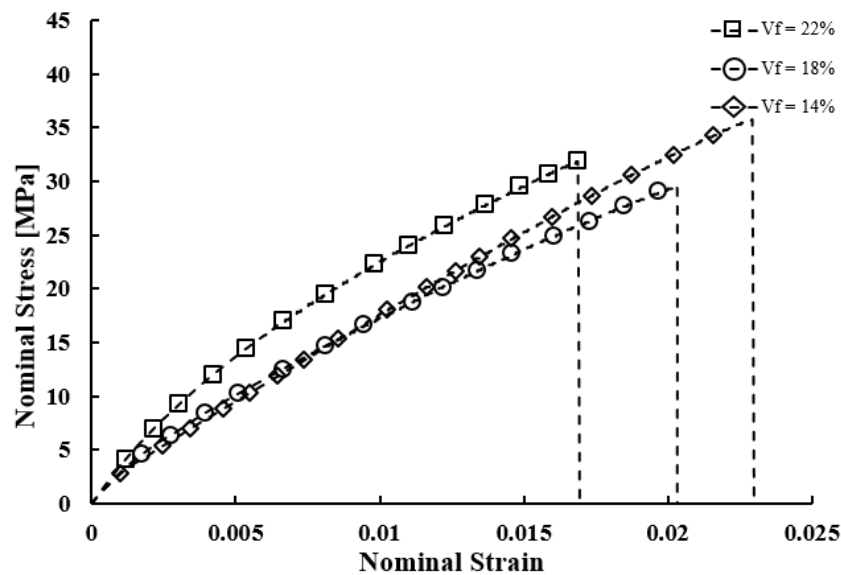


Figure 5-13 Tensile nominal stress vs strain curves for three different nonwoven Flax/Polyester panels of varying fibre contents represented in their averaged values for: $V_f = 22\%$, $V_f = 18\%$, $V_f = 14\%$

Flexural moduli and strengths of the tested specimen Flax/UPE with varying fibre contents are presented in Table 5-5. There is an increase in modulus and strength of the Flax/UPE samples, however at fibre loading of 14% and 18%, the modulus reported of 3001 (± 295 MPa) and 3490 (± 179 MPa) respectively fell short of the typically reported average value of virgin polyester of 4000 (± 500 MPa) (Gouanve et al., 2006). Furthermore, strength increased from 31 (± 2.62 MPa) to 44.8 (± 2.77 MPa) corresponding to fibre loading of 14% to 22% respectively. However, the flexural strength reported herein is well below the typical reported values in literature (Yu et al., 2009). This may be due to the quality of the reinforcement as the mat manufacturing which may have had an effect on the void formation hence the poor fibre matrix interface led to the load transfer inefficiency. While the modulus increase reported in this study is well in agreement with current literature the strength is mostly in agreement (Rassmann et al., 2010) (Dhakal et al., 2007), however with some exceptions. As others reported a decrease of strength with increased hemp fibre contents from 0% to 30% (Sawpan et al., 2012). For this particular study, this was explained by stress concentrations and population of fibre defects (kink bands).

Table 5-5 Flexural modulus and strength averaged values and their corresponding standard deviations (S.D.) of the five specimen tested under 3pt bending for three levels of fibre volume contents.

Fibre volume content ($V_f\%$)	Flexural Modulus [MPa]		Flexural Strength [MPa]	
	Average	S.D.	Average	S.D.
14	3001	± 295	31.0	± 2.62
18	3490	± 179	34.9	± 5.91
22	4706	± 817	44.8	± 2.77

The extent of specimen deflection under flexure testing is observed to vary across the three levels of fibre loading. The flexural strain at failure is therefore found to increase with an increased flax content, this may be attributed to the fibre arrangements within the polyester matrix. The fibre reinforcement is also thought to have created a flexible structure with higher resilience as demonstrated in the 22% fibre content with a strain at failure of 3.6%. Meanwhile, the other two specimens of 14% and 18% exhibited lower but comparable deflections of 2.4% and 2.6% respectively.

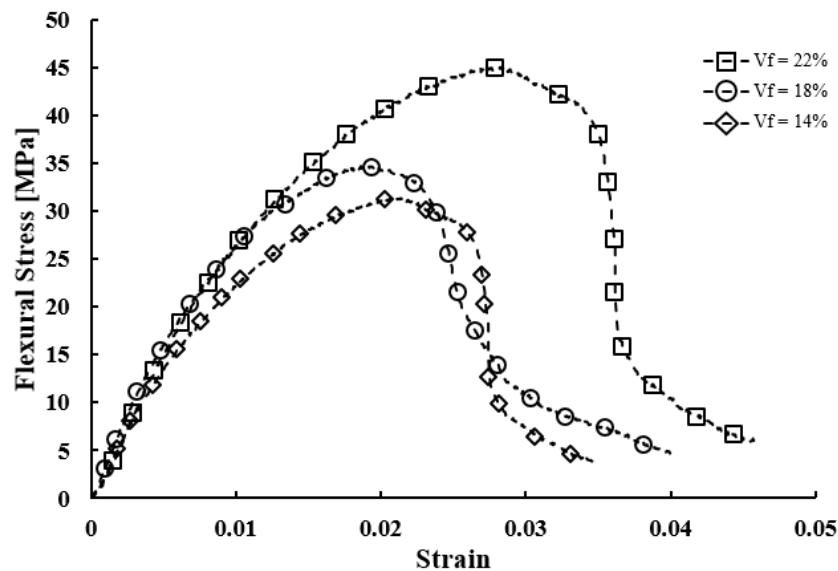


Figure 5-14 Flexural nominal stress vs strain curves for three different nonwoven Flax/Polyester panels of varying fibre contents represented in their averaged values for: $V_f = 22\%$, $V_f = 18\%$, $V_f = 14\%$

Introduction of flax fibres to the polyester matrix imparted the material with some form of plastic properties. Increase in fibre content led to an enhanced limit of proportionality and a larger plastic region.

5.1.3. The effect of In-Situ Temperature on NFCs under Tension

The selection of flax based biocomposite materials to be considered for investigation in terms of *in-situ* temperature effects on the tensile properties were based on a number of considerations and the preliminary results reported in sections 5.1.1 and 5.1.2. These considerations included primarily the ease to manufacture and end-use application, in addition to, the mechanical performance and thermal stability of flax fibres as demonstrated in TGA studies in section 4.1.1.2. Flax fibres when exposed to a ramping temperature show no sign degradation until up to temperatures as high as 200°C. Therefore the range selected to investigate the thermal stability of the biocomposite in temperature range of 30–70°C is deemed well below the degradation effects. The aim of this investigation is to determine the thermal conditioning on the interface between the fibre and matrix and how this would affect the mechanical performance.

5.1.3.1. Flax/Poly-lactic continuous reinforcement

The preliminary results of the continuous flax reinforced with PLA with a 0°/90° revealed their potential to be used in structural applications. It is well established that thermoplastic polymers tend to be affected by temperature during the life service of such products due to its linear molecular arrangement. This structure causes thermal instability of thermoplastics as temperature increases to approach the glass transition temperature which inadvertently affects their mechanical performance. It is therefore necessary to evaluate the effect of increasing *in-situ* temperature on the tensile behaviour of flax reinforced PLA over the range of 30 – 70 °C. Table 5-6 lists the average tensile moduli and strength values and their corresponding standard deviations of five specimen tested under each temperature condition. Specimen exhibited a significant decrease in both tensile modulus and strength as temperature was raised to surpass the glass transition of PLA typically in the range of 55- 65 °C. With regard to modulus a decrease of 76% from 30 to 70°C while 66% decrease in tensile strength was recorded over the same temperature range. For the modulus in particular, it can be noticed that the reduction was severe at temperatures below and up to 50 °C from 30 °C with values axed by 35% then again by 47% through the 10 °C increments. Above 50 °C the modulus reduction tends to be comparatively lower with 15% and 12% as temperature progresses to 60 °C then 70 °C respectively. On the other hand, strength was found to be decreasing steadily over the same range with a 25 % reduction from 30 to 40 °C after which strength shows no significant change as temperature increases to 50 °C. Further reductions of 28% and 32% with 10 °C temperature increments up to 70 °C.

Table 5-6 Tensile modulus and strength averaged values of continuous aligned of Flax/PLA and their corresponding standard deviations (S.D.) of the five specimen tested under varying temperatures 30°C to 70°C.

Temperature °C	Tensile Modulus [MPa]		Tensile Strength [MPa]	
	Average	S.D.	Average	S.D.
30	10946	261	47.29	0.32
40	6784	206	37.46	2.32
50	3581	71	33.75	1.6
60	3027	120	24.11	2.64
70	2650	179	16.24	1.45

There is a clear trend of tensile properties deterioration as temperature increases from ambient up to 70°C as shown in Figure 5-15. All specimen tested across this range of temperatures exhibited the same expected behaviour as stress increases non-linearly with strain increase. This continues up to a maximum load indicating the tensile strenght of the specimen before a sudden drop in load wich signifies the failure point. This typical response is a characteristic of reinforcement with flax fibres. The effects of temeprature on polymeric composites can be identified from the stress-strain trace and found to be opposite to the effect of increased strain rate. For instance, at low temeprature the stress–strain behavior is much like that of a brittle material. Specimen tested under temperatures below 50 °C may

not exhibit any signs of yielding and the strain-to-failure is low. As the temperature is increased, yielding may occur; but the yield strength decreases with increasing temperature.

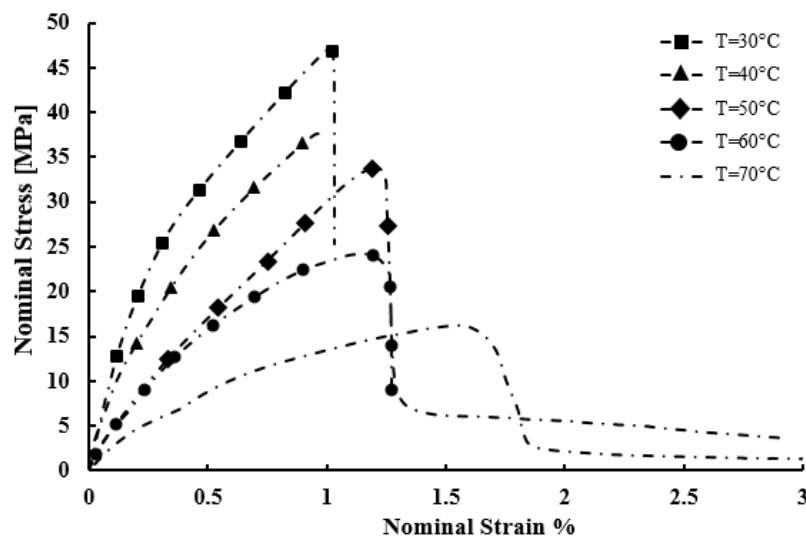


Figure 5-15 Tensile nominal stress vs strain averaged curves of five test repetitions of Flax/PLA panels tested under a range of temperatures 30°C- 70°C

The contribution of flax reinforcement within a PLA matrix is to increase its fracture toughness, through the increased modulus of elasticity due to adequate stress transfer from the fibres to the matrix. Meanwhile, the polymeric matrix of PLA presence induces the brittleness observed from the curves, however this effect is diminished as temperature increases. With regard to the strain to failure, an increase from 1.02% to 1.62% corresponds to an increase in temperature from 30°C to 70°C. This behaviour is attributed to the thermal degradation of PLA as specimen approach glass transition temperature. At this stage, thermal transitions occur which can impart dramatic step-changes in the biocomposite behaviour since temperature weakens the interfacial bonding between flax fibres and PLA matrix.

5.1.3.2. Flax/Polypropylene nonwoven mats

Tensile test results of flax and thermoplastic based biocomposites using both continuous and discontinuous reinforcements under ambient conditions were reported in previous sections. Furthermore, in light of what was reported for Flax/PLA in terms of *in-situ* thermal conditioning on tensile properties deterioration, tensile properties of Flax/PP nonwoven mats have been evaluated with respect to the same temperature range to identify common behaviour characteristics of these biocomposites. It has been previously established that nonwoven mats possess lower load bearing abilities when compared to continuous reinforcement such that of Flax/PLA. This is shown to deteriorate further with temperature increase. Table 5-7 summarises the average tensile modulus and strength values and their corresponding standard deviations of five specimen tested under each temperature condition. Upon increasing temperature from 30 to 70°C, a very similar temperature dependency was observed for both tensile modulus and strength with a significant loss of 58% and 60%

respectively. Although the progressive deterioration (calculated in increment of 10°C) of modulus and strength differ, as modulus recorded steeper reductions of 28% and 24% with temperature above 50°C. On the other hand, specimen exhibited the highest strength reduction of 41% at the lower range (i.e. 30-50°C) in comparison to 33% for the upper temperature range (above 50°C). This observation suggests that while the stiffness is controlled by the fibres themselves which is also affected by the interface, strength is more susceptible to matrix cracking as evidenced here with PP vulnerability to heat. A temperature increase introduces internal stresses caused by differential thermal coefficients of the flax and the PP matrix.

Table 5-7 Averaged tensile modulus and strength values with calculated standard deviations of five test repetitions of Flax/PP panels tested under the effect of temperature 30°C- 70°C

Temperature °C	Tensile Modulus [MPa]		Tensile Strength [MPa]	
	Average	S.D.	Average	S.D.
30	1399	55	11.99	0.89
40	1222	88	9.56	0.58
50	1056	96	7.06	0.49
60	760	58	5.82	0.5
70	577	77	4.72	0.43

The acquired load-displacement traces have been transformed into nominal stress-strain curves using individual specimen geometry. Averaged curves of at least five repetitions tested after conditioning to the allocated temperature are included in Figure 5-16. A soak duration has been predetermined as part of pre-test trials. All specimen exhibited non-linear response over the entire strain history, with some specimen having no clear peak, thus the absence of a yield point indicates the poor interaction between flax fibres and PP. This phenomena was previously explained by discontinuity in the composites structure due to lack of matrix aggregates to form interlock points. The flax to PP weight ratio employed in this study (52:48) and processing parameters may have affected the microstructure of the final biocomposite. Specimen tested below 50°C, yield strength after which failure manifests through a sharp drop in load capacity is explicitly noted. Otherwise, specimen tested above 50°C, the yield point does not exist instead the curves prolonged up to 4% strain with minimal relative reduction to stress. This invalidates the analysis of strain-to-failure with respect to temperature effect, nevertheless, it is evident that by increasing the temperature the elongation of flax/PP composite increases. Strain values of all specimen ranged between 2.7% and 4%.

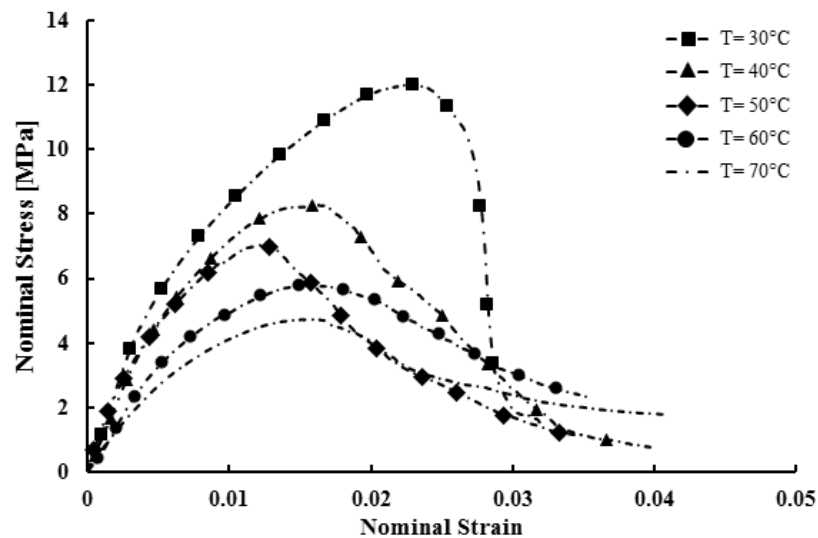


Figure 5-16 Tensile nominal stress vs strain averaged curves of five test repetitions of nonwoven Flax/PP panels tested under a range of temperatures 30°C- 70°C

5.1.3.3. Flax/Furan continuous reinforcement

Thermoset based biocomposites are not exempt from property-degradation when exposed to elevated temperature. Therefore the effect of increased temperature, identical range considered for thermoplastic based counterparts, has been evaluated. Here, samples of unidirectional Flax/PLA tapes in weight ratio of 90:10 used for reinforcement with Biorez PFA in a 1:1 fibre to matrix ratio were simultaneously exposed to conditioning while loaded in tension. The specimen demonstrated temperature dependency over the range 30-70°C for modulus and strength as they undergo a gradual decrease up to 35% and 22% respectively. This performance loss is considered less significant when compared to thermoplastic based specimen. PFA is a bio-resin which demonstrates higher thermal stability at temperatures below 80°C, owed to its high heat distortion temperature (HDT). The tensile properties described in our study are much higher than those reported by Kumar and Anandjiwala (Kumar and Anandjiwala, 2013) for a 60:40 resin to fabric ratio as they found a tensile strength of 15.53 MPa.

Table 5-8 Averaged tensile modulus and strength values with calculated standard deviations of five test repetitions of thermoset based aligned continuous Flax/Biorez panels tested under the effect of temperature 30°C- 70°C

Temperature °C	Tensile Modulus [MPa]		Tensile Strength [MPa]	
	Average	S.D.	Average	S.D.
30	8548	262	49.9	1.4
40	7907	352	48.02	4.2
50	6939	634	45.52	1.9
60	6013	208	43.39	1.2
70	5563	234	38.76	1.1

Averaged curves of at least five Flax/PFA tested specimen across the range of temperatures are presented in Figure 5-17. As a general trend, it can be observed that as temperature increases the peak stress and initial slope decrease while the strain-to-failure increases. This strain-to-failure was found to

be as low as 0.88% at 30°C increasing to 1.2% as temperature reaches 70°C. These strain values are even lower than the flax fibres (2.7-3.2%) but closer to the reported elongation of virgin PFA ~0.8% (Kumar and Anandjiwala, 2013). This suggests that the failure is matrix dominated. The curves shape is notably different to those recorded for PLA biocomposites as non-linear effect brought in by the presence of fibres is replaced by a bi-linear like curve. This demonstrates the good flax/PFA interface and the degree of crosslinking achieved at the PFA matrix level. In addition, the failure mode of these specimen is found to be consistently brittle indicated by the sharp drop in stress without further extension beyond yield point. It therefore appears that the ductility effect commonly caused by temperature increase is not observed here.

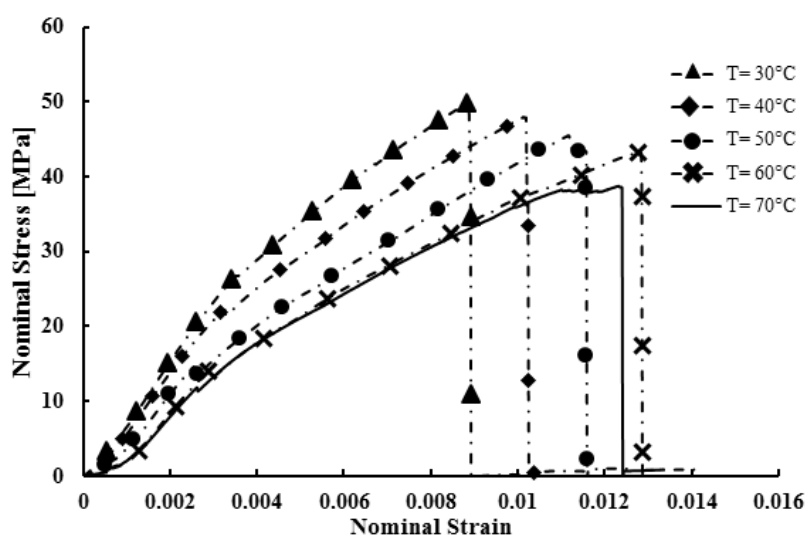


Figure 5-17 Tensile nominal stress vs strain averaged curves of five test repetitions of nonwoven Flax/Biorez panels tested under a range of temperature 30°C- 70°C.

The thermal stability of furan resins at temperatures below 80°C has limited the molecular chain mobility unlike the relaxation reactions around T_g observed in thermoplastic counterparts. Furthermore, flax fibres are reported to increase the elasticity of PFA as they effectively immobilise the polymeric chain segments as the cross-linking of the furan is enhanced in the presence of the fibres leading to the glass transition and subsequent softening not being observed to a temperature up to 70°C.

5.2. 3D-Printed PLA Structures

5.2.1. Dimensional accuracy

The dimensional accuracy and tolerances of the MakerBot Replicator 2 printer are not clearly stated apart from the positioning precision of the stepping motor of 11 μm in the x - y directions and 2.5 μm in the z - direction, as well a maximum layer resolution of 100 μm . Ensuring geometrical stability of 3D-printed parts through the optimisation of printing parameters increases the chances of adopting FDM technology and its scale-up to commercialisation. As can be seen in Figure 5-18 all samples fell well above the specified CAD dimensions 6 mm and 3 mm for width and thickness respectively. The mean

width of all 15 samples was 6.49 mm however is still within the upper tolerances of the ASTM standards of ± 0.5 mm. Although all specimen for raster orientation of $-30^\circ/+60^\circ$ fell within the control limits, they all had widths higher than the mean as well as the accepted upper tolerance. Otherwise specimen of $0^\circ/90^\circ$ and $\pm 45^\circ$ fell within the accepted upper tolerance.

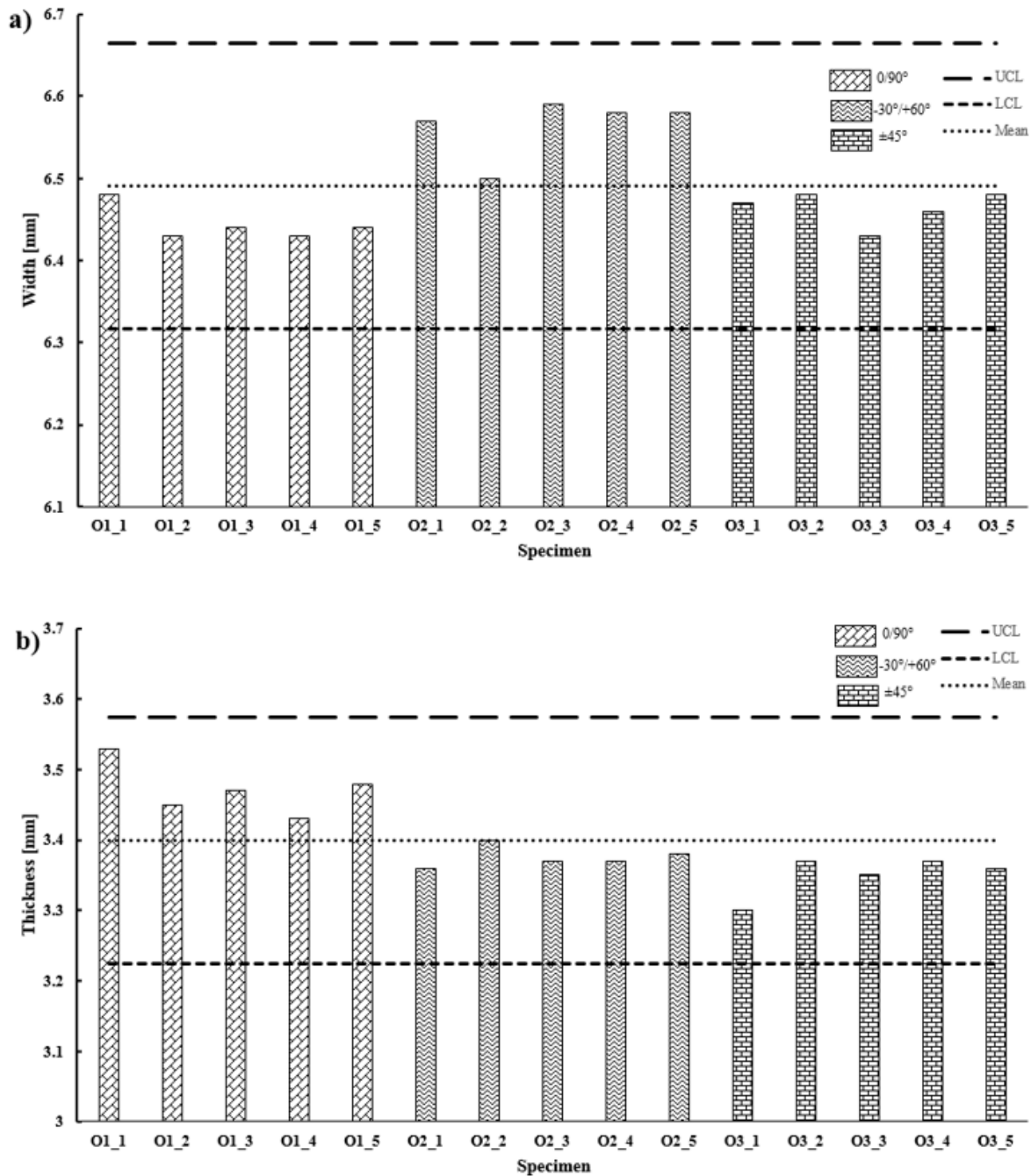


Figure 5-18 Dimensions of all printed specimen compared to the UCL and LCL of the full population sample: a) width and b) thickness

Specimen geometry as per ASTM International D638-14 “The Standard Test Method for Tensile Properties of Plastics” prescribes a thickness of 3.2 ± 0.4 mm for all injection moulded parts (ASTM, 2015). Since this standard is the most suitable in the absence of a specific standard for FDM parts, the

accepted upper limit is therefore 3.6 mm and the lower limit is 2.8 mm. Looking at Figure 5-18 b), the mean thickness of all 15 samples is 3.4 mm. This value fell within the upper tolerance according to the standard specifications while it was found that the lower control limit from the 3 standard deviations analysis is 3.22 mm which is only 0.02 mm higher than the recommended width value. It was also noticed that while specimens of $-30^{\circ}/+60^{\circ}$ and $\pm 45^{\circ}$ were within the lower segment of the mean thickness, $0^{\circ}/90^{\circ}$ specimen were all above the mean value.

Overall printing with MakerBot Replicator demonstrated statistically significant dimensional deviations from the input CAD file geometry however these deviations are all within the accepted tolerances as specified in the standards. Furthermore the MakerBot demonstrated the ability of printing low cost components in a relatively short time. Nevertheless, designers must be aware of inherent limitations in this technology when designing functional components to tight dimensional tolerances.

5.2.2. Tensile testing

Load displacement curves were acquired during each test which were analysed and later converted into the stress-strain curve, Figure 5-19 reports the full set of repetitions for each orientation. The applied stress was computed as the ratio between the applied load and the initial minimum cross-section area, while the strain was derived by dividing the crosshead displacement over the initial gripping length of the specimen (150 mm). It is worth mentioning that the calculated minimum cross-section area was based on the externally measured dimensions. However, the potential voids within the built structure are not accounted for in this calculation. The average values of the mechanical properties with the corresponding standard deviation have been computed for each group of five specimens considered at a given orientation and temperature. The ultimate tensile strength (UTS), Young's modulus (E), the stress at failure and the strain at failure have been derived in accordance with ASTM: D638 Standard and reported in Table 5-9.

Table 5-9 Experimental values of tensile properties reported in terms of Young's modulus, ultimate tensile strength, stress at failure and strain at failure

Test Model	Young's Modulus [MPa]	UTS [MPa]	Stress at failure [MPa]	Strain at failure [%]
O1_1	2511	45.38	44.18	1.96
O1_2	2608	47.01	45.48	1.93
O1_3	2664	45.87	45.27	1.83
O1_4	2535	45.69	45.13	1.93
O1_5	2782	44.98	44.55	1.73
O2_1	2602	47.52	44.33	2.2
O2_2	2328	44.13	43.44	2.1
O2_3	2225	45.23	43.64	1.99
O2_4	2515	44.15	43.36	1.91
O2_5	2504	47.25	42.57	2.1
O3_1	3306	50.58	50.13	1.7
O3_2	3077	49.76	48.86	1.8
O3_3	3210	49.75	48.83	1.7
O3_4	3254	48.31	47.86	1.7
O3_5	3210	50.22	48.44	1.8

All test specimens for all raster orientations exhibited elastic and plastic deformation with a linear increase of load with increased displacement to a certain extension point after which a short region of nonlinearity is recorded. The plastic deformation region is a sign of necking until a pronounced peak stress is achieved indicating the tensile strength of the specimen. Following this, a sudden drop of stress which indicates a complete failure by total separation of the specimen around its minimum width part. Failure is mainly attributed to the raster damage, as tensile strain increases failure of the weakest raster followed by the next weakest raster break in sequence until total failure. In terms of variations of obtained results for samples within the same orientation batch, high level of repeatability was maintained across all raster orientations as demonstrated through identical trend shown in the curves of Figure 5-19.

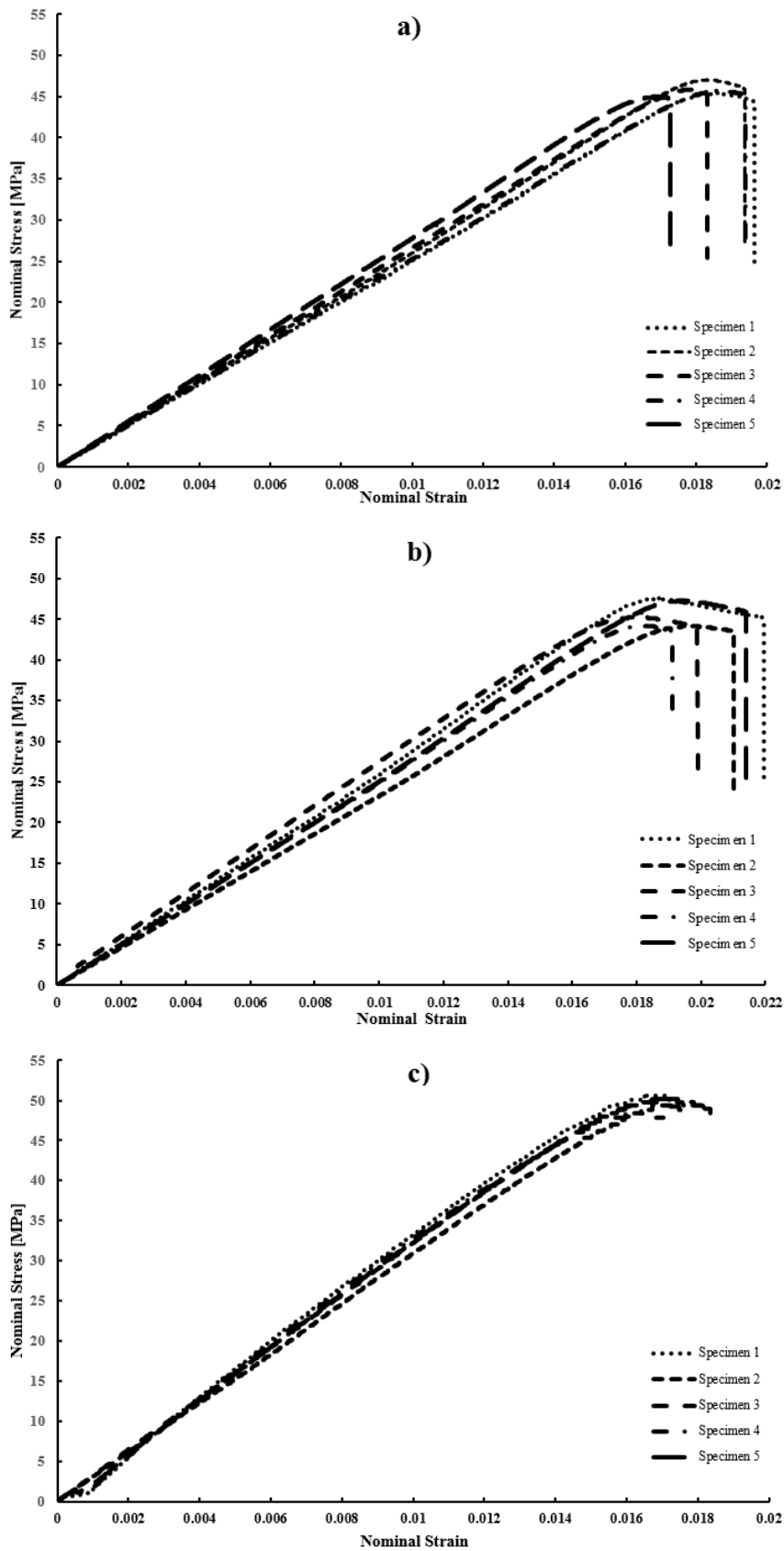


Figure 5-19 Tensile curves of nominal stress vs strain for the three raster orientations each reported for five sample repetitions: a) $0^\circ/90^\circ$, b) $-30^\circ/+60^\circ$, c) $\pm 45^\circ$

The results acquired at room temperature through tensile tests have confirmed the well-known dependency of the stiffness and strength on the infill orientation (Lanzotti et al., 2015), as shown in Figure 5-20 with variation in the elastic linear region and peak of the three orientations. Garrett and co-authors evaluated the dimensional accuracy and tensile properties of samples produced with MakerBot 3D printer and reported while layer height does not affect the elastic properties, the print orientation and per cent infill have an effect over the elastic modulus (Eujin Pei et al., 2015).

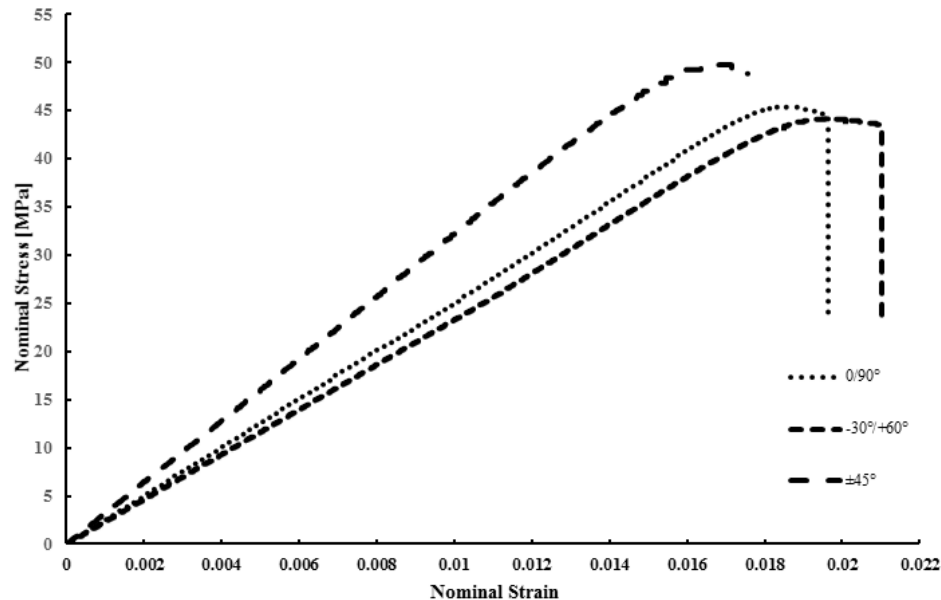


Figure 5-20 Tensile stress vs strain of averaged samples of the three orientations overlapped, samples oriented in $\pm 45^\circ$ exhibit higher slope of elastic region indicating higher stiffness and higher peak corresponding to maximum UTS

The maximum average value of the Young's modulus is at 3211 (± 76 MPa) for samples of $\pm 45^\circ$ orientation compared to the values of 2620 (± 97 MPa) and 27945 (± 621 MPa) recorded for specimen orientations of 0/90° and -30°/+60° respectively. These results are in accordance with some current literature as reported for ABS FDM fabricated parts (Dawoud et al., 2016). Other works reported different findings as polypropylene samples with raster orientations of 0/90° displayed slightly higher values of Young's modulus in excess of 1000 MPa compared to those of $\pm 45^\circ$ both built with 100% infill and 0.2 mm layer thickness (Carneiro et al., 2015). Within the same study it was also proven that the tensile strength and stiffness increase linearly with increasing infill from 20 to 60 then 100%. However, with increasing layer thickness to 0.35 mm a negligible difference was noticed in terms of stiffness whereas strength increased which is potentially a consequence of the lower number of interfaces among beads.

5.2.3. The effect of temperature on extruded filaments

Tensile tests were carried out on the PLA filament before and after printing. The average curves obtained from the tests performed at the four different temperature values (30°C, 40°C, 50°C and 60°C) are reported in Figure 5-21. Apart from the highest temperature test (60°C) which did not fail, the

remaining specimens failed after their nominal extension had been recorded. As expected, increasing the temperature results in a significant higher strain at failure. As the temperature increases, the molecular segments motion is triggered enabling free chain movement up to the glass transition phase (approximately 60° C) which explains the continuous extension of the filament without a defined failure point (Saeidlou et al., 2012). Ductile polymers tend to have a well-defined yield point with high strain typically of the order 5-10 % because of their semicrystalline state, whereas most amorphous glassy polymers are typically brittle and rupture at definite low strains. These effects are generally controlled by the addition of plasticisers or temperature variation (Kendall and Siviour, 2014).

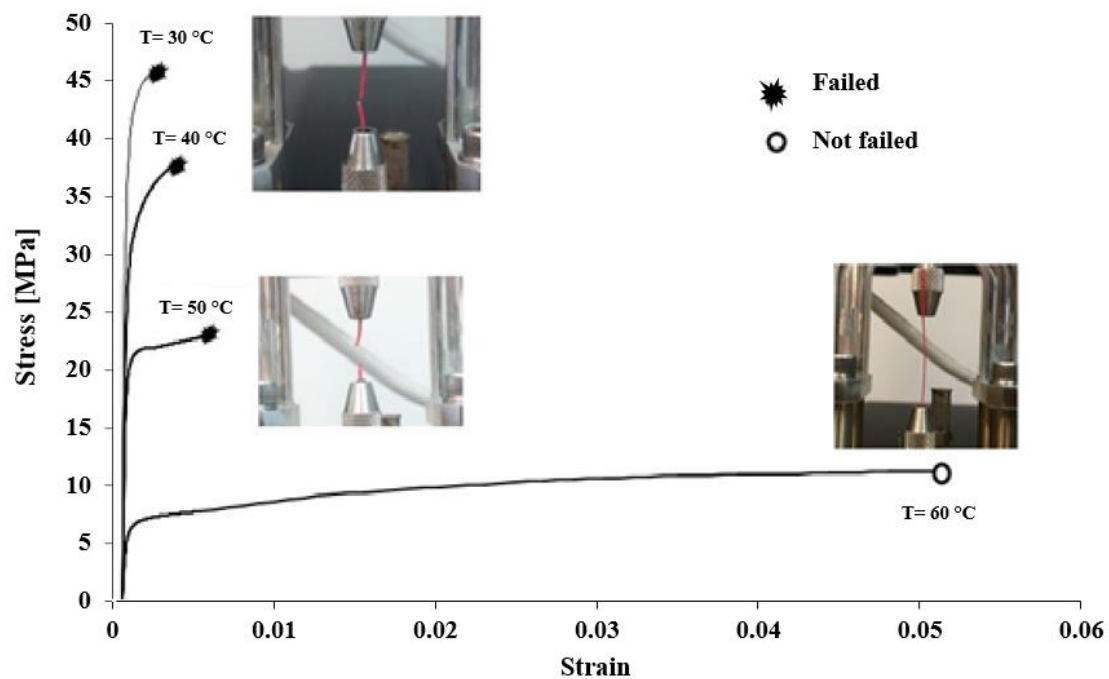


Figure 5-21 Stress vs strain for printed PLA curve: tensile strength decreased while strain increased as temperature increases

Results reported in Table 5-10 reveal that the thermal history undergone by the polymer during the deposition phase will affect inherently the mechanical property of the final fused (printed) polymer. For this reason, a modelling approach should take into account the variations on the mechanical properties, from the original feeding material, induced by the printing operations.

According to the tensile stiffness recorded for both plain and 3D-printed PLA, it can be observed that there is an inverse relationship between temperature increase and modulus reduction. However, it is worthwhile to mention the comparable reduction in stiffness from 30 % in plain PLA to 16 % for the freely extruded filaments as the temperature increases from 40°C to 50°C. This can be explained by the cold crystallisation effects of such polymers and molecular chain re-alignment along the testing direction (Martin and Avérous, 2001). The thermal dependence of PLA properties is explained by the direct influence of its thermal history on the crystallinity of PLA (Farah et al., 2016). Therefore, the melting process, within the nozzle, during 3D printing results in α growth of PLA crystals. The dramatic

drop in stiffness as the temperature approaches the glass transition 60°C is associated with the glass transition of the polymer into a semi-liquid or rubbery state.

Table 5-10 Experimental result for neat and printed filaments from the tensile test

Temperature (°C)	Young's Modulus (MPa)	
	Neat PLA	3D-printed PLA
30	1175 ± 89	1400 ± 78
40	1011 ± 75	1143 ± 82
50	701 ± 54	961 ± 54
60	247 ± 16	350 ± 12

5.2.4. The effect of In-Situ Temperature on Tensile Parameters

Tensile tests carried out on the 3D-printed specimens by means of the electromechanical INSTRON machine. For each group, the average over the five values acquired together with the standard deviation is reported. In correspondence to temperature values 50°C and 60°C, the transition in the mechanical behaviour because of the T_g changes the constraint of the polymeric chains allowing them to move and slide under the action of the applied load. This condition results in a continuous elongation under a constant applied load. As the failure condition is not reached, the tensile test was stopped once a strain of 0.1 equivalent to 10 % was reached. It has been assumed that this elongation corresponds to the condition for which the functionality of the component is lost, even if separation is not accomplished.

Figure 5-22 depicts the comparison between the values of the elastic modulus (E) of specimen built in the three considered orientations namely 0°/90°, -30°/+60° and ±45° under a combined effect of tension and *in-situ* temperatures varied from 20°C to 60°C. Similarly, the results presented in Figure 5-23 displays parallel comparison of ultimate strengths (UTS). A general trend indicates the strong influence of temperature increase on both stiffness and ultimate strength of the FDM specimen. It can be clearly observed that as the temperature increases the stiffness and UTS decrease. Although, some specimens exhibited higher standard deviations exceeding other ranges under comparison, the trend of temperature and orientation on mechanical behaviour can still be identified. This observation is explained by means of fractography analysis in later section herein.

The stiffness values, at temperatures below 40°C, fluctuate within a narrow range with the exception of the outlier specimen, ±45° orientation, at room temperature. This is then followed by a significant fall in stiffness as temperatures approach the glass transition region between 50°C and 60°C. However, UTS values experienced a gradual decrease with respect to temperature increase up to 50°C at which

point a dramatic fall in strength is recorded and continues to drop at 60°C, with values axed to below 100 MPa.

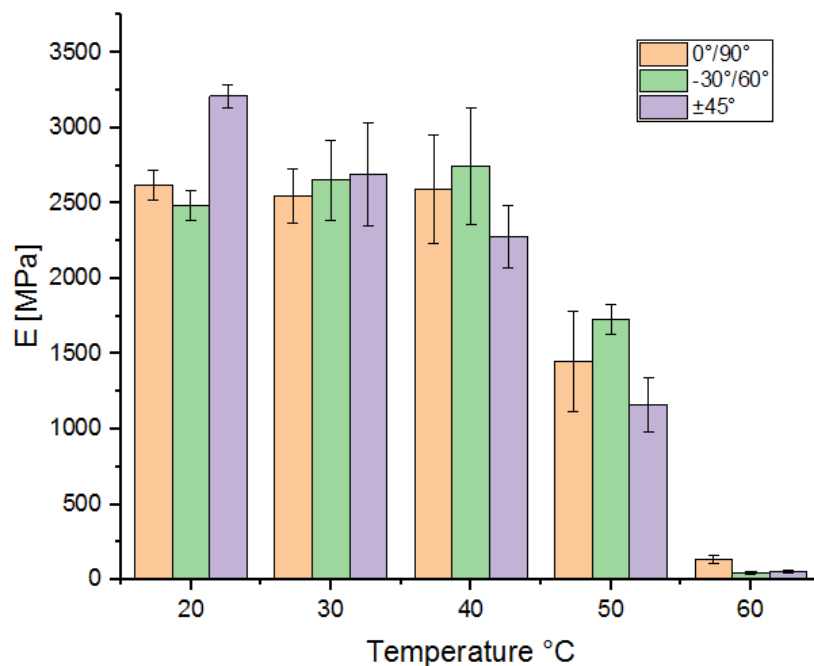


Figure 5-22 Comparison of the Young's Modulus values of the three different orientations across temperatures (20-60 °C) – Standard deviations are included for all averages. For -30°/+60° and ±45° samples tested at 60°C low modulus values under 100 MPa and their respective standard deviations are presented but considerably low compared to the scale used.

At room temperature i.e. 20 °C, a significant dominance recorded for the ±45° specimen in terms of their Young's modulus with an average value of 3211 (±75.9 MPa) while both orientations 0°/90° and -30°/+60° showed relatively lower stiffness of 2620 (±97.4 MPa) and 2487 (±99.5 MPa) respectively. The latter orientations exhibit similar stiffness as their averages and corresponding deviations align them within the same range. This observation is in agreement with Dawoud and coworkers' study on ABS specimen (Dawoud et al., 2016). Whereas Tymrak and coworkers' study on ABS specimen revealed a slight advantage in terms of stiffness for the 0°/90° orientation over the ±45° orientation (Tymrak et al., 2014). However, in the same study, PLA specimen were also tested for comparison whereby their reported stiffness values agree well with our values for specimen with ±45° orientation while this was not the case for specimen of 0°/90° orientation.

When considering specimen tested under 30 °C temperature, all stiffness values for all orientations fluctuate within a narrow range around a value of 2630 MPa with more spread deviation ranges in comparison to what has been recorded for room temperature. It is however noteworthy to mention the marginally superior average stiffness of the ±45° specimen with its considerably wider deviation range encompassing the 0°/90° and -30°/+60° specimen average stiffness values and their deviations.

At 40 °C, the maximum value of the stiffness is reached at orientation $-30^{\circ}/+60^{\circ}$ with mean value of 2745 (± 390 MPa) and the minimum at $\pm 45^{\circ}$ with mean value of 2279 MPa while $0^{\circ}/90^{\circ}$ specimen exhibited intermediate stiffness value of 2591 (± 206 MPa). However, the variation of all orientations stiffness values when considering standard deviations, fluctuate within a wide range. This observation may be attributed to the build process of the $-30^{\circ}/+60^{\circ}$ whereby the final structure is much denser with minimal air gaps as displayed by the fractographic assessment in section 6.2.3 thus higher thermal mass. Therefore thermal mass variations inevitably shift the onset softening point. This trend is dissimilar to those tested under 30 °C as their stiffness proved to be scarcely influenced by the combined effect of the temperature and raster orientation.

At 50 °C, a significant drop in the stiffness values across all orientations however it can be noticed that the trend reported for the tests under temperature of 40 °C is maintained. Overall, values of stiffness of all specimen seem to have been approximately halved. Specimen $-30^{\circ}/+60^{\circ}$ exhibited the highest value of stiffness, 1728 (± 98 MPa), which maintain its consistent superiority similarly to those tested under 40 °C yet with less deviations from the mean value. Meanwhile, specimen $\pm 45^{\circ}$ demonstrated the lowest stiffness of 1162 (± 182 MPa) and a median value of 1448 (± 333 MPa) was found for the $0^{\circ}/90^{\circ}$ specimen.

Further substantial reduction in stiffness was observed for all specimen orientations at temperature of 60 °C. Apart from the $0^{\circ}/90^{\circ}$ specimen with their mean stiffness of 134 (± 29 MPa) which exceeded the mark of 100 MPa, the other specimen exhibited considerably lower mean stiffness with one order of magnitude less as values of 43 MPa and 53 MPa for $-30^{\circ}/+60^{\circ}$ and $\pm 45^{\circ}$ specimen respectively were recorded.

As far as strength is concerned, as expected a gradual decrease as temperature increases was noted and displayed in Figure 5-23. While the same logic as the stiffness was observed at room temperature since specimen of $\pm 45^{\circ}$ orientation exhibited the highest strength with mean value 49.7 (± 0.7 MPa), the other orientations $0^{\circ}/90^{\circ}$ and $-30^{\circ}/60^{\circ}$ indicated more or less identical strengths 45.8 (± 0.7 MPa) and 45.7 (± 1.5 MPa) respectively. This trend was reversed as temperature increased, for instance, at 30 °C temperature the $0^{\circ}/90^{\circ}$ and $-30^{\circ}/+60^{\circ}$ specimen maintained their strength similarity with mean values of 41.0 (± 0.5 MPa) and 41.5 (± 1.6 MPa) respectively while minimum strength was recorded for $\pm 45^{\circ}$ at 38.8 (± 1.2 MPa). Similarly at 40 °C, although the strength of all orientations continued to decrease an identical trend was observed. The minimum strength value 29.2 (± 0.6 MPa) was reached at orientation $\pm 45^{\circ}$ while the maximum of 34.4 (± 1.4 MPa) at $0^{\circ}/90^{\circ}$ which was very comparable to that of $-30^{\circ}/+60^{\circ}$ orientation at mean value of 34.1 (± 0.9 MPa). The lowest stiffness value at $\pm 45^{\circ}$ corresponds to a lowest value of the strength with the minimum value of the UTS.

As temperature approaches the glass transition range, 50 to 60 °C, strength plummeted to very low levels across all orientations which signifies deterioration of load bearing capabilities. Surprisingly, at

50 °C, the strength of -30°/+60° specimen exceeded the other orientations by almost double at a mean value of 12.4 (±1.8 MPa) compared to 6.4 (±1 MPa) and 6.7 (±1.8 MPa) for 0°/90° and ±45° respectively. This observation may indicate that a good inter-beads interface is still in place at this temperature due to the high thermal mass, thus maintaining the stress transfer among the bonding surfaces.

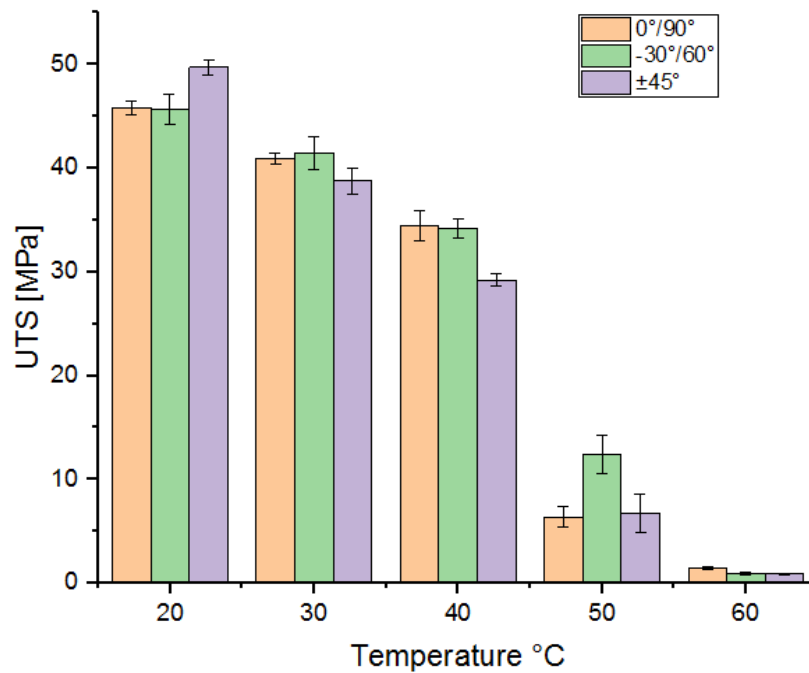


Figure 5-23 Comparison of the tensile strength values of the three different orientations across temperatures (20-60 °C) – Standard deviations are included for all averages. For samples tested at 60°C low strength values under 1 MPa and their respective standard deviations are presented but considerably low compared to the scale used.

At 60 °C further reduction to minimum level of strength with values of all orientations fluctuating around a mean value of 1 MPa. At this point no separation occurred however a consideration to the specimen loss of functionality in correspondence with poor performance in terms of strength and stiffness suggests its eventual failure.

Stress at failure σ_f values across all orientations with respect to the temperature at which the tensile specimen were tested is presented in Figure 5-24. As a general observation increasing the temperature up to a value 40 °C causes a gradual reduction of the stress at failure for the 0°/90° and -30°/+60°. In comparison, the other orientation i.e. ±45° exhibited lower values of stress at failure consistently across all temperatures however an average value of 34 (±2 MPa) was maintained for specimen tested under 20 and 30 °C. This stress at failure of ±45° specimen however drastically decreases at temperature of 40 °C to a level as low as 7.7 MPa with a high range standard deviation ±5.3 MPa. This value is comparable to those specimen (all orientations) tested at a higher temperature 50 °C but considerably lower than their counterparts i.e. 0°/90° and -30°/+60° tested at 40 °C that recorded an average of 30 (±2 MPa). For the tests carried out at 50 °C and 60 °C, the stress at failure is identified as the constant stress under which the material flow at high strain values. Therefore all specimen of the three

orientations exhibited values well under 10 MPa when tested at 50 °C which then carry on to further drop to even lower values ~1 MPa at 60 °C.

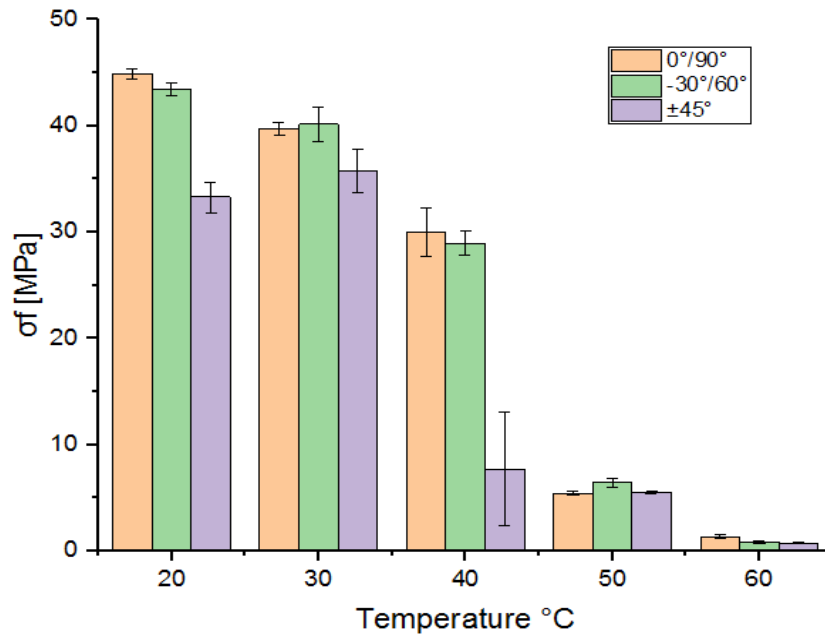


Figure 5-24 Comparison of the stress at failure values of the three different orientations across temperatures (20-60 °C) – Standard deviations are included for all averages. For samples tested at 60°C low values under 1 MPa and their respective standard deviations are presented but considerably low compared to the scale used.

The strain at failure at 50°C and 60°C were evaluated at 10 % since failure with the complete separation of the two ends of the sample was never reached. For that reason, it is not possible to make any comparisons as shown in Figure 5-25.

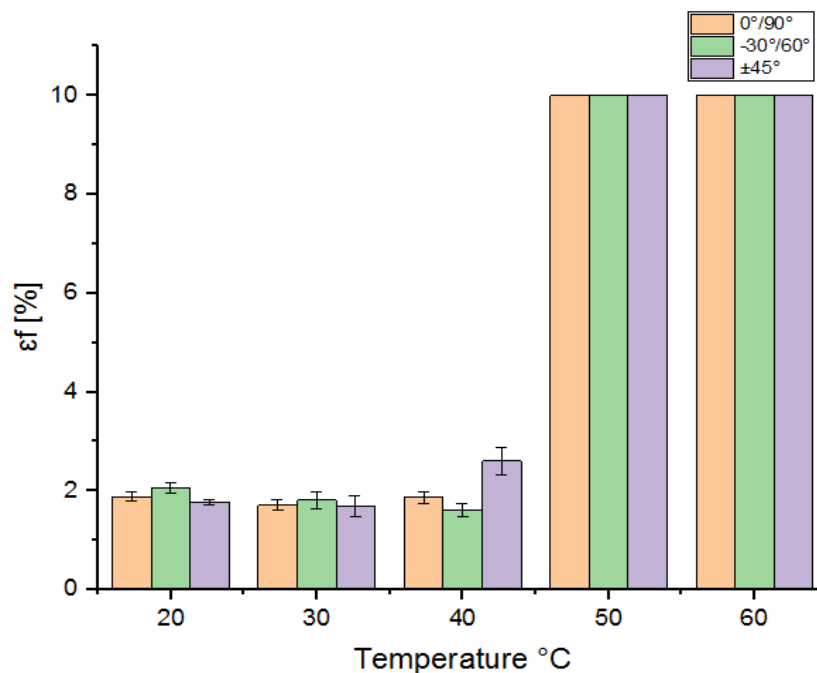


Figure 5-25 Comparison of the strain at failure values of the three different orientations across temperatures (20-60 °C) – Standard deviations are included for all averages. A very marginal influence of the temperature up to 40 °C after which total failure cannot be reached at 50 °C and 60 °C.

At room temperature, the maximum strain at failure is reached at $-30^{\circ}/60^{\circ}$ as the overall longitudinal strain is mainly composed by the elongation of the beads along the loading line. The lowest strain at failure at 20°C occurs at $\pm 45^{\circ}$, as the strain is mostly contributed by the bonding surfaces without any significant axial elongation of the beads. As the temperature increases to 40°C , the highest strain at failure value is reached at $\pm 45^{\circ}$, whereas the lowest value is at $-30^{\circ}/60^{\circ}$.

6. Discussions

6.1. Discussion of the biocomposites properties

6.1.1. Quasi-static Properties under Ambient Conditions

In this research, the approach adopted is to establish the performance differences among NFCs composed of continuous and discontinuous reinforcement with either a thermoplastic or thermoset matrix. Knowing that the selection of the appropriate combination is merely end-application driven i.e. the performance, the ease of manufacture, cost and product end of life disposal methods and impact.

6.1.1.1. Continuous reinforcement

This type of reinforcement can be used in a number of forms, as well as in combination with different thermoplastics and thermosets. The idea was to evaluate the optimum properties that can be achieved based on the choice of matrix type. As a start, three matrices PLA, PP and MAPP were employed with twill flax reinforcement at fibre content of 40%. Results have shown that the PLA based biocomposites exhibited the highest tensile properties attributed to adequate adhesion between the flax fibres and matrix. An improvement of strength as high as 50% when 30-40 wt% flax fibres were reinforced with PLA as compared to PP based composites (Oksman et al., 2003). Abaca fibres and cellulose fibres with 30 wt% were incorporated in each of PLA and PP matrices, tensile strength for both reinforcement increased by 68% for abaca/PLA and 28% for cellulose/PLA as compared to their PP based counterparts (Bledzki et al., 2009). The Flax/PLA interfacial strength is responsible for efficient load transfer resulting in the optimal strength and stiffness. It is possible to quantify the stress transfer efficiency of reinforcement using the single fibre micro-fragmentation tests to assess the fibre/matrix compatibility. Previous studies evaluated the apparent shear stress for various natural fibres added to PLA and PP matrices, an example, kenaf fibres reinforced PP yielded $\tau=12\text{MPa}$ (Tripathy et al., 2001). Another study on interfacial strength of Flax/PLA found $\tau=15.3\text{MPa}$ which increased with slower cooling rate since during rapid cooling the matrix structure, which shows visco-elastic behaviour, does not have time to relax (Le Duigou et al., 2010). The polar nature of both flax fibres and PLA enhance the adhesion. Furthermore, using maleic PP (MAPP) improves the fibre/matrix interfacial properties which can be observed from the high tensile strength exceeding the PLA based biocomposite. A common disadvantage associated with using biocomposites is the polarity of natural fibres and hydrophobic character of the non-polar matrix polymer which impedes the proper dispersion of fibres in thermoplastic polymers. Therefore, due to strong intermolecular hydrogen bonding between bio-fillers, they tend to agglomerate during the compounding process with the matrix polymer. The maleic anhydride forms a covalent bond between the anhydride group of the hydrophobic PP and the OH group of the cellulose in the hydrophilic flax. Fracture analysis confirmed the good wetting of fibres with

MAPP matrix evidenced by the absence of holes around the matrix and scarcity of breakage during pull-out fracture (Kim et al., 2007).

The effect of flax reinforcement architecture was considered in this research, as a comparison between Flax/PLA specimens fabricated from twill 2x2 and 0°/90° was made, the former type exhibited better strength and stiffness due to the interlacing of fibres which prevented matrix cracking i.e. crack propagation can be restricted between weave cells in woven composites and cannot spread as fast as would be the case for UD. The balanced arrangement of fibres within the 0°/90° specimen only have half the fibre contents aligned along the load direction while the remaining fibres are in the transverse direction, therefore only 50% contribution in modulus and strength. In another study to compare tensile and dynamic properties of flax/epoxy architectures (UD, 0°/90° and twill), the opposite was reported as twill based composites suffered lower properties. This was attributed to few factors, the high twist angle of yarns (>20°), also the high crimp can cause distortion and misalignment within the yarns (Duc et al., 2014a). Furthermore, crimp zones experience high stress concentrations as fibres at the cross-over points are subjected to a considerably higher local stress than the average stress and are more susceptible to rupture.

The effect of fibre loading on the tensile and flexural properties of Flax/PLA tapes with stacking sequence of 0°/90° has been evaluated. The increased fibre contents although did not significantly improve the tensile modulus up to 50wt%, when this was raised to 60wt% stiffness increased. Strength on the other hand increased with fibre contents increase up to contents of 55wt% after which no further improvement noted due to improper wetting and potential fibre agglomerate. Flexural modulus increased linearly with fibre contents until peaking at 55wt% then decreased again for 60wt%, strength also followed the same trend. Upon close examination, the compressive side suffered severe debonding as a result of stress concentration at the flax/PLA interface, this worsen as fibre contents increased. The quality of flax fibres is crucial in flexure mode as these need to be defects free, a common cause of failure is kink bands presence. Furthermore, flax fibres are much stiffer than PLA in addition to adequate bonding in place, effective load transfer can be achieved.

With regard to the PP based biocomposite with 50wt% fibre, a similar comparison in terms of reinforcement architecture was made among UD (0°), cross ply and twill which revealed the clear dominance of the unidirectional. When all fibres are aligned along the loading direction 100% contribution is achieved in both modes tensile and flexural. In addition, MAPP incorporation within the flax reinforcement have increased the tensile and flexural properties as compared to the PP based composites. It is worth mentioning that the use of PP and MAPP caused thermal shrinkage at temperatures above 155°C which worsen to cause sticking as temperature reaches 160°C. Selecting the appropriate temperature and heating time to achieve a good balance between complete melting to ensure fibres wetting and avoid shrinkage was also reported elsewhere (Shibata et al., 2006). However as

observed from Figure 6-1 and Figure 6-2, increasing the fibre content can lead to increased contact area and prevented shrinkage.

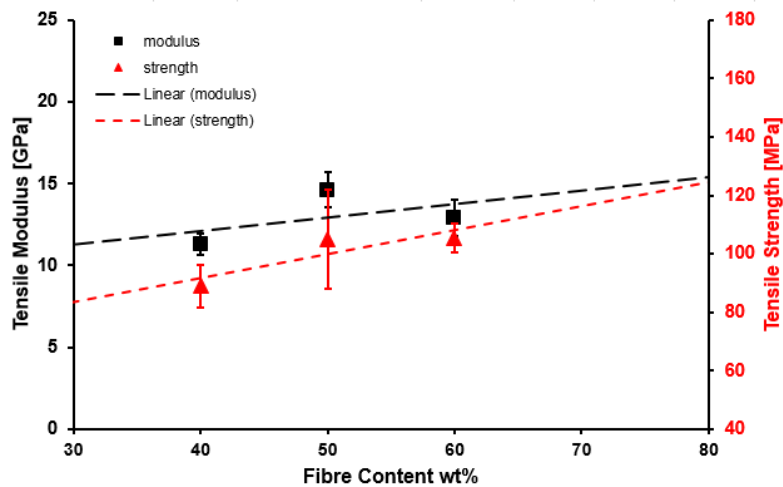


Figure 6-1 Tensile modulus and strength variations of flax/MAPP composites with respect to the increasing fibre wt%

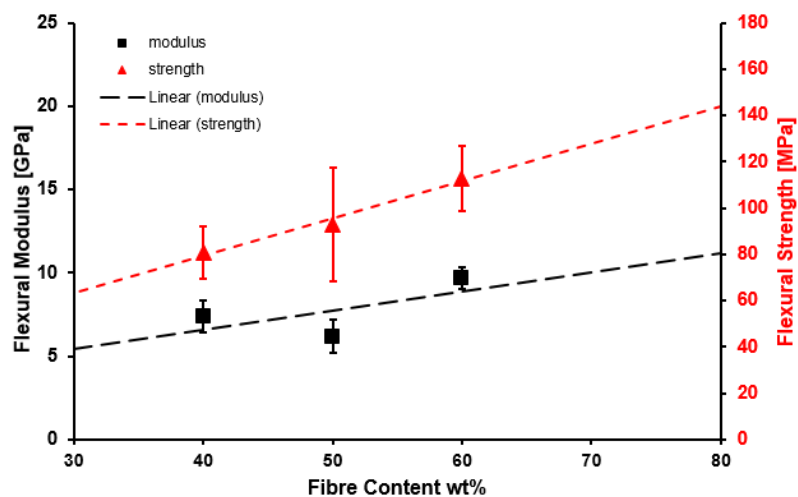


Figure 6-2 Flexural modulus and strength variations of flax/MAPP composites with respect to the increasing fibre wt%

Although thermoplastic materials currently dominate as matrices for bio-fibres, current efforts to move toward more thermosets use. This is because thermoset polymers outperform thermoplastics in some areas, including mechanical properties, chemical resistance, thermal stability, and overall durability. The use of thermoset matrix generally provides higher mechanical properties due the enhanced matrix to fibre interlocking. Other advantages are flexibility in structural fibre configuration and the ability to be processed at ambient conditions opposed to thermoplastics that require high temperatures to process which is less desirable considering the vulnerability of natural fibres to heat. One of the resins considered in this research is Biorez PFA reinforced with hybrid fabrics layered from flax tapes and glass veils. This biocomposite was compared against Flax/PLA/PFA tapes and 100% laminates Flax/UPE, all specimen were arranged in UD (0°). Hybridisation of natural fibres with glass fibres have

been attempted and proved to while enhancing the mechanical properties it also reduce the overall density of the composite which can be beneficial in the production of lightweight structures (Petrucci et al., 2013). This process although can be desired for its performance advantage but can be both labour and energy intensive. The tensile behaviour of the hybrid samples is controlled by the breaking strain of individual reinforcing fibres, since glass fibres are characterised by a high stiffness and low strain-to-failure while flax fibres are moderate strain-to failure and modulus. Under tension load, all fibres are evenly strained up to a limit of the lowest level which in this case corresponds to the glass fibres. After which any increase in load leads to a sudden transfer of load to the weak natural fibres that would result in the failure of the natural fibres and eventually triggering imminent overall failure.

Biorez PFA based biocomposites have been tested in tensile and flexural modes, the fibre loading was maintained at constant range 50-55wt% yielding a comparable $V_f = 46-47\%$, however, the reinforcement arrangement varied. As expected the UD samples had the highest tensile properties which also corresponded to the highest flexural properties. This was also observed for UD polyester based biocomposites as it exhibited the highest tensile and flexural properties followed by the cross-ply $0^\circ/90^\circ$ then twill samples. UD flax reinforced with resins are generally found to be dependent on factors including the steps undertaken in the fibres extraction and yarn preparation process. Furthermore, the level of yarn twist determines both the strength of the dry fibre bundle and also the extent of fibres wetting in the composite manufacturing stage. The level of twist should also be carefully exercised as any excessive twist can impact the wettability and render impregnation difficult. In comparison to other studies (Shah et al., 2012) (Phillips et al., 2013) in which woven flax/epoxy was investigated in equivalent fibre contents, the reported tensile properties were higher than our flax/furan and flax/UPE twill but similar to the polyester based cross-ply $0^\circ/90^\circ$. Values obtained in our study for furan based samples are found to be higher than reported properties of Cordenka/PFA (Malaba and Wang, 2015). A possible explanation to the variation, is that Cordenka fibres have lower mechanical properties and fibres were of zero twist. According to most published work on furan based biocomposites, the proportion of the fibre contents has been below 50% (Giannis et al., 2008). Therefore, it has been suggested that to attain high mechanical strength levels above 200MPa, the fibre content must exceed 50% (Tumolva et al., 2009). Rightly so, Tumolva suggested the UD laminate to be pressed prior to the addition of resin to achieve higher volume fraction which has been the case in our UD Flax/PLA laminates as they undergo thermal bonding prior to impregnation. With regard to other orientations, results can be grouped in two categories, $\pm 45^\circ$ and $0^\circ/90^\circ$ due to the comparable performance both under tension and flexure. For instance, the stitched NCF $\pm 45^\circ$ samples performed better than the multilayer $\pm 45^\circ$ which can be justified by the effective fibre alignment prior composite impregnation with resin that can cause non-uniform distribution of fibres. Similar justification can be adopted for the bi-directional twill and $0^\circ/90^\circ$ as the former outperformed the latter, but all found to be considerably lower than the $\pm 45^\circ$ samples. In direct comparison to published results elsewhere for woven glass/furan

of equivalent $V_f = 47\%$ (Arnold et al., 2009), the flexural stiffness and strength reported of 9 GPa and 104 MPa respectively are very comparable to our reported results herein, see Figure 5-8.

6.1.1.2. Discontinuous reinforcement

Nonwoven mats of flax/PP needle-punched have been produced and tested. During tension testing of flax fibres, they show a non-linear stress–strain response. This is due to their microstructure, which is a multi-layer composite with oriented cellulose microfibrils in the cell walls. These can be aligned under tensile load and can also slide. The cell walls of flax fibres contain numerous defects (cross marks), known variously as nodes, slip planes, kink bands, dislocations or micro-compressive defects. Figure 6-3 shows examples, observed with a scanning electronic microscope (SEM), of kink bands at the surface of the fibre. When the reinforcing fibres are in bundles form, upon loading these bundles are also prone to internal sliding among themselves in addition to damage mechanism of debonding of fibre outer layers. Further, the PP matrix exhibit a highly non-linear behaviour which can contribute to the nonlinear response of the nonwoven mats when loaded in longitudinal and transverse directions. The transverse properties were low but not with high margin as the mats are thought to be quasi-unidirectional due to effect of needle punch in the z-direction which can cause a proportion of the fibres to change orientation. Fibres also have low transverse strength coupled with low stiffness of PP.

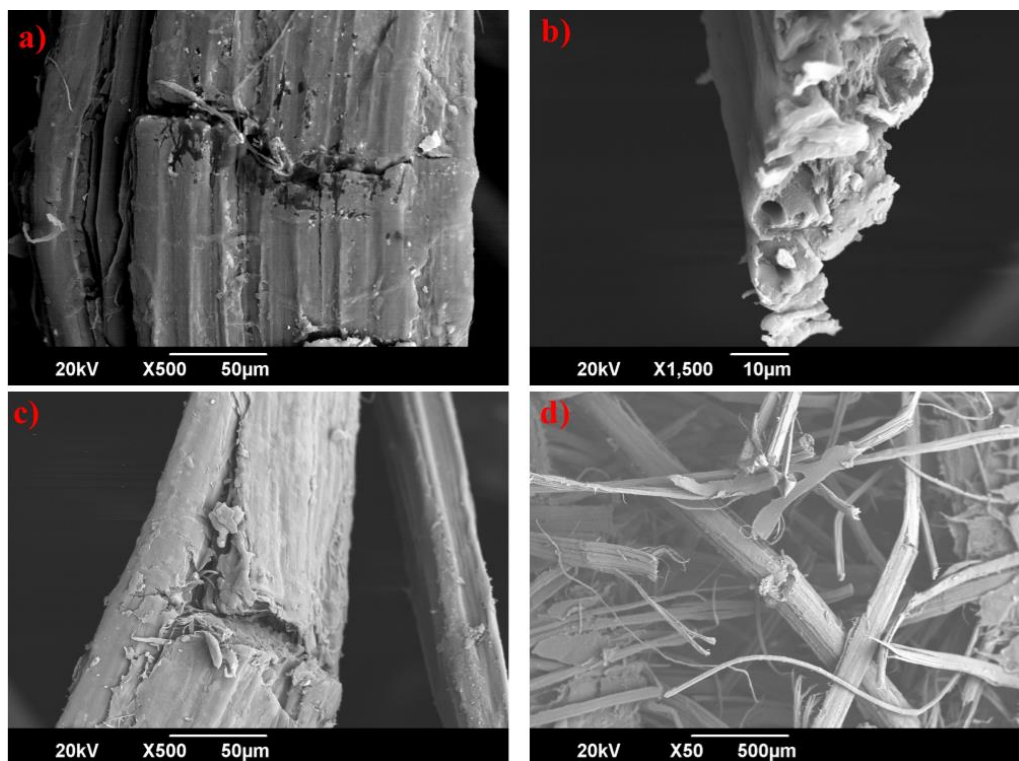


Figure 6-3 SEM images of internal geometry of flax/PP fractured samples: a) kink bands at the surface of the fibre; b) fibre internal pull-out of microfibrils; c) surface fracture of fibre under compressive load; d) a view of a dense zone of fibres damaged due to pull and twist loading

The mechanical properties of discontinuous fibre-reinforced composites are expected to depend (i) on the intrinsic properties of both matrix and fibres, (ii) on aspect ratio, content, length distribution and

orientation of the fibres in the composite, and (iii) on fibre–matrix adhesion that is responsible for the efficiency of load transfer in the composite. SEM analysis shows that the diameter of the flax fibres within samples of this study varies as well as the cross section as some fibres have other shapes than circular, see Figure 6-4. Further to the inconsistent diameter, fibre length variation is another variable controlling the aspect ratio. The original work of Cox (Cox, 1952), which has been since developed by several authors, shows that the efficiency of the reinforcement increases with aspect ratio reaching a maximum in continuous fibre composites. It also shows that there is a minimum ‘critical’ fibre length as a function of the matrix/fibre interfacial strength (Baiardo et al., 2004). Comparisons of NFCs mechanical properties with published results can be complicated due to the high dependency on the height of the plant stem from which the fibres are taken.

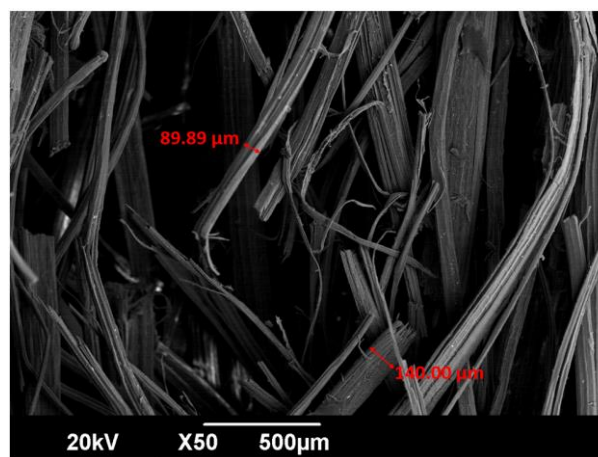


Figure 6-4 SEM image to show the variations of diameter and shape of fibres within the same sample.

Polyester based nonwoven flax mats have been fabricated through hand lay-up yielding three levels of fibre contents ($V_f\%$) 14, 18 and 22%. The effects of processing and the different constituent proportions (fibre, matrix and void) on the tensile and flexural properties have been evaluated. The low stiffness of the composite at low fibre content can be explained by the poor load transfer between the fibres and matrix. It is commonly reported in literature that the strength of such composite drops from the initial value of the virgin matrix then increases again from the critical value of fibre contents. This effect is explained by the discontinuity of reinforcement within the composite that weakens it. The hollow feature within individual natural fibres enable them to absorb some of the resin which can affect the results.

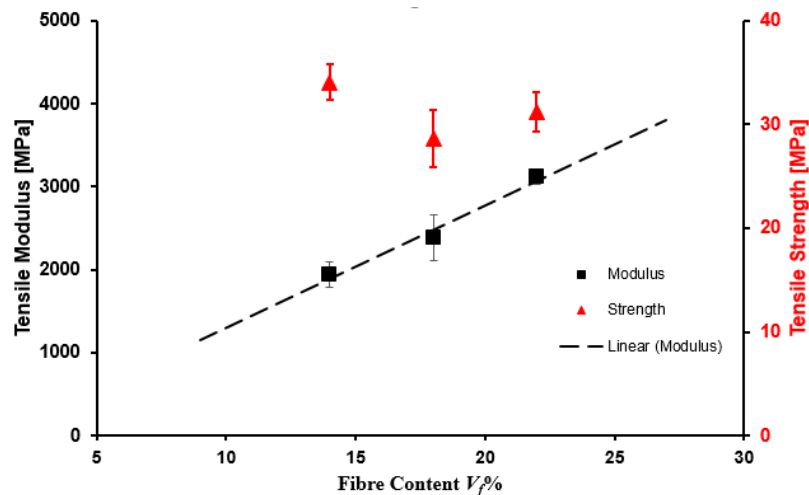


Figure 6-5 The variation of tensile strength and modulus of flax/UPE composites with respect to fibre volume fraction increase

The non-linear response within the individual fibres themselves is attributed to the microfibril orientation angle (MFA) within the secondary layer S2 cell walls. There is a direct effect of the MFA on the strength and stiffness of single fibres as smaller orientation angles increase the strength of the fibre and ultimately the composite too. The typical range of the microfibril angle for flax fibres is 8°-10°, (Reiterer et al., 1999) (McLaughlin and Tait, 1980) it was noted that any increase in microfibril angle leads to even more non-linear response in tension. Furthermore, beside MFA effect, it is worth noting that the variation in cellulosic contents with respect to fibre lumen diameter and porosity should also be responsible for the scattering of the tensile properties. The effect of the natural fibres reinforcement on the composite in terms of strain at break is shown in Figure 6-6.

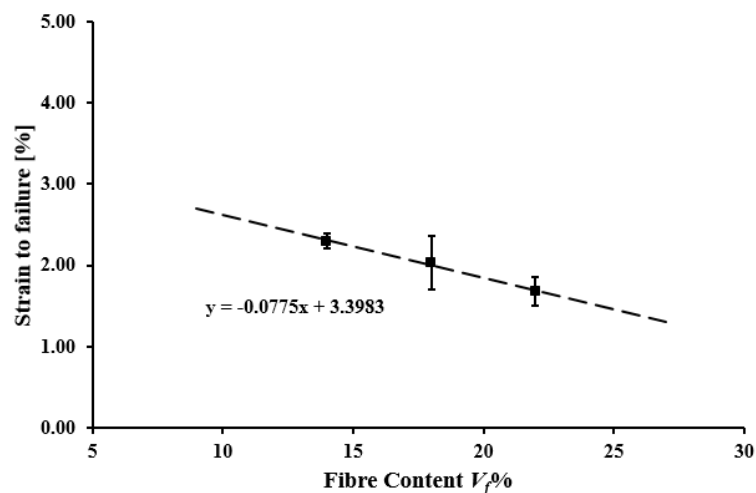


Figure 6-6 strain-to-failure linear reduction with increased fibre contents within the composites

There was a clear trend of reduction in strain-to-failure with increasing fibre contents. Taking into account voids and data scattering, the decrease is found to be perfectly linear. It would also appear that strength is controlled by the fibres fracture strain, and potentially strength can be substantially improved using fibre with higher strain capability (Bader and Bowyer, 1972). Overall, it can be concluded that

reinforcing the polyester matrix with nonwoven mats using flax did not necessarily improve the tensile strength of the composite. Unlike UD laminate composites, the nonwoven irregular shaped fibres and misalignment can cause fibre entanglement which consequently hinder the overall properties of such composites. This fibre entanglement creates resin rich areas contributing to the formation of voids and porosity (Dhakal et al., 2007)

Figure 6-7 illustrates the failure locations of fibres under tension which demonstrates the fibres role. This proves that during composite loading, the fibre-matrix interface resists some load before debonding occur after which only fibres become responsible for carrying load beyond the matrix strength to some limit. At this limit fibres exhibit brittle failure hence the sharp drop observed in the stress-strain curve.

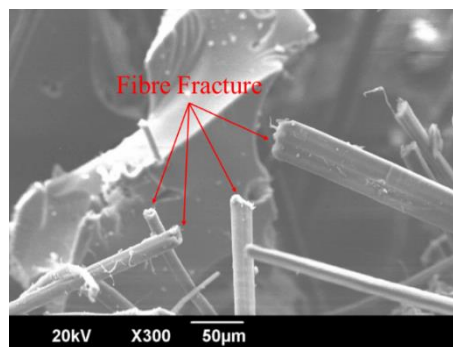


Figure 6-7 SEM image of brittle fracture of flax fibres under the tensile load

Flexural moduli and strengths of the tested specimen Flax/UPE with varying fibre contents are presented in Figure 6-8. There is an increase in modulus and strength of the Flax/UPE as fibre-matrix interface improved. The properties of virgin polyester may be higher than the reported here due to the quality of the reinforcement through mat manufacturing which may have had an effect on the void formation hence the poor fibre matrix interface led to the load transfer inefficiency. In fact the samples exhibit more commonly agreed flexural modulus and strength among published data (Rassmann et al., 2010). The considerably lower reported flexural properties in this study can be explained by the cure mechanism of samples prompted the formation sandwich structure of top/ bottom layers resin rich and middle layer fibres rich, this non-uniformity caused the composite to respond differently under bending load. From the bending theory it is known that beams under flexure, the bottom layer experiences tension whereas top layer experiences compression. Microscopic images validate this claim as shown in Figure 6-9b), the excessive bending load which initiate fibre fracture at the kink bands region, Figure 6-9d).

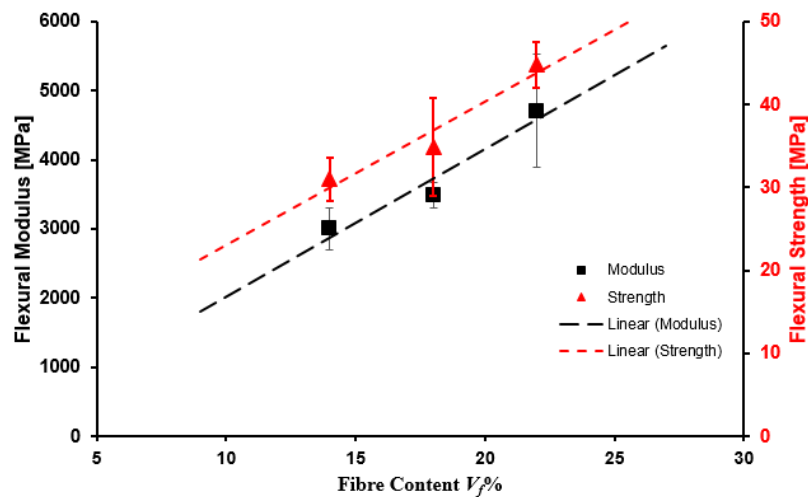


Figure 6-8 The variation of flexural strength and modulus of flax/UPE composites with respect to fibre volume fraction increase

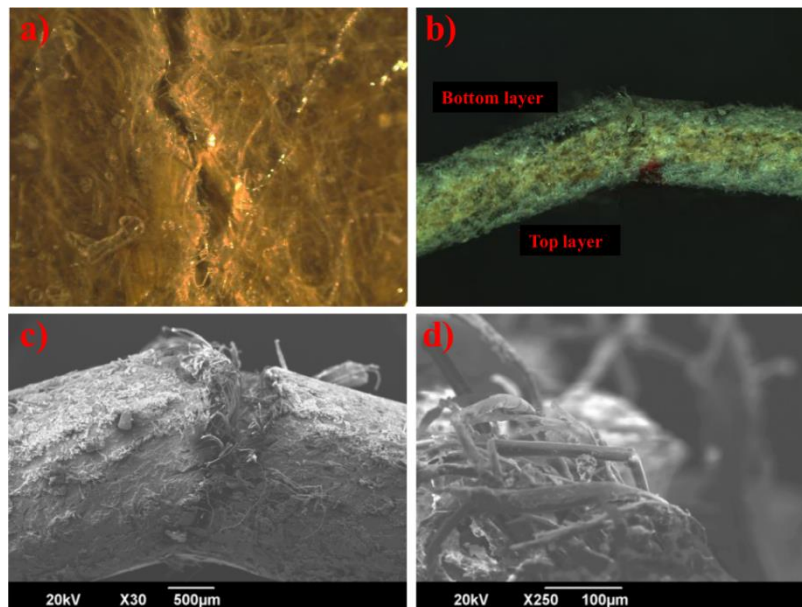


Figure 6-9 a) optical microscope image of bottom surface fracture with evident resin rich zones; b) microscopic image of through thickness view of the sandwich like arrangement of flax/UPE; c) mid-span damage initiation and propagation through the specimen thickness; d) failure of individual fibres due to stress concentration at the weak nodes due to bending.

According to Baley (Baley, 2004) the cell walls of flax fibres inevitably consists of regions of defects in longitudinal direction referred to in different terms such as slip planes, kink bands, dislocations and micro-compressive defects. These corresponds to the change of the crystalline orientation i.e. change of fibrillary orientation resulting from the decortication process. Therefore, in bending scenario as depicted in our flexure test, these locations represent weak nodes as fibre bundles are prone to buckle. Fibre-matrix de-bonding and formation of micro-cracks in the matrix are initiated around the micro-compressive defects due to stress concentrations which contribute to the global fracture of the composite (Hughes et al., 2000).

6.1.1.2.1. Interlaminar Shear Strength

In light of flexural results, through thickness stresses can be a detrimental factor due to non-uniform dispersion of fibres. The interlaminar shear strength (ILSS) of reinforced plastics is a function of the fibre-matrix adhesion, matrix strength, moisture and void content (Francucci et al., 2014). A short beam test was conducted as an additional approach to flexural test using the same test setup. However to obey to the length to thickness ratio ($l:d$) requirement of 5:1 as per to BS EN ISO 14130: 1998, 2 layers have been stacked up which only produced samples of $V_f=17\%$. A shorter span may be necessary to produce interlaminar shear failure, since some tested samples have been omitted due to their unacceptable mode of failure. Possible unacceptable modes of failure can be mixed mode i.e. shear and tension or shear and compression, non-shear mode i.e. tension or compression and plastic. The apparent interlaminar shear strength is calculated using Eq. (6-1):

$$\tau_M = \frac{3}{4} \times \frac{F_M}{bh} \quad \text{Eq. (6-1)}$$

Where τ_M is the maximum stress, F_M is the maximum force, b is the width and h is the thickness. The samples tested recorded ILSS of 5.4 ± 1.03 MPa. It has been reported in literature that the matrix strength contribute towards the ILSS to certain point before the influence of voids becomes more dominant in the failure mechanism (Ahmed and Vijayarangan, 2008). During the samples consolidation, air bubbles can form under high vacuum conditions and remain in the fabric after cure as voids. The comparable range of ILSS with other published work suggests similar fibre-matrix interface achieved in processing, microscopic images prove this claim.

6.1.1.2.2. Thermo-mechanical properties

Storage modulus (E') of 3pt bending dynamic tests of Flax/UPE composites with different fibre contents 14, 18 and 22 % are represented in Figure 6-10 a). There is a clear improvement in storage modulus with increasing fibre fraction for the PE-F/H samples as an enhancement by a factor of 1.41 from fibre contents of 14 to 22 % at initial temperature of 25°C. The polyester chains movements are highly restricted due the increased fibre loading in the composite which then results in stress transfer enhancement at the fibre-matrix interface. Examining the E' variation with increasing temperature (25 – 180°C), it can be clearly noticed that all composites do not display any glassy plateau before the transition phase into rubbery state. This effect was recorded across all fibre contents but more prominent as seen in the sharp drop of E' at lower temperatures. This observation can be explained by the insufficient crosslinking of the polyester during the cure, this can be validated by the microscopic images. Few studies investigated the effect of fillers on the dynamic moduli using a parameter C the effectiveness coefficient as a ratio of the glassy to rubbery moduli ratio between the composite and resin (Poathan et al., 2003) (Romanzini et al., 2013). The higher C value is, the lower the effectiveness of the filler is. Both studies revealed that the higher reinforcement fractions the more effective is the

composite, up to a certain limit after which any increase in the fibre content will adversely increase fibre-fibre contact reducing the fibre-matrix load transfer efficiency (Idicula et al., 2005).

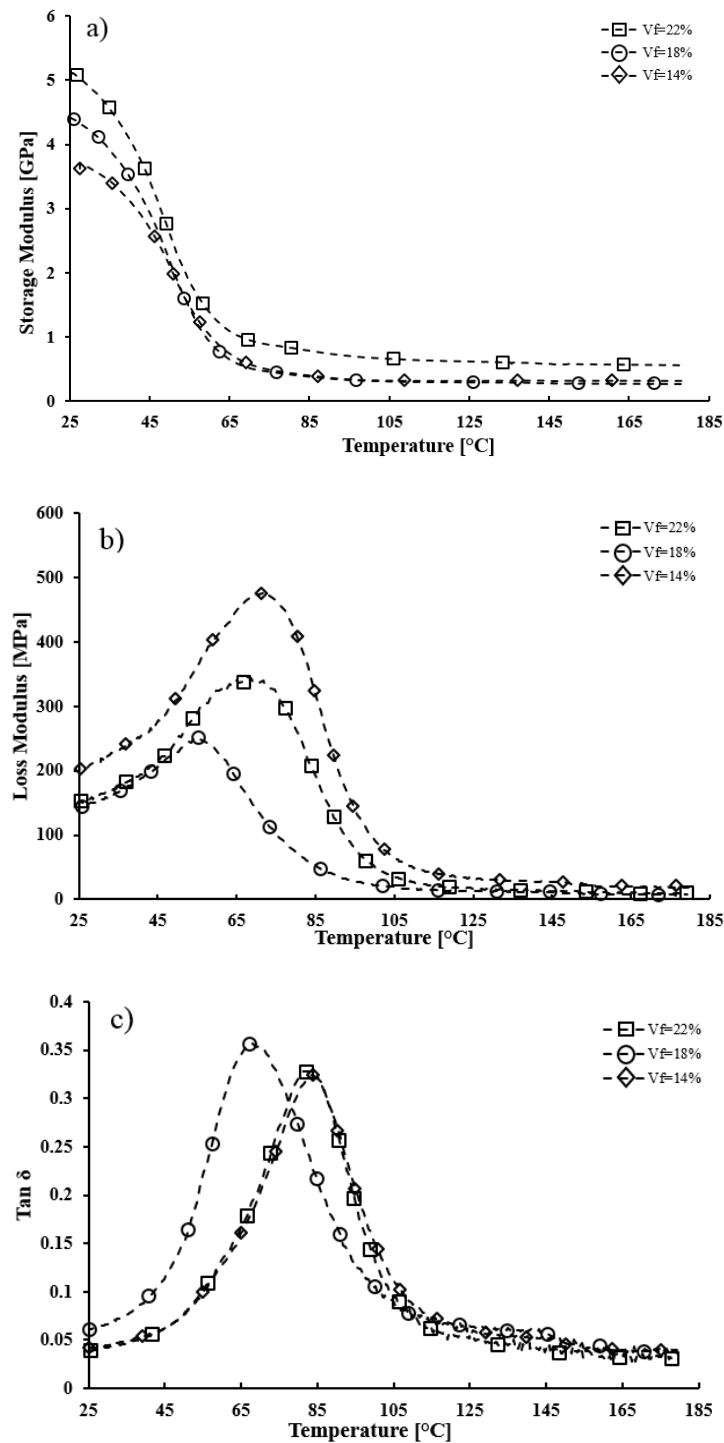


Figure 6-10 DMA results for the flax/UPE composites of three levels of fibre contents $V_f = 22\%$, $V_f = 18\%$, $V_f = 14\%$: a) storage modulus; b) loss modulus; c) $\tan \delta$

Another important observation, the notable variation in storage modulus at lower temperatures diminishes as temperature increased above T_g within the rubbery state. This confirms that once the

polymer molecular chains are unlocked and free volume mobility is induced the fibre role vanishes showing lesser contribution of fibres towards stiffness.

As previously mentioned, the glass transition temperature T_g as indication of several parameters e.g. thermal stability of composite, bonding strength, damping ratio, dynamic stiffness, polymer relaxations etc. is identified from either loss modulus (E'') or $\tan \delta$ curves. Peaks temperatures and curve widths have significance of the level of dynamic damping due to the incorporation of fibres into polymeric systems. Loss moduli of samples increased with increasing temperature up to T_g indicating maximum mechanical energy dissipation then decreases at higher temperatures in the rubbery range, Figure 6-10 b) represents the loss modulus of all levels of fibre contents. Furthermore, there is no clear indication of the effect of reinforcement contents on the shift of the T_g , however heights of E'' decreased with increasing the fibre contents which can only suggests reduced polymer chains mobility which agrees with other studies.

$\tan \delta$ curves of all reinforcements are shown in Figure 6-10 c), a highest damping ratio found for fibre contents of 18% while the others recorded almost identical ratios. It is therefore less evident that the incorporation of fibres leads to lowering the damping ratio due to greater restriction of the movement of polymer molecules caused by the presence of stiff fibres (Ornaghi Jr et al., 2010). An important observation regarding the T_g peaks as an odd shift was noted for V_f 14% at temperature of 83°C aligning with that of the 22% V_f , while the outlier V_f 18% peaking at 68°C. This observation can be attributed to the quality of composites processing. In fact, similar to the E'' curves, glass transition temperatures obtained for the $\tan \delta$ curves did not exhibit a clear trend, however, peaks indicating T_g from both curves were consistent. It has been established that as interfacial bonding improves with the incorporation of fibres the damping reduces. As insufficient fibre-matrix bonding induces defects and discontinuity of load transfer dissipating more energy, therefore increasing the fillers amount decreased the damping ratio from 0.35 for 18 % V_f to 0.32 for 22 % V_f . The positive T_g shift along the temperature range with increasing fibre contents up to 22 % can be attributed to the change in free volume between the monomeric units during the curing reaction affecting the molecular motion and diffusion.

6.1.2. Tensile properties of conditioned specimen

The effect of temperature on flax reinforced biocomposites have been evaluated. Natural fibres are prone to thermal degradation mainly during processing into composites, this is typically in temperatures range 160 -200°C. However, at lower temperatures such as the normal operational range when a product is in use, the matrix stability and fibre/matrix interface are the most susceptible to degradation. This has been proven through the tensile performance decline of a number of flax biocomposites in Figure 6-11, Figure 6-12 and Figure 6-13 corresponding to Flax/PLA, Flax/PP and Flax/PFA respectively. With regard to the thermoplastic based, PLA and PP, tensile properties suffer the most severe degradation up to 50°C at which these are halved. The thermal stability of these materials are dependent on the glass

transition and crystallinity of these polymers post thermal consolidation. This is controlled by the temperature cycling during fabrication and resulting molecular weight M_w of molecular chains.

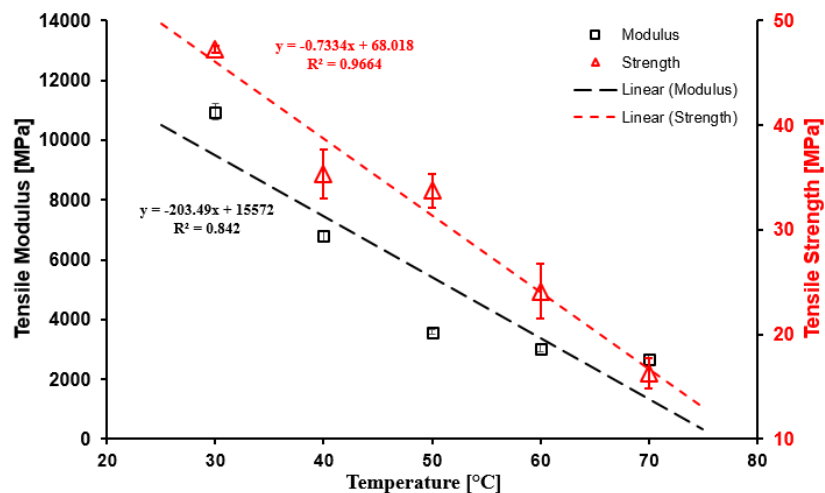


Figure 6-11 Effect of *in-situ* temperature increase on the tensile modulus and strength of Flax/PLA biocomposites, standard deviations values of the modulus are very small are difficult to see— a linear decrease with respect to temperature increase

Modulus is reduced to more than 50% of that in room temperature, with a higher gradient reduction between 30-50°C than 50-70 °C. Adding flax fibres to PLA shift the glass transition towards a higher temperature, as flax restricts the mobility of the PLA polymeric chains. Further, internal stresses are introduced by the differential thermal coefficients of composite components which can change magnitude with temperature, and control the matrix cracking. Increased ductility induced by higher mobility of the PLA chains at elevated temperatures above glass transition results in less debonding between the resin and fibres, thus better load transfer.

Similar response to that of Flax/PLA was observed for the Flax/PP and Flax/PFA, although furan based samples demonstrated higher thermal stability. To establish a quantitative comparison among these materials, a percentage decrease per 1°C was computed as the fraction of the best fit line gradient value to the reference property (modulus and strength) value recorded at 30°C. A reduction in modulus of 1.9%/°C, 1.5%/°C and 0.9%/°C; while 1.6%/°C, 1.5%/°C and 0.5%/°C reduction in strength for each of the biocomposite based on PLA, PP and PFA respectively.

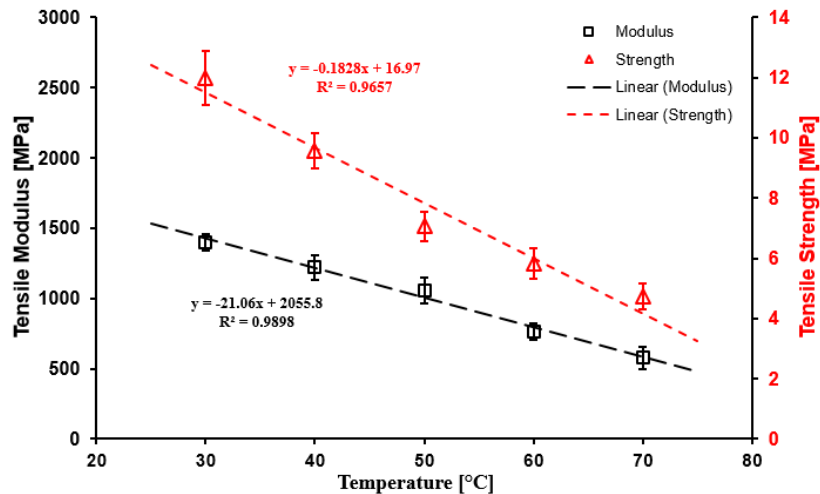


Figure 6-12 Effect of *in-situ* temperature increase on the tensile modulus and strength of Flax/PP biocomposites – a linear decrease with respect to temperature increase

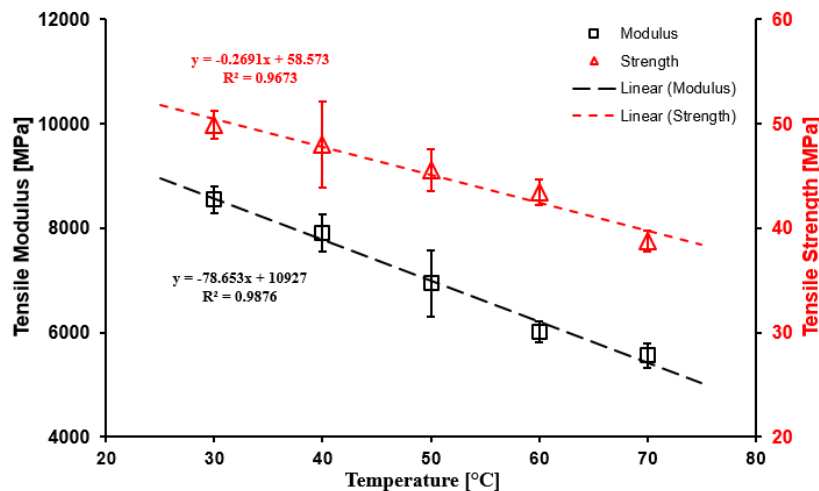


Figure 6-13 Effect of *in-situ* temperature increase on the tensile modulus and strength of Flax/PFA biocomposites – a linear decrease with respect to temperature increase

6.1.3. Toughness and resilience of conditioned biocomposites

The tensile testing conducted on the biocomposite specimen provides the primary data comprising the Young's modulus, ultimate strength (UTS), stress at failure and strain at failure. However, further analysis of such output can generate more properties which can assist in determining other characteristics such as fracture toughness. Toughness is a property that can be evaluated through other purposely designed methods of testing such as impact test, this includes Charpy and Izod testing. However the tensile stress-strain history can be used as an indication of how energy is absorbed or dissipated. Modulus of toughness is typically indicated by the absorbed mechanical energy up to a point of failure. Resilience though is the ability of a material to absorb energy when deformed elastically and release energy upon unloading, in other words, the maximum energy that can be absorbed up to the elastic limit without sustaining permanent distortion. This can be measured by the modulus of resilience which is the strain energy per unit volume required to stress the material from zero to yield stress.

Both toughness and resilience can be given by the area under the stress-strain curve, up to fracture and elastic limit respectively, this area is calculated by the following equation:

$$U_t = \int \sigma d\epsilon \quad \text{Eq. (6-2)}$$

U_t is the energy measured in J/m^3 , σ is the stress in MPa (either up to elastic limit or up to fracture) and ϵ is the strain.

Figure 6-14 illustrates the effect of temperature increase on the ability of biocomposites to absorb energy as both modulus of toughness and resilience have been computed by area integration from the stress-strain curves. The general trend was deterioration of properties with temperature increase however the strain-to-failure increased. Due to the fact that Flax/PFA tensile tests displayed no plastic deformation after reaching the yield point which explains that both modulus of toughness and resilience are identical. Otherwise, thermoplastic based materials exhibited ductile behaviour as temperature increased which caused extended deformation allowing the modulus of toughness to be higher than resilience.

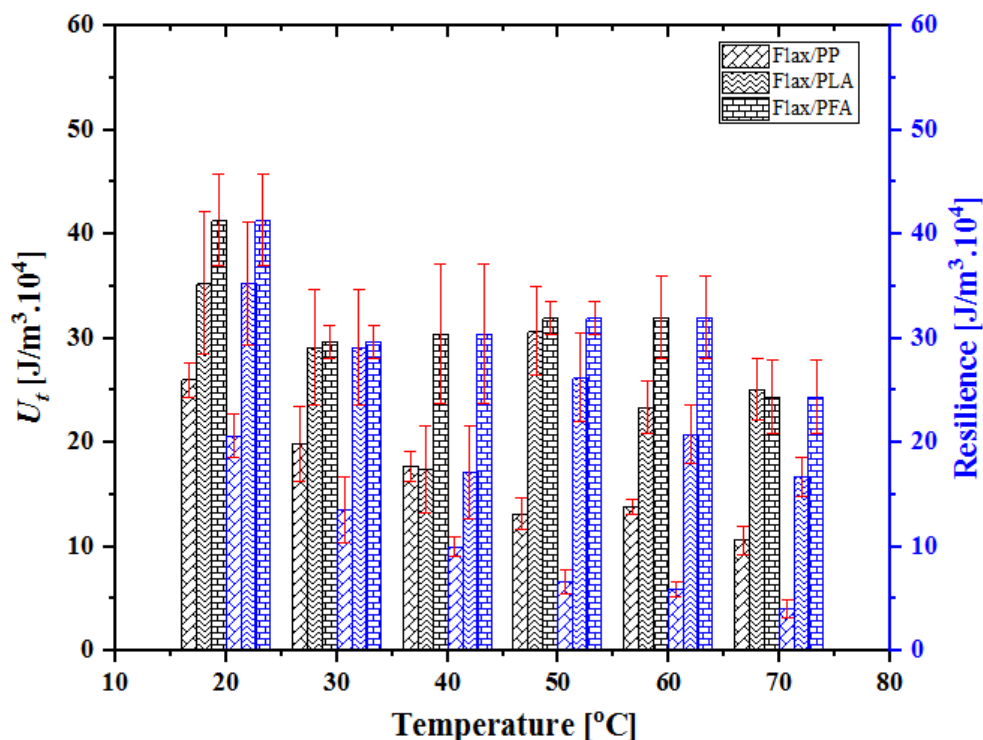


Figure 6-14 modulus of toughness and resilience of the biocomposites Flax/PLA, Flax/PP and Flax/PFA as temperature increases from 20-70°C

6.2. Discussion of 3D-Printed PLA properties

6.2.1. Effect of internal geometry

The tensile properties of 3D-printed specimen fabricated from PLA have been evaluated and results were presented in Chapter 5. The effect of infill orientation, also known as raster angle, has been widely discussed in literature as it was found to significantly affect the anisotropy and strength of 3D-printed parts (Rodríguez et al., 2003) (Rodríguez et al., 2003). The examination of the modes of failure exhibited by the specimen is directly linked to the loading mechanism experienced by beads either longitudinally, transversely or $\pm\theta$ angled to support the evidence of tensile test data. Figure 6-15 confirms the tensile behavior dependency on the internal geometry in a similar manner to a reinforced composite-like material. Unlike unidirectional structures, such that of reinforced composites, when load bearing is 100% shared by aligned fibres along a single direction (typically line of load application), the alternating layers as used in the 3D-printed specimen ($\pm\theta$) bear a fractional capacity of the load applied. This causes either specimen with failures of tough or brittle characteristics. The superior strength and modulus associated with $\pm 45^\circ$ with variation in stiffness as high as 29% and 22% as compared with specimen of the $-30/+60$ and $0/90$ builds respectively. This variation falls in the range of reported values of 11 to 37% (Rodríguez-Panes et al., 2018). The literature states that parts are stronger when beads are arranged in the load direction for tensile tests (Ziemian et al., 2012) (Vega et al., 2011) (Sood et al., 2010), while the current study focuses on the criss-cross layout for which response to load is supported by the interaction of two orientations thus controlling the part strength. The optimum response observed for $\pm 45^\circ$ specimen is attributed to the inter-raster bonding and reduced air gap between individual beads that forms during fabrication where only the layers with orientation higher than 45° positively contribute to the behaviour.

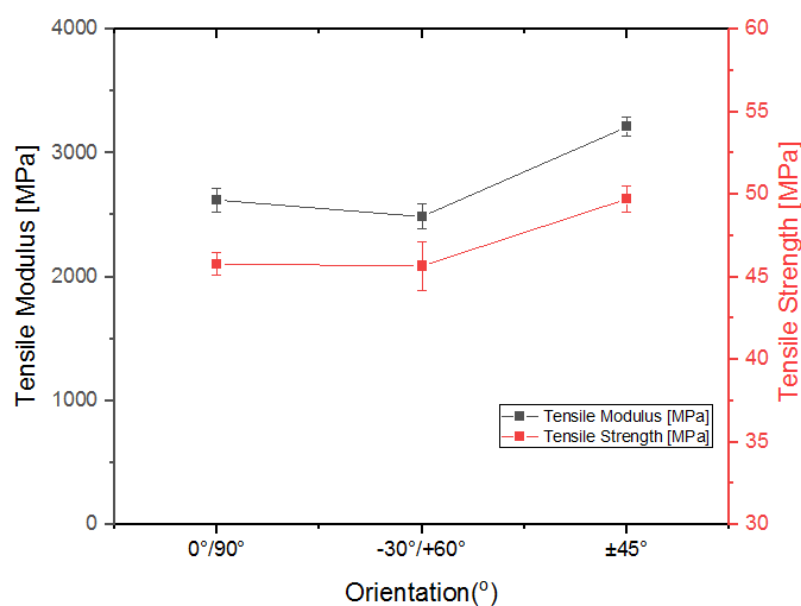


Figure 6-15 tensile strength and modulus variation of 3D-printed PLA with respect to the infill orientation of internal beads

For $0^\circ/90^\circ$, the axial load is taken partially by half of the layers oriented along the loading direction and partially by the rest of the layers oriented along the orthogonal direction. The contribution of the latter in sustaining the load is limited to the bonding surfaces that are weaker than the beads. However, the deformability of the cross section is limited; hence, the brittle failure is dominant as shown in Figure 6-16. The irregular shape of the beads, as well as the bonding region between beads locally increases the stress promoting failure.

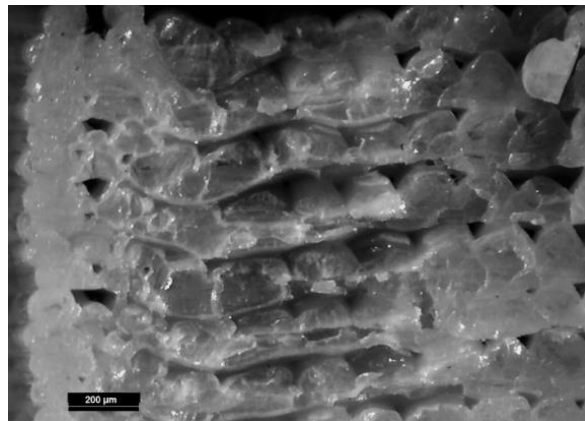


Figure 6-16 cross section view of specimen of $0/90^\circ$ orientation after the tensile test and full rupture of mid-section. Image portrays beads in criss-cross layering arrangement and bonding surfaces

As already described by Durgun and Ertan (Durgun and Ertan, 2014), the failure mode is a result of the material separation in a plane approximately normal to the tensile stress. The failure is caused by pulling with high tensile strength and eventual rupture, as the tensile loads were taken by beads themselves as presented in Figure 6-17.

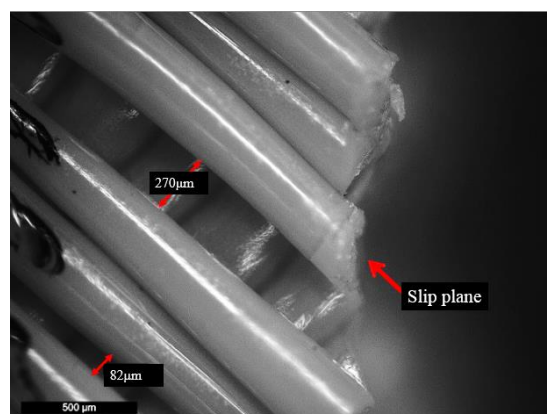


Figure 6-17 Micrograph of tensile failure surface perpendicular along the slip plane

When the beads are oriented along $-30^\circ/+60^\circ$ in each layer, the axial load has a component along the direction of the beads. As seen in Figure 6-18 the presence of more beads that withstand the load compensate the less part of the load taken by the more extended bonding surfaces resulting in a limited reduction of the stiffness value. Regarding the strength, similar performance of specimen at $-30^\circ/+60^\circ$ to that of the $0^\circ/90^\circ$ as equivalent UTS values were recorded, with slight advantage for the latter. This

is due to the fact that the bonding surfaces at $-30^{\circ}/+60^{\circ}$ orientation play a crucial role in reducing the load sustained by the specimen (Grasso et al., 2018). The criss-cross arrangement reduced the strength variability between these two orientations, however, marginal decrease in strength can be attributed to the reduction of effective load bearing area.

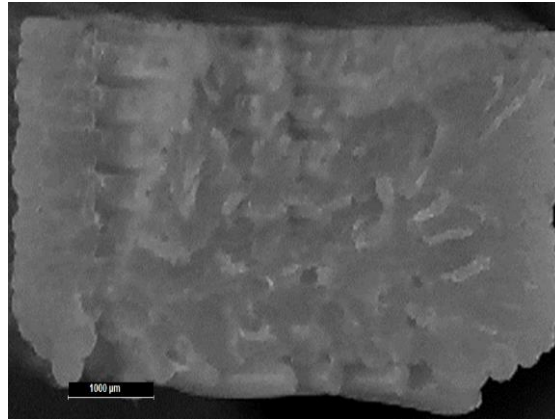


Figure 6-18 cross section view of specimen of $-30^{\circ}/+60^{\circ}$ orientation after the tensile test and full rupture of mid-section. Image portrays beads in criss-cross layering arrangement and bonding surfaces

When the beads are oriented along $\pm 45^{\circ}$, the diamond arrangement of the oriented beads Figure 6-19 enables the increased load taken with minimal extension compared to the two previous orientations, having at the same time a lower extension of the bonding surfaces.

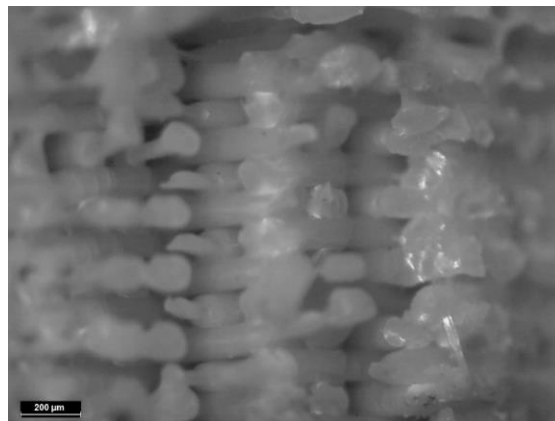


Figure 6-19 cross section view of specimen of $\pm 45^{\circ}$ orientation after the tensile test and full rupture of mid-section. Image portrays beads in criss-cross diamond arrangement and bonding surfaces

Another factor contributing to the variations of tensile properties among batches with the same orientation is the fact that printing of layers can be defective with either regions of beads not in contact creating an undesired positive air gap or non uniform shape of beads along the plane perpendicular to the load line as shown in Figure 6-20.

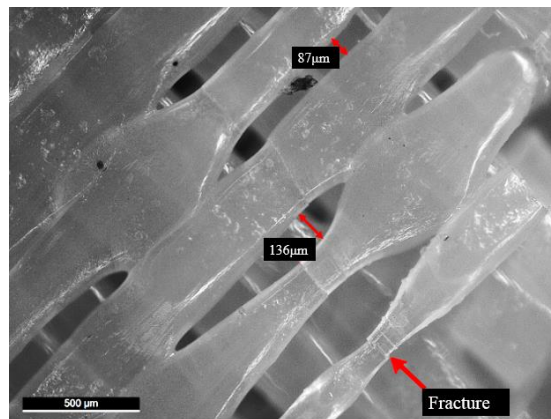


Figure 6-20 Micrograph of individual bead necking promoting local fracture and regions of air gaps between beads reducing the load bearing contribution of bonding surfaces

6.2.2. Extruded Filaments

The process of FDM typically entails exposing input feedstock filament to a thermal cycling as it undergoes heating above its melting temperature to flow through the nozzle. Upon its cooling, solidification takes place to ambient state, a condition which favours an amorphous and thus less strong polymer structure. This process at times results in deterioration of mechanical properties due to thermal shrinkage which result in molecular re-orientation. This shrinkage is normally experienced when the material is exposed to temperatures higher than its glass transition temperature T_g . Although there is no existing data concerning the effect of printing process on PLA extruded beads, a study on ABS reported stiffness reduction in the range of 11- 37 % when compared to raw feedstock (Rodríguez et al., 2001). However, in our study, opposite effects were observed as extruded monofilaments' stiffness increased by 19, 13, 37 and 41 % from the pre-extrusion filaments i.e. raw filament used as 3D-P input feedstock when subject to combined tension and temperatures 30, 40, 50 and 60°C respectively. A possible justification is the fact that upon PLA cooling from molten phase to solidification, PLA recrystallise inducing new crystals growth in the form of α and α' which evidently increases the crystalline fraction. This crystallisation window is controlled by the molecular weight of these crystals more specifically the D-lactate as an increase of its presence leads to a rise in T_g . This is in agreement with reported increased PLA mechanical properties post-annealing effect (Perego et al., 1996). Furthermore, with regard to the gradual decrease of stiffness as temperature increases, this is expected and can be explained by the increased chain mobility of PLA molecules that impart the micro-level structural integrity. The expanded free volume which promotes free particles movement and consequently reduces the interlocking mechanism; hence, lowering the measured stiffness (Nikzad et al., 2011).

6.2.3. Tensile Properties of 3D-printed Conditioned Specimen

To aid the discussion of obtained results, visual simulations of primary experimental results have been generated in the form of contour plots by means of data analysis and graphing specialist software OriginLab Corporation (Northampton, USA). A learning edition was acquired and used in the analysis provided herein. The combined effects of *in-situ* temperature increase and infill orientation variation

is illustrated in the contour plot of Figure 6-21, to be read in colour as per the legend. There is clear indication of modulus deterioration as temperature increases in a uniform manner as depicted by the explicit regions. Note that the highest modulus is interpreted from the contour plot to be associated with those specimen of orientation approaching the zone of $\pm 45^\circ$ at which the peak is recorded. This trend is however found to differ when temperature is increased to 40°C with highest modulus being associated with region of $-30^\circ/+60^\circ$. As temperature approaches 50°C , the infill orientation seems to have minimal to no effect on the modulus from what can be observed.

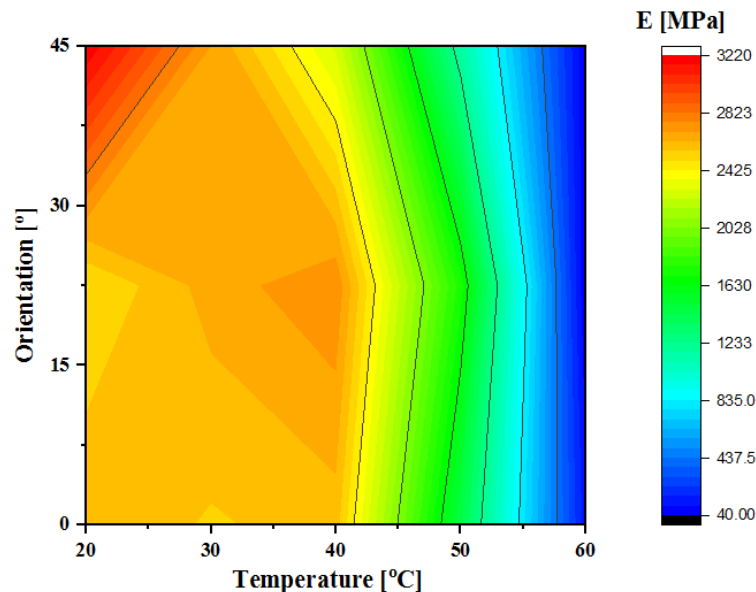


Figure 6-21 Contour plot of young's modulus variation for 3D-printed PLA to illustrate the combined effects of temperature increase and infill orientation angle. Y-axis labels identification: 0= ($0^\circ/90^\circ$), 30= ($-30^\circ/+60^\circ$) and 45= ($\pm 45^\circ$)

Similarly, strength variation with increased temperature while considering the infill orientation, is illustrated in Figure 6-22. The strength trend corresponds to that found for modulus as the highest strength is found to be for the $\pm 45^\circ$ at 20°C . However this observation is only true for lower temperatures below 40°C as the other orientations tend to have higher stability and retain performance. At 40°C the minimum value of strength is reached at $\pm 45^\circ$ and the maximum at $0^\circ/90^\circ$. For all orientations, necking plays a major role in the failure mechanism resulting in immediate failure after the ultimate strength is reached.

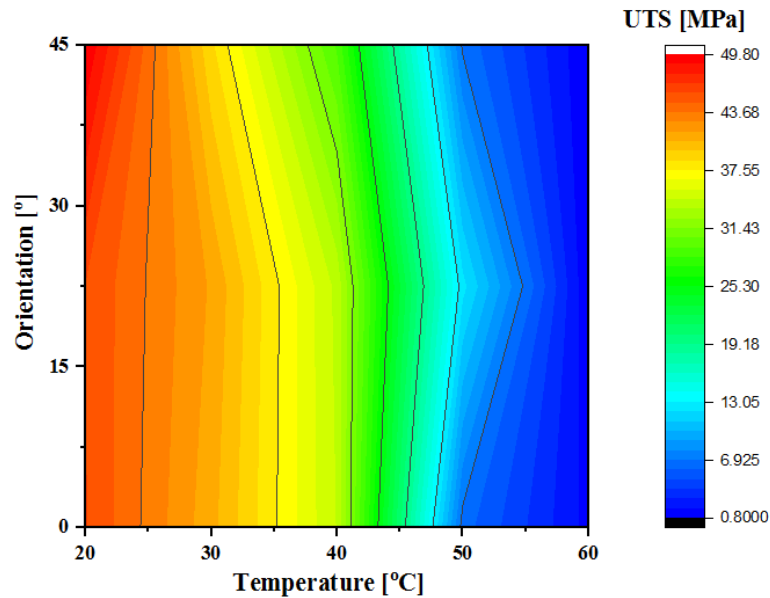


Figure 6-22 Contour plot of strength variation for 3D-printed PLA to illustrate the combined effects of temperature increase and infill orientation angle. Y-axis labels identification: 0= (0°/90°), 30= (-30°/+60°) and 45= (±45°)

Bonding surfaces are the contact regions created among adjacent beads. In fact when all beads are all broken as they exhibit ductile fracture, the load is then primarily carried by the bonding surfaces which will tend to creep along the directional planes due to the shear forces. Moreover, the inspection of the fracture surfaces as shown in Figure 6-23 of the ±45° specimen together with the analysis of the stress-strain curves reveal that the response is characterised by evident softening because of the shear response resulting in a higher strain at failure. The effects of the temperature promote creep which contributes to the greater elongation (Yang et al., 2006).

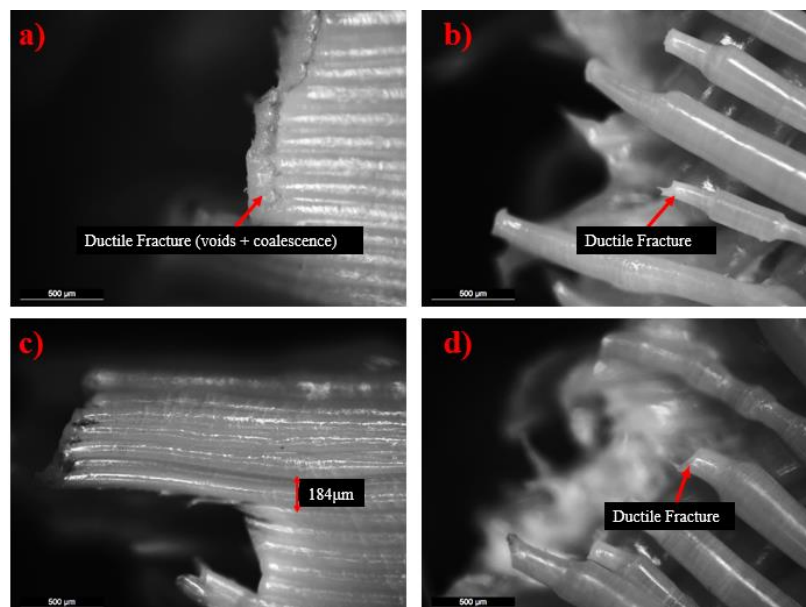


Figure 6-23 Optical images of fractured specimen ±45°: a) and b) for tests under 30°C, c) and d) for tests under 40°C

Specimen tested at 40°C have shown a failure mode mainly ductile with necking in the beads and visible necking in the cross section of the specimen, see Figure 6-25. As a result the combined effects of infill orientation and temperature result in the failure of beads. The combination of infill orientation and temperature trigger the shear failure of the samples. Shear is induced by the force acting in parallel planes, consequently sliding movement of beads layers along the raster direction as depicted in Figure 6-24.

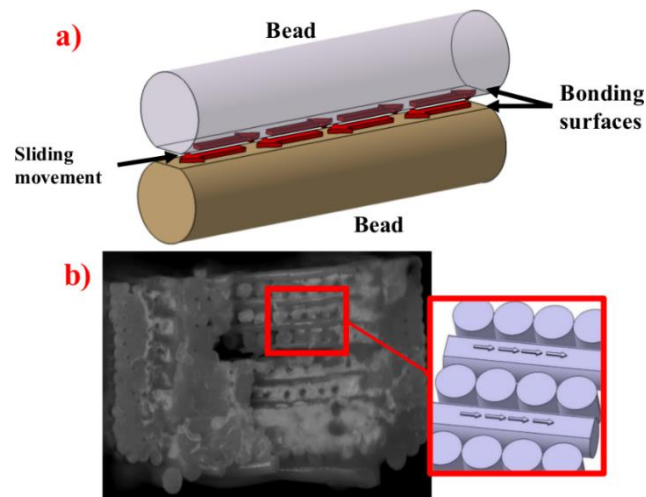


Figure 6-24 a) illustration of sliding movement of bonding surfaces under the induced shear due to tension acting on the adjacent beads; b) optical microscopic image close-up illustrated in a representative volume of shear failure within a cross section of fractured specimen.

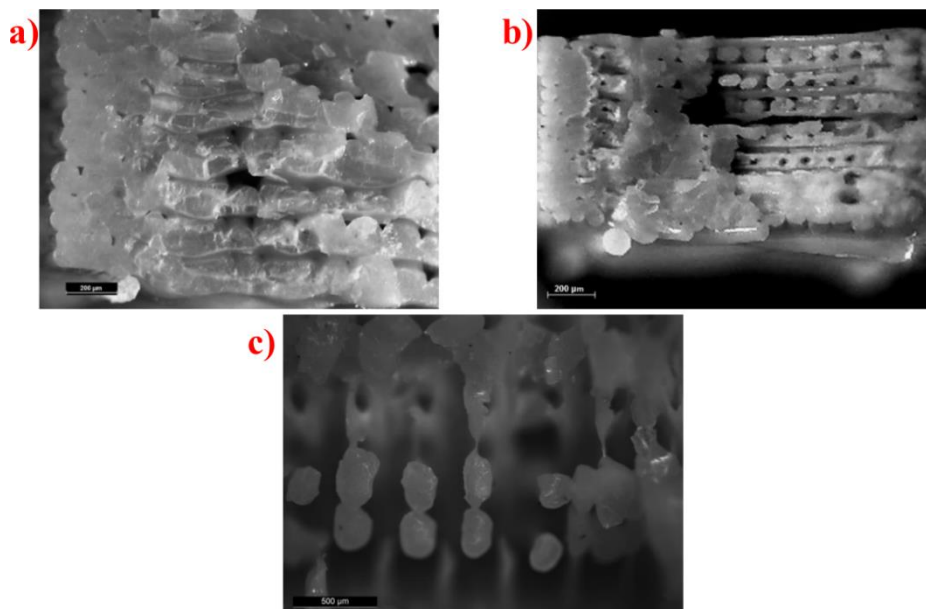


Figure 6-25 Microscopic images of specimen printed at: a) 0°/90°, b) -30°/+60° and c) ±45° after testing at 40°C. The fractography evidence of specimen tested at both 50°C and 60°C was not possible as these did not reach separation due to rupture although stiffness continued to drop with differences among the various orientations. At 50°C the effect of temperature on the strength and stiffness is different as the highest values of 12.4MPa and 1728MPa respectively for the -30°/+60° because of the different contributions

from the beads and the bonding surfaces. In this particular case, most of the beads are orientated closer to the loading line resulting in most of the load being taken by the beads rather than the bonding surfaces. By further increasing the temperature to 60°C, no significant variances in stiffness and strength is observed among the three orientations as depicted from the contour plots. These values are considerably low for all orientations as the test temperature is greater than the glass transition of PLA, however, differences can be identified as in particular the maximum value is reached for 0°/90° whilst the minimum at -30°/+60°. Below this temperature any dimensional changes are dominated by the temporary distortions of the primary valence bonds. Polymers in general, including PLA which its structure and thermal stability characteristics have been already discussed, are either semi-crystalline or amorphous. Therefore the resulted structure after extrusion is considered to be in a semi-crystalline phase with repeating crystals which are responsible for enhancing the tensile stiffness and strength. These properties decrease drastically above the glass transition (Van de Velde and Kiekens, 2002). Furthermore, the glass transition temperature depends on the mobility and flexibility of polymeric chains i.e. ease of the chain segment to rotate along the chain backbone.

With regard to the stress at failure, the variation of values among orientations can be clearly observed at temperatures below 50°C. Above this temperature, i.e. approaching the glass transition point, values are very small for all orientations with insignificant differences as shown in Figure 6-26.

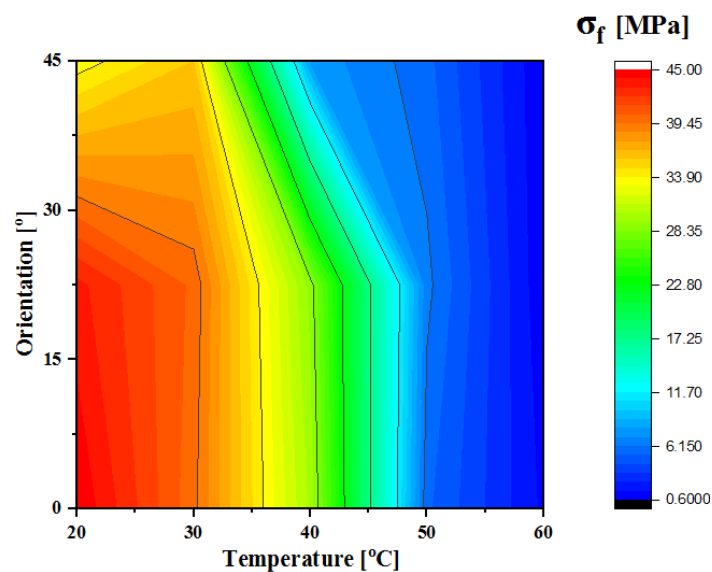


Figure 6-26 Contour plot of stress at failure variation for 3D-printed PLA to illustrate the combined effects of temperature increase and infill orientation angle. Y-axis labels identification: 0= (0°/90°), 30= (-30°/+60°) and 45= (±45°)

At room temperature, the highest stress at failure was recorded for specimen of 0°/90° orientation while the minimum corresponded to ±45° specimen. This was found to be a general trend consistent as the temperature increased up to 50°C, the 0°/90° and -30°/+60° maintained higher stress at failure values while the ±45° values plummeted more sharply. The explanation of this observation can be provided

with reference to the optical microscopic images Figure 6-23 and Figure 6-25. The extended necking, plastic deformation and the brittleness of the bonding surfaces which are predominantly contributing in the load bearing role for the $\pm 45^\circ$ orientation, are affecting the beads as well as the entire cross section. On the other hand, for the other two orientations i.e. $0^\circ/90^\circ$ and $-30^\circ/+60^\circ$, the contribution from the beads is predominant compared the bonding surfaces and consequently the stress at failure is much higher. To include the specimen tested under temperatures 50°C and 60°C , the stress at failure was identified as the constant stress under which the material flow at high strain values.

Considering the strain at failure, the specimen tested at temperature of 50°C and 60°C , the extension was infinite and therefore strain at failure was not possible to be determined hence this was fixed at 10%. The graphical analysis presented in Figure 6-27 is therefore limited to the temperature range of $20\text{--}40^\circ\text{C}$ since complete failures were not achieved at 50°C and 60°C , thus comparisons cannot be made. At room temperature the maximum strain at failure is reached at $-30^\circ/+60^\circ$ as the overall longitudinal strain is mainly composed by the elongation of the beads along the loading line. Meanwhile, specimen of $\pm 45^\circ$ attain the lowest strain at failure as the strain is mostly contributed by the bonding surfaces without any significant axial elongation of the beads.

With regard to specimen tested at 30°C , a similar response to that of the room temperature as the maximum strain at failure is again for those specimens oriented at $-30^\circ/+60^\circ$ while the minimum is attributed to the $\pm 45^\circ$. However as the temperature is increased to 40°C , the trend is the opposite as the highest strain at failure is reached at $\pm 45^\circ$ whereas the lowest at $30^\circ/+60^\circ$. The combination of bonding surfaces deformation with the axial elongation of the beads is thought to cause the dissimilar performance at that temperature.

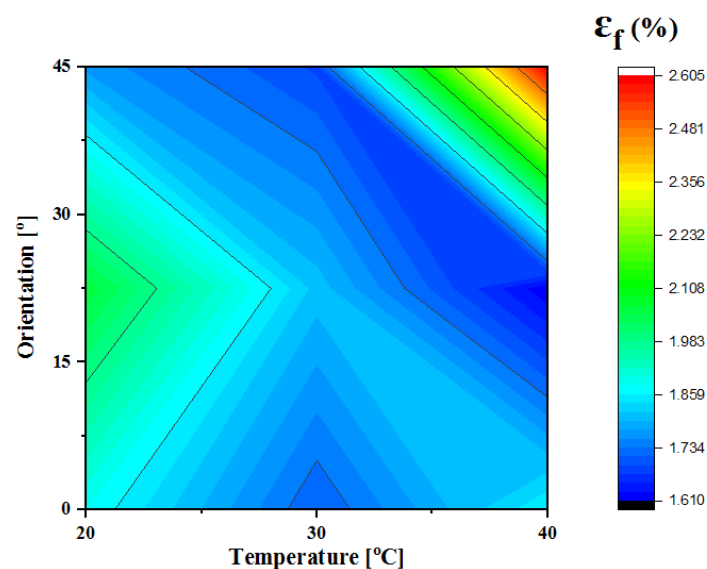


Figure 6-27 Contour plot of strain at failure variation for 3D-printed PLA to illustrate the combined effects of temperature increase and infill orientation angle. Y-axis labels identification: 0= ($0^\circ/90^\circ$), 30= ($-30^\circ/+60^\circ$) and 45= ($\pm 45^\circ$)

At low temperatures, the macroscopic examination of $\pm 45^\circ$ specimen displayed multiple failures of individual beads in both shear and tension owed to the diamond arrangement. At elevated temperatures, the softening effect causes a drop in the shear strength of the bonding surface among beads, resulting in a ductile failure. The increased load sustained by the beads results in more elongation and a dominant necking all over the cross section.

6.2.4. Resilience and toughness of 3D-printed specimen

Similar calculation methods to that used for the of resilience and toughness of biocomposite specimen in Section 6.1.3 are used for the 3-D printed specimen. Figure 6-28 summarises all calculated values of the fracture toughness and resilience of specimen built in three orientations $0^\circ/90^\circ$, $-30^\circ/+60^\circ$ and $\pm 45^\circ$ and tested across a range of temperatures 20-60°C. These calculations enable better interpretation of the experimental results considering the variations in failure mechanisms between samples with respect to plastic deformations before rupture. Samples tested at 50 and 60°C did not fail and therefore the calculation of toughness was set to span up to 6% strain for all specimen.

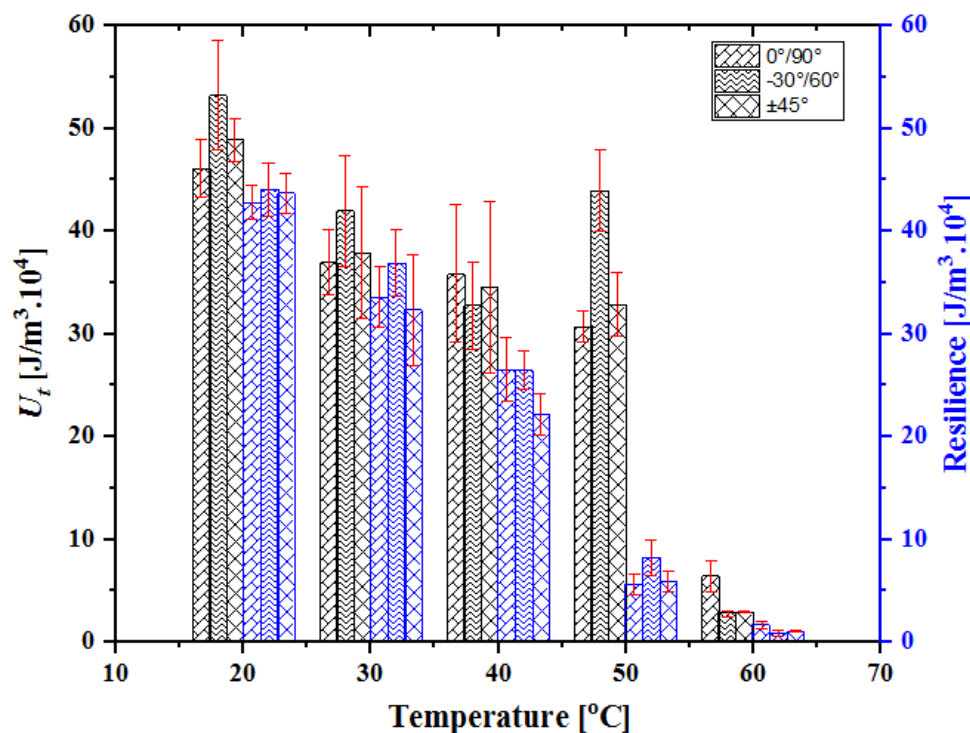


Figure 6-28 Fracture toughness and resilience of 3D-printed PLA of the three orientations and across a range of temperatures 20-60°C

The differences associated with adopting the toughness calculation as integration of area up to fracture can cause discrepancies due to the variation of material response beyond the point of UTS. Since some specimen experienced immediate rupture at the UTS while others experienced large plastic deformation before rupture. A general observation from the chart is that both toughness and resilience decreased as temperature increased. Although it is coherent to have resilience values to be consistently below those of the toughness for the respective samples, the gap in values widens as temperature increased. This can

be an indication that specimen experienced higher elongation under constant stress which is considerably low, this typically corresponds to high temperature testing. Overall, specimen $-30^{\circ}/+60^{\circ}$ demonstrated higher energy absorbance compared to the other orientations.

One can observe that toughness of all specimen plummeted after temperature of 50°C , an indication of glass transition effects on tensile behaviour of 3D-printed parts represented by a reduced strength. Further to this, at this temperature i.e. 50°C a noticeable peak of toughness for specimen $-30^{\circ}/+60^{\circ}$ reaching values as high as the lower range of those recorded for ambient conditions.

Figure 6-29 illustrates the values of resilience calculated from the area under stress-strain curve of all tested across all temperature using Eq. (6-2) and represented in a contour plot. For which the combined effect of temperature and orientation is represented and correlates with the strength behaviour due to its effect on how energy is absorbed. As temperature increased, specimen $-30^{\circ}/+60^{\circ}$ showed marginal superiority of resilience which fades away beyond the point of glass transition.

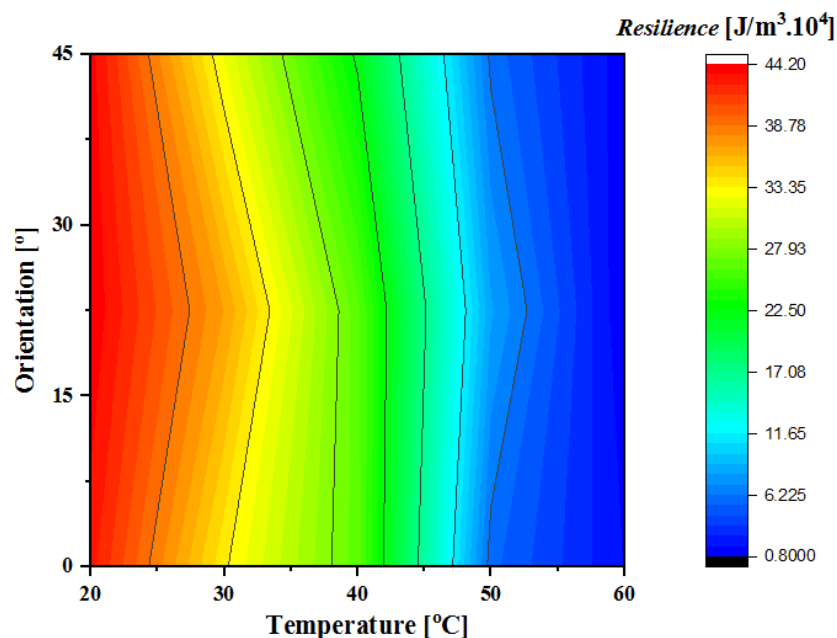


Figure 6-29 Contour plot of resilience variation for 3D-printed PLA to illustrate the combined effects of temperature increase and infill orientation angle. Y-axis labels identification: 0= ($0^{\circ}/90^{\circ}$), 30= ($-30^{\circ}/+60^{\circ}$) and 45= ($\pm 45^{\circ}$)

The modulus of toughness, represented in Figure 6-30, tends to gradually decrease as temperature increased and is directly related to the strain-to-failure. At low temperatures $-30^{\circ}/+60^{\circ}$ exceeded other orientations. For instance, as high strain-to-failure values are recorded such as that for the $-30^{\circ}/+60^{\circ}$ specimen the toughness is the highest. This advantage is maintained as temperature increases up to 40°C .

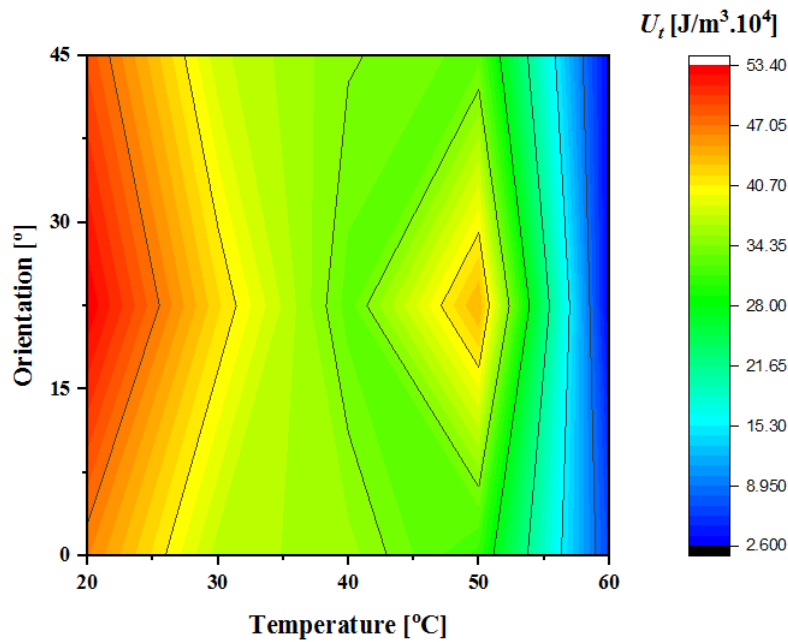


Figure 6-30 Contour plot of modulus of toughness variation for 3D-printed PLA to illustrate the combined effects of temperature increase and infill orientation angle. Y-axis labels identification: 0= (0°/90°), 30= (-30°/+60°) and 45= (±45°)

From the contour plot, in the vicinity of 40°C temperature range all orientations have equivalent toughness. Whereas a sudden increase of the -30°/+60° specimen toughness can be observed around a temperature of 50°C which can be linked to a corresponding high UTS and the fact that no failure occurred. At temperatures above 50°C, all specimen of various orientations absorb equivalent amounts of energy indicating that toughness is independent of build orientation. Consistent results were obtained as all specimens tested above this temperature did not rupture. This observation can be attributed to the weakening of bonding surfaces as well as the individual beads triggered by the unlocking mechanism of PLA molecular chains above glass transition. This change of molecular structure is significantly visible at the macrostructure level as displacement in the load direction is infinite with no obvious failure.

7. Case Study: Sandwich Panels of 3-D Printed Lattice Core and Biocomposite Skins

7.1. Introduction

The advanced development in sandwich structures and polymer/natural fibre composites open up the potential to overcome one of the primary limitations of FFF/FDM in load bearing applications: highly anisotropic properties having particularly low stiffness and strength in the direction of layer deposition i.e. z-direction. Amongst the complex geometries that can be produced using FFF/FDM is the lattice or cellular structure for load-bearing applications, and it is expected that the mechanical properties of the sandwich cellular structures for load-bearing applications could be improved by fibre reinforced thermoplastics. Therefore, in order to probe these potentials, a study was designed to take advantage of the more advanced work in PP-flax composites to make up the top and bottom layer of the sandwich structure and PLA to form 3-D printed truss-like lattice units of a non-stochastic structures making up the internals. The aim of this work thus was to collect sufficient mechanical properties of three selected lattice topologies of PLA and PP + flax composites to be used in the structure optimisation process for sandwich structures. Mechanical tests included compression both in-plane and out-of-plane (edgewise and flatwise), core shear and sandwich flexural. Force vs displacement curves were generated, which were then processed accordingly to interpret the achieved results and later discussed the overall response to draw conclusions on stress distributions within the structures and identify high-stress regions which may require reinforcement and low-stress regions where with potential weight savings. The potential for FFF/FDM to provide load-bearing structures for various applications with these materials are discussed, and conclusions are drawn.

7.2. Methodology

7.2.1. Lattice Structures

Cellular solids are divided into two main groups: 1) stochastic structures (or foams) are classified according to their porosity type open-cell or closed-cell, whereas 2) the non-stochastic are categorised according to their building unit cell either 2-D lattice unit (honeycomb) or 3-D lattice unit (truss-like) (Bellini and Güçeri, 2003). The lattice structure is a truss-like structure with a repeating unit cell that forms intersecting struts and nodes with a specific recurring arrangement over a volumetric region. The internal design of these struts whether hollow, circular, square or any desired shape cross sections is application dependent and more specifically dependent on the strength and stiffness requirements (Tao and C.Leu, 2016). Kagome truss core structures perform better than conventional honeycomb core structures in terms of their specific compressive and shear strength. In order to maximise the compressive and shear strength of the kagome structure, the internal angle can be adjusted closer to 45° or 60° respectively.

Three unit cell structures were developed with the CAD software CATIA V5 (Dassault Systemes, Velizy-Villacoublay, France), motivated from the previously investigated structures in literature. However modifications to the geometry and dimensions have been applied to improve the print quality and reduce manufacturing times. Lattice structures are generated by repeating unit cells, which are cylindrical struts built at different orientations connected through nodes. For comparison purposes a fixed envelop of width and height of 10×10 mm is used. The STL files of the base unit cells designs can be found at the Open Science Framework (Azzouz et al., 2018) and are shown in Figure 7-1.

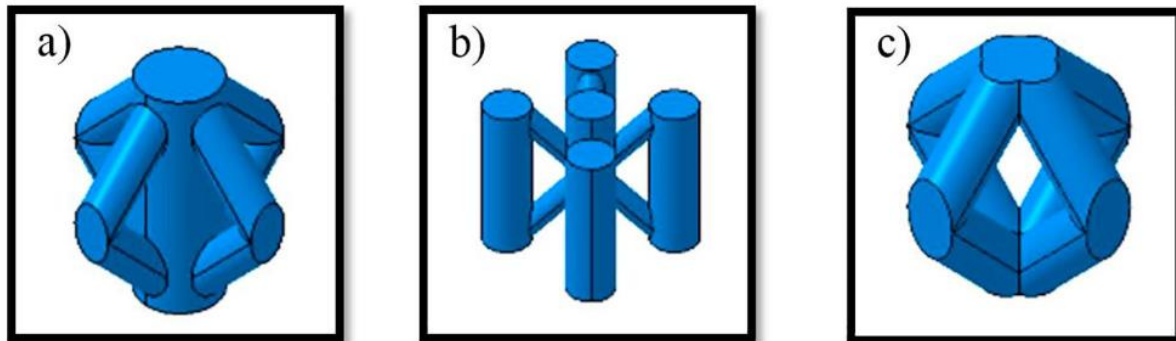


Figure 7-1 (a) Lattice 1: BCC-Z structure, diamond design that has a vertical strut that runs through the middle of the unit cell (b) Lattice 2: cube-like format, circumferential rectangular pattern of 4 vertical struts on each corner, with 5th vertical struts in the centre, and eight smaller struts that meet at the middle of the vertical strut in the centre of the cell, and (c) Lattice 3: diamond form BCC unit cell like that of unit lattice 1 without the vertical strut.

Lattice 1 is a diamond design that has a vertical strut that runs through the middle of the unit cell. The vertical strut in the centre of the cell has a diameter of 2.5 mm whilst the remaining diagonal struts have a reduced thickness of 1.5 mm. With the vertical strut present in the layout of the unit cell, the compressive capabilities of the cell should see greater improvement compared to the same design without. For the second unit cell, a cube-like format has been utilised, with five vertical struts (4 corners with 1 in the centre), and eight smaller struts that meet at the middle of the vertical strut in the centre of the cell. Similar to unit cell 1, the vertical struts have a thickness of 2.5 mm whereas the smaller diagonal struts bear a thickness of 1.5 mm. This cell structure is expected to perform especially well under compression due to an increase in mass as a result of the additional vertical struts in comparison to unit cell 1. The third unit cell to be observed is a cell that also takes a diamond form like that of unit cell 1. However, it differs in the fact that it does not have the vertical strut present in the centre of the cell. As a result, it is expected to perform to a lower standard to unit cell 1 under compression. Due to the absence of vertical struts in this cell, the thickness of the struts is marginally thicker than the other two cells, with a diameter of 2 mm instead of the original 1.5 mm.

7.2.2. Manufacturing Procedures

7.2.2.1. Materials and equipment of the core

Manufacturing of specimens was carried out using an Ultimaker 3 Extended dual extruder equipped with 0.4 mm nozzles compatible for printing PLA on a 215 x 215 mm heated glass build plate. The

printer uses the layer by layer build approach by which a nozzle travel deposition in x - y direction with active build plate levelling in z direction. CAD files were imported into Cura 2.7.0 in STL format to be sliced and a list of printing parameters were adjusted accordingly, these instructions are subsequently generated in a G-code script which the printer uses to perform the print. A process of fine tuning the printing parameters to attain an optimum quality, where visual investigation of printed parts were carried out to identify physical defects which would potentially yield inconsistent results. No support material used for all printing operations, this was decided due to poor quality prints and to reduce manufacturing lead times. The feedstock for the 3-D printed cores used in this study was a PLA filament made of starch promoting its biodegradability and biocompatibility. Spools of blue PLA 750 g of 2.75 mm diameter, melting temperature range of 145–160 °C and a specific density of 1.24 purchased from RS Components Ltd, UK. The mechanical properties of bulk PLA were reported in the datasheet [41] with a tensile modulus of 2852 MPa and yield stress of 38.5 MPa, which were tested in accordance with ISO 527. During the printing process, a spool of Blue PLA 2.85 mm was placed on a holder located at the back of the printer and fed to a 225 °C preheated print-core through pulling gears to ensure continuous and steady flow of filament. An electrically generated heat is conducted from a steel plate through the glass build bed set at the recommended temperature of 60°C.

7.2.2.2. Printing problems resolution

i. Build plate adhesion

It is worthwhile mentioning the problems encountered with poor adhesion to the plate since no raft nor support were used, this was mitigated by the use of a thin layer of general use glue stick being applied on the print area before the start of each print. Furthermore, the build bed levelling influences the amount of extruded material as with an increased gap deposition is random and the layer is distorted and consequently produce a poor quality print. Whereas a decreased clearance i.e. close print-core (nozzle) results in under-extrusion, these are illustrated in zone 2 within Figure 7-2 a).

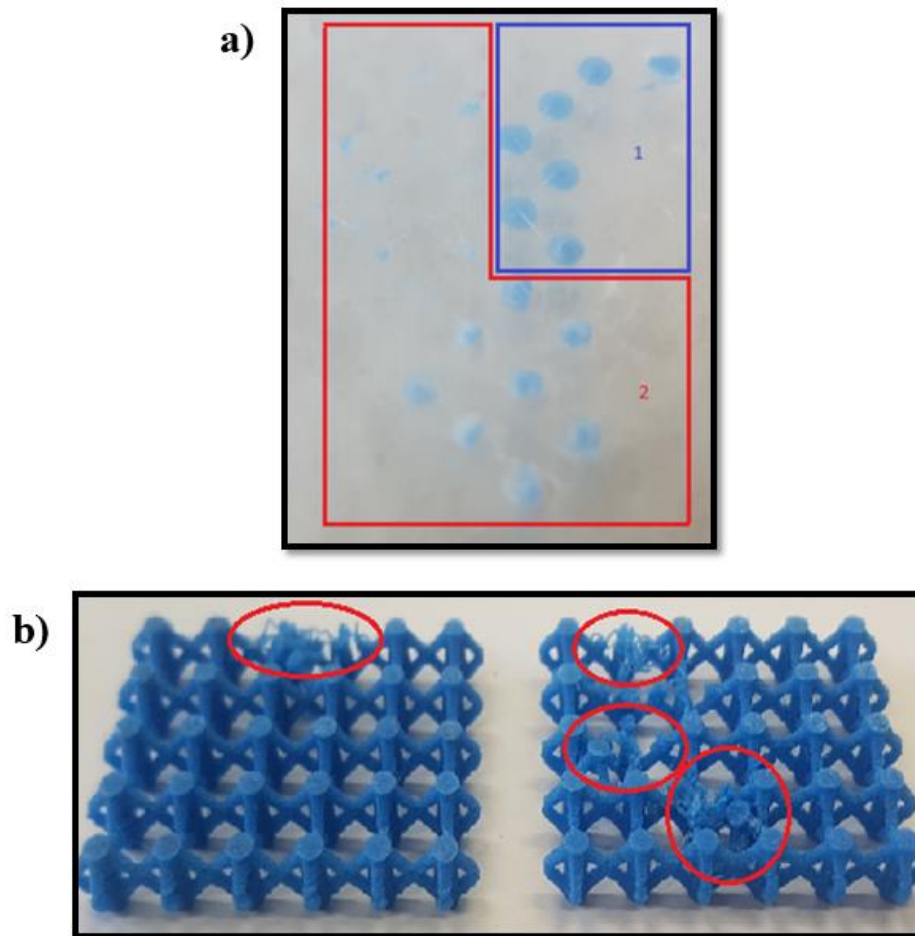


Figure 7-2 the effect of the reduced build plate adhesion and the plate levelling on the quality of the extruded filaments: a) the use of glue on surface build plate instead of raft; b) the plate/print-core nozzle spacing affects the quality of extrusion as shown is zones of poorly printed unit cells

ii. *Temperature and speed effects*

Similarly, environmental conditions influence the printing process, the surrounding temperature and humidity are common factors to be considered when selecting the printing temperature. Since the material used is PLA which is extremely sensitive to heat and moisture, a progressive increase of 5 °C in printing temperature from 205 °C to 225 °C to identify the most suitable revealed that the latter produced the best parts. Figure 7-3 highlights the defects of some layers associated with the inadequate temperature or moisture contestants. It was also noted that daily weather conditions contribute to either improving or decreasing the part quality. Furthermore, the spool was regularly removed and packed in its original metallic sealable bag to prevent exposure to surrounding humidity. In the case of filament exposed to high moisture, a common practice accepted and implemented by the 3D-printing community is to oven dry the spool. Although this technique is considered efficient however more care is required not to overheat the thermoplastic thus softening it. In general, about 60-70 °C is just about right for most materials, except may be a bit hot for lower temp materials like PLA, therefore 40 °C can be

considered as the highest. Once the oven is up to temperature, place the spooled material inside and leave it there for four to six hours. If you have a convection oven, this drying time may be shortened since the circulated air removes more moisture from the material more quickly.

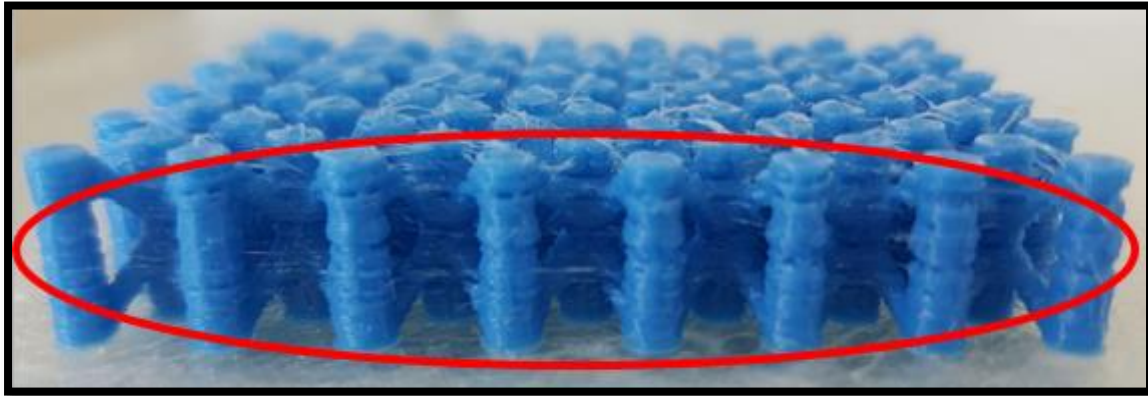


Figure 7-3 Filament extrusion poor quality due to the inadequate printing temperature and the moisture content in the surrounding environment creates layers with multiple defects such as high porosity and geometrical faults.

These observations were recorded across all three different lattice structures, however lattice 2 experienced a trend of missing layers in the same location upon repetitive trials. After a close monitoring of the print-core travel, it was evident that the combination of deposition speed being too high and complexity of the geometry prevented a good quality print. Therefore single unit cells were generated with reduced speeds from 40 mm/s to 15 mm/s and a noticeable improvement within prints at speeds lower than 40 mm/s until the ghost layer completely disappeared at a speed as low as 15 mm/s which was decided for all future prints. Figure 7-4 displays these improvements, nonetheless this resulted in extended printing times but with reassured quality.

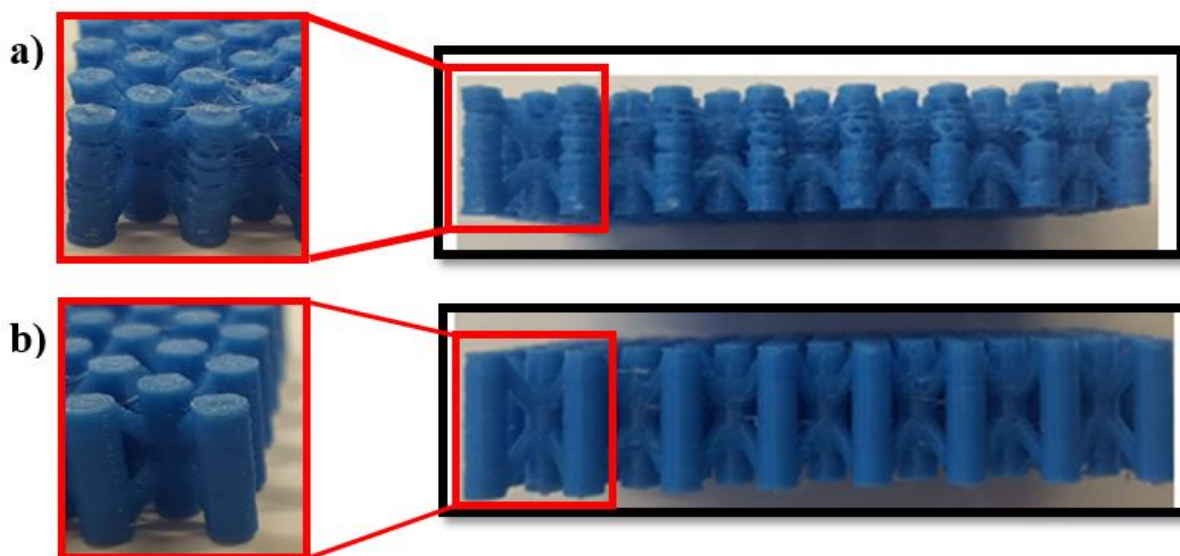


Figure 7-4 Printing speed optimised to overcome the ghost layers of the complex parts: a) Lattice 2 printed at speed of 40 mm/s and missing layers are clearly noticed, b) Lattice 2 printed at speed of 15 mm/s which is defect-free

The complete list of parameters used to manufacture all types of specimen have been included in Table 7-1.

Table 7-1 Printing parameters used to manufacture all specimen considered for this study

Layer Thickness (mm)	0.1
Infill density (%)	100
Print temperature (°C)	225
Build bed temperature (°C)	60
Print speed (mm/s)	15
Flow rate (%)	100
Build bed adhesion	Glue stick

7.2.2.3. Sandwich panels production

Natural fibre composites (NFC) face sheets made of discontinuous flax fibres and polypropylene and preformed with a mass content ratio 52:48 Flax/PP were produced at EcoTechnilin Ltd, Cambridgeshire, UK. These consolidated mats called fibriplast sheets are a mixture of discontinuous flax fibres, and PP interlocked using needle punch process with 30,000 needles/s resulting in the aerial weight of 1200 gsm. Consolidation using heated press with applied pressure of 20 MPa and 120 °C temperature for 5 min yield a reduced thickness of 2 mm. The motivation for the use of NFC as opposed to the use of virgin polypropylene is the eco-friendliness of flax fibres and reduced carbon footprint. Furthermore, polypropylene is a fossil fuel based thermoplastic with a maximum tensile modulus of 1.5 GPa and strength of 30 MPa.

For the sandwich panel's production, the adhesion of the 3-D printed core to the NF face sheets was achieved using Araldite 2015 (AV5308/HV5309-1) bi-component epoxy paste adhesive purchased from RS Components Ltd, Northants, UK. The two-part epoxy resin and hardener were mixed in an equal amounts and allowed to react for 5 min in room temperature before being applied on the face sheets only. This adhesive was also used to attach the 3-D printed core specimen to the metallic shear fixture as described in section 7.2.3.3.

7.2.3. Mechanical testing

This research considered the full mechanical characterisation of all constituents to capture the different modes of loading of a given sandwich panel. Typically sandwich panels are structurally considered as load bearing structure whereby the increased second moment of area by increasing the thickness results in resistance to high bending moments. Bending loading of a sandwich panel consists of mixed mode of tensile and compressive stresses of the bottom and top face sheets respectively, whereas the core's dominating mode is pure shear with accompanying compression loading in the both in-plane and out-of-plane directions.

7.2.3.1. Tensile testing of NFC

The tensile properties (i.e. stiffness and strength) of NFC have been evaluated in accordance with ISO 527-4:1997 and standard test specimen type 1B. The results and discussions of this can be found in section 5.1.2.1 and 6.1.1.2 respectively.

7.2.3.2. Compression testing of core lattice structures

Quasi-static compression tests in-plane and out-of-plane were performed on the three core lattice structures using the same Tinius Olsen 25 ST machine. In-plane test also called edgewise compression is a method to determine the compressive strength and stiffness in the direction parallel to the sandwich facing plane. Specimens tested were only lattice cores without face sheets therefore buckling was insignificant. These tests were constructed to replicate the ASTM C364-99 standard as closely as possible with some modifications to the geometry for clamping purposes. Dimensions of the cubic tested specimen were dependent on the unit cell dimensions however for comparison purposes the number of cells was chosen as $4 \times 4 \times 1$ cells in the x, y and z directions, respectively as shown in Figure 7-5.

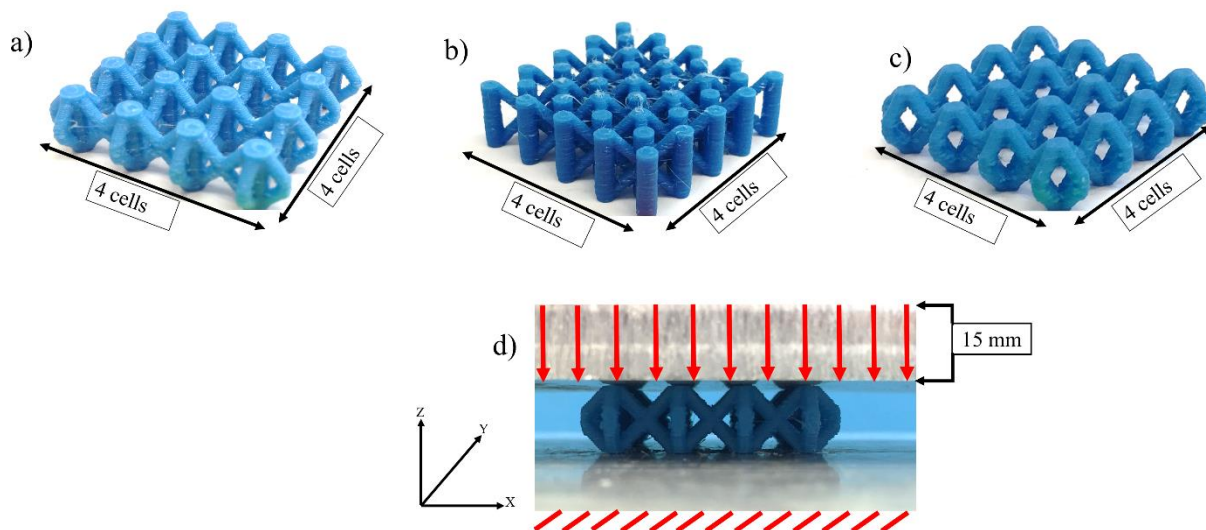


Figure 7-5 3D-printed PLA cellular lattice fabricated for compression test: (a) Lattice 1, (b) Lattice 2, (c) Lattice 3, (d) out-of-plane compression test set up.

The out-of-plane or flatwise compressive testing consists of subjecting the three lattice structures to a uniaxial load in the z-direction normal to the plane of the face sheets. Since the top and bottom of specimen are flat, the loading platens transmit the force with no geometrical modifications. Whereas strut brackets like on the Lattice 1 and 3 specimen edges have been sanded down to create a flat surface on both the bottom and top ends on which the loading platens rest as illustrated in Figure 7-6.

Nominal dimensions and weights were verified for each specimen before carrying out compression tests. For the compression tests the crosshead displacement rate was set at 1 mm/min, load cell recording the applied force.

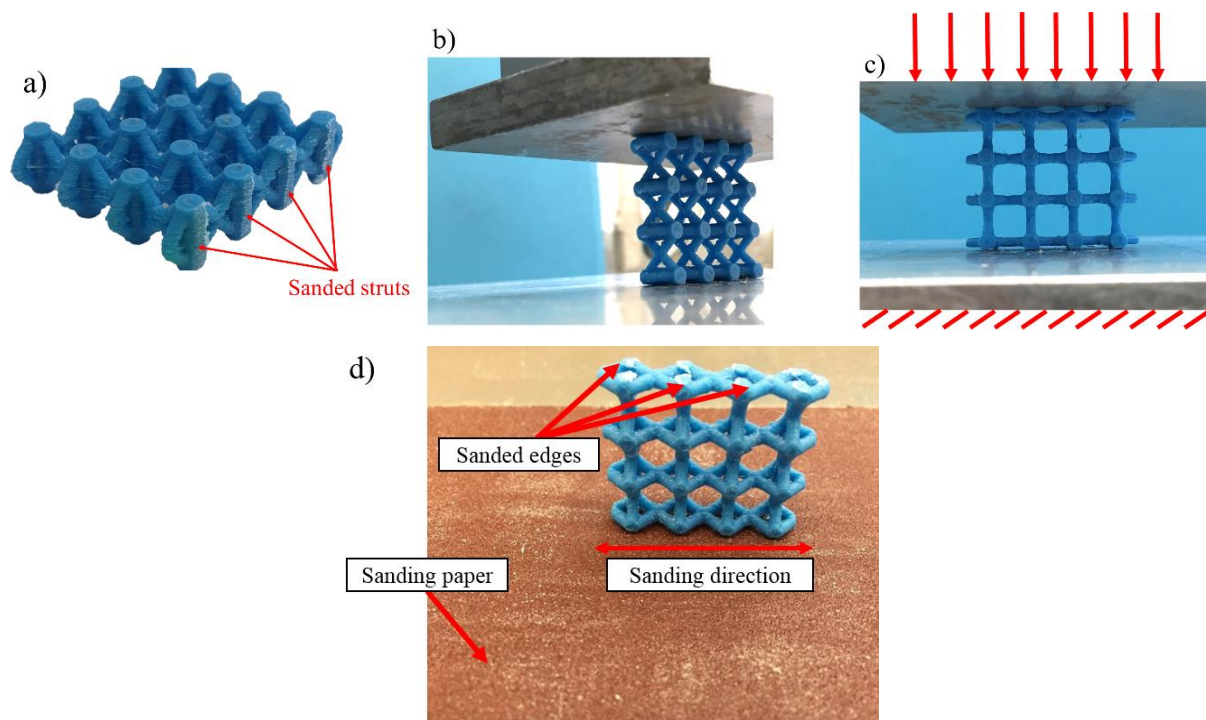


Figure 7-6 In-plane compression test set up: (a) inclined struts sanded down, (b) perfect alignment, (c) load line direction with specimen under testing, (d) illustration of manual sanding operation of a compression specimen.

7.2.3.3. Shear testing of core lattice structures

A customised shear test setup fixture was designed to replicate the procedure described in the ASTM C273-00. Shear tests for the core structures were to determine their strength and modulus parallel to the plane of sandwich. The tests were conducted solely on the core material bonded to the thick loading plates. This method provides the load-deflection behaviour of core structures when loaded parallel to the facings. However, this method of testing does not produce pure shear as the secondary forces acting normal to the faces are present, but the prescribed specimen geometry and fixture setup reduce their effects on the obtained results. Test specimen dimensions were decided according to the ASTM recommendations as the three unit cells height were within the 10 mm envelope, the 120 mm long core met the 12 times thickness minimum requirement and 60 mm width. The core adhesion to the steel plate was achieved using Araldite epoxy on the plate in the 50:50 by weight mixture and cured at 50 °C for 4 h to obtain the optimum lap shear strength. The external load applied on the shear test rig produces a rotation of the steel plates that causes secondary peeling stresses at the interface with the core. Since the desired failure mode is 100% shear, specimen experiencing cohesive failures were rejected. Tensile load was applied on the rigid plate through the bolted bracket to the steel plates at crosshead displacement rate of 1 mm/min. Figure 7-7 illustrates the details of the testing methods.

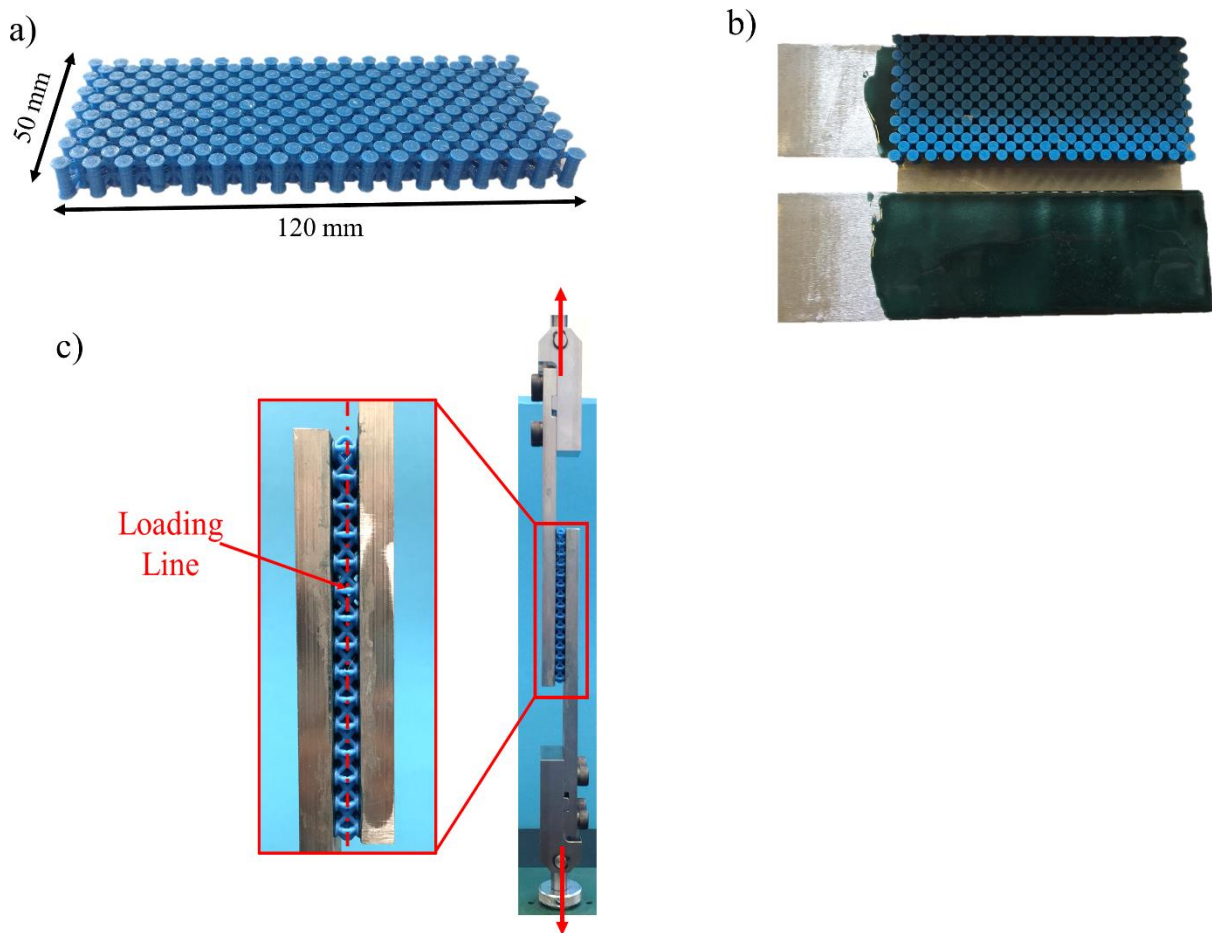


Figure 7-7 (a) Dimensions of the tested core, (b) sample preparation, (c) test setup and loading direction.

The contact areas of the core lattice structures have an effect on the quality of adhesion to the steel plates. In order to mitigate the premature debonding of the 3-D printed cores from the steel plates, the region adjacent to the bonding surfaces struts were modified. The diameter of the struts was increased only at the ends of the struts to double the contact areas. This modification was not needed for the compressive and flexural tests. The data for load-deflection can be used to derive the ultimate shear strength and the effective shear modulus using Eq. (7-1) and Eq. (7-2) respectively as per ASTM standard C273 test method for shear properties of sandwich core materials :

$$\tau = \frac{P}{Lb} \quad \text{Eq. (7-1)}$$

where τ , P , L and b are the core shear stress (MPa), load on specimen (N), length of specimen and width of specimen (mm), respectively. Eq. (7-2) uses the specimen geometry and the load-deflection response to derive the shear modulus G of the core:

$$G = \frac{St}{Lb} \quad \text{Eq. (7-2)}$$

Where S and t are the slope of the initial portion of load-deflection curve (N/mm) and thickness of the core (mm).

7.2.3.4. Flexural testing of sandwich panels

Flexural behaviour of the sandwich structures is affected by the core shear limits during deformation. Whereas the facings are responsible for the tensile and compressive load carrying providing directional stiffness and strength while being protected by the core against local buckling. Three-point bending tests were conducted on the NF/3DP core sandwich panels according to ASTM C393-06 to determine their flexural properties. A Tinius Olsen testing machine equipped with 25 kN load cell was used to perform the bending tests with a loading rate of 1 mm/min. Sample preparation using the 3-D printed lattice cores permanently bonded to the NF face sheets with Araldite 2015 epoxy resin in a 50:50 by weight mixture. Specimens with dimensions of 160 mm length, 40 mm width and overall thickness of 12 mm were put under testing with a setup of span length of 125 mm, support and loading nose radius of 5 mm as illustrated in Figure 7-8. The NF face sheets were cut off a panel using a laser cutter in the above-mentioned dimensions and 2 mm thickness. To avoid indentation failure within the face sheets a face to core ratio of 1:5 was adopted (Kabir et al., 2014). Sandwich beams were then placed in the oven for 4 h for curing. The load F and the crosshead displacement were recorded. Force-deflection curves were plotted, and subsequently flexural stiffness and failure loads were determined. Three pieces of specimen per test condition were tested in room temperature 23 ± 2 °C and 50% humidity.

The loading mechanism in terms of nose location with respect to the internal geometry of the core structure had an effect on the obtained results. In particular, a different effect was observed when the moving nose was placed directly on a vertical strut or when it was placed between two inclined struts, which was only a concern within Lattice 1 and 3. The effect of this positioning was quantified in the analysis.

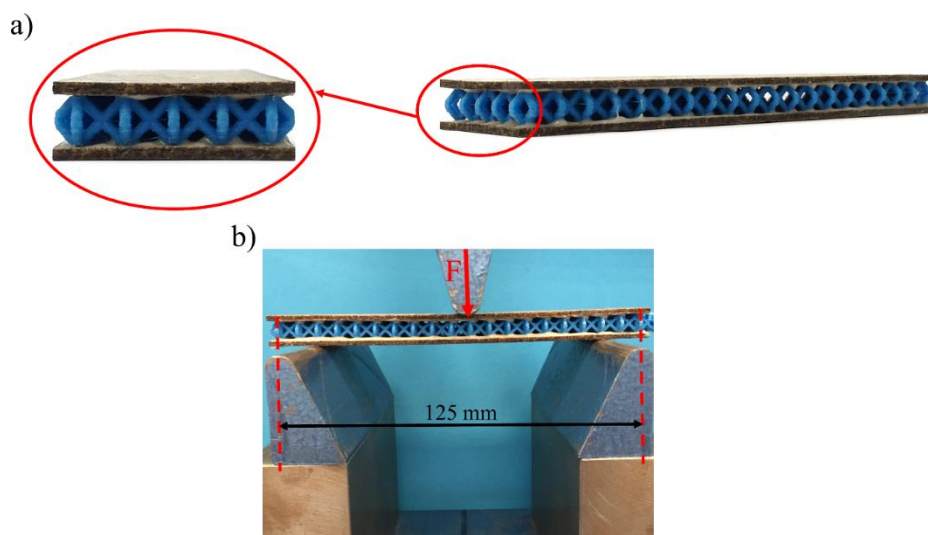


Figure 7-8 (a) Specimen with lattice core bonded to the NFC skins, (b) sandwich panel flexural test set up.

7.3. Results and discussions

7.3.1. Compression results of core lattice structures

The load-displacement curves obtained from testing the three proposed lattice designs under flatwise and edgewise quasi-static compressions are summarised in Figure 7-9 and Figure 7-10 respectively, it appears that the internal geometry of the lattice structures affected their behaviour. The responses in all cases were elastic followed by either a plateau as load was maintained for higher displacement as observed within Lattice 1 or a dip of load after reaching the maximum over a longer displacement as observed in Lattices 2 and 3. Lattice 2 represented in Figure 7-9 b depicted a variability over the three repeated measurements, which can be explained by the variability of specimen manufacturing as L2_S1 failure mechanisms of its vertical struts as the global buckling is clearly observed in Figure 7-9 d).

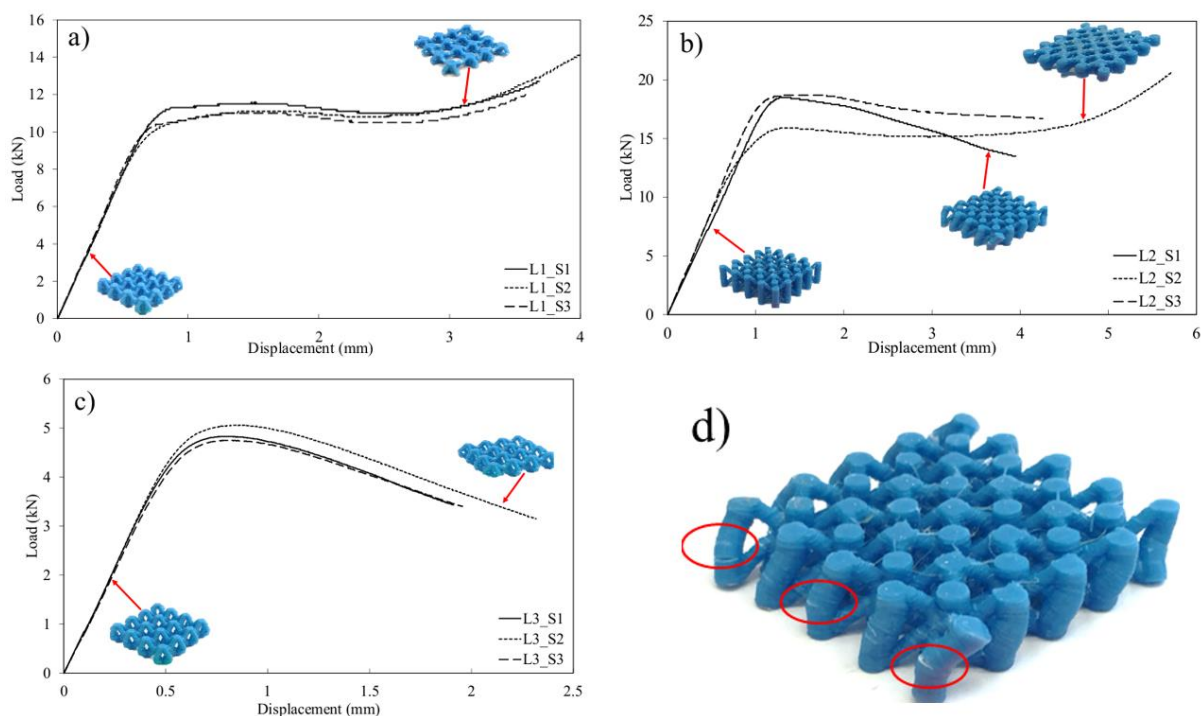


Figure 7-9 Load vs displacement curves obtained from the out-of-plane compression test showing the three sample repetitions denoted as S1, S2 and S3: (a) Lattice 1, (b) Lattice 2, (c) Lattice 3 and (d) L2_S1 deformation mechanism with vertical struts fracture z

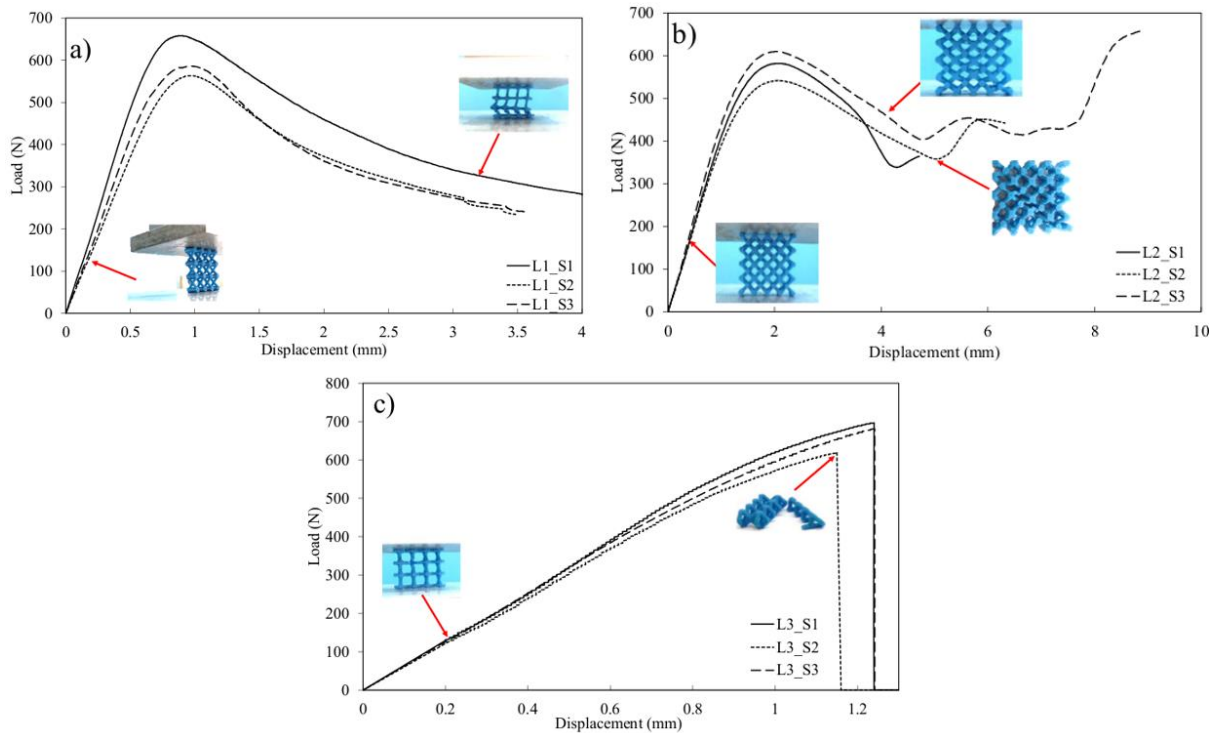


Figure 7-10 Load vs displacement curves from the in-plane compression test for the three repetitions with the observed in-situ deformation during and after testing: (a) Lattice 1, (b) Lattice 2 and (c) Lattice 3.

The stiffness recorded for the three structures was obtained from the slope of the load-displacement curve. It was observed that compressive stiffness of Lattice 1 out-of-plane was 15.5 kN/m whereas the highest stiffness was from Lattice 2 peaked at 18.02 kN/m and the lowest recorded was from Lattice 3 at 8.5 kN/m. The maximum peak load and the stiffness values observed for similar lattice structures reported in literature (Mercer et al., 2018), (Yin et al., 2017) are comparable to those measured for Lattice 1 and Lattice 2. However, the mechanical behaviour of Lattice 3 is lower than the other two structures, although it is comparable to results reported in literature for metallic cores (Mines et al., 2013). An effect of the internal geometry on the mechanical response of the overall structure can be clearly noticed in a way that the vertical struts tend to withstand high compressive loads at higher deformation. This phenomena is then followed by the densification of the struts to act like bulk materials as the load increases at higher displacement. However, in some cases where the printing process has an effect on the performance, the vertical struts tend to buckle under high compressive loads, which explains the relatively maximum load carried by the structure before plummeting with no sign of the densification phase. The buckling mechanism as illustrated in Figure 7-9_d) initiates at mid-distance through the struts height which then triggers the overall structure sideways collapse. Considering L1, L2 and L3 curves, as shown in Figure 7-10, their performances in terms of stiffness and strength values can be classified in a descending order of L2, L1 then L3 as the crucial contribution of the vertical struts towards the structural integrity was demonstrated.

The in-plane compression tests performed on the L1, L2 and L3 revealed their structural differences in terms of stiffness and strength in addition to their failure mechanisms. All specimens show typical characteristics of cellular structures exhibiting an elastic response region, yield, plastic strain hardening up to a peak load and post-yield buckling or fracture. Overall the maximum load taken by each structure was much lower compared to the out-of-plane in the range of 500–700 N. The in-plane testing direction is normal to the printing direction (i.e. layer by layer, therefore, the interlayer bonding strength is examined). L1 and L2 demonstrated higher strain energy capability as the load was maintained for higher displacement and an apparent ductile failure mechanism through the structure was observed across the three repetitions. In contradiction of L3 for which the failure across all repetitions was consistently brittle with minimal deformation along the displacement direction. This can be explained by the missing vertical struts, which supplied L1 and L2 with additional support allowing load distribution flowing through the constituents struts of individual unit cells. Lattice 1 samples tend to collapse layer by layer as the connecting struts fold triggering side movements of layers. It can be noticed that the slope and maximum load recorded for the tested specimen showed trivial variability with L1_S1 demonstrated the highest stiffness and strength this can be related to the printing process. Structural imperfections within additively manufactured parts can be categorised into micro-pores or non-uniform diameter of struts which directly affect the deformation mechanism within the lattice structures. Due to the less dense structure of Lattice 1 compared to Lattice 2, an elongated region of diagonal struts buckling before densification of the bottom row of cells was observed as illustrated in Figure 7-11 a). Apart from Lattice 3 in which minimal deformation due to the post-yield hardening, which occurred at low strains followed by a sharp drop of load signifying a brittle fracture, Lattice 1 and 2 displayed shear band regions due the broken diagonal struts in the vertices, these are shown in Figure 7-11 b). Shear band formation due to bending of the diagonal struts results in the formation of plastic hinges.

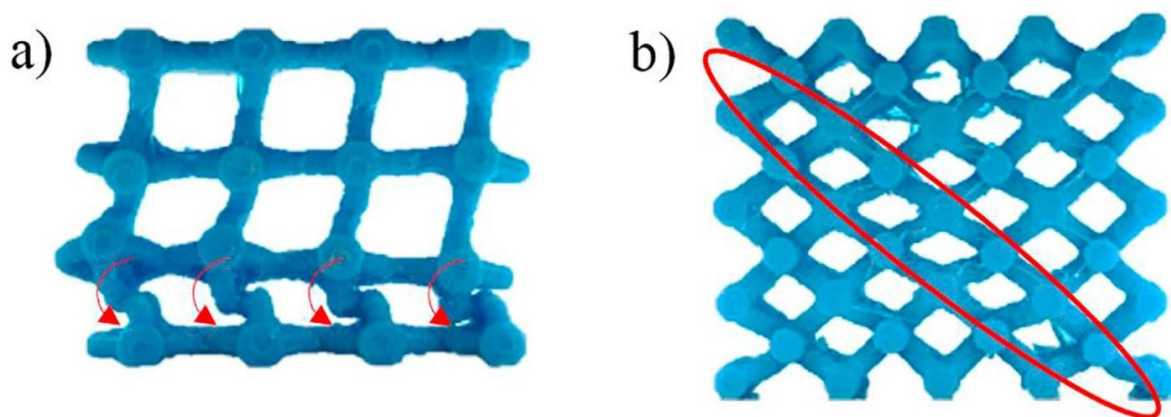


Figure 7-11 Deformation mechanisms of lattice structures under in-plane compression tests: (a) Lattice 1 shows layer by layer collapse through node rotation, (b) Lattice 2 shear band formation with stretch dominant deformation of bottom layer.

7.3.2. Shear results of core lattice structures

The shear experiments provide the equivalent stiffness and strength of the different core structures with their consequent failure modes. The increased contact surface between the 3D Printed core and the platens improved the adhesion strength and reduced the debonding effects induced due to the minimal bending effects. Intersection points represent the weakest link of the structure making them common failure locations for all three lattice structures as illustrated in Figure 7-12. Consistent results for all tests in terms of stiffness through load vs displacement slope repeatability, responses in all three configurations were linear elastic followed by either a brittle failure (Lattice 2 and 3) or gradual load drop at increasing strains. The shear strength and modulus have been computed from the experimental results using Eq. (7-1) and Eq. (7-2) and the apparent cross section area. It can be seen that Lattice 2 exhibited the highest shear capabilities with maximum taken load of 16 kN equivalent to a shear strength of 2.3 MPa and shear modulus of 17.8 MPa. The sharp load drops within Lattice 2 and 3 after 1.5 mm displacement signify the brittle failure of the overall structure at its critical connection points compared to the elongated displacement for Lattice 1 up to 3 mm with gradual loss of strength. Comparing the obtained results which are summarised in Figure 7-12 d, it can be clearly noticed that the slope and maximum load (i.e. stiffness and strength) are affected by the internal topology of each lattice structure. The vertical struts within Lattice 1 provide structural stability under shear loading as the shear modulus is maintained at 17.8 MPa and a slight reduction of strength to 2 MPa as progressive failure of inclined struts under excessive bending causes the immediate load drop with a tensile failure of connecting struts between adjacent unit cells. Figure 7-12 b) explains the overall response of Lattice 2 as the high load capacity is owed to the vertical struts taking most of it, but as the connecting struts within individual cells fail under a combined tensile and compressive modes, a subsequent abrupt load drop is associated with a harmonised layer slide closer to the moving platens parallel to the loading plane. Although the similar features between Lattice 1 and 3 apart from the missing vertical strut, it is evident that Lattice 3 suffered a reduced shear strength and modulus of 1.7 MPa and 15.5 MPa respectively as the individual cells shifted along the displacement direction through the dislocation of the weakest link at the intersecting node (Figure 7-12 c). In addition to the latter, an evident rotation of diagonal struts as rupture occurs at both upper and lower nodes due to excessive bending.

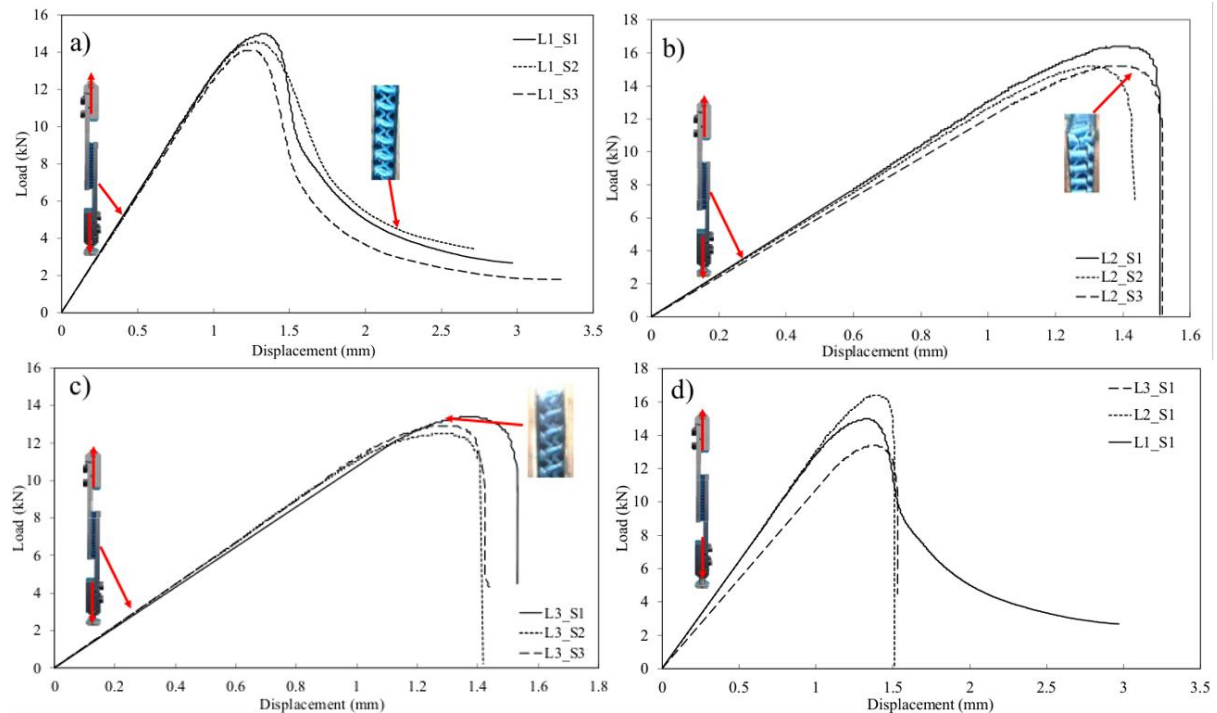


Figure 7-12 Load vs displacement curves from the shear test of bonded core lattice: (a) Lattice 1, (b) Lattice 2, (c) Lattice 3 and (d) Comparison of the three structures

Deformation mechanisms of the three core lattice structures under shear loading showing the collapse and fracture of the struts are illustrated in Figure 7-13 a) Lattice 1 the vertical strut provides high stiffness and extended deformation within the plastic region as ductile failure was demonstrated, b) Lattice 2 clear, brittle failure as sharp cuts develop through the thickness, c) Lattice 3 decreased stiffness and lower shear load resistance as top and bottom nodes show a brittle fracture.

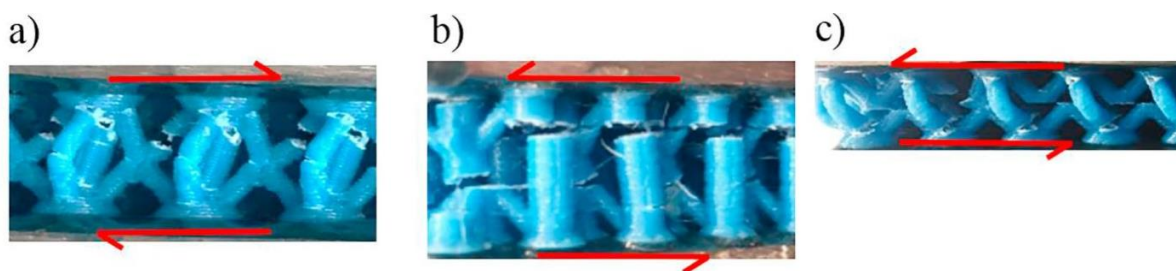


Figure 7-13 Failure mechanisms of the three core lattice structures under shear: (a) Lattice 1, (b) Lattice 2, (c) Lattice 3.

7.3.3. Flexural results of sandwich panels

Having investigated the compression and shear behaviour of the 3D Printed core structures, the obtained results provide an insight into the significance of bending loads on the sandwich structure. In flexural testing, the applied bending moment and transverse shear load are distributed between the constituents of a sandwich panel (i.e. face-sheets and core, respectively). Figure 7-14 illustrates the load vs deflection under the flexural test; three specimens have been tested under the same conditions to ensure the

findings integrity. However, tests revealed inconsistency as testing of one lattice structure showed diverging responses in terms of flexural strength and plastic strains after the post yielding point.

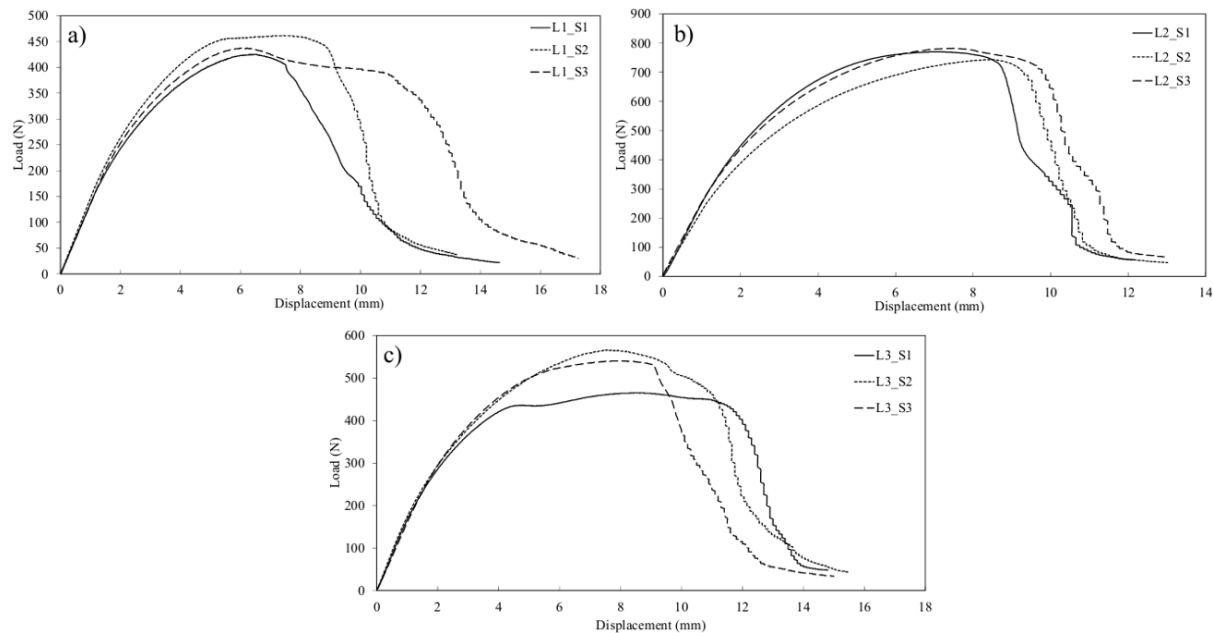


Figure 7-14 Bending characteristics of sandwich panels shown on the load vs displacement. Three sample repetitions to show repeatability: (a) Lattice 1, (b) Lattice 2 and (c) Lattice 3.

The overall response of the all cell topologies was consistently highly nonlinear as the initial portion of the curve represented the calculated bending rigidity of the sandwich panel up to a displacement of ~ 2 mm. The sandwich panels continue to withstand increasing loads under high plastic deformations beyond the elastic limit point up to a crosshead displacement of ~ 10 mm. It has been observed that the failure mechanism and flexural strength have been affected by the moving nose placement with respect to the internal geometry of the lattice structure.

In a set up in which the moving load is placed directly on a unit cell, an increased load-bearing capacity was observed with minimal deflection and consequent tensile failure of bottom face-sheet. Whereas if the load is applied over the intersecting node of two adjacent cells, compression of the top face-sheet initiated folding into a V-like shape promoting the panel energy absorption at the cost of its flexural strength. Despite the latter, the bending rigidity values have not been affected in which repeatability was validated by the consistent initial slope. The averaged bending rigidity values recorded for L1, L2 and L3 were 142, 242 and 162 kN/m, respectively. Good skin-core adhesion was observed throughout all tested specimens as no evidence of delamination was observed, which implies that it can be eliminated as a variable to understand the performance.

Figure 7-15 a) shows Lattice 1 (L1_S1) local dislocation of the diagonal strut along the loading line due to stretching whereas the bottom face-sheet exhibited tensile fracture. The maximum load of this particular test was 425 N, which was considered lower than L1_S2 (Figure 7-14 a) exhibiting 462 N as the top face-sheet wrinkles at increasing deflection and maintained load. L1_S3 experienced similar

response to L1_S1 at a maximum load held within an equivalent deflection region ~ 6.3 mm, however beyond 8 mm deflection load dropped through two stages. This dissimilarity can be explained by higher strength of the bottom face-sheet as the tensile fracture was less severe within L1_S3, hence the strut dislocation distance. The progressive diagonal struts failure along the panel width on the normal plane to Figure 7-15 is associated with the near plateau load before the sharp drop of load. Results obtained from Lattice 2 tests were consistent in terms of the high stiffness and maximum load as well as the failure mechanism due to its dense topology. This has also reduced the wrinkling effect of the top face-sheet and promoted the tensile fracture of the bottom face and struts dislocation at significantly higher loads ~ 765 N due to the relatively highly packed structure with vertical struts. Geometrical differences between L1 and L3 being the missing central vertical strut and increased diameter of all struts provided the latter with slightly improved stiffness and strength. The results reported in our paper are in coherence with several studies on the failure mechanisms of the sandwich structures components (Kazemahvazi et al., 2009), (Rathbun et al., 2004), (Wadley et al., 2003). Although the reported studies focused on metallic truss cores, the parameters affecting the experimental programme are the same. Moreover, Zok et al. (Zok et al., 2004) developed mechanism maps for possible failures of pyramidal metallic truss cores based on beam theory with respect to face and core dimensions.

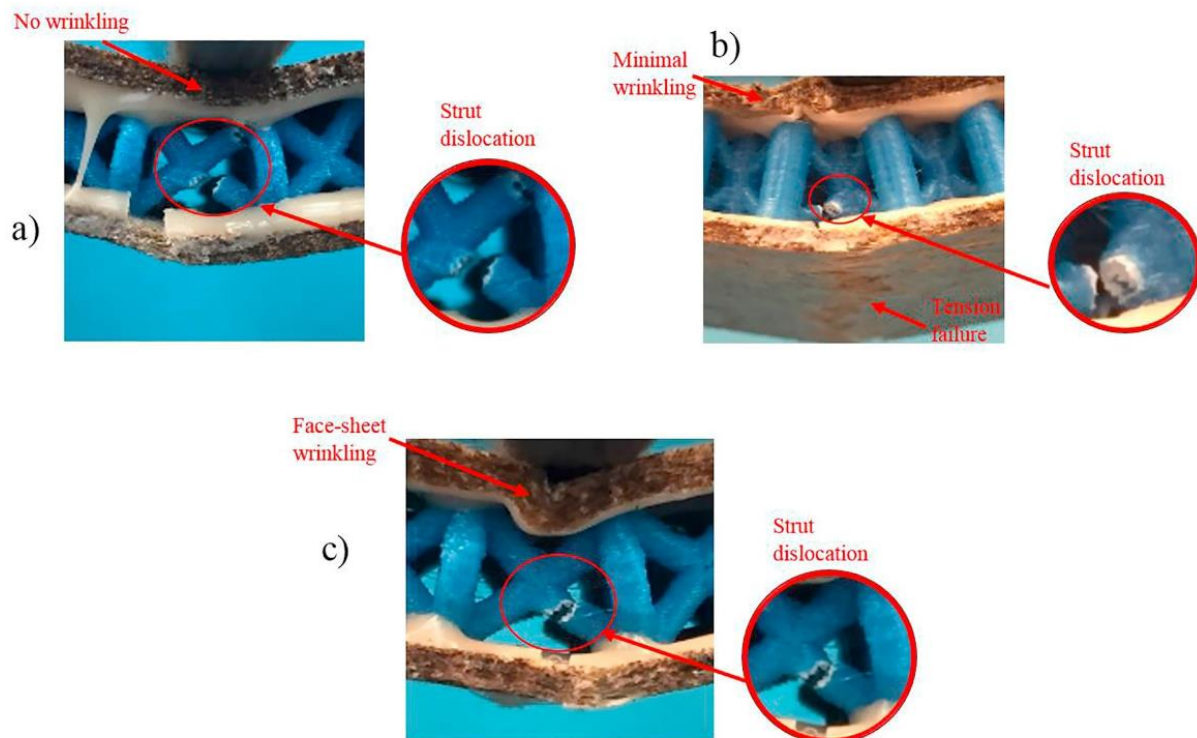


Figure 7-15 Deflection and failure mechanisms under bending loading: (a) Lattice 1, (b) Lattice 2, (c) Lattice 3. In the past, many researchers have studied the potential use of AM lattice structures for various applications (Kantareddy et al., 2016), (Mahmoud and Elbestawi, 2017), (Liu et al., 2018), (Ferro et al., 2017). Yoon et al. (Yoon et al., 2014) investigated the compressive strength and modulus of 3-D printed

ABS engineered trabecular bone and honeycomb biomimetic structures. Results proved that 3DP technology could be an efficient technique for comparative studies. Lee and Kang (Lee and Kang, 2010) carried out an experimental analysis on the compressive behaviour of woven Kagome stainless steel wires as a periodic cellular metal structure within two steel face sheets; they found that as the number of layers increases along the out of plane direction the strength decreases. In order to study the effects of variation in strut diameter on the compressive elastic modulus and collapse stress of cellular lattices, Ravari and co-authors (Karamooz Ravari et al., 2014) fabricated PLA lattice structures using FFF for the mechanical characterisation and also developed beam and solid elements based FEM. To achieve realistic elastic modulus and strength each strut needed to be divided into ten and twelve equally spaced intervals respectively. The results found in this study compliment these past works as they can be used to predict mechanical properties of appropriately modelled sandwich structures.

The maximum load values obtained from averaging the three maximum loads recorded from samples repetitions have been normalised with the nominal weight and reported in Table 7-2. From the comparison, the diamond structure with vertical strut (Lattice 1) performs the best in compression out of the plane and shear whilst the diamond structure without vertical strut (Lattice 3) performs better under compression in plane and three-point bending load. However, the latter diamond structure was modified increasing the diameter of the struts from 1.5 mm to 2 mm. This change justifies the increase in normalised maximum load for the in-plane and the flexural since the diagonal struts are primarily contributing to the bending and in-plane strength of the cell.

Table 7-2 Maximum load values normalised with the nominal weight.

	Normalised maximum load F/m (N/g)		
	Lattice 1	Lattice 2	Lattice 3
Compression out-of-plane	5090	5000	2360
Compression in-plane	290	164	368
Shear	860	533	724
Flexural	32	26	34

These results are promising. However, there are several limitations to this study that can be improved in future work. First, the top and bottom sheets made of the PP-flax composite were different materials to the struts (PLA), and they were held together with an adhesive. Although no delamination occurred in testing, and therefore the results are reliable, this introduces a suboptimal method of assembly and materials mixing into the final sandwich structure. As both NF PLA composites have been previously investigated and PP 3-D is possible, it would be interesting to investigate single material sandwich structures of both PP + flax and PLA + flax in the future. To make this realistic from a manufacturing

perspective, the lattice structures could be printed in a multi-head 3-D printer (Laureto and Pearce, 2017) using the sheets as substrates. The final layer of the sandwich could be bonded thermally or with adhesives. In addition, the lattice structures were fabricated using relatively thin layers using a high-resolution nozzle that is inadequate for timely manufacturing. Future work should investigate large layer thicknesses from a large nozzle to enable rapid manufacturing of bio-composite sandwich structures. Finally, work should expand applications beyond flat bio-compatible sandwich panels with natural fibre composite skins to more advanced shapes where the skin itself could be 3-D printed.

8. Conclusions and Recommendations

8.1. Conclusions

- I. As part of the development of a novel flax based biocomposite to be considered as a potential replacement of glass fibre reinforced composites in structural applications, this study involved developing a number of flax reinforced biocomposites then experimentally characterising their macro-mechanical response under quasi-static loading scenario. The characterisation of materials encompassed stress-strain response and failure mechanisms under combined effect of mechanical loading and temperature conditioning:
 - The flax/matrix interface efficiency using twill fabrics with PLA, PP and MAPP in 50:50 wt% was investigated through comparison of tensile strength and stiffness and flax/PLA showed the highest properties due to better adhesion and higher intrinsic PLA properties compared to those of PP. Also, unlike PLA, processing PP can be challenging due to its thermal shrinkage during thermal bonding with flax.
 - Reinforcement orientation effects on the tensile properties were evaluated for flax/PLA, flax/PP and flax/MAPP among UD, cross ply 0°/90° and bidirectional 2D woven twill whereby the twill samples consistently exhibited higher properties than the 0°/90°. Nevertheless cross ply arrangement of flax tapes exhibited comparable performance enabling them to be considered for structural application. Similar observation was made with regard to flax/PP
 - Blend ratio optimisation of the continuous flax and thermoplastic commingled tapes has been carried out, for example, the 0°/90° flax/PLA tapes tensile and flexural results revealed that optimum wetting is achieved at fibre 55% by weight as any further increase of fibre contents causes improper wetting and therefore inefficient load transfer.
 - Polyester and furan based composites with continuous flax reinforcement were compared in terms of like-to-like architecture comparison using bio-based PFA and UPE where the former exhibited higher tensile modulus while tensile strength was identical. Reinforcement architecture and orientations have also been evaluated, as for furan samples the effect of orientation is more significant than the architecture.
 - The ease of fabrication and sustainability advantage of nonwoven Flax/PP preforms as these are produced from by-products of fibre extraction is opposed by the lower tensile properties as compared to continuous reinforcement. This is attributed to the fact of thickness variation, increased void contents, fibre damage during needle-punch, and potential discontinuity of molten matrix which hinders the effective load transfer at the fibre/matrix interface. On the other hand, nonwoven flax/UPE showed clear dependency

on the fibre content as demonstrated through the increase of tensile and flexural properties as fibre volume fractions increased.

- The effect of *in-situ* temperature on tensile performance of NFCs was investigated in this study, a general trend of a progressive property drop as temperature increases which tends to specifically intensify around temperatures of the matrix thermal transition such as T_g . Thermoset based biocomposites were found to be more stable compared to their thermoplastic counterparts. For example, flax/PLA has a modulus decrease of 76% from 30 to 70°C while 66% decrease in tensile strength. Overall, a reduction in modulus of 1.9%/°C, 1.5%/°C and 0.9%/°C; while 1.6%/°C, 1.5%/°C and 0.5%/°C reduction in strength was computed for each of the biocomposite based on PLA, PP and PFA respectively.
- II. The combined effects of infill orientation of FDM parts and *in-situ* temperature conditioning were investigated in this project to identify the correlations between the impact of printing parameters and the temperature values. The response surfaces were used to derive the required relationship among process parameters, temperature, the tensile stiffness, the UTS, the strain and stress at failure. The findings of the experimental analysis are:
- Tensile tests carried out on single filament before and after the extrusion process with the 3D printer have shown a reduction in stiffness from 30% in plain PLA filaments to 16% in 3D-printed filament, as temperature increases from 40°C to 50°C. This was explained by the cold crystallisation effects of such polymers and molecular chain re-alignment along the testing direction.
 - At ambient, the $\pm 45^\circ$ had the highest strength and modulus with variation in stiffness as high as 29% and 22% when compared to specimen of the $-30^\circ/+60^\circ$ and $0^\circ/90^\circ$ builds respectively. This is supported by the fracture analysis as the diamond internal structure showed higher bead density which enables the increased load taken with minimal extension.
 - As temperature increases to 40°C the highest tensile modulus is found for $-30^\circ/+60^\circ$ after which no variation with respect to raster orientation was detected. However, for all orientations, necking plays a major role in the failure mechanism resulting in immediate failure after the ultimate strength is reached.
 - Regarding the UTS, it is possible to identify a continuous reduction in values as the temperature increases and the three configurations follow the same path.
 - At ambient, the highest stress at failure was recorded for specimen of $0^\circ/90^\circ$ orientation while the minimum corresponded to $\pm 45^\circ$ specimen. The temperature variation from 20°C to 30°C for $\pm 45^\circ$ lowers the strength of the bonding surface which is counterbalanced by the

beads robustness into the overall force loading balance of the sample. As temperature approaches T_g for PLA, the weakness of the beads induces a redistribution of the stresses to the bonding surfaces for which failure is controlled by the shear strength of the interface.

- Regarding strain-to-failure, at room temperature, the maximum is reached at $-30^\circ/+60^\circ$ while specimen of $\pm 45^\circ$ attained the lowest strain at failure. However, this observation is reversed for 40°C .
- High temperature testing corresponds to higher elongation under constant stress, which contributes the modulus of toughness. Overall, specimen $-30^\circ/+60^\circ$ demonstrated higher energy absorption compared to the other orientations. Furthermore, all specimen plummeted after temperature of 50°C , an indication of glass transition effects on tensile behaviour of 3D-printed parts as previously indicated on strength.

III. From the case study, the mechanical properties of 3DP PLA cores under compression both in-plane and out-of-plane, shear and flexural of the bio-sandwich panel have assessed. The key findings established in this work are listed as follow:

- A comparison between the investigated geometries shows that the diamond structure with vertical strut (Lattice 1) performs the best in compression out of the plane and shear whilst the diamond structure without vertical strut (Lattice 3) performs better under compression in plane and three-point bending load.
- The failure mechanisms of the core structures observed under the different loading conditions have been discussed. Under compression in-plane shear band and rotation of the struts have been observed. For the compression out of plane, the main mechanism is plastic hinges followed by densification. In some cases buckling of the vertical struts has been noted. Under shear load, the failure generally occurred at the nodes where the diagonal struts intersect the vertical strut. In addition for the diamond structure without vertical strut, the failure also starts in the middle plane at the intersect node. Under flexural load, the failure always appeared in one of the lower diagonal struts closer to the middle plane under tension load.
- The experimental results discussed in this work prove the feasibility of AM technology in the process of manufacturing lightweight polymer-based sandwich panels for structural applications. Based upon experimental results, this category of core structures could compete with high performing honeycomb structures used for aerospace applications. However, as quality assurance of parts produced with this technology, repeatability is still an issue to be addressed.

8.2. Recommendations

In a fast-paced environment of product development process, considering the global market competition it is both economically and logistically necessary to reduce the time and cost involved in the design, manufacture and test life cycle. Therefore, numerical modelling by means of computer-based simulations can efficiently reduce the associated high costs and time of early stage product development through optimisation and improvement processes. As part of the process of numerical modelling, the evaluation and selection of materials used are key to correctly make the decision on their type and amount at early stages of the product development. This will provide the expected behaviour of the material within its intended application and full or partial representation of the real-life scenario of its properties and limitations upon its functional integration. The process of obtaining complex models of materials behaviour is known as the constitutive modelling.

Constitutive modelling covers the study of extreme working conditions of structural components at the base material level. These conditions can be either high mechanical or thermal loads and can also be the combination of both which influence the engineering material in use and contribute to the deterioration of the material properties through concurrent process of damage and deformation. The need for near accurate lifetime prediction of engineering components and structures is crucial to avoid unexpected serious events affecting human safety within critical applications such as aviation and nuclear industries. This necessitates thorough calculations and in-depth engineering analyses based on exhaustive empirical methods.

Various types of engineering materials such as metals, polymers, composites and concrete have different approaches of modelling their physical mechanisms of deterioration and deformation at the macroscopic level. Therefore, constitutive modelling facilitates the understanding of these materials' behaviour through simplified mathematical modelling of complex physical behaviour. Despite the non-existence of exact models for materials it is still possible to develop common material behaviour models through the use of continuum mechanics. An efficient model should:

- Be relevant for describing the physical phenomena at hand,
- Provides sufficiently accurate prediction for given application,
- Be easily implemented in a robust mechanical algorithm for obtaining the truly operational condition.

Selecting the most appropriate material model to better describe its behaviour can be challenging and is considered as the most crucial part of solid mechanics. As aforementioned that constitutive models are sets of stress strain equations with various assumptions on variables (temperatures, strain history, strain rate... etc.) that potentially affect the materials response. Experimental characterisation tests allow the classification of materials into response categories: elastic, rigid, plastic and perfectly plastic.

Experimental characterisation of the various properties can be challenging in both setting up and consistency of results. However, these are essential to be used in the process of generating the model which best replicate the case under investigation. For most engineering applications, the behaviour of a material can be quite accurately represented with relatively simple mathematical formulations. In simple cases, the material is considered for its linear elastic limit with displacement to a maximum point within the elastic region and the induced load is measured using the Hook's law principle in matrix format at the nodal level. However, the interest in simulating components in their working conditions is focused on their extreme points of loading up to failure. This requires a more sophisticated mathematical modelling to replicate the whole scenario from the beginning of the load up to failure. Due to plasticity effects in which the material deforms beyond its point of recovery, the material behaviour follows a complex unexpected trend with high nonlinearity. Plastic deformation of solids are characterised by the irreversible straining associated with a certain level of stress controlled by the damage evolution at both micro and macro level.

Therefore, with the aim to expand on the achievement of this research, the author proposes the following:

- Develop semi-empirical models for all constituents and use an iterative approach to validate the constitutive model of each material with respect to experimental data.
- Fully develop a model of 3D printed sandwich structure and biocomposite
- Damage evolution analysis of both the PLA 3D printed truss-like core structure and biocomposite
- Numerical modeling through finite element analysis of the full characterisation of all constituents of the biocomposite, this however needs to begin with establishing robust models using representative volume element approach to tackle the quasi-static behavior and dynamic transient behaviour of all components of the biocomposite

References

- ADAMSEN, A. P. S., AKIN, D. E. & RIGSBY, L. L. 2002. Chelating agents and enzyme retting of flax. *Textile Research Journal*, 72, 296-302.
- AHMED, K. S. & VIJAYARANGAN, S. 2008. Tensile, flexural and interlaminar shear properties of woven jute and jute-glass fabric reinforced polyester composites. *Journal of Materials Processing Technology*, 207, 330-335.
- AHN, S.-H., MONTERO, M., ODELL, D., ROUNDY, S. & WRIGHT, P. K. 2002. Anisotropic material properties of fused deposition modeling ABS. *Rapid prototyping journal*, 8, 248-257.
- AKIL, H., OMAR, M., MAZUKI, A., SAFIEE, S., ISHAK, Z. M. & BAKAR, A. A. 2011. Kenaf fiber reinforced composites: A review. *Materials & Design*, 32, 4107-4121.
- AKIN, D. E., HENRIKSSON, G., EVANS, J. D., ADAMSEN, A. P. S., FOULK, J. A. & DODD, R. B. 2004. Progress in enzyme-retting of flax. *Journal of Natural Fibers*, 1, 21-47.
- AKIN, D. E., MORRISON, W. H., RIGSBY, L. L. & DODD, R. B. 2001. Plant Factors Influencing Enzyme Retting of Fiber and Seed Flax. *Journal of Agricultural and Food Chemistry*, 49, 5778-5784.
- ALIMUZZAMAN, S. 2014. *Nonwoven Flax Fibre Reinforced PLA Biodegradable Composites*. University of Manchester.
- ANANDJIWALA, R. D. & BOGUSLAVSKY, L. 2008. Development of needle-punched nonwoven fabrics from flax fibers for air filtration applications. *Textile Research Journal*, 78, 614-624.
- ANDERSONS, J. & JOFFE, R. 2011. Estimation of the tensile strength of an oriented flax fiber-reinforced polymer composite. *Composites Part A: Applied Science and Manufacturing*, 42, 1229-1235.
- ARBELAIZ, A., FERNANDEZ, B., RAMOS, J., RETEGI, A., LLANO-PONTE, R. & MONDRAGON, I. 2005. Mechanical properties of short flax fibre bundle/polypropylene composites: Influence of matrix/fibre modification, fibre content, water uptake and recycling. *Composites Science and Technology*, 65, 1582-1592.
- ARNOLD, E., WEAGER, B., HOYDONCKX, H. & MADSEN, B. Next generation sustainable composites: Development and processing of furan-flax biocomposites. 17th international conference on composite materials, 2009. British Composites Society, 27-31.
- ARROYO, M., ZITZUMBO, R. & AVALOS, F. 2000. Composites based on PP/EPDM blends and aramid short fibres. Morphology/behaviour relationship. *Polymer*, 41, 6351-6359.
- ASHORI, A. & NOURBAKHS, A. 2009. Polypropylene cellulose-based composites: The effect of bagasse reinforcement and polybutadiene isocyanate treatment on the mechanical properties. *Journal of applied polymer science*, 111, 1684-1689.
- ASSOCIATION, E. I. H. 2011. Hemp Fibres for Green Products—An assessment of life cycle studies on hemp fibre applications. June.
- ASTM, I. 2015. *ASTM D638-14, Standard Test Method for Tensile Properties of Plastics*, ASTM International.
- AURAS, R., SINGH, S. P. & SINGH, J. 2006. Performance evaluation of PLA against existing PET and PS containers. *Journal of Testing and Evaluation*, 34, 530-536.
- AUSIAS, G., BOURMAUD, A., COROLLER, G. & BAILEY, C. 2013. Study of the fibre morphology stability in polypropylene-flax composites. *Polymer Degradation and Stability*, 98, 1216-1224.
- AZIZ, S. H. & ANSELL, M. P. 2004. The effect of alkalization and fibre alignment on the mechanical and thermal properties of kenaf and hemp bast fibre composites: Part 1 – polyester resin matrix. *Composites Science and Technology*, 64, 1219-1230.
- AZIZ, S. H., ANSELL, M. P., CLARKE, S. J. & PANTENY, S. R. 2005. Modified polyester resins for natural fibre composites. *Composites Science and Technology*, 65, 525-535.

- AZZOUZ, L., CHEN, Y., ZARRELLI, M., PEARCE, J. M., MITCHELL, L., REN, G. & GRASSO, M. 2018. *3-D printed truss-like lattice structures* [Online]. Available: <https://osf.io/mrjzw/> [Accessed 06/02/2019].
- AZZOUZ, L., CHEN, Y., ZARRELLI, M., PEARCE, J. M., MITCHELL, L., REN, G. & GRASSO, M. 2019. Mechanical properties of 3-D printed truss-like lattice biopolymer non-stochastic structures for sandwich panels with natural fibre composite skins. *Composite Structures*, 213, 220-230.
- BADER, M. & BOWYER, W. 1972. The mechanical properties of thermoplastics strengthened by short discontinuous fibres. *Journal of Physics D: Applied Physics*, 5, 2215.
- BAIARDO, M., ZINI, E. & SCANDOLA, M. 2004. Flax fibre–polyester composites. *Composites Part A: Applied Science and Manufacturing*, 35, 703-710.
- BAJPAI, P. K., SINGH, I. & MADAAN, J. 2014. Development and characterization of PLA-based green composites: A review. *Journal of Thermoplastic Composite Materials*, 27, 52-81.
- BALEY, C. 2002. Analysis of the flax fibres tensile behaviour and analysis of the tensile stiffness increase. *Composites Part A: Applied Science and Manufacturing*, 33, 939-948.
- BALEY, C. 2004. Influence of kink bands on the tensile strength of flax fibers. *Journal of materials science*, 39, 331-334.
- BALEY, C., KERVOËLEN, A., LAN, M., CARTIÉ, D., LE DUIGOU, A., BOURMAUD, A. & DAVIES, P. 2016. Flax/PP manufacture by automated fibre placement (AFP). *Materials & Design*, 94, 207-213.
- BECKERMANN, G. W. & PICKERING, K. L. 2009. Engineering and evaluation of hemp fibre reinforced polypropylene composites: Micro-mechanics and strength prediction modelling. *Composites Part A: Applied Science and Manufacturing*, 40, 210-217.
- BELLINI, A. & GÜÇERİ, S. 2003. Mechanical characterization of parts fabricated using fused deposition modeling. *Rapid Prototyping Journal*, 9, 252-264.
- BENSADOUN, F. 2016. In-service behaviour of flax fibre reinforced composites for high performance applications.
- BENSADOUN, F., VERPOEST, I., BAETS, J., MÜSSIG, J., GRAUPNER, N., DAVIES, P., GOMINA, M., KERVOELEN, A. & BALEY, C. 2017. Impregnated fibre bundle test for natural fibres used in composites. *Journal of Reinforced Plastics and Composites*, 36, 942-957.
- BIAGIOTTI, J., PUGLIA, D. & KENNY, J. M. 2004a. A review on natural fibre-based composites-part I: structure, processing and properties of vegetable fibres. *Journal of Natural Fibers*, 1, 37-68.
- BIAGIOTTI, J., PUGLIA, D., TORRE, L., KENNY, J. M., ARBELAIZ, A., CANTERO, G., MARIETA, C., LLANO-PONTE, R. & MONDRAGON, I. 2004b. A systematic investigation on the influence of the chemical treatment of natural fibers on the properties of their polymer matrix composites. *Polymer Composites*, 25, 470-479.
- BIKAS, H., STAVROPOULOS, P. & CHRYSSOLOURIS, G. 2016. Additive manufacturing methods and modelling approaches: a critical review. *The International Journal of Advanced Manufacturing Technology*, 83, 389-405.
- BLAINE, R. L. 2002. Thermal Applications Note. *Polymer Heats of Fusion*.
- BLEDZKI, A. & GASSAN, J. 1999. Composites reinforced with cellulose based fibres. *Progress in polymer science*, 24, 221-274.
- BLEDZKI, A., REIHMANE, S. & GASSAN, J. 1996. Properties and modification methods for vegetable fibers for natural fiber composites. *Journal of applied polymer science*, 59, 1329-1336.

- BLEDZKI, A. K., FRANCISZCZAK, P., OSMAN, Z. & ELBADAWI, M. 2015. Polypropylene biocomposites reinforced with softwood, abaca, jute, and kenaf fibers. *Industrial Crops and Products*, 70, 91-99.
- BLEDZKI, A. K., JASZKIEWICZ, A. & SCHERZER, D. 2009. Mechanical properties of PLA composites with man-made cellulose and abaca fibres. *Composites Part A: Applied Science and Manufacturing*, 40, 404-412.
- BLEDZKI, A. K., SPERBER, V. & FARUK, O. 2002. *Natural and wood fibre reinforcement in polymers*, iSmithers Rapra Publishing.
- BODROS, E., PILLIN, I., MONTRELAY, N. & BALEY, C. 2007. Could biopolymers reinforced by randomly scattered flax fibre be used in structural applications? *Composites Science and Technology*, 67, 462-470.
- BOEY, F. Y. C. & LYE, S. W. 1992. Void reduction in autoclave processing of thermoset composites: Part 1: High pressure effects on void reduction. *Composites*, 23, 261-265.
- BOGOEVA-GACEVA, G., AVELLA, M., MALINCONICO, M., BUZAROVSKA, A., GROZDANOV, A., GENTILE, G. & ERRICO, M. 2007. Natural fiber eco-composites. *Polymer composites*, 28, 98-107.
- BOS, H., VAN DEN OEVER, M. & PETERS, O. 2002. Tensile and compressive properties of flax fibres for natural fibre reinforced composites. *Journal of Materials Science*, 37, 1683-1692.
- BOS, H. L., MÜSSIG, J. & VAN DEN OEVER, M. J. A. 2006. Mechanical properties of short-flax-fibre reinforced compounds. *Composites Part A: Applied Science and Manufacturing*, 37, 1591-1604.
- BOURELL, D., KRUTH, J. P., LEU, M., LEVY, G., ROSEN, D., BEESE, A. M. & CLARE, A. 2017. Materials for additive manufacturing. *CIRP Annals*, 66, 659-681.
- BOWYER, W. & BADER, M. 1972. On the re-reinforcement of thermoplastics by imperfectly aligned discontinuous fibres. *Journal of Materials Science*, 7, 1315-1321.
- BRENNE, F., NIENDORF, T. & MAIER, H. J. 2013. Additively manufactured cellular structures: Impact of microstructure and local strains on the monotonic and cyclic behavior under uniaxial and bending load. *Journal of Materials Processing Technology*, 213, 1558-1564.
- CAO, X. & LEE, L. J. 2003. Control of shrinkage and residual styrene of unsaturated polyester resins cured at low temperatures: I. Effect of curing agents. *Polymer*, 44, 1893-1902.
- CARNEIRO, O. S., SILVA, A. F. & GOMES, R. 2015. Fused deposition modeling with polypropylene. *Materials & Design*, 83, 768-776.
- CHAISHOME, J., BROWN, K., BROOKS, R. & CLIFFORD, M. Thermal Degradation of Flax Fibres as Potential Reinforcement in Thermoplastic Composites. *Advanced Materials Research*, 2014. Trans Tech Publ, 32-36.
- CHARLET, K., BALEY, C., MORVAN, C., JERNOT, J. P., GOMINA, M. & BRÉARD, J. 2007. Characteristics of Hermès flax fibres as a function of their location in the stem and properties of the derived unidirectional composites. *Composites Part A: Applied Science and Manufacturing*, 38, 1912-1921.
- CHOURA, M., BELGACEM, N. M. & GANDINI, A. 1996. Acid-catalyzed polycondensation of furfuryl alcohol: mechanisms of chromophore formation and cross-linking. *Macromolecules*, 29, 3839-3850.
- CICALA, G., CRISTALDI, G., RECCA, G., ZIEGMANN, G., EL-SABBAGH, A. & DICKERT, M. 2009. Properties and performances of various hybrid glass/natural fibre composites for curved pipes. *Materials & Design*, 30, 2538-2542.
- CICHOCKI JR, F. R. & THOMASON, J. L. 2002. Thermoelastic anisotropy of a natural fiber. *Composites Science and Technology*, 62, 669-678.

- COMPTON, B. G. & LEWIS, J. A. 2014. 3D-printing of lightweight cellular composites. *Advanced materials*, 26, 5930-5935.
- COUTURE, A., LEBRUN, G. & LAPERRIÈRE, L. 2016. Mechanical properties of polylactic acid (PLA) composites reinforced with unidirectional flax and flax-paper layers. *Composite Structures*, 154, 286-295.
- COX, H. 1952. The elasticity and strength of paper and other fibrous materials. *British journal of applied physics*, 3, 72.
- CÓZAR, A., ECHEVARRÍA, F., GONZÁLEZ-GORDILLO, J. I., IRIGOIEN, X., ÚBEDA, B., HERNÁNDEZ-LEÓN, S., PALMA, Á. T., NAVARRO, S., GARCÍA-DE-LOMAS, J. & RUIZ, A. 2014. Plastic debris in the open ocean. *Proceedings of the National Academy of Sciences*, 111, 10239-10244.
- CROCCOLO, D., DE AGOSTINIS, M. & OLMI, G. 2013. Experimental characterization and analytical modelling of the mechanical behaviour of fused deposition processed parts made of ABS-M30. *Computational Materials Science*, 79, 506-518.
- ĆWIKŁA, G., GRABOWIK, C., KALINOWSKI, K., PAPROCKA, I. & OCIEPKA, P. 2017. The influence of printing parameters on selected mechanical properties of FDM/FFF 3D-printed parts. *IOP Conference Series: Materials Science and Engineering*, 227, 012033.
- DA LUZ, F. S., CANDIDO, V. S., DA SILVA, A. C. R. & MONTEIRO, S. N. 2018. Thermal Behavior of Polyester Composites Reinforced with Green Sugarcane Bagasse Fiber. *JOM*, 70, 1965-1971.
- DAVALOS, J. F., QIAO, P., FRANK XU, X., ROBINSON, J. & BARTH, K. E. 2001. Modeling and characterization of fiber-reinforced plastic honeycomb sandwich panels for highway bridge applications. *Composite Structures*, 52, 441-452.
- DAVID, C. & FORNASIER, R. 1986. Utilization of waste cellulose. 7. Kinetic study of the enzymatic hydrolysis of spruce wood pretreated by sodium hypochlorite. *Macromolecules*, 19, 552-557.
- DAVIS, J. R. 2004. *Tensile testing*, ASM international.
- DAWOUD, M., TAHA, I. & EBEID, S. J. 2016. Mechanical behaviour of ABS: An experimental study using FDM and injection moulding techniques. *Journal of Manufacturing Processes*, 21, 39-45.
- DE OBALDIA, E. E., JEONG, C., GRUNENFELDER, L. K., KISAILUS, D. & ZAVATTIERI, P. 2015. Analysis of the mechanical response of biomimetic materials with highly oriented microstructures through 3D printing, mechanical testing and modeling. *Journal of the mechanical behavior of biomedical materials*, 48, 70-85.
- DEKA, H., MISRA, M. & MOHANTY, A. 2013. Renewable resource based “all green composites” from kenaf biofiber and poly(furfuryl alcohol) bioresin. *Industrial Crops and Products*, 41, 94-101.
- DHAKAL, H., ZHANG, Z., BENNETT, N., LOPEZ-ARRAIZA, A. & VALLEJO, F. 2014. Effects of water immersion ageing on the mechanical properties of flax and jute fibre biocomposites evaluated by nanoindentation and flexural testing. *Journal of Composite Materials*, 48, 1399-1406.
- DHAKAL, H. N., ZHANG, Z. Y. & RICHARDSON, M. O. W. 2007. Effect of water absorption on the mechanical properties of hemp fibre reinforced unsaturated polyester composites. *Composites Science and Technology*, 67, 1674-1683.
- DHOLAKIYA, B. 2012. *Unsaturated polyester resin for specialty applications*, InTech Rijeka.
- DISSANAYAKE, N. P. 2011. LIFE CYCLE ASSESSMENT OF FLAX FIBRES.
- DOAN, T.-T.-L., BRODOWSKY, H. & MÄDER, E. 2007. Jute fibre/polypropylene composites II. Thermal, hydrothermal and dynamic mechanical behaviour. *Composites Science and Technology*, 67, 2707-2714.

- DUC, F., BOURBAN, P.-E. & MÅNSON, J.-A. E. 2014a. Dynamic mechanical properties of epoxy/flax fibre composites. *Journal of reinforced plastics and composites*, 33, 1625-1633.
- DUC, F., BOURBAN, P. E., PLUMMER, C. J. G. & MÅNSON, J. A. E. 2014b. Damping of thermoset and thermoplastic flax fibre composites. *Composites Part A: Applied Science and Manufacturing*, 64, 115-123.
- DURGUN, I. & ERTAN, R. 2014. Experimental investigation of FDM process for improvement of mechanical properties and production cost. *Rapid Prototyping Journal*, 20, 228-235.
- DWEIB, M. A., HU, B., O'DONNELL, A., SHENTON, H. W. & WOOL, R. P. 2004. All natural composite sandwich beams for structural applications. *Composite Structures*, 63, 147-157.
- ECOTECHNILIN. 2017. Available: <https://eco-technilin.com/en/page/11-transport> [Accessed 03/05/2019].
- ETAATI, A., MEHDIZADEH, S. A., WANG, H. & PATHER, S. 2014. Vibration damping characteristics of short hemp fibre thermoplastic composites. *Journal of Reinforced Plastics and Composites*, 33, 330-341.
- EUJIN PEI, D., MELENKA, G. W., SCHOFIELD, J. S., DAWSON, M. R. & CAREY, J. P. 2015. Evaluation of dimensional accuracy and material properties of the MakerBot 3D desktop printer. *Rapid Prototyping Journal*, 21, 618-627.
- EUROPEAN BIOPLASTICS, N.-I. 2018. *Bioplastics market data 2018: Global production capacities of bioplastics 2018-2023* [Online]. Available: <https://www.european-bioplastics.org/market/> [Accessed 06/02/2019].
- FAGES, E., GIRONÉS, S., SÁNCHEZ-NACHER, L., GARCÍA-SANOQUERA, D. & BALART, R. 2012. Use of wet-laid techniques to form flax-polypropylene nonwovens as base substrates for eco-friendly composites by using hot-press molding. *Polymer composites*, 33, 253-261.
- FARAH, S., ANDERSON, D. G. & LANGER, R. 2016. Physical and mechanical properties of PLA, and their functions in widespread applications — A comprehensive review. *Advanced Drug Delivery Reviews*, 107, 367-392.
- FARUK, O., BLEDZKI, A. K., FINK, H.-P. & SAIN, M. 2012. Biocomposites reinforced with natural fibers: 2000–2010. *Progress in polymer science*, 37, 1552-1596.
- FARUK, O., BLEDZKI, A. K., FINK, H. P. & SAIN, M. 2014. Progress report on natural fiber reinforced composites. *Macromolecular Materials and Engineering*, 299, 9-26.
- FERREIRA, R. T. L., AMATTE, I. C., DUTRA, T. A. & BÜRGER, D. 2017. Experimental characterization and micrography of 3D printed PLA and PLA reinforced with short carbon fibers. *Composites Part B: Engineering*, 124, 88-100.
- FERRO, C. G., VARETTI, S., VITTI, F., MAGGIORE, P., LOMBARDI, M., BIAMINO, S., MANFREDI, D. & CALIGNANO, F. 2017. A Robust Multifunctional Sandwich Panel Design with Trabecular Structures by the Use of Additive Manufacturing Technology for a New De-Icing System. *Technologies*, 5, 35.
- FORUZANMEHR, M., ELKOUN, S., FAM, A. & ROBERT, M. 2016. Degradation characteristics of new bio-resin based-fiber-reinforced polymers for external rehabilitation of structures. *Journal of Composite Materials*, 50, 1227-1239.
- FRANCK, R. R. 2005. *Bast and other plant fibres*, Crc Press.
- FRANCUCCI, G., MANTHEY, N. W., CARDONA, F. & ARAVINTHAN, T. 2014. Processing and characterization of 100% hemp-based biocomposites obtained by vacuum infusion. *Journal of Composite Materials*, 48, 1323-1335.
- FRANCUCCI, G., RODRÍGUEZ, E. S. & VÁZQUEZ, A. 2012. Experimental study of the compaction response of jute fabrics in liquid composite molding processes. *Journal of Composite Materials*, 46, 155-167.

- GARKHAIL, S., HEIJENRATH, R. & PEIJS, T. 2000. Mechanical properties of natural-fibre-mat-reinforced thermoplastics based on flax fibres and polypropylene. *Applied Composite Materials*, 7, 351-372.
- GASSAN, J. & BLEDZKI, A. K. 2001. Thermal degradation of flax and jute fibers. *Journal of Applied Polymer Science*, 82, 1417-1422.
- GASSAN, J., CHATE, A. & BLEDZKI, A. K. 2001. Calculation of elastic properties of natural fibers. *Journal of materials science*, 36, 3715-3720.
- GIANNIS, S., ARNOLD, E., HOYDONCKX, H., WEAGER, B. & MARTIN, R. Development of high performance bio-composites based on furan bio-resins for vehicle panels. Proceedings of the 13th European Conference on Composite Materials (ECCM'08), 2008.
- GIBSON, I., ROSEN, D. W. & STUCKER, B. 2010. *Additive manufacturing technologies*, Springer.
- GOERTZEN, W. K. & KESSLER, M. 2007. Dynamic mechanical analysis of carbon/epoxy composites for structural pipeline repair. *Composites Part B: Engineering*, 38, 1-9.
- GONZALEZ, J., ALBANO, C., ICHAZO, M. & DÍAZ, B. 2002. Effects of coupling agents on mechanical and morphological behavior of the PP/HDPE blend with two different CaCO₃. *European Polymer Journal*, 38, 2465-2475.
- GONZÁLEZ, R., FIGUEROA, J. M. & GONZÁLEZ, H. 2002. Furfuryl alcohol polymerisation by iodine in methylene chloride. *European Polymer Journal*, 38, 287-297.
- GOUANVE, F., MEYER, M., GRENET, J., MARAIS, S., PONCIN-EPAILLARD, F. & SAITER, J.-M. 2006. Unsaturated polyester resin (UPR) reinforced with flax fibers, untreated and cold He plasma-treated: thermal, mechanical and DMA studies. *Composite Interfaces*, 13, 355-364.
- GRAND.VIEW.RESEARCH. 2018. *Natural Fiber Composites (NFC) Market Size, Share & Trends Analysis Report By Raw Material, By Matrix, By Technology, By Application, And Segment Forecasts, 2018 - 2024* [Online]. Available: <https://www.grandviewresearch.com/industry-analysis/natural-fiber-composites-market> [Accessed 31/10/2019].
- GRASSO, M., AZZOUZ, L., RUIZ-HINCAPIE, P., ZARRELLI, M. & REN, G. 2018. Effect of Temperature on the Mechanical Properties of 3DPrinted PLA Tensile Specimens. *Rapid Prototyping Journal*, 25.
- GUO, C.-G., SONG, Y.-M., WANG, Q.-W. & SHEN, C.-S. 2006. Dynamic-mechanical analysis and SEM morphology of wood flour/polypropylene composites. *Journal of Forestry Research*, 17, 315-318.
- HABIBI, M., LAPERRIÈRE, L., LEBRUN, G. & TOUBAL, L. 2017. Combining short flax fiber mats and unidirectional flax yarns for composite applications: Effect of short flax fibers on biaxial mechanical properties and damage behaviour. *Composites Part B: Engineering*, 123, 165-178.
- HAGHDAN, S. & SMITH, G. D. 2015. Natural fiber reinforced polyester composites: A literature review. *Journal of Reinforced Plastics and Composites*, 34, 1179-1190.
- HAN, C., VAN DEN WEGHE, T., SHETE, P. & HAW, J. 1981. Effects of coupling agents on the rheological properties, processability, and mechanical properties of filled polypropylene. *Polymer Engineering & Science*, 21, 196-204.
- HARDING, K. G., DENNIS, J. S., VON BLOTTNITZ, H. & HARRISON, S. T. L. 2007. Environmental analysis of plastic production processes: Comparing petroleum-based polypropylene and polyethylene with biologically-based poly- β -hydroxybutyric acid using life cycle analysis. *Journal of Biotechnology*, 130, 57-66.
- HARRIS, B. 1999. Engineering composite materials.
- HATTON, J. 1974. Polymerizable unsaturated polyester resin compositions and articles made therefrom. Google Patents.
- HAYWARD, J. & HARRIS, B. 1990. Effect of process variables on the quality of RTM mouldings. *SAMPE J.*, 26, 39-46.

- HENTON, D. E., GRUBER, P., LUNT, J. & RANDALL, J. 2005. Polylactic acid technology. *Natural fibers, biopolymers, and biocomposites*, 16, 527-577.
- HERRMANN, A. S., ZAHLEN, P. C. & ZUARDY, I. 2005. Sandwich structures technology in commercial aviation. *Sandwich structures 7: Advancing with sandwich structures and materials*. Springer.
- HINE, P. J., DAVIDSON, N., DUCKETT, R. A. & WARD, I. M. 1995. Measuring the fibre orientation and modelling the elastic properties of injection-moulded long-glass-fibre-reinforced nylon. *Composites Science and Technology*, 53, 125-131.
- HO, M.-P., WANG, H., LEE, J.-H., HO, C.-K., LAU, K.-T., LENG, J. & HUI, D. 2012. Critical factors on manufacturing processes of natural fibre composites. *Composites Part B: Engineering*, 43, 3549-3562.
- HODZIC, A., SHANKS, R. A. & LEORKE, M. 2002. Polypropylene and Aliphatic Polyester Flax Fibre Composites. *Polymers and Polymer Composites*, 10, 281-290.
- HORNSBY, P., HINRICHSEN, E. & TARVERDI, K. 1997. Preparation and properties of polypropylene composites reinforced with wheat and flax straw fibres: part I fibre characterization. *Journal of materials science*, 32, 443-449.
- HSU, C. & LEE, L. J. 1991. Structure formation during the copolymerization of styrene and unsaturated polyester resin. *Polymer*, 32, 2263-2271.
- HU, W., TON-THAT, M. T., PERRIN-SARAZIN, F. & DENAULT, J. 2010. An improved method for single fiber tensile test of natural fibers. *Polymer Engineering & Science*, 50, 819-825.
- HUDA, M. S., DRZAL, L. T., MOHANTY, A. K. & MISRA, M. 2008. Effect of fiber surface-treatments on the properties of laminated biocomposites from poly(lactic acid) (PLA) and kenaf fibers. *Composites Science and Technology*, 68, 424-432.
- HUGHES, M., SÈBE, G., HAGUE, J., HILL, C., SPEAR, M. & MOTT, L. 2000. An investigation into the effects of micro-compressive defects on interphase behaviour in hemp-epoxy composites using half-fringe photoelasticity. *Composite Interfaces*, 7, 13-29.
- IDICULA, M., MALHOTRA, S., JOSEPH, K. & THOMAS, S. 2005. Dynamic mechanical analysis of randomly oriented intimately mixed short banana/sisal hybrid fibre reinforced polyester composites. *Composites Science and Technology*, 65, 1077-1087.
- JAWAID, M. & KHALIL, H. A. 2011. Cellulosic/synthetic fibre reinforced polymer hybrid composites: A review. *Carbohydrate Polymers*, 86, 1-18.
- JOFFE, R., ANDERSONS, J. & WALLSTRÖM, L. 2003. Strength and adhesion characteristics of elementary flax fibres with different surface treatments. *Composites Part A: Applied Science and Manufacturing*, 34, 603-612.
- JOHN, M. J. & THOMAS, S. 2008. Biofibres and biocomposites. *Carbohydrate polymers*, 71, 343-364.
- JUSOH, M. S. M., YAHYA, M. Y. & HUSSEIN, N. I. S. The effect of fibre layering pattern in resisting bending loads of natural fibre-based hybrid composite materials. MATEC Web of Conferences, 2016. EDP Sciences.
- KABIR, K., VODENITCHAROVA, T. & HOFFMAN, M. 2014. Response of aluminium foam-cored sandwich panels to bending load. *Composites Part B: Engineering*, 64, 24-32.
- KALAY, G. & BEVIS, M. J. 1997. Processing and physical property relationships in injection-molded isotactic polypropylene. 1. Mechanical properties. *Journal of Polymer Science Part B: Polymer Physics*, 35, 241-263.
- KALIA, S., KAITH, B. & KAUR, I. 2009. Pretreatments of natural fibers and their application as reinforcing material in polymer composites—a review. *Polymer Engineering & Science*, 49, 1253-1272.

- KANNAN, T. G., WU, C. M., CHENG, K. B. & WANG, C. Y. 2013. Effect of reinforcement on the mechanical and thermal properties of flax/polypropylene interwoven fabric composites. *Journal of Industrial Textiles*, 42, 417-433.
- KANTAREDDY, S., ROH, B., SIMPSON, T., JOSHI, S., DICKMAN, C. & LEHTIHET, E. Saving Weight With Metallic Lattice Structures: Design Challenges With a Real-World Example. Solid Freeform Fabrication Symposium (SFF), Austin, TX, Aug, 2016. 8-10.
- KARADUMAN, Y., SAYEED, M. M. A., ONAL, L. & RAWAL, A. 2014. Viscoelastic properties of surface modified jute fiber/polypropylene nonwoven composites. *Composites Part B: Engineering*, 67, 111-118.
- KARAMOOZ RAVARI, M. R., KADKHODAEI, M., BADROSSAMAY, M. & REZAEI, R. 2014. Numerical investigation on mechanical properties of cellular lattice structures fabricated by fused deposition modeling. *International Journal of Mechanical Sciences*, 88, 154-161.
- KAZEMAHVAZI, S., TANNER, D. & ZENKERT, D. 2009. Corrugated all-composite sandwich structures. Part 2: Failure mechanisms and experimental programme. *Composites Science and Technology*, 69, 920-925.
- KENDALL, M. J. & SIVIOUR, C. R. Rate dependence of poly (vinyl chloride), the effects of plasticizer and time-temperature superposition. Proc. R. Soc. A, 2014. The Royal Society, 20140012.
- KESSLER, R. W., BECKER, U., KOHLER, R. & GOTH, B. 1998. Steam explosion of flax — a superior technique for upgrading fibre value. *Biomass and Bioenergy*, 14, 237-249.
- KHONDKER, O. A., ISHIAKU, U. S., NAKAI, A. & HAMADA, H. 2005. Fabrication mechanical properties of unidirectional jute/PP composites using jute yarns by film stacking method. *Journal of Polymers and the Environment*, 13, 115-126.
- KHONDKER, O. A., ISHIAKU, U. S., NAKAI, A. & HAMADA, H. 2006. A novel processing technique for thermoplastic manufacturing of unidirectional composites reinforced with jute yarns. *Composites Part A: Applied Science and Manufacturing*, 37, 2274-2284.
- KIM, H.-S., LEE, B.-H., CHOI, S.-W., KIM, S. & KIM, H.-J. 2007. The effect of types of maleic anhydride-grafted polypropylene (MAPP) on the interfacial adhesion properties of bio-flour-filled polypropylene composites. *Composites Part A: Applied Science and Manufacturing*, 38, 1473-1482.
- KRENCHER, H. 1964. Fibre reinforcement; theoretical and practical investigations of the elasticity and strength of fibre-reinforced materials. *Akademisk Forlag*.
- KUMAR, R. & ANANDJIWALA, R. D. 2013. Compression-moulded flax fabric-reinforced polyfurfuryl alcohol bio-composites. *Journal of thermal analysis and calorimetry*, 112, 755-760.
- LA MANTIA, F. & MORREALE, M. 2011. Green composites: A brief review. *Composites Part A: Applied Science and Manufacturing*, 42, 579-588.
- LANZOTTI, A., GRASSO, M., STAIANO, G. & MARTORELLI, M. 2015. The impact of process parameters on mechanical properties of parts fabricated in PLA with an open-source 3-D printer. *Rapid Prototyping Journal*, 21, 604-617.
- LAURETO, J. J. & PEARCE, J. M. 2017. Open source multi-head 3D printer for polymer-metal composite component manufacturing. *Technologies*, 5, 36.
- LAUTENSCHLÄGER, M. I., SCHEIWE, M. H., WEIDENMANN, K. A., HENNING, F. & ELSNER, P. 2017. Study of Influencing Factors on the Flowability of Jute Nonwoven Reinforced Sheet Molding Compound. *World Academy of Science, Engineering and Technology, International Journal of Chemical, Molecular, Nuclear, Materials and Metallurgical Engineering*, 11, 50-55.
- LE DUGOU, A., CASTRO, M., BEVAN, R. & MARTIN, N. 2016. 3D printing of wood fibre biocomposites: From mechanical to actuation functionality. *Materials & Design*, 96, 106-114.

- LE DUGOU, A., DAVIES, P. & BAILEY, C. 2010. Interfacial bonding of flax fibre/poly (l-lactide) bio-composites. *Composites Science and Technology*, 70, 231-239.
- LE TROEDEC, M., SEDAN, D., PEYRATOUT, C., BONNET, J. P., SMITH, A., GUINEBRETIERE, R., GLOAGUEN, V. & KRAUSZ, P. 2008. Influence of various chemical treatments on the composition and structure of hemp fibres. *Composites Part A: Applied Science and Manufacturing*, 39, 514-522.
- LEE, B.-K. & KANG, K.-J. 2010. A parametric study on compressive characteristics of Wire-woven bulk Kagome truss cores. *Composite Structures*, 92, 445-453.
- LI, J., WU, B. & MYANT, C. 2016. The Current Landscape for Additive Manufacturing Research.
- LIN, M. S., LIU, C. C. & LEE, C. T. 1999. Toughened interpenetrating polymer network materials based on unsaturated polyester and epoxy. *Journal of Applied Polymer Science*, 72, 585-592.
- LIU, F. W. 2007. *Rapid prototyping and engineering applications: a toolbox for prototype development*, Crc Press.
- LIU, S., LI, Y. & LI, N. 2018. A novel free-hanging 3D printing method for continuous carbon fiber reinforced thermoplastic lattice truss core structures. *Materials & Design*, 137, 235-244.
- LUMMERSTORFER, T., GRETHENBERGER, G. & TRANNINGER, M. 2019. Polypropylene compositions for automotive applications. Google Patents.
- MACAULEY, N., HARKIN-JONES, E. & MURPHY, W. 1998. The influence of nucleating agents on the extrusion and thermoforming of polypropylene. *Polymer Engineering & Science*, 38, 516-523.
- MADDAH, H. A. 2016. Polypropylene as a promising plastic: A review. *Am. J. Polym. Sci*, 6, 1-11.
- MADSEN, B. & LILHOLT, H. 2003. Physical and mechanical properties of unidirectional plant fibre composites—an evaluation of the influence of porosity. *Composites Science and Technology*, 63, 1265-1272.
- MADSEN, B., THYGESEN, A. & LILHOLT, H. 2007. Plant fibre composites – porosity and volumetric interaction. *Composites Science and Technology*, 67, 1584-1600.
- MADSEN, B., THYGESEN, A. & LILHOLT, H. 2009. Plant fibre composites – porosity and stiffness. *Composites Science and Technology*, 69, 1057-1069.
- MAHMOUD, D. & ELBESTAWI, M. 2017. Lattice Structures and Functionally Graded Materials Applications in Additive Manufacturing of Orthopedic Implants: A Review. *Journal of Manufacturing and Materials Processing*, 1, 13.
- MAITY, S., GON, D. P. & PAUL, P. 2014. A review of flax nonwovens: Manufacturing, properties, and applications. *Journal of Natural Fibers*, 11, 365-390.
- MAITY, S. & SINGHA, K. 2012. Structure-property relationships of needle-punched nonwoven fabric. *Frontiers in Science*, 2, 226-234.
- MALABA, T. & WANG, J. 2015. Unidirectional Cordenka Fibre-Reinforced Furan Resin Full Biocomposite: Properties and Influence of High Fibre Mass Fraction. *Journal of Composites*, 2015.
- MALLICK, P. K. 2007. *Fiber-reinforced composites: materials, manufacturing, and design*, CRC press.
- MARTIN, N., DAVIES, P. & BAILEY, C. 2016. Evaluation of the potential of three non-woven flax fiber reinforcements: Spunlaced, needlepunched and paper process mats. *Industrial Crops and Products*, 83, 194-205.
- MARTIN, O. & AVÉROUS, L. 2001. Poly(lactic acid): plasticization and properties of biodegradable multiphase systems. *Polymer*, 42, 6209-6219.
- MCLAUGHLIN, E. & TAIT, R. 1980. Fracture mechanism of plant fibres. *Journal of Materials Science*, 15, 89-95.

- MEHTA, G., DRZAL, L. T., MOHANTY, A. K. & MISRA, M. 2006. Effect of fiber surface treatment on the properties of biocomposites from nonwoven industrial hemp fiber mats and unsaturated polyester resin. *Journal of applied polymer science*, 99, 1055-1068.
- MEISEL, N. A., WILLIAMS, C. B. & DRUSCHITZ, A. Lightweight metal cellular structures via indirect 3D printing and casting. Proceedings of the international solid freeform fabrication symposium, 2012. 162-176.
- MERCER, C., LEE, J. & BALINT, D. S. 2018. An investigation of the mechanical behavior of three-dimensional low expansion lattice structures fabricated via laser printing. *Composite Structures*, 206, 80-94.
- MIAO, M. & SHAN, M. 2011. Highly aligned flax/polypropylene nonwoven preforms for thermoplastic composites. *Composites Science and Technology*, 71, 1713-1718.
- MINES, R. A. W., TSOPANOS, S., SHEN, Y., HASAN, R. & MCKOWN, S. T. 2013. Drop weight impact behaviour of sandwich panels with metallic micro lattice cores. *International Journal of Impact Engineering*, 60, 120-132.
- MODNIKS, J. & ANDERSONS, J. 2013. Modeling the non-linear deformation of a short-flax-fiber-reinforced polymer composite by orientation averaging. *Composites Part B: Engineering*, 54, 188-193.
- MOHAMED, O. A., MASOOD, S. H. & BHOWMIK, J. L. 2015. Optimization of fused deposition modeling process parameters: a review of current research and future prospects. *Advances in Manufacturing*, 3, 42-53.
- MOHANTY, A., MISRA, M. & HINRICHSEN, G. 2000. Biofibers, biodegradable polymers and biocomposites: an overview. *Macromolecular materials and Engineering*, 276, 1-24.
- MOHANTY, A. K., MISRA, M. & DRZAL, L. T. 2005. *Natural fibers, biopolymers, and biocomposites*, CRC press.
- MOHANTY, S., NAYAK, S., VERMA, S. & TRIPATHY, S. 2004. Effect of MAPP as a coupling agent on the performance of jute-PP composites. *Journal of reinforced plastics and composites*, 23, 625-637.
- MORALEJO-GÁRATE, H., MAR'ATUSALIHAT, E., KLEEREBEZEM, R. & VAN LOOSDRECHT, M. C. 2011. Microbial community engineering for biopolymer production from glycerol. *Applied microbiology and biotechnology*, 92, 631-639.
- MORITOMI, S., WATANABE, T. & KANZAKI, S. 2010. Polypropylene compounds for automotive applications. *Sumitomo Kagaku*, 1, 1-16.
- MOURITZ, A. P., GELLERT, E., BURCHILL, P. & CHALLIS, K. 2001. Review of advanced composite structures for naval ships and submarines. *Composite Structures*, 53, 21-42.
- MURARIU, M. & DUBOIS, P. 2016. PLA composites: From production to properties. *Advanced drug delivery reviews*, 107, 17-46.
- NACOS, M., KATAPODIS, P., PAPPAS, C., DAFERERA, D., TARANTILIS, P., CHRISTAKOPOULOS, P. & POLISSIOU, M. 2006. Kenaf xylan-A source of biologically active acidic oligosaccharides. *Carbohydrate polymers*, 66, 126-134.
- NANNAN GUO, M. C. L. 2013. Additive manufacturing: technology, applications and research needs. *Front. Mech. Eng.*, 8, 215-243.
- NANNI, G., HEREDIA-GUERRERO, A. J., PAUL, C. U., DANTE, S., CAPUTO, G., CANALE, C., ATHANASSIOU, A., FRAGOULI, D. & BAYER, S. I. 2019. Poly(furfuryl alcohol)-Polycaprolactone Blends. *Polymers*, 11.
- NASSIOPOULOS, E. 2015. Localised low velocity impact performance of FLAX/PLA biocomposites.
- NEMAT-NASSER, S., KANG, W. J., MCGEE, J. D., GUO, W. G. & ISAACS, J. B. 2007. Experimental investigation of energy-absorption characteristics of components of sandwich structures. *International Journal of Impact Engineering*, 34, 1119-1146.

- NGO, T. D., KASHANI, A., IMBALZANO, G., NGUYEN, K. T. Q. & HUI, D. 2018. Additive manufacturing (3D printing): A review of materials, methods, applications and challenges. *Composites Part B: Engineering*, 143, 172-196.
- NIKZAD, M., MASOOD, S. & SBARSKI, I. 2011. Thermo-mechanical properties of a highly filled polymeric composites for fused deposition modeling. *Materials & Design*, 32, 3448-3456.
- NORLANDER, B. W. 1946. Resinous products from furfuryl alcohol and process of making the same. Google Patents.
- O'DONNELL, A., DWEIB, M. & WOOL, R. 2004. Natural fiber composites with plant oil-based resin. *Composites science and technology*, 64, 1135-1145.
- OKSMAN, K., SKRIFVARS, M. & SELIN, J.-F. 2003. Natural fibres as reinforcement in polylactic acid (PLA) composites. *Composites science and technology*, 63, 1317-1324.
- ORNAGHI JR, H. L., BOLNER, A. S., FIORIO, R., ZATTERA, A. J. & AMICO, S. C. 2010. Mechanical and dynamic mechanical analysis of hybrid composites molded by resin transfer molding. *Journal of Applied Polymer Science*, 118, 887-896.
- OSMAN, Y., ELRAZAK, A. A. & KHATER, W. 2016. Bioprocess optimization of microbial biopolymer production. *Journal of Biobased Materials and Bioenergy*, 10, 119-128.
- PAN, N. 1993. Theoretical determination of the optimal fiber volume fraction and fiber-matrix property compatibility of short fiber composites. *Polymer composites*, 14, 85-93.
- PANTHAPULAKKAL, S. & SAIN, M. 2007. Injection-molded short hemp fiber/glass fiber-reinforced polypropylene hybrid composites—Mechanical, water absorption and thermal properties. *Journal of applied polymer science*, 103, 2432-2441.
- PARKER, E. E. & MOFFETT, E. 1954. Physical properties of polyester resin. *Industrial & Engineering Chemistry*, 46, 1615-1618.
- PEARCE, J. M. 2012. Building research equipment with free, open-source hardware. *Science*, 337, 1303-1304.
- PEIJS, T., GARKHAIL, S., HEIJENRATH, R., VAN DEN OEVER, M. & BOS, H. Thermoplastic composites based on flax fibres and polypropylene: influence of fibre length and fibre volume fraction on mechanical properties. *Macromolecular Symposia*, 1998. Wiley Online Library, 193-203.
- PEREGO, G., CELLA, G. D. & BASTIOLI, C. 1996. Effect of molecular weight and crystallinity on poly (lactic acid) mechanical properties. *Journal of Applied Polymer Science*, 59, 37-43.
- PETRUCCI, R., SANTULLI, C., PUGLIA, D., SARASINI, F., TORRE, L. & KENNY, J. 2013. Mechanical characterisation of hybrid composite laminates based on basalt fibres in combination with flax, hemp and glass fibres manufactured by vacuum infusion. *Materials & Design*, 49, 728-735.
- PHILLIPS, S., BAETS, J., LESSARD, L., HUBERT, P. & VERPOEST, I. 2013. Characterization of flax/epoxy prepregs before and after cure. *Journal of Reinforced Plastics and Composites*, 32, 777-785.
- PICKERING, K. L., EFENDY, M. G. A. & LE, T. M. 2016a. A review of recent developments in natural fibre composites and their mechanical performance. *Composites Part A: Applied Science and Manufacturing*, 83, 98-112.
- PICKERING, K. L., EFENDY, M. G. A. & LE, T. M. 2016b. A review of recent developments in natural fibre composites and their mechanical performance. *Composites Part A: Applied Science and Manufacturing*, 83, 98-112.
- PIL, L., BENSADOUN, F., PARISET, J. & VERPOEST, I. 2016. Why are designers fascinated by flax and hemp fibre composites? *Composites Part A: Applied Science and Manufacturing*, 83, 193-205.

- POTHAN, L. A., OOMMEN, Z. & THOMAS, S. 2003. Dynamic mechanical analysis of banana fiber reinforced polyester composites. *Composites Science and Technology*, 63, 283-293.
- QIN, C., SOYKEABKAEW, N., XIUYUAN, N. & PEIJS, T. 2008. The effect of fibre volume fraction and mercerization on the properties of all-cellulose composites. *Carbohydrate Polymers*, 71, 458-467.
- QIN, Z., COMPTON, B. G., LEWIS, J. A. & BUEHLER, M. J. 2015. Structural optimization of 3D-printed synthetic spider webs for high strength. *Nature communications*, 6.
- RAHEEM, D. 2013. Application of plastics and paper as food packaging materials-An overview. *Emirates Journal of Food and Agriculture*, 177-188.
- RAMOS, M., JIMÉNEZ, A., PELTZER, M. & GARRIGÓS, M. C. 2012. Characterization and antimicrobial activity studies of polypropylene films with carvacrol and thymol for active packaging. *Journal of Food Engineering*, 109, 513-519.
- RANA, A., MITRA, B. & BANERJEE, A. 1999. Short jute fiber-reinforced polypropylene composites: Dynamic mechanical study. *Journal of Applied Polymer Science*, 71, 531-539.
- RANA, S. & FANGUEIRO, R. 2016. *Fibrous and Textile Materials for Composite Applications*, Springer.
- RASHED, M. G., ASHRAF, M., MINES, R. A. W. & HAZELL, P. J. 2016. Metallic microlattice materials: A current state of the art on manufacturing, mechanical properties and applications. *Materials & Design*, 95, 518-533.
- RASSMANN, S., REID, R. G. & PASKARAMOORTHY, R. 2010. Effects of processing conditions on the mechanical and water absorption properties of resin transfer moulded kenaf fibre reinforced polyester composite laminates. *Composites Part A: Applied Science and Manufacturing*, 41, 1612-1619.
- RATHBUN, H., WEI, Z., HE, M., ZOK, F., EVANS, A., SYPECK, D. & WADLEY, H. 2004. Measurement and simulation of the performance of a lightweight metallic sandwich structure with a tetrahedral truss core. *Journal of Applied Mechanics*, 71, 368-374.
- RAY, D., SARKAR, B. K., DAS, S. & RANA, A. K. 2002. Dynamic mechanical and thermal analysis of vinyl ester-resin-matrix composites reinforced with untreated and alkali-treated jute fibres. *Composites Science and Technology*, 62, 911-917.
- REIMSCHUESSEL, H. 1985. *Handbook of Fiber Science and Technology-Fiber Chemistry*, Vol. IV. Marcel Dekker, New York.
- REITERER, A., LICHTENEGGER, H., TSCHEGG, S. & FRATZL, P. 1999. Experimental evidence for a mechanical function of the cellulose microfibril angle in wood cell walls. *Philosophical Magazine A*, 79, 2173-2184.
- REN, G., PATEL, H., HAPUARACHCHI, D., CROWTHER, S., FAN, M. & HOGG, P. Development of natural HEMP fibre sheet mould composites (NF-SMC). The 17 th International Conference on Composite Materials, Edinburgh, UK, 2009.
- RODRÍGUEZ, J. F., THOMAS, J. P. & RENAUD, J. E. 2003. Design of fused-deposition ABS components for stiffness and strength. *J. Mech. Des.*, 125, 545-551.
- RODRÍGUEZ-PANES, A., CLAVER, J. & CAMACHO, A. M. 2018. The influence of manufacturing parameters on the mechanical behaviour of PLA and ABS pieces manufactured by FDM: A comparative analysis. *Materials*, 11, 1333.
- RODRÍGUEZ, J. F., THOMAS, J. P. & RENAUD, J. E. 2001. Mechanical behavior of acrylonitrile butadiene styrene (ABS) fused deposition materials. Experimental investigation. *Rapid Prototyping Journal*, 7, 148-158.
- RODRÍGUEZ, J. F., THOMAS, J. P. & RENAUD, J. E. 2003. Mechanical behavior of acrylonitrile butadiene styrene fused deposition materials modeling. *Rapid Prototyping Journal*.

- ROMANZINI, D., LAVORATTI, A., ORNAGHI, H. L., AMICO, S. C. & ZATTERA, A. J. 2013. Influence of fiber content on the mechanical and dynamic mechanical properties of glass/ramie polymer composites. *Materials & Design*, 47, 9-15.
- ROMHÁNY, G., KARGER-KOCSIS, J. & CZIGÁNY, T. 2003. Tensile fracture and failure behavior of thermoplastic starch with unidirectional and cross-ply flax fiber reinforcements. *Macromolecular Materials and Engineering*, 288, 699-707.
- RUBIO-LÓPEZ, A., OLMEDO, A., DÍAZ-ÁLVAREZ, A. & SANTIUSTE, C. 2015. Manufacture of compression moulded PLA based biocomposites: A parametric study. *Composite Structures*, 131, 995-1000.
- RYAN, P. G., MOORE, C. J., VAN FRANEKER, J. A. & MOLONEY, C. L. 2009. Monitoring the abundance of plastic debris in the marine environment. *Philosophical Transactions of the Royal Society B: Biological Sciences*, 364, 1999-2012.
- SABA, N., JAWAID, M., ALOTHMAN, O. Y. & PARIDAH, M. T. 2016. A review on dynamic mechanical properties of natural fibre reinforced polymer composites. *Construction and Building Materials*, 106, 149-159.
- SAEIDLOU, S., HUNEALUT, M. A., LI, H. & PARK, C. B. 2012. Poly(lactic acid) crystallization. *Progress in Polymer Science*, 37, 1657-1677.
- SAHEB, D. N. & JOG, J. P. 1999. Natural fiber polymer composites: a review. *Advances in polymer technology*, 18, 351-363.
- SANCHEZ, E. M. S., ZAVAGLIA, C. A. C. & FELISBERTI, M. I. 2000. Unsaturated polyester resins: influence of the styrene concentration on the miscibility and mechanical properties. *Polymer*, 41, 765-769.
- SAWALLISCH, K. 1984. Compounding of Sheet Molding Compound. *Polymer-Plastics Technology and Engineering*, 23, 1-36.
- SAWPAN, M. A., PICKERING, K. L. & FERNYHOUGH, A. 2012. Flexural properties of hemp fibre reinforced polylactide and unsaturated polyester composites. *Composites Part A: Applied Science and Manufacturing*, 43, 519-526.
- SERRANO, A., ESPINACH, F. X., JULIAN, F., DEL REY, R., MENDEZ, J. A. & MUTJE, P. 2013. Estimation of the interfacial shears strength, orientation factor and mean equivalent intrinsic tensile strength in old newspaper fiber/polypropylene composites. *Composites Part B: Engineering*, 50, 232-238.
- SHAFIZADEH, J., SEFERIS, J., CHESMAR, E. & GEYER, R. 1999. Evaluation of the in-service performance behavior of honeycomb composite sandwich structures. *Journal of Materials Engineering and Performance*, 8, 661-668.
- SHAH, D. U., SCHUBEL, P. J., LICENCE, P. & CLIFFORD, M. J. 2012. Determining the minimum, critical and maximum fibre content for twisted yarn reinforced plant fibre composites. *Composites Science and Technology*, 72, 1909-1917.
- SHIBATA, S., CAO, Y. & FUKUMOTO, I. 2006. Lightweight laminate composites made from kenaf and polypropylene fibres. *Polymer Testing*, 25, 142-148.
- SHUBHRA, Q. T., ALAM, A. & QUAIYYUM, M. 2013. Mechanical properties of polypropylene composites: A review. *Journal of thermoplastic composite materials*, 26, 362-391.
- SIMÃO, J. A., CARMONA, V. B., MARCONCINI, J. M., MATTOSO, L. H. C., BARSBERG, S. T. & SANADI, A. R. 2016. Effect of fiber treatment condition and coupling agent on the mechanical and thermal properties in highly filled composites of sugarcane bagasse fiber/PP. *Materials Research*, 19, 746-751.
- SINGH, S., RAMAKRISHNA, S. & SINGH, R. 2017. Material issues in additive manufacturing: A review. *Journal of Manufacturing Processes*, 25, 185-200.

- SINGLETON, A., BAILLIE, C., BEAUMONT, P. & PEIJS, T. 2003. On the mechanical properties, deformation and fracture of a natural fibre/recycled polymer composite. *Composites Part B: Engineering*, 34, 519-526.
- SOOD, A. K., OHDAR, R. K. & MAHAPATRA, S. S. 2010. Parametric appraisal of mechanical property of fused deposition modelling processed parts. *Materials & Design*, 31, 287-295.
- SOOD, A. K., OHDAR, R. K. & MAHAPATRA, S. S. 2012. Experimental investigation and empirical modelling of FDM process for compressive strength improvement. *Journal of Advanced Research*, 3, 81-90.
- SREEKUMAR, P. A., JOSEPH, K., UNNIKRISHNAN, G. & THOMAS, S. 2007. A comparative study on mechanical properties of sisal-leaf fibre-reinforced polyester composites prepared by resin transfer and compression moulding techniques. *Composites Science and Technology*, 67, 453-461.
- STAMBOULIS, A., BAILLIE, C. & PEIJS, T. 2001. Effects of environmental conditions on mechanical and physical properties of flax fibers. *Composites Part A: Applied Science and Manufacturing*, 32, 1105-1115.
- SUH, D. J., LIM, Y. T. & PARK, O. O. 2000. The property and formation mechanism of unsaturated polyester-layered silicate nanocomposite depending on the fabrication methods. *Polymer*, 41, 8557-8563.
- SUMMERSCALES, J. & GROVE, S. 2014. 7 - Manufacturing methods for natural fibre composites. In: HODZIC, A. & SHANKS, R. (eds.) *Natural Fibre Composites*. Woodhead Publishing.
- SUN, X., XU, F., SUN, R., FOWLER, P. & BAIRD, M. 2005. Characteristics of degraded cellulose obtained from steam-exploded wheat straw. *Carbohydrate research*, 340, 97-106.
- TAO, W. & C.LEU, M. 2016. Design of lattice structure for additive manufacturing.
- TAO, Y., WANG, H., LI, Z., LI, P. & SHI, S. 2017. Development and application of wood flour-filled polylactic acid composite filament for 3d printing. *Materials* 10 (4): 339.
- THOMAS, J. P. & RENAUD, J. E. 2003. Design of fused-deposition ABS components for stiffness and strength. *Journal of Mechanical Design*, 545-551.
- TORIZ, G., ARVIDSSON, R., WESTIN, M. & GATENHOLM, P. 2003. Novel cellulose ester-poly (furfuryl alcohol)-flax fiber biocomposites. *Journal of applied polymer science*, 88, 337-345.
- TRAN, P., NGUYEN, Q. T. & LAU, K. T. 2018. Fire performance of polymer-based composites for maritime infrastructure. *Composites Part B: Engineering*, 155, 31-48.
- TRIPATHY, S., LEVITA, G. & DI LANDRO, L. 2001. Interfacial adhesion in jute-polyolefin composites. *Polymer composites*, 22, 815-822.
- TUMOLVA, T., KUBOUCHI, M. & SAKAI, T. Evaluating the carbon storage potential of furan resin-based green composites. Proceedings of the 17th international conference on composite materials, Edinburgh, UK, 2009. 27-31.
- TYMRAK, B. M., KREIGER, M. & PEARCE, J. M. 2014. Mechanical properties of components fabricated with open-source 3-D printers under realistic environmental conditions. *Materials & Design*, 58, 242-246.
- UTELA, B., STORTI, D., ANDERSON, R. & GANTER, M. 2008. A review of process development steps for new material systems in three dimensional printing (3DP). *Journal of Manufacturing Processes*, 10, 96-104.
- VALLEJOS, M. E., ESPINACH, F. X., JULIÁN, F., TORRES, L., VILASECA, F. & MUTJÉ, P. 2012. Micromechanics of hemp strands in polypropylene composites. *Composites Science and Technology*, 72, 1209-1213.
- VAN DE VELDE, K. & KIEKENS, P. 2002. Biopolymers: overview of several properties and consequences on their applications. *Polymer Testing*, 21, 433-442.

- VAN DE VELDE, K. & KIEKENS, P. 2003. Effect of material and process parameters on the mechanical properties of unidirectional and multidirectional flax/polypropylene composites. *Composite Structures*, 62, 443-448.
- VAN DEN OEVER, M. & BOS, H. 1998. Critical fibre length and apparent interfacial shear strength of single flax fibre polypropylene composites. *Advanced Composites Letters*, 7, 096369359800700303.
- VAN VOORN, B., SMIT, H. H. G., SINKE, R. J. & DE KLERK, B. 2001. Natural fibre reinforced sheet moulding compound. *Composites Part A: Applied Science and Manufacturing*, 32, 1271-1279.
- VAS, L. & BAKONYI, P. 2012. Estimating the creep strain to failure of PP at different load levels based on short term tests and Weibull characterization. *Express Polymer Letters*, 6.
- VEGA, V., CLEMENTS, J., LAM, T., ABAD, A., FRITZ, B., ULA, N. & ES-SAID, O. S. 2011. The effect of layer orientation on the mechanical properties and microstructure of a polymer. *Journal of materials engineering and performance*, 20, 978-988.
- VILLANUEVA, G. R. & CANTWELL, W. 2003. Low velocity impact response of novel fiber-reinforced aluminum foam sandwich structures. *Journal of materials science letters*, 22, 417-422.
- VINK, E. T., RABAGO, K. R., GLASSNER, D. A. & GRUBER, P. R. 2003. Applications of life cycle assessment to NatureWorks™ polylactide (PLA) production. *Polymer Degradation and stability*, 80, 403-419.
- WADLEY, H. N. G., FLECK, N. A. & EVANS, A. G. 2003. Fabrication and structural performance of periodic cellular metal sandwich structures. *Composites Science and Technology*, 63, 2331-2343.
- WANG, H. & YAO, J. 2006. Use of poly (furfuryl alcohol) in the fabrication of nanostructured carbons and nanocomposites. *Industrial & engineering chemistry research*, 45, 6393-6404.
- WANG, X., JIANG, M., ZHOU, Z., GOU, J. & HUI, D. 2017. 3D printing of polymer matrix composites: A review and prospective. *Composites Part B: Engineering*, 110, 442-458.
- WIELAGE, B., LAMPKE, T., MARX, G., NESTLER, K. & STARKE, D. 1999. Thermogravimetric and differential scanning calorimetric analysis of natural fibres and polypropylene. *Thermochimica Acta*, 337, 169-177.
- WILLIAMS, C. B., COCHRAN, J. K. & ROSEN, D. W. 2011. Additive manufacturing of metallic cellular materials via three-dimensional printing. *The International Journal of Advanced Manufacturing Technology*, 53, 231-239.
- WILLIAMS, C. D., GROVE, S. M. & SUMMERSCALES, J. 1998. The compression response of fibre-reinforced plastic plates during manufacture by the resin infusion under flexible tooling method. *Composites Part A: Applied Science and Manufacturing*, 29, 111-114.
- WITTBRODT, B. & PEARCE, J. M. 2015. The effects of PLA color on material properties of 3-D printed components. *Additive Manufacturing*, 8, 110-116.
- WITTBRODT, B. T., GLOVER, A. G., LAURETO, J., ANZALONE, G. C., OPPLIGER, D., IRWIN, J. L. & PEARCE, J. M. 2013. Life-cycle economic analysis of distributed manufacturing with open-source 3-D printers. *Mechatronics*, 23, 713-726.
- WOOL, R. & SUN, X. S. 2011. *Bio-based polymers and composites*, Academic Press.
- YAN, L., CHOUW, N. & JAYARAMAN, K. 2014. Flax fibre and its composites – A review. *Composites Part B: Engineering*, 56, 296-317.
- YANG, J.-L., ZHANG, Z., SCHLARB, A. K. & FRIEDRICH, K. 2006. On the characterization of tensile creep resistance of polyamide 66 nanocomposites. Part I. Experimental results and general discussions. *Polymer*, 47, 2791-2801.

- YANG, L. 2015. Experimental-assisted design development for an octahedral cellular structure using additive manufacturing. *Rapid Prototyping Journal*, 21, 168-176.
- YANG, Y. & LEE, L. J. 1988. Microstructure formation in the cure of unsaturated polyester resins. *Polymer*, 29, 1793-1800.
- YAZDANI SARVESTANI, H., AKBARZADEH, A. H., NIKNAM, H. & HERMENEAN, K. 2018. 3D printed architected polymeric sandwich panels: Energy absorption and structural performance. *Composite Structures*, 200, 886-909.
- YIN, S., LI, J., LIU, B., MENG, K., HUAN, Y., NUTT, S. R. & XU, J. 2017. Honeytubes: Hollow lattice truss reinforced honeycombs for crushing protection. *Composite Structures*, 160, 1147-1154.
- YOON, Y.-J., MOON, S. K. & HWANG, J. 2014. 3D printing as an efficient way for comparative study of biomimetic structures—trabecular bone and honeycomb. *Journal of Mechanical Science and Technology*, 28, 4635-4640.
- YOUNG, D., KESSLER, J. & CZABAJ, M. Interlayer fracture toughness of additively manufactured unreinforced and carbon-fiber-reinforced acrylonitrile butadiene styrene. 31st Annual Technical Conference of the American Society for Composites, ASC 2016, 2016. DEStech Publications Inc.
- YU, Z., ALCOCK, M., ROTHWELL, E. & MCKAY, S. Development of non-woven biofibre mats for composite reinforcement. Proceedings of International Conference on Composite Materials, ICCM, 2009.
- YUANJIAN, T. & ISAAC, D. 2007. Impact and fatigue behaviour of hemp fibre composites. *Composites Science and Technology*, 67, 3300-3307.
- ZAINI, L. H., JONOBI, M., TAHIR, P. M. & KARIMI, S. 2013. Isolation and characterization of cellulose whiskers from kenaf (*Hibiscus cannabinus* L.) bast fibers. *Journal of Biomaterials and Nanobiotechnology*, 4, 37.
- ZHU, J., ZHU, H., NJUGUNA, J. & ABHYANKAR, H. 2013. Recent development of flax fibres and their reinforced composites based on different polymeric matrices. *Materials*, 6, 5171-5198.
- ZIEMIAN, C., SHARMA, M. & ZIEMIAN, S. 2012. Anisotropic mechanical properties of ABS parts fabricated by fused deposition modelling. *Mechanical engineering*, 23, 2397.
- ZOK, F. W., WALTNER, S. A., WEI, Z., RATHBUN, H. J., MCMEEKING, R. M. & EVANS, A. G. 2004. A protocol for characterizing the structural performance of metallic sandwich panels: application to pyramidal truss cores. *International Journal of Solids and Structures*, 41, 6249-6271.